THE UNIVERSITY OF HULL

MICROEMULSION AND MACROEMULSION BEHAVIOUR OF SYSTEMS CONTAINING OIL, WATER AND NONIONIC SURFACTANT

being a Thesis submitted for the Degree of

Doctor of Philosophy

in the University of Hull

by

David Ian Horsup, B.Sc.

August 1991

ACKNOWLEDGEMENTS

I would like to express my sincere gratitude to my supervisor, Dr. Paul Fletcher for his assistance and advice during the period of my research and for his encouragement of my interest in surface and colloid chemistry. Thanks are also due to Dr. Robert Aveyard, Dr. Bernard Binks and my fellow colleagues for many fruitful discussions.

I am also grateful to the Agricultural and Food Research Council and Unilever (Colworth) for the provision of a three year studentship.

August 1991

To my parents for providing me with the opportunity

to pursue my academic studies.

Scientist alone is true poet,

he gives us the moon, he promises the stars,

he'll make us a new universe if it comes to that.

Allen Ginsberg, "Poem Rocket,"
Kaddish and Other Poems (1961).

ABSTRACT

In this thesis, attempts have been made to correlate some equilibrium properties of microemulsions with the formation and stability of macroemulsions. Studies have been mainly limited to water-in-oil (W/O) systems stabilised by pure nonionic surfactants of the poly-oxyethylene alkyl ether (C_nE_m) type. Initially however, a brief account is presented of the behaviour of W/O microemulsions stabilised by commercial nonionic surfactants of the type used in foods.

A detailed study of the equilibrium behaviour of W/O microemulsions stabilised by tetra-oxyethylene mono-n-dodecyl ether, $C_{12}E_4$, in hydrocarbon oils is presented. Aggregates form above a certain surfactant concentration in the oil, designated the *critical microemulsion concentration*, cμc. Changes in the monolayer curvature induced through changing the temperature, salt concentration and the nature of the oil phase, are discussed in terms of an effective surfactant molecular geometry. The effect of solubilisation of protein into the dispersed aqueous phase is also presented.

The corresponding W/O macroemulsions prepared with these systems at concentrations in excess of the cμc breakdown primarily by droplet sedimentation. There appears to be an optimum surfactant concentration at which maximum stabilisation is achieved. This is approximately equal to the cμc of the surfactant in the oil phase. Addition of microemulsion droplets to the oil dramatically increases the rate of oil phase resolution. For a fixed concentration of aggregated surfactant, the acceleration rate is rather insensitive to the size of the microemulsion droplets. These findings are reasonably consistent with a depletion flocculation mechanism in which microemulsions are assumed to behave as hard spheres and are excluded from the intervening region between approaching emulsion droplets.

Microemulsion phase behaviour is also reported for oil phases containing different concentrations of medium and long chain length triglycerides (MCT, LCT) in heptane. The critical microemulsion concentration is observed to increase dramatically

upon increasing the concentration of triglyceride. Additionally, the enthalpy change upon transfer of a mole of $C_{12}E_4$ monomers from the oil phase to the preferred microemulsion droplet curvature becomes significantly less exothermic as the concentration of MCT in the oil phase increases.

The breakdown of W/O macroemulsions produced with these triglyceride systems is also consistent with a depletion flocculation mechanism. Emulsions prepared with 75% MCT as the oil phase undergo coalescence once an approximately close-packed droplet volume fraction is achieved. It is shown that as the cμc increases (through the addition of MCT or increasing the temperature), the stability of the emulsion dramatically decreases.

Using a technique of time-resolved fluorimetry, the rate of exchange of probe molecules between microemulsion droplets has been determined. The exchange rate is always slowest at the solubilisation phase boundary where inter-droplet attractions are a minimum. The rate constants at this phase boundary are similar for aggregates formed in both heptane and in an equal volume ratio mixture of heptane : MCT. The possible relevance to the magnitude of the exchange rate constant of energies associated with bending the surfactant monolayer and desorbing surfactant from the droplet surface are considered.

This technique has also been applied to three surfactant systems for which monolayer bending rigidities have previously been reported. Microemulsion exchange rates measured at equivalent positions on the solubilisation phase boundary increase as the monolayer rigidity decreases. The stability of the corresponding W/O macroemulsions is also observed to follow this order, the fastest water resolution rates being observed for the systems with the lowest monolayer rigidities.

PUBLICATIONS

The work contained within this thesis has given rise to the following publications:

(1) Chapters 5 & 7. *Effect of microemulsified surfactant in destabilising water-in-oil emulsions containing* $C_{12}E_4$. B.P. Binks, P.D.I. Fletcher and D.I. Horsup.
Accepted for publication in Colloids and Surfaces.

(2) Chapter 6. *Droplet dynamics in water-in-oil microemulsions and macroemulsions stabilised by nonionic surfactants. Correlation of measured rates with monolayer bending elasticity.* P.D.I. Fletcher and D.I. Horsup.
Submitted to the Journal of the Chemical Society, Faraday Transactions.

GLOSSARY

Some of the abbreviations and terms used in this thesis are given below. Others are defined locally within the text.

A	area per surfactant molecule within a planar oil-water interface
a	emulsion droplet radius
A_s	area per surfactant molecule at the interface between the droplet core and the surfactant monolayer
A_h	effective area of a surfactant head group within a curved microemulsion interface
A_t	effective area of a surfactant tail group within a curved microemulsion interface
AOT	di-ethylhexyl sodium sulphosuccinate
BSA	bovine serum albumin
C	concentration of aggregated surfactant in g/cm^3
cmc	critical micelle concentration
cμc	critical microemulsion concentration
C_nE_m	nonionic surfactant of the polyoxyethylene alkyl ether type
C.P.	cloud point
α-CT	α-chymotrypsin
D	apparent diffusion coefficient
D_o	diffusion coefficient at infinite particle dilution
G	Gibbs free energy
$G(\tau)$	intensity autocorrelation function
HLB	hydrophile-lipophile balance
i	general index for component i

I_0	fluorescence intensity at time t = zero
I_t	fluorescence intensity at time t
j	auxiliary index for all components other than the i^{th}
K	monolayer bending rigidity constant
$\bar{K}$	Gaussian curvature elastic modulus
k_B	Boltzmann's constant
k_c	second order rate constant for the exchange of probe molecules between microemulsion droplets
k_{dc}	second order diffusion controlled rate constant
k_0	first order fluorescence intensity decay rate constant
k_q	first order fluorescence intensity decay rate constant for a microemulsion droplet containing a single quencher molecule
k_t	first order rate constant for microemulsion droplet exchange
LCT	long chain length triglyceride
M	molecular weight
MCT	medium chain length triglyceride
m_s	surfactant concentration
MV	methyl viologen
N	average number of protein molecules per microemulsion droplet
N_A	Avogadro's constant
N_{agg}	number of surfactant molecules constituting one micelle/microemulsion
n	refractive index
n_i	number of moles of species i
O/W	oil-in-water (microemulsion/macroemulsion)
P	geometrical packing factor
p	as a subscript denotes pressure
P_{osm}	osmotic pressure

Q	magnitude of the scattering vector
r	general abbreviation for a microemulsion droplet radius
RB	ruthenium tris-bipyridyl
r_c	microemulsion core radius
r_o	spontaneous radius of curvature
r_1	principal radius of curvature
r_H	microemulsion hydrodynamic radius
R	molar gas constant
R_{oil}	mole ratio of dispersed oil to *total* surfactant
R_{water}	mole ratio of dispersed water to *total* surfactant
R'	mole ratio of dispersed component to surfactant within an aggregate
R'_{oil}	mole ratio of dispersed oil to surfactant within a microemulsion droplet
R'_{water}	mole ratio of dispersed water to surfactant within a microemulsion droplet
t	an arbitrary time
T*	temperature at which the oil-water interfacial tension is a minimum
$t_{x\%}$	time for x% resolution of oil or water
SDS	sodium dodecyl sulphate
T	temperature (absolute or Celsius specified in text)
V	a general volume specified in the text
V_d	depletion flocculation interaction energy
v_i	molecular volume of species i
W/O	water-in-oil (microemulsion/macroemulsion)
$[x]_s$	average number of quenchers in aggregates containing excited fluorescent probes in the steady-state phase of the fluorescence decay
[A]	concentration of species A

α	first virial coefficient of the apparent diffusion coefficient
γ	general symbol for the tension at an oil (or air) - water interface
γ_c	interfacial tension at a surfactant concentration in excess of the cmc or cμc
δ	effective surfactant interfacial film thickness
ϕ	volume fraction of droplets
Γ_s	interfacial surface excess concentration of surfactant
η	viscosity
ρ	density
λ	wavelength of light
ω	angular velocity

CONTENTS

1. INTRODUCTION.

THE BEHAVIOUR OF SURFACTANTS IN OIL - WATER MIXTURES.

CHAPTER 1

1.1 Surfactants in Solution.

1.1.1 What are surfactants ?

A surfactant (a contraction of the term surface-active agent) is an amphiphilic molecule consisting of a nonpolar hydrophobic part, usually a hydrocarbon chain, attached to a hydrophilic portion. A schematic representation of a surfactant is given below in Figure 1.1.

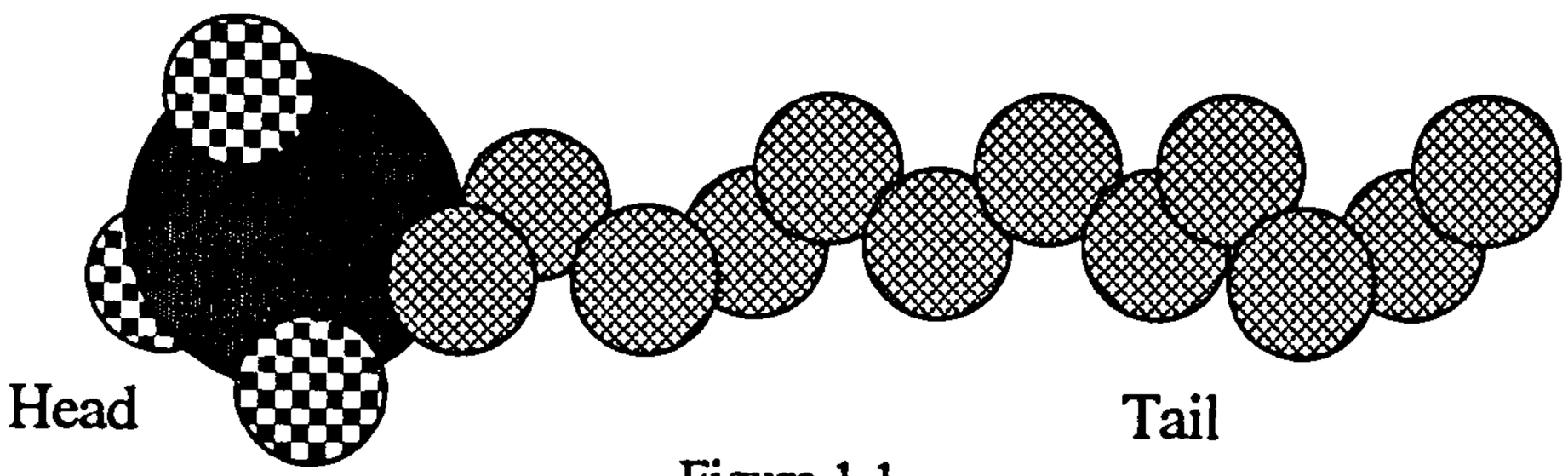

Figure 1.1

The hydrophilic and hydrophobic portions within the molecule are commonly referred to as the head and tail groups respectively. The hydrocarbon tail group may be linear or branched and may consist of more than one chain and may contain an aromatic group. Surfactants are classified according to the nature of their head group. Anionic surfactant head groups include sulphonate, sulphate, carboxylate, etc. Cationic surfactants, in which the head groups are positively charged, are generally molecules derived from substituted ammonium compounds e.g. dodecyl trimethyl-ammonium bromide (D.T.A.B.). An important class of nonionic surfactants is based on polyoxyethylene and has the general formula $C_nH_{2n+1}(OCH_2CH_2)_mOH$ (usually abbreviated to C_nE_m), e.g. tetra-oxyethylene mono-n-dodecyl ether, $C_{12}H_{25}(OCH_2CH_2)_4OH$. Finally, surfactants in which the head group comprises of both anionic and cationic groups are termed zwitterionic surfactants. Many important examples of zwitterionic surfactants are commonly found in the biological membranes of many animal cells (1), e.g. lecithin.

The special properties of surfactant molecules in solution have made them of major industrial importance and they are now used extensively throughout many different areas of the chemical industry. For example, surfactants are encountered in many foodstuffs (2) and pharmaceutical preparations (3), in detergents (4) and insecticide/herbicide applications (5) and in a number of processes encountered in the oil industry (6, 7).

Most of the work described in this thesis is concerned with nonionic surfactants of the type C_nE_m. In this chapter the behaviour of surfactants in water, in oil and in oil + water mixtures will be described. As far as possible, the behaviour will be illustrated with examples based on C_nE_m type surfactants.

1.1.2. Surfactants in water.

When a surfactant is added to water at low concentrations, the molecules exist in solution as monomers. Some surfactant also resides at the air-water interface such that the hydrophobic tail groups protrude out of the water surface as illustrated schematically in Figure 1.2a below.

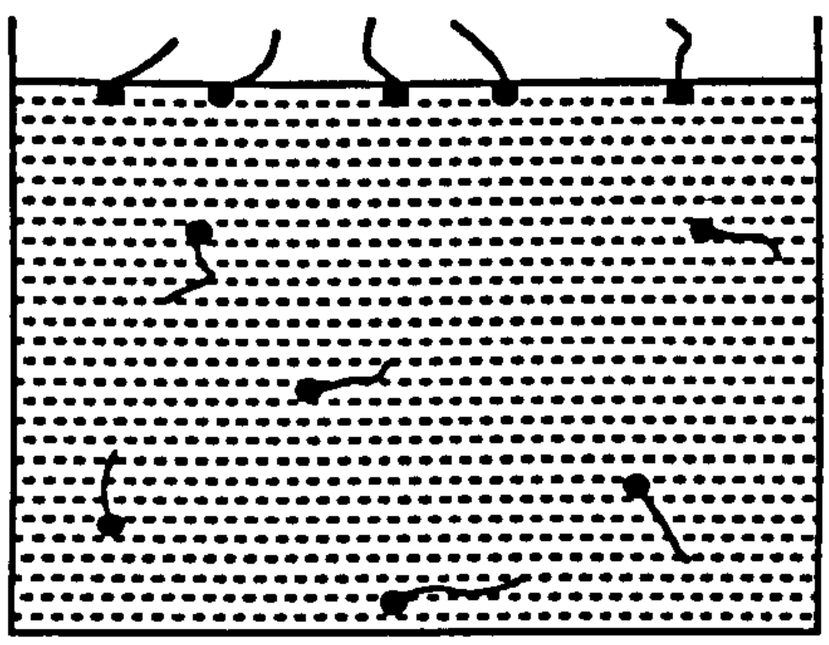

Figure 1.2a

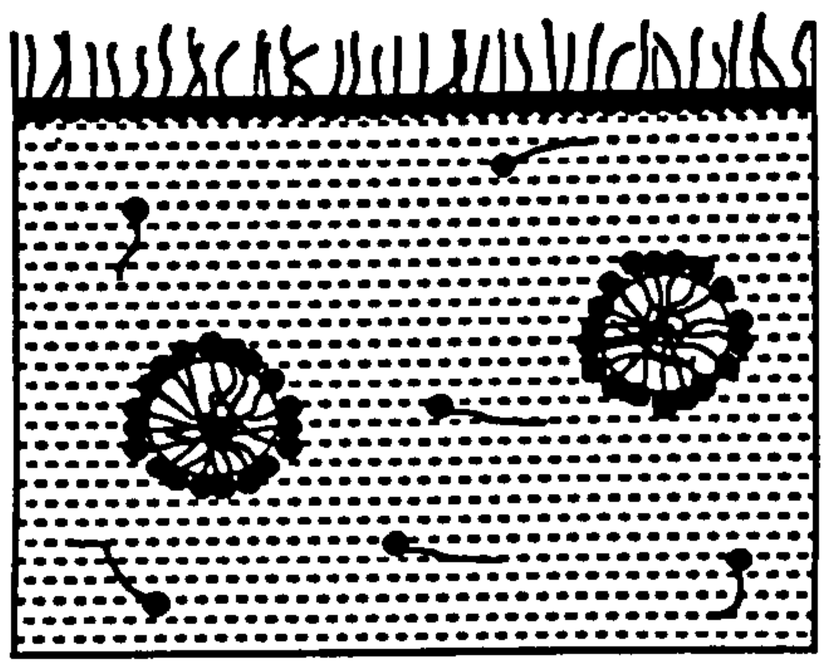

Figure 1.2b

Upon increasing the concentration of surfactant, a concentration can be reached (for a particular surfactant and temperature) at which aggregates are formed as shown in Figure 1.2b. These aggregates are called *normal micelles* (8) and the minimum concentration at which they are formed is called the *critical micelle concentration*

(cmc). The cmc can be determined from abrupt changes in most solution properties which include surface tension, conductivity, dye solubilisation, light scattering, osmotic pressure, etc. A detailed compilation of cmc values can be found in the book by Mukerjee and Mysels (9).

Formation of micelles in solution is a direct consequence of the amphiphilic nature of the molecule. In solution at low concentrations, the hydrophobic tail group of the surfactant interacts with the solvent producing an increased ordering of the water molecules around it. This entropically unfavourable process, known as the *hydrophobic effect* (10), leads to a tendency to minimise the hydrocarbon chain-water contact. One way this may be achieved is through adsorption at the air-water interface with orientation of the hydrophobic groups away from the solvent. Alternatively, the surfactant molecules may aggregate into micelles with their hydrophobic groups directed towards the interior of the structure and the hydrophilic groups forming the exterior surface. In this way, the hydrophobic tails again minimise their contact with water.

As discussed above, the main driving force for aggregation arises from the hydrophobicity of the surfactant tail group. If this was the only force operating then aggregation would proceed all the way to phase separation of the surfactant. Since this does not occur, there must be forces present which serve to limit the aggregation. In the case of ionic surfactants, electrostatic repulsion between adjacent surfactant head groups is mainly responsible for opposing and limiting aggregation. For nonionic surfactants the opposing force is probably a combination of steric and hydration forces. Qualitatively, the formation of micelles can be understood in terms of a balance of opposing forces. Attraction between tails favours aggregation and micellar growth, whereas repulsion between headgroups opposes aggregation and limits micellar growth. The balance is known as the *principle of opposing forces* (10).

The head and tail group contributions to the free energy changes involved in micelle formation can be quantified to some extent as follows. For a nonionic surfactant, the standard free energy required to micellise one mole of surfactant (ΔG°) is simply related to the cmc as follows.

$$\Delta G^\circ = RT \ln(cmc) \qquad (1.1)$$

For a homologous series of surfactants of varying hydrophobic tail length, it is generally found that ΔG° decreases linearly with increasing number of methylene groups in the tail. For many different series of surfactants it is found that each methylene group of the tail contributes approximately -3 kJ mol^{-1} to the free energy of micellisation (11, 12). This general observation is equivalent to the general rule that an increase in surfactant chain length by two methylene groups decreases the cmc by approximately ten fold.

Comparison of cmc values for surfactants containing the same tail group but different head groups allows some generalisations to be made. Surfactants with ionic head groups generally have cmc values which are typically 100 times larger than corresponding nonionics. The addition of electrolyte to ionic surfactant solutions reduces the cmc as it screens the headgroup charge and thus reduces the unfavourable electrostatic repulsion between adjacent heads. For C_nE_m nonionic surfactants, increasing the value of m generally increases the cmc by approximately 1.1 times per additional ethylene oxide group (13).

The number of surfactant molecules constituting one micelle, the aggregation number, is dependent upon the balance of opposing forces as discussed previously. For many systems the aggregation number is in the range 30 - 200 (14). Micelles with low aggregation numbers are spherical with diameters which are usually somewhat less than twice the length of the fully extended surfactant molecule (i.e. a few nm). Increasing the attractive forces between surfactant molecules (e.g. by increasing the tail length) or

decreasing the repulsive forces (by decreasing the head group size or by increasing the ionic strength for ionic surfactants) leads to an increase in aggregation number of the micelles formed. Since the maximum radius of a spherical micelle cannot exceed the all-trans length of the surfactant molecule, micellar growth beyond a certain aggregation number can only proceed if the micelle adopts a non-spherical shape. Thus, addition of electrolyte or increasing the surfactant concentration generally leads to the formation of either rod or disc-shaped micelles whose aggregation numbers can exceed several thousand.

Such rod or disc micelles are the pre-cursors of lyotropic liquid crystalline phases which are generally formed at high surfactant concentrations (typically greater than 10 wt%). Figure 1.3 shows schematically the progression of organised structures that may form upon increasing the concentration of the surfactant (15, 16). Figure 1.4 below shows an example of a two component phase diagram showing the progression of lyotropic liquid crystalline phases observed with increasing concentration of hexa-oxyethylene-mono n-dodecyl ether ($C_{12}E_6$) in water (17). The annotation refers to the types of structures given in Figure 1.3.

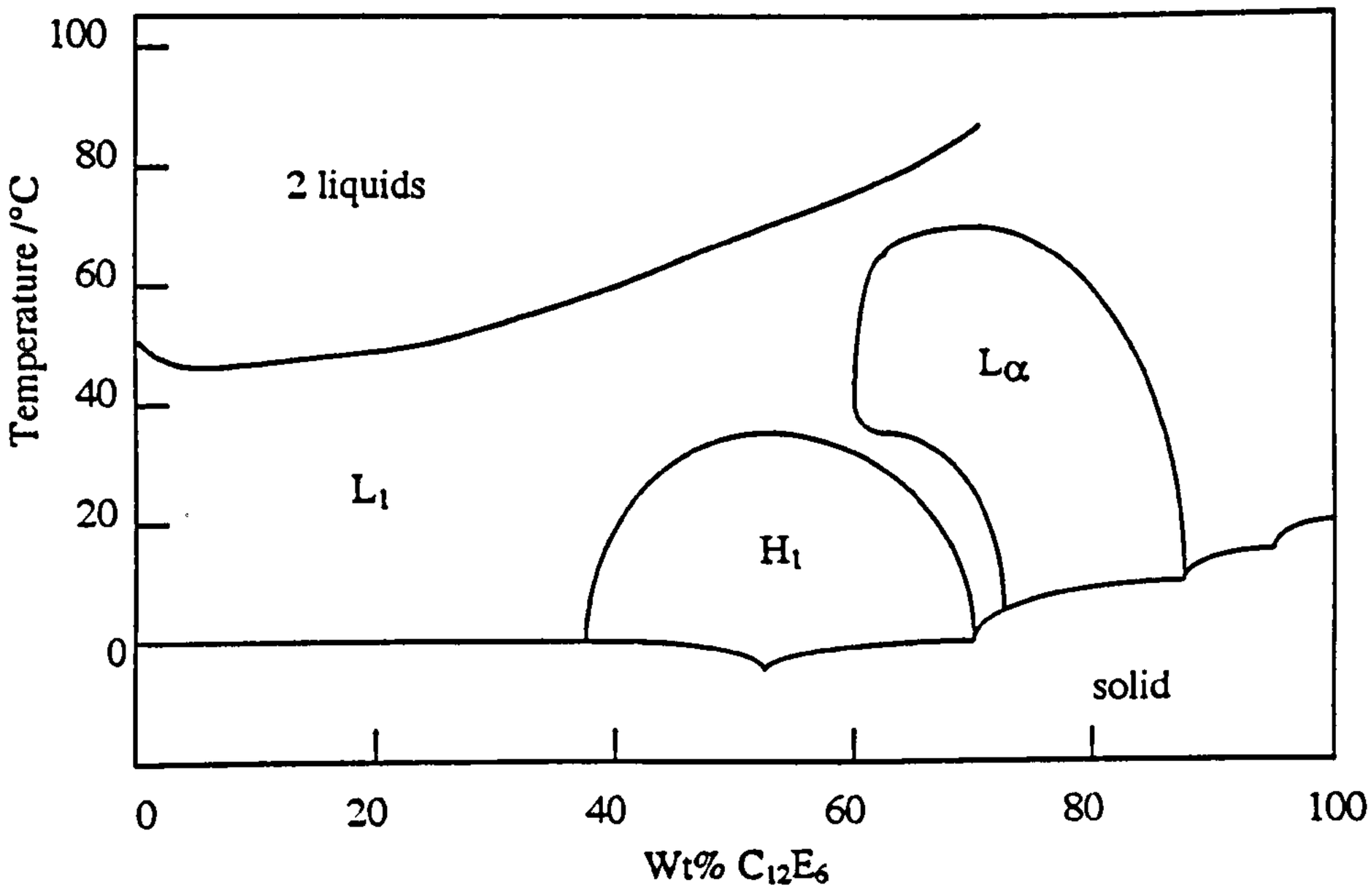

Figure 1.4

Figure 1.3

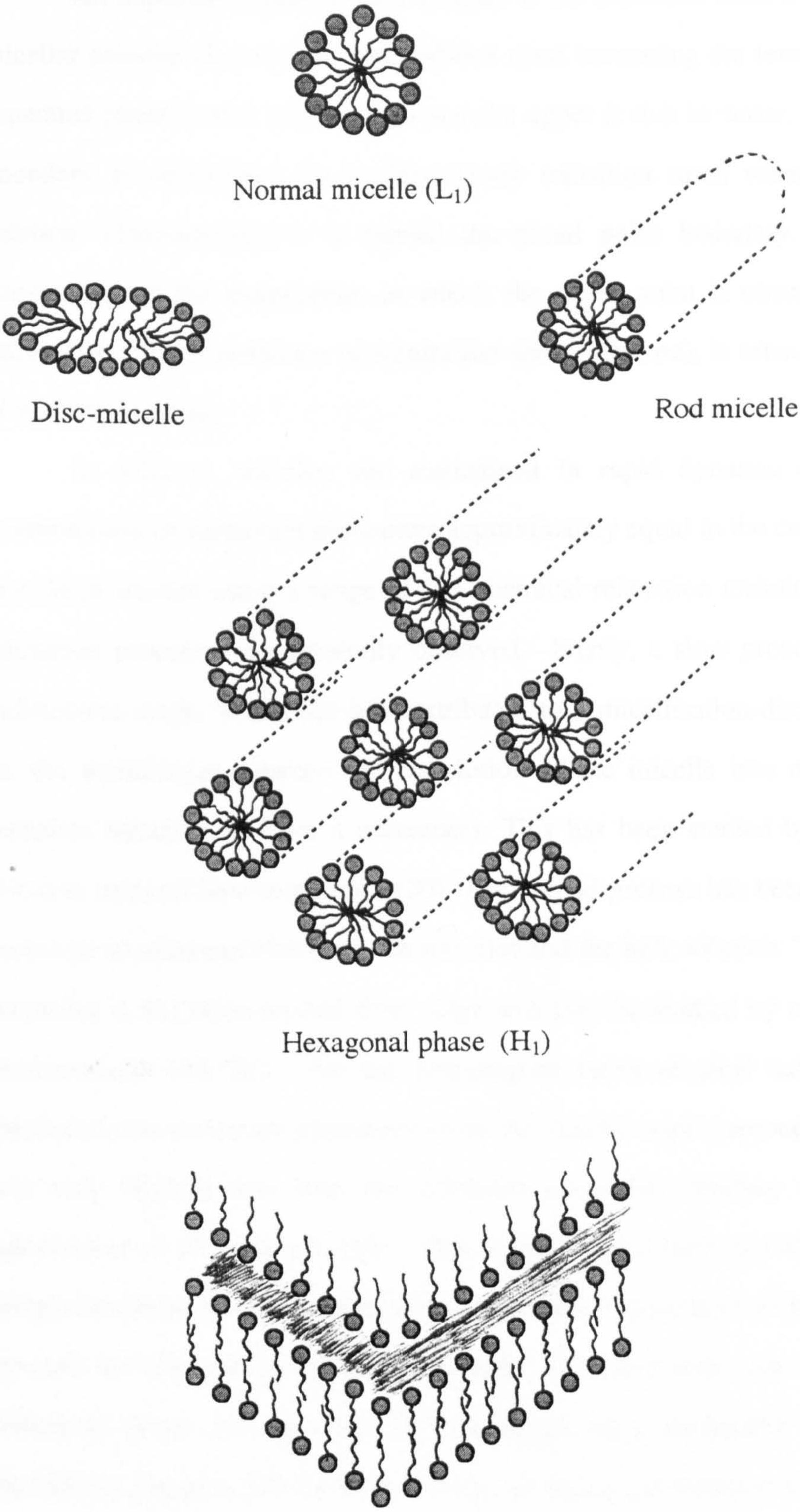
Normal micelle (L_1)
Disc-micelle
Rod micelle
Hexagonal phase (H_1)
Lamella phase (L_α)
INCREASING SURFACTANT CONCENTRATION

An important feature of this diagram is the transition from a one phase isotropic micellar solution (L_1) to two liquid phases upon increasing the temperature. The lower separated phase is rich in surfactant and the upper is rich in water. The position of this boundary is determined by a clear-cloudy transition upon warming the surfactant solution. Consequently, it is termed the cloud point boundary. Experimentally, a comparison of the temperature at which the cloud point is observed with literature values (for a fixed surfactant concentration above the cmc), is often performed as a test of surfactant purity.

In solution, micelles are maintained in rapid dynamic equilibrium with a concentration of surfactant monomers approximately equal to the cmc. Micellar kinetics have been studied using a range of fast chemical relaxation techniques (18, 19). Two relaxation processes are generally observed. Firstly, a slow process occurring in the millisecond range, which has been attributed to a micellisation-dissolution equilibrium i.e. the equilibrium between the dissolution of the micelle into n monomers and its complete reformation from n monomers. This has been studied by temperature jump (19) and stopped flow techniques (20). The second process has been identified with the exchange of monomers between the micelles and the bulk solution. This is a fast process occurring in the microsecond time range and may be studied by ultrasonic absorption measurements (18, 21). For the homologous series of alkyl sulphates, it has been concluded that surfactant monomers enter the micelle with a second order rate constant (k^+) only slightly less than the diffusion controlled limiting value and virtually independent of chain length (18). This indicates that there is only a relatively small energy barrier to monomer entry which is probably associated with electrical repulsion between the charged monomer and micelle. The first order rate constant for exit of monomers from the micelles (k^-) decreases with increasing chain length. The equilibrium constant (K) for the exchange of monomers between micelles and the bulk solution is given by equation 1.2 below.

$$K = k+/k- = 1/cmc \qquad (1.2)$$

Thus, it is the monomer exit rate that primarily determines the chain length dependence of the equilibrium constant for micelle formation (i.e. the cmc).

1.1.3 Surfactants in oils.

Addition of surfactant to apolar solvents produces aggregates in which the polar head groups form the interior and the hydrophobic tails extend outwards into the solvent. This type of structure is known as a reverse micelle. In contrast to surfactant aggregates in water, the main driving force for aggregation in apolar solvents is the energy change due to interactions between the polar head groups of the surfactant molecules. In certain cases, hydrogen bond formation between head groups may also occur. Jones *et al.* have investigated the aggregation behaviour of nonionic surfactants of the type C_nE_m in hydrocarbons (22). They have shown that the degree of surfactant aggregation is low and only very small micelles containing between 5 and 15 monomers are formed. The aggregation number increases as the number of oxyethylene units in the head group increases whereas the length of the alkyl tail has little influence on the aggregation behaviour. Opposing micelle formation is the possible loss of translational, vibrational and rotational freedom of the monomers when incorporated in the micelle.

In contrast to surfactants in water where aggregation occurs over a very narrow range of concentration, aggregation in oils generally occurs over a wide concentration range. This is a consequence of their much lower aggregation numbers. The notion of a cmc in the oil is therefore not strictly applicable. For some systems, aggregation has been presumed to occur through a step-wise association process (23). For oils

containing significant quantities of water, the aggregation numbers are dramatically increased and consequently a cmc can usefully be defined.

As in the case of micelles formed in water, reverse micelles are maintained in rapid dynamic equilibrium with surfactant monomers in the continuous phase. The monomer-micelle equilibrium has been studied by an ultra-sonic absorption technique for a series of polyoxyethylene alkyl ethers in heptane (22). It is observed that the monomer entry rate is close to the diffusion controlled limit and effectively independent of the degree of head group ethoxylation. The first order rate constant for exit of monomers from the micelles is of the order of 10^8 s^{-1} and decreases slightly with an increasing number of ethylene oxide units in the head group.

1.2 Surfactants in Oil - Water Mixtures : Microemulsions.

1.2.1 One phase oil-water mixtures.

It is well known that oil and water do not mix. Upon addition of surfactant however, oil may be taken up into the aqueous phase or water into the apolar phase. This was first described by Hoar and Schulman in 1943 (24). They observed that transparent systems formed *spontaneously* when oil and water were mixed with a sufficient amount of an ionic surfactant in the presence of a medium chain length alcohol. These one phase systems contain the dispersed phase solubilised within the cores of surfactant aggregates formed in the continuous phase and are termed *microemulsions*. Depending upon the type of surfactant employed and the solution conditions (see later) the aggregates formed may consist of dispersed oil in a continuous aqueous medium, termed oil-in-water (O/W) microemulsions, or dispersed water in an

apolar medium, termed water-in-oil (W/O) microemulsions. These are shown schematically in Figure 1.5.

Oil-in-water Water-in-oil

Figure 1.5

If the degree of solubilised material is low i.e. only sufficient to solvate the surfactant head groups (for W/O aggregates) or tail groups (for O/W aggregates), the aggregates are referred to as swollen micelles. The distinction between swollen micelle and microemulsion is not well defined, but generally it is accepted that when "free" dispersed phase (i.e. not involved in solvation of the surfactant) exists in the aggregate it may be classified as a microemulsion.

In recent years microemulsions have attracted a great deal of attention in relation to their possible use in enhanced oil recovery (25). Additionally, investigations have also been performed into the micro-synthesis of colloidal catalysts (26) and into the possible selective extraction and purification of biopolymers using W/O microemulsion systems (27).

Typically, microemulsion droplet sizes range between 5 - 100 nm and consequently they appear transparent or slightly bluish. This is in contrast to macroemulsions where the larger droplet sizes (typically μm) result in a milky/white appearance. The most important distinction between microemulsions and macroemulsions is that microemulsions are *thermodynamically stable.*

Since the formation of microemulsion aggregates involves the production of very large areas of oil-water interface, the free energy associated with the interface is of

considerable importance in determining the stability of the aggregates. The energy required to form a unit area of interface is the interfacial tension, γ. This is defined as

$$\gamma = (\delta G/\delta A)_{T,p,ni} \qquad (1.3)$$

where G is the Gibbs energy of the system, A is the interfacial area and T, p and n_i are the absolute temperature, pressure and the number of moles of species i respectively. It has been shown by Ruckenstein and Chi, that for microemulsions to form spontaneously, the oil-water interfacial tension must be of the order of 10^{-2} mN m^{-1} (28). If this is not the case then mechanical work is required to mix the two phases and a thermodynamically unstable macroemulsion will result.

The solubilisation capacity of a microemulsion can be expressed as the mole ratio of dispersed phase to surfactant within the aggregate. This is denoted by R'. For water-in-oil microemulsions this is given by

$$R'_{water} = [water]/([surfactant] - c\mu c) \qquad (1.4)$$

where the cμc represents the *critical microemulsion concentration* which is the minimum concentration of surfactant required for the formation of microemulsion aggregates (29). This is analogous to the cmc in a surfactant-solvent system. However, since the aggregates formed here are microemulsions not micelles, the distinction is required. This concentration of surfactant remains in solution as monomers in equilibrium with the microemulsion aggregates. For oil-in-water microemulsions

$$R'_{oil} = [oil]/([surfactant] - c\mu c). \qquad (1.5)$$

If the microemulsion droplets are assumed to be spherical and monodisperse, simple geometry gives the dependence of the hydrodynamic radius (r_H) on the droplet composition R' to be

$$r_H = \frac{3\,R'\,v_{molec}}{A_s} + \delta \qquad (1.6)$$

where v_{molec} is the molecular volume of the dispersed phase and A_s is the area occupied by a single surfactant molecule at the interface between the droplet core and the surfactant monolayer. The length δ is the thickness of the surfactant monolayer and contains a contribution from any entrapped solvent.

For a particular microemulsion composition (i.e. R') there exists a well defined temperature range over which one phase stability is preserved. This is shown schematically below in Figure 1.6 for oil-in-water and water-in-oil microemulsions stabilised by a nonionic surfactant.

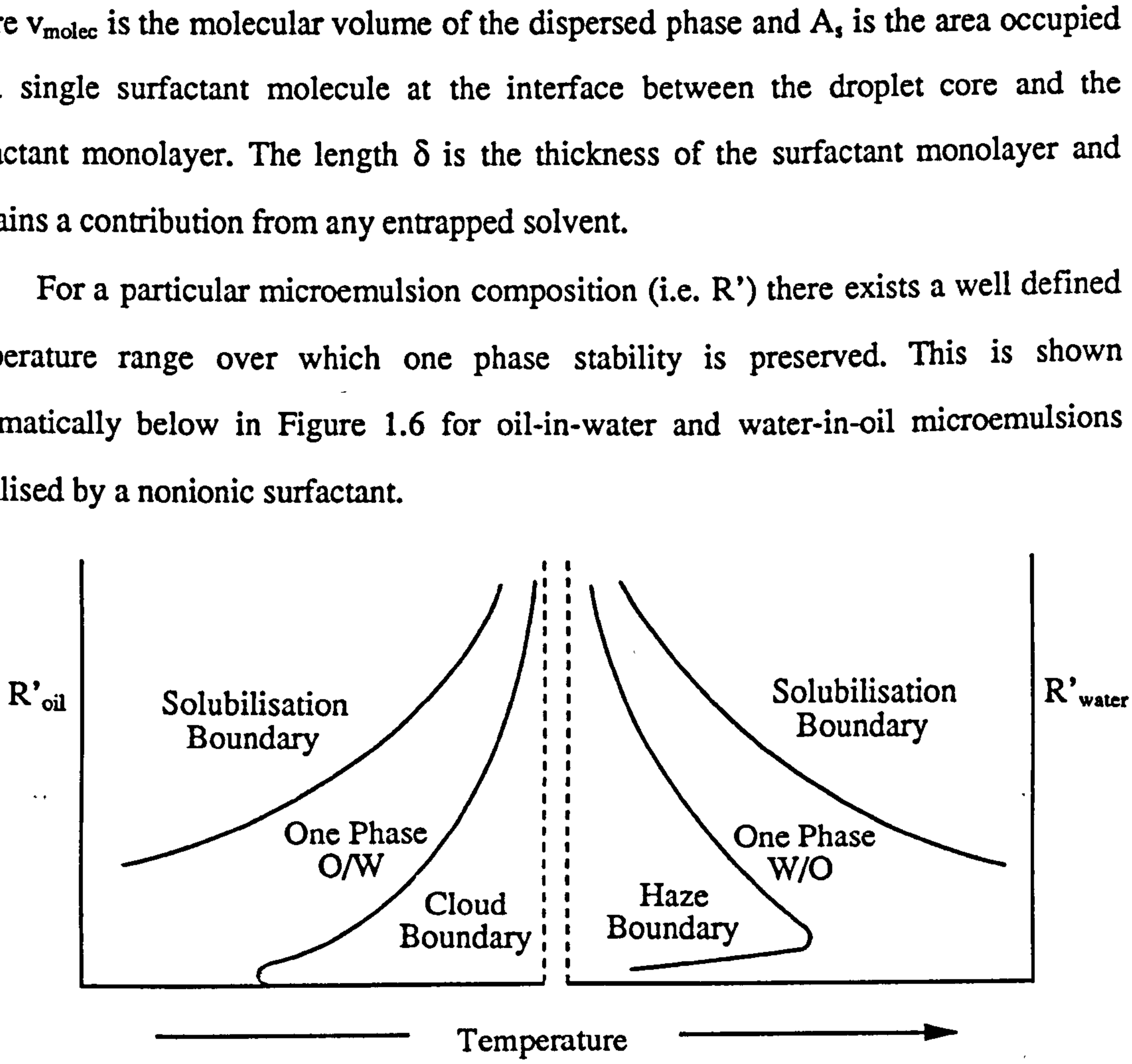

Figure 1.6

The one phase microemulsion regions are bounded by the cloud or haze boundaries which correspond to the separation of surfactant-rich and surfactant-lean phases, and the solubilisation boundaries which correspond to the separation of either excess oil (for O/W microemulsions) or excess water (for W/O microemulsions). The

order of the two boundaries is reversed with respect to temperature for O/W and W/O aggregates. The solubilisation boundary corresponds to the point at which attractive interactions between microemulsion droplets are a minimum for these nonionic systems (30).

1.2.2. Multi-phase oil-water mixtures.

In a two phase oil-water system containing surfactant, the type of microemulsion aggregate produced at equilibrium is dependent upon the nature of the surfactant and the solution conditions. For nonionic surfactant systems this type of phase behaviour has been investigated extensively by Shinoda *et al.* (31, 32) and Kahlweit *et al.* (33, 34). For a fixed concentration of nonionic surfactant, the effect of temperature on the phase behaviour of a ternary water + oil + surfactant system can be represented as shown in Figure 1.7a. Between the two one phase O/W and W/O microemulsion regions (which are equivalent to those shown in Figure 1.6), there exists a central region where three phases coexist in equilibrium. The progression of phases observed within an oil + water + surfactant mixture upon changing, for example, the temperature, was first described by Winsor (35). Consider for example, an oil/water mixture containing nonionic surfactant at a composition given by the dashed line in Figure 1.7a (i.e. equal weight fraction of oil and water). At low temperatures, oil-in-water aggregates form in the aqueous phase in equilibrium with an excess oil phase. This type of two-phase system is termed a Winsor I microemulsion system. Upon increasing the temperature aggregates may form in a third surfactant-rich phase in equilibrium with oil and water phases. This type of three-phase system is called a Winsor III system. A further increase in temperature results in the formation of a water-in-oil microemulsion phase in equilibrium with excess water. This is termed a Winsor II microemulsion system.

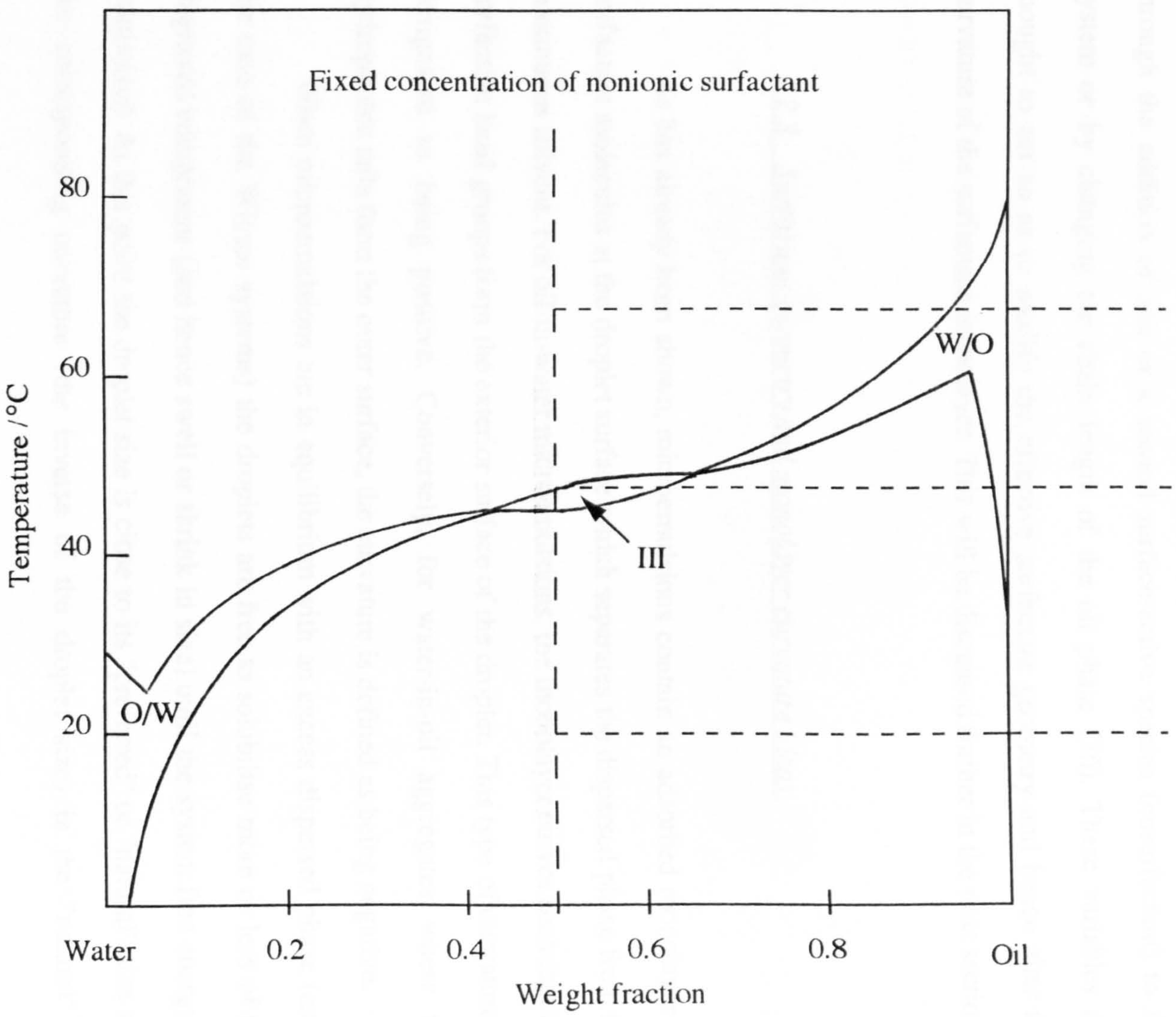

Figure 1.7a

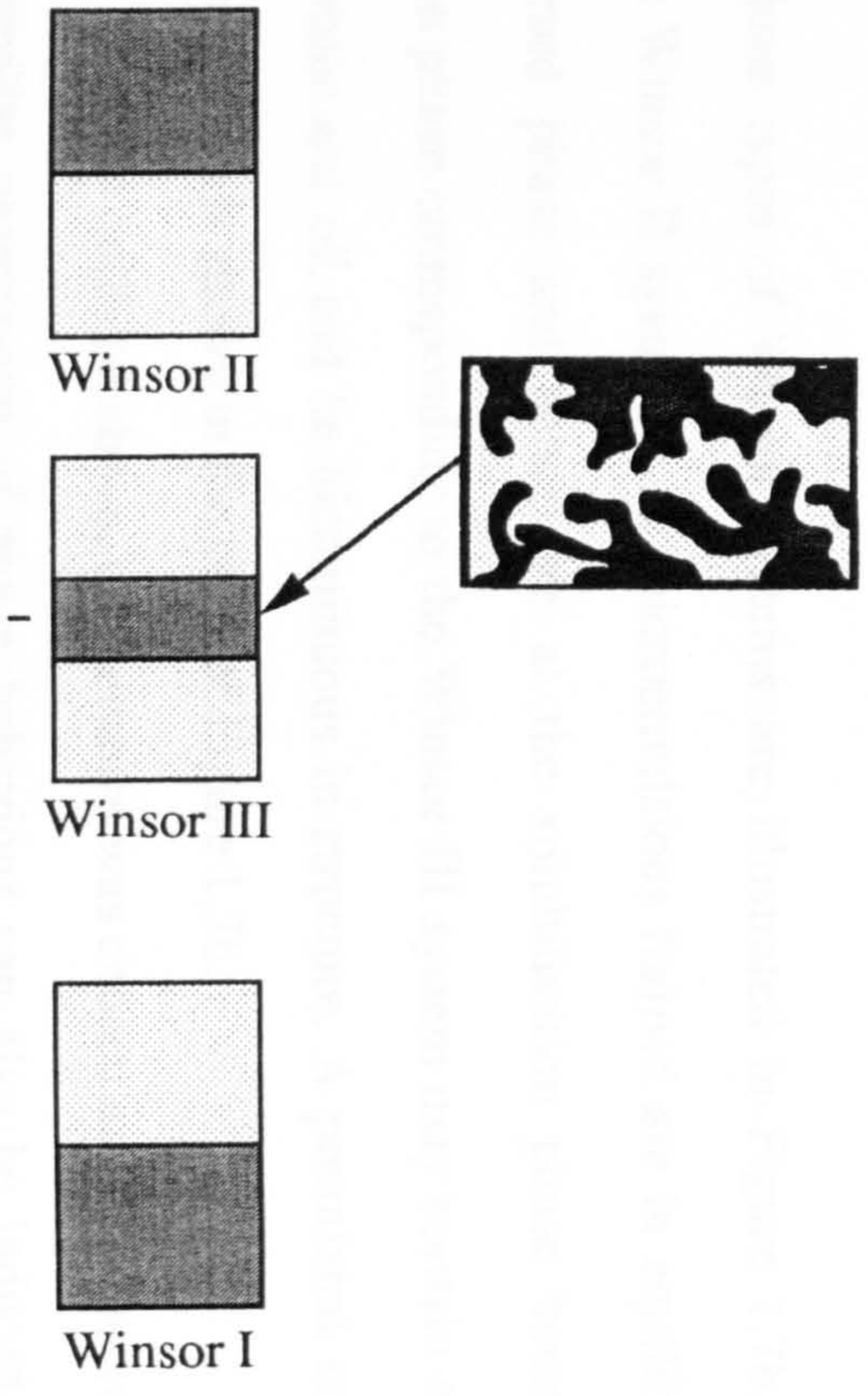

Figure 1.7b

The three types of Winsor systems are illustrated in Figure 1.7b. For both Winsor I and Winsor II systems, the microemulsions formed are in equilibrium with excess dispersed phase and hence are at the solubilisation phase boundary. The microemulsion phase corresponding to the Winsor III system may contain comparable amounts of water and oil and be bicontinuous in structure. A postulated structure for such a microemulsion is shown in the inset of Figure 1.7b.

In the example outlined above, temperature was chosen as the structure inducing variable. A similar progression of phase behaviour can also be induced, however, through the addition of salt or a second surface-active species (cosurfactant) to the system or by changing the chain length of the oil phase (36). These variables are thought to act so as to modify the effective surfactant geometry and hence alter the curvature of the surfactant monolayer. This will be discussed further in the next section.

1.2.3 Surfactant geometry and monolayer curvature ideas.

As has already been shown, microemulsions contain an adsorbed monolayer of surfactant molecules at the droplet surface which separates the dispersed phase from the continuous solvent. For oil-in-water microemulsions, the monolayer curves such that the surfactant head groups form the exterior surface of the droplet. This type of curvature is designated as being positive. Conversely, for water-in-oil aggregates where the hydrophobic tails form the outer surface, the curvature is defined as being negative.

When microemulsions are in equilibrium with an excess dispersed phase (as in the case of the Winsor systems) the droplets are free to solubilise more or less of the dispersed component (and hence swell or shrink in size) until the system free energy is minimised. At this point the droplet size is close to its "preferred" or "natural" size and the corresponding curvature (the inverse of the droplet size) is the "natural" or

"spontaneous" curvature of the surfactant monolayer. It has been shown previously that the degree of solubilisation (R') is proportional to the droplet size and may be dramatically altered by changing the solution conditions. Since the *type* of aggregate produced is dependent on the solution conditions the microemulsion size can pass through a maximum as shown in Figure 1.8a. This corresponds to a situation in which the monolayer curvature changes progressively from positive in the Winsor I system, through zero in the Winsor III case, to negative in the Winsor II system. This is shown in Figure 1.8b. The formation of microemulsion phases is clearly strongly associated with the tendency of the monolayer to curve, which in turn, may be determined by the molecular geometry of the surfactant.

A simple schematic representation of the molecular structure of a surfactant is shown below in Figure 1.9. The relative sizes of the head and tail groups are characterised by the cross-sectional areas A_h and A_t.

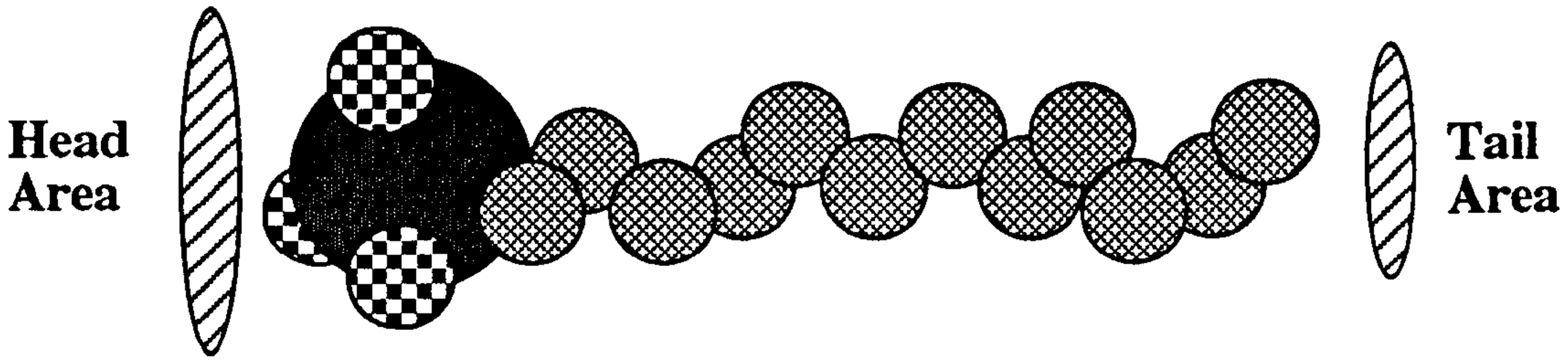

Figure 1.9

Mitchell and Ninham introduced a packing factor P to predict the type of microemulsion that would form (37).

$$P = A_t/A_h \qquad (1.7)$$

However, if the surfactant geometry was determined solely by the surfactant molecular structure, then a particular surfactant would always yield a single preferred monolayer curvature (and hence droplet size) in a two phase oil-water system, i.e. independent of the solution conditions such as temperature, salt concentration, nature of the oil phase,

Figure 1.8a

Effect of Solution Variables on Microemulsion Droplet size

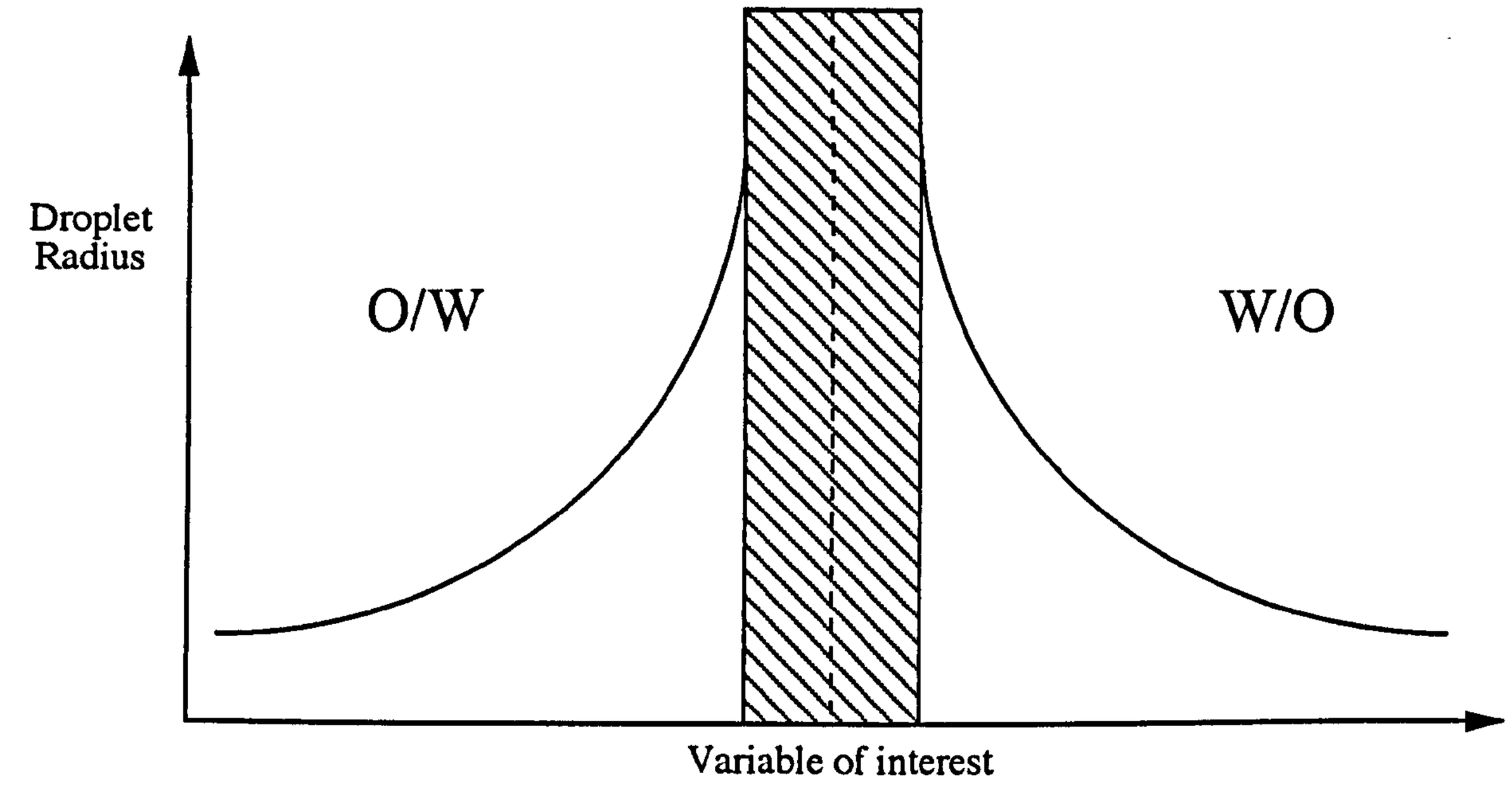

Figure 1.8b

Effect of Solution Variables on Monolayer Curvature

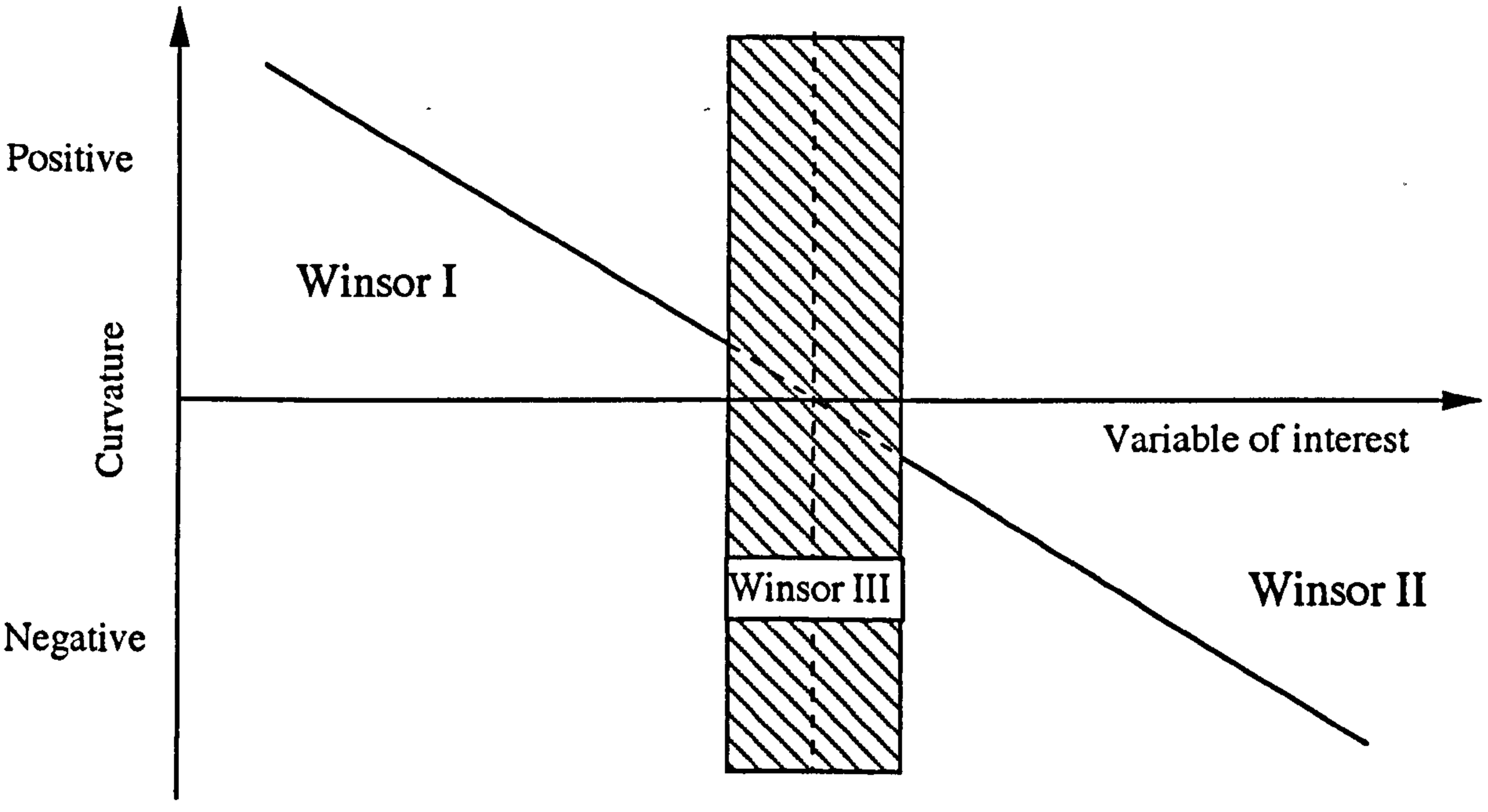

etc. It has already been shown (for nonionic surfactants) that the microemulsion type changes from O/W to W/O upon increasing the temperature with a corresponding change in the monolayer curvature from positive to negative. Hence it is the *effective* molecular geometry *in situ* in the monolayer that is changing and it is this which must be considered.

If the effective geometry of a surfactant in a monolayer is such that $A_h > A_t$ (i.e. $P < 1$) then in a two phase system, aggregates will be produced in which the bulky head groups form the exterior surface, and an O/W microemulsion will result. Similarly, if $A_h < A_t$ (i.e. $P > 1$) then a water-in-oil microemulsion will be formed. An alternative possibility may arise if $A_h = A_t$ ($P = 1$). In this case the net monolayer curvature will be zero and either a random bicontinuous phase will result or an ordered lamellar liquid crystalline phase will be formed.

It is clear from the above discussion that the effective surfactant geometry within the monolayer is determined by a combination of the surfactant molecular structure *and* the solution conditions e.g. temperature, salt concentration, addition of cosurfactant and the nature of the oil phase. The effect of each of these parameters on the monolayer curvature will be considered in turn.

(1) Surfactant molecular geometry.

The molecular structure of a surfactant is one of the prime considerations when selecting a surfactant for a particular application. For many surfactants, the head group area of a molecule is greater than that of the tail group and, if the effective geometry resulting from the influence of the solution conditions is neglected, oil-in-water aggregate formation is promoted. Surfactants exhibiting branched alkyl tail groups or more than one tail may however, favour negative curvature and produce aggregates in the oil phase.

(2) Temperature.

For nonionic surfactants, an increase in temperature promotes an increase in negative curvature of the surfactant film (i.e. a change from O/W to W/O aggregates as shown previously in Figure 1.7a). This may be a consequence of dehydration of the surfactant head group reducing its effective area (31). Additionally, an increase in temperature appears to produce an increase in the effective area per surfactant tail group (38). This may arise due to an increased penetration of alkane into the tail region or from changes in the conformation of the surfactant molecule at the droplet surface.

For ionic surfactants, increasing the temperature increases the positive curvature of the surfactant film (i.e. transition from W/O to O/W aggregates) (39). This may be due to an increased dissociation of the surfactants head groups which results in a larger repulsive electrostatic interaction between heads. The effective head group size is therefore increased, favouring positive curvature.

(3) Salt concentration.

Increasing the salt concentration in a two phase system produces a shift towards more negative curvature for both nonionic and ionic surfactant systems. For ionics, this is due to a screening of the electrostatic repulsive interactions between the head groups reducing their effective size (14). For nonionics, larger salt concentrations are required to produce a significant change in the monolayer curvature. The salt is thought to reduce the effective area per surfactant head group by a "salting-out" process. This may occur through the formation of a salt-free layer at the interface which leads to an increased free energy cost of forming interfacial area (40). Alternative "salting-out" mechanisms have also been postulated. One of these interprets the effect of the salt as disrupting the hydrogen bonding network between the water molecules and the hydrophilic head groups (41).

(4) *Addition of a cosurfactant or second surfactant.*

Cosurfactants are surface-active molecules which adsorb together with the surfactant at the oil-water interface forming a mixed film. They are generally alcohols. Depending upon their structure, they may occupy different locations within the surfactant monolayer. For medium chain length alcohols, the "head" group is small in comparison with the alkyl tail and consequently increased negative curvature is imparted to the monolayer. However, in the case of the addition of a second surfactant for which A_h is greater than A_t, e.g. Tween 20 (a polyethoxylated sorbitan ester), a shift towards more positive curvature may be achieved.

(5) *Nature of the oil phase.*

The effective area per surfactant tail group is strongly dependent upon the degree of solvation by the apolar phase. In general, it is observed that short chain alkanes favour a shift towards more negative curvature and are therefore assumed to penetrate the tail region to a greater extent than long chain alkanes (40). Substitution of alkane by an aromatic hydrocarbon is observed to generally favour an increased negative curvature.

The effects of each variable outlined above are summarised below in Table 1.1.

Table 1.1

Increase in Parameter	Nature of Surfactant	Effect on Curvature
Temperature	ionic	more positive
"	nonionic	more negative
[Salt]	ionic or nonionic	more negative
[Cosurfactant]*	ionic or nonionic	more negative
Alkane chain length	ionic or nonionic	more positive

* e.g. octanol.

1.2.4 Oil-water interfacial tension.

As surfactant is added to an oil-water system, the monomers present partition between the two bulk phases. Nonionic surfactants typically partition extensively in favour of the oil phase (42). The oil-water interfacial tension (γ) decreases as the surfactant adsorbs at the interface. This is shown schematically in Figure 1.10 below.

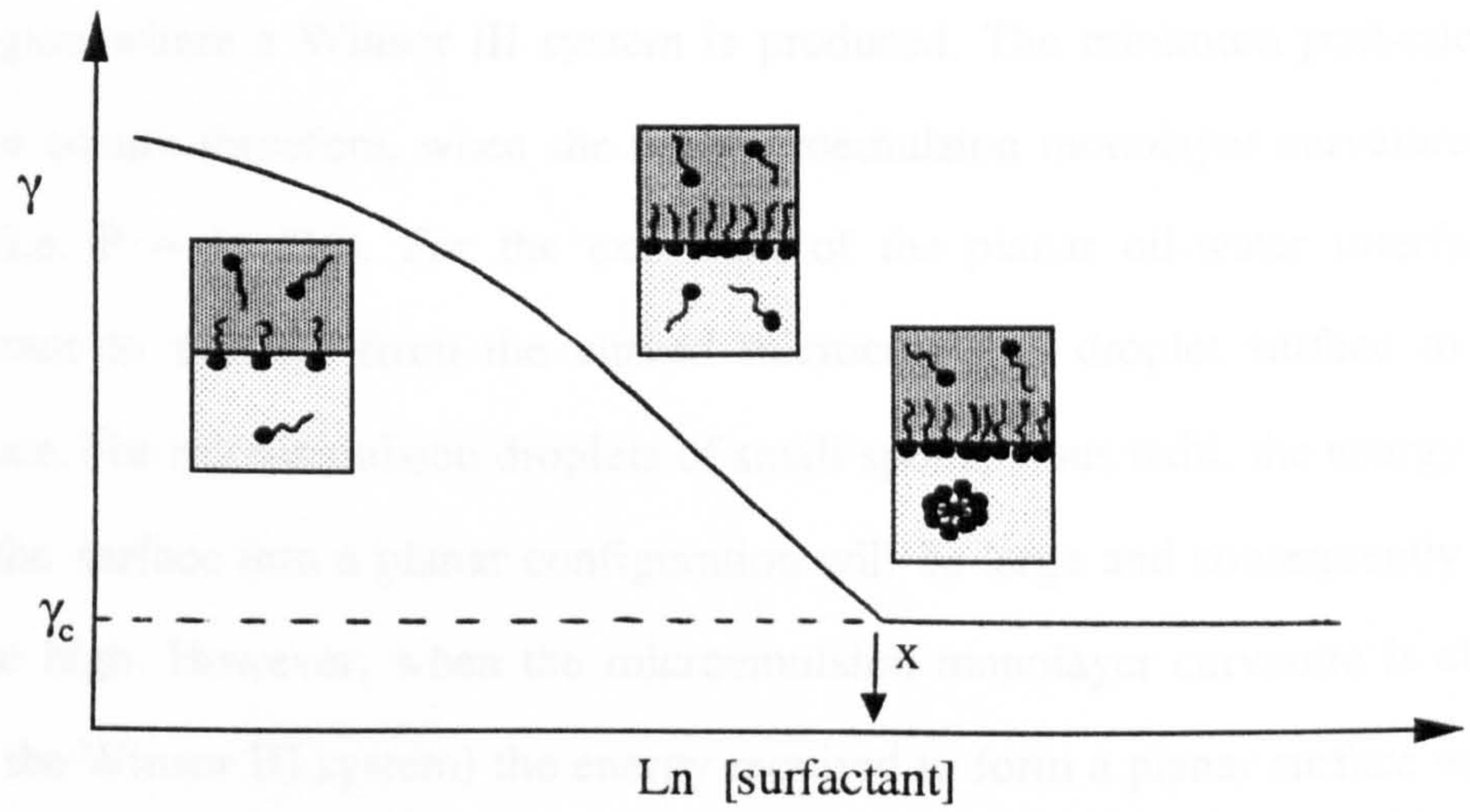

Figure 1.10

In the region where the interfacial tension is falling, the interfacial surface excess concentration of surfactant Γ_s is given, for a nonionic surfactant, by

$$-d\gamma = \Gamma_s \, RT \, d\ln m_s \qquad (1.8)$$

where m_s is the surfactant concentration. It is assumed that the activity coefficient of the surfactant in solution is unity. When ($d\gamma/d\ln m_s$) is constant, Γ_s is effectively constant and the adsorbed monolayer is saturated. The tension then drops linearly with ln [surfactant] until point x is reached. At this point the critical microemulsion concentrations in both the water and oil phases are reached. Further addition of surfactant produces aggregates in either the water, oil or a third phase depending on the

solution conditions. The aggregates are not themselves surface active and so the tension is not lowered further and remains at a virtually constant value, γ_c.

Variation of this post-cμc interfacial tension γ_c as a function of the various curvature determining variables, e.g. temperature, salt concentration etc., is shown schematically in Figure 1.11 for a nonionic surfactant system. It can be seen that the interfacial tension passes through a minimum value (which may be $< 10^{-3}$ mN m^{-1}) in the region where a Winsor III system is produced. The minimum post-cμc interfacial tension occurs therefore, when the net microemulsion monolayer curvature is close to zero (i.e. P ≈ 1) (36). For the extension of the planar oil-water interface requires surfactant to transfer from the curved microemulsion droplet surface to the planar interface. For microemulsion droplets of small spontaneous radii, the energy required to bend the surface into a planar configuration will be large and consequently the tension will be high. However, when the microemulsion monolayer curvature is close to zero (as in the Winsor III system) the energy required to form a planar surface will be much reduced and hence the interfacial tension will be a minimum. It is evident therefore, that an inverse relationship exists between the planar oil-water interfacial tension and the microemulsion droplet size.

1.2.5 The relationship between interfacial tension and droplet size.

The interfacial tension is related to the free energy difference between the interfacial film at the planar interface separating the bulk phases and the curved monolayer surrounding the droplets. This contains contributions from the energies required to bend the monolayer and also energies associated with dispersing the droplets within the medium and inter-droplet interactions (43). Generally it is observed that the interfacial tension is independent of surfactant concentration (above the cμc) over a

Figure 1.11

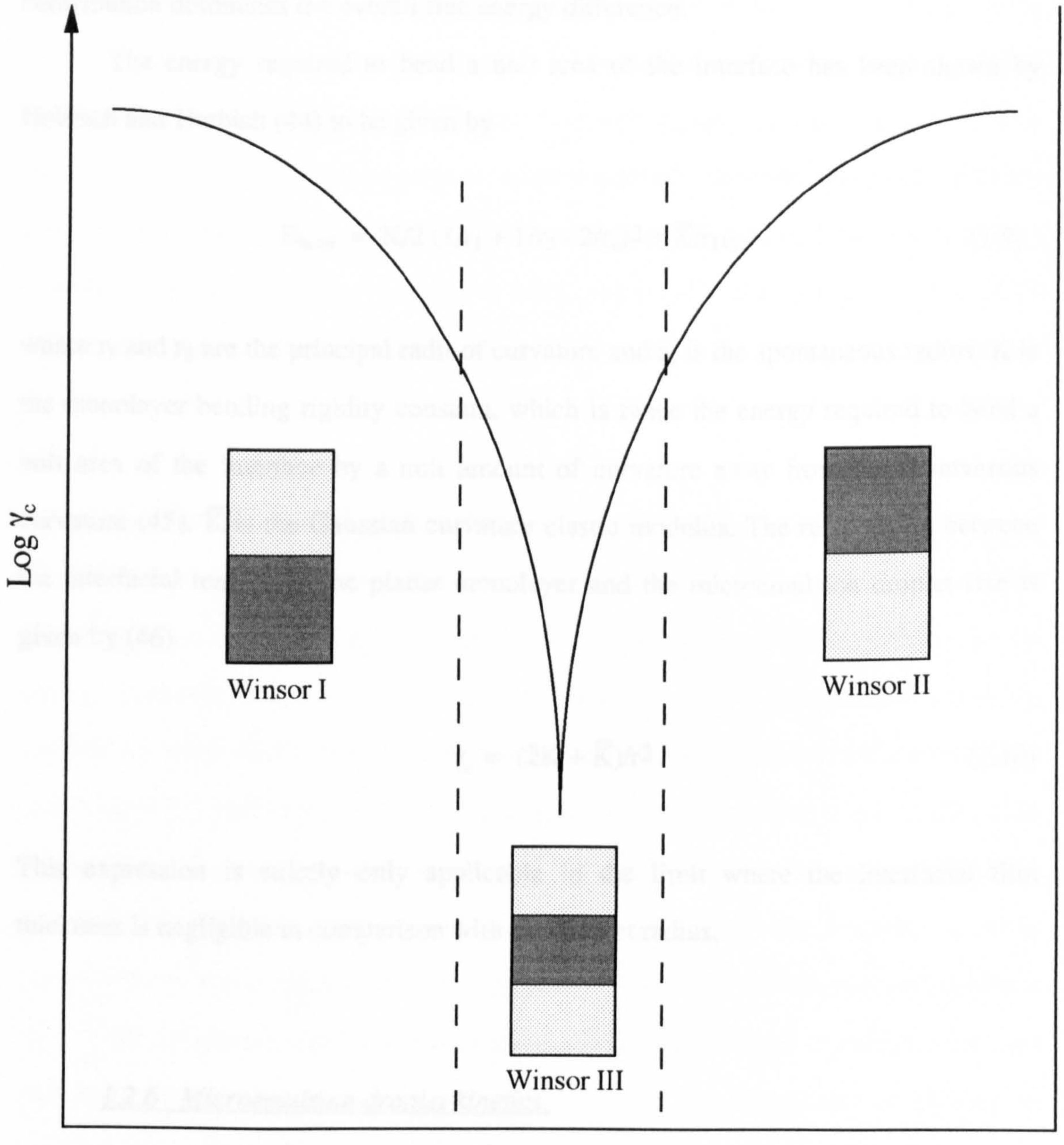
Log γ_c
Winsor I
Winsor II
Winsor III
Temperature
Salt concentration
Alkane chain length

wide range of droplet concentration (as shown in Figure 1.10). Since the free energies associated with dispersing the droplets and interactions between the droplets should be dependent upon the droplet concentration, this implies that the bending energy contribution dominates the overall free energy difference.

The energy required to bend a unit area of the interface has been shown by Helfrich and Harbich (44) to be given by

$$E_{bend} = K/2\,(1/r_1 + 1/r_2 - 2/r_o)^2 + \bar{K}/r_1 r_2 \qquad (1.9)$$

where r_1 and r_2 are the principal radii of curvature and r_0 is the spontaneous radius. K is the monolayer bending rigidity constant, which is twice the energy required to bend a unit area of the interface by a unit amount of curvature away from the spontaneous curvature (45). $\bar{K}$ is the Gaussian curvature elastic modulus. The relationship between the interfacial tension of the planar monolayer and the microemulsion droplet size is given by (46)

$$\gamma_c = (2K + \bar{K})/r^2 \qquad (1.10)$$

This expression is strictly only applicable in the limit where the interfacial film thickness is negligible in comparison with the droplet radius.

1.2.6 Microemulsion droplet kinetics.

Like micellar and reversed micellar solutions, microemulsion droplet dispersions are maintained in rapid, *dynamic* equilibrium. One process likely to occur in these systems is the exchange of surfactant monomer between the continuous solvent and the

microemulsion aggregates. At the present time, there have been no experimental investigations of this process for three component microemulsions. However, as has been discussed, the second order rate constant for monomer entry (k^+) for both normal and reversed micelles is close to the diffusion controlled limiting value (approx. 10^{10} M^{-1} s^{-1}) and the rate constant for monomer exit from the aggregates (k^-) can be determined from the relationship given previously in equation 1.2. If it is assumed that microemulsion aggregates behave similarly, then the monomer exchange rate constants can be estimated from a knowledge of the viscosity (which allows an estimation of the diffusion controlled entry rate) (47) and the cμc. For W/O microemulsions stabilised by nonionic surfactants with cμc values of the order of 0.05 M, it is estimated that k^+ is of the order of 10^{10} M^{-1} s^{-1} and k^- is of the order of 10^8 s^{-1}.

Microemulsion droplets differ from micelles in that they contain a liquid droplet of either water or oil. Clearly, the dynamics of these droplets will differ from those of two component surfactant aggregate solutions. The equilibrium microemulsion droplet size is primarily determined by the mole ratio R'. If a low-R' microemulsion (containing small droplets) is mixed with a large-R' microemulsion (containing large droplets), it is found that intermediate size droplets (corresponding to the intermediate R' value) are formed "instantaneously" (i.e. within the experimental mixing time of a minute or so). Clearly, exchange of solubilised material between droplets can occur rapidly. Part of the work described in this thesis is concerned with investigations of this type of droplet dynamic process and in this section some relevant experimental studies and ideas for their interpretation are briefly outlined. The importance of gaining an insight into the dynamics of aggregates arises since many applications of oil + water + surfactant systems are centred around their ability to *kinetically* stabilise structures e.g. in emulsions and foams.

Microemulsion droplet dynamics have been investigated using a range of fast kinetic techniques including time-resolved fluorescence (TRF) (48, 49), stopped flow (50) and temperature jump methods (51). For most of these studies, the rate of exchange of material between microemulsion aggregates has been monitored using probe molecules added to the system (52 - 55). Although there is some ambiguity of interpretation owing to the use of probe molecules, the following picture of microemulsion droplet dynamics seems to be reasonably well established. In solution, the equilibrium distribution of microemulsion droplet sizes is maintained in a rapid dynamic equilibrium via a mechanism of continual droplet coalescence and re-separation (50, 56, 57). The overall process of the coalescence of two droplets to form a short lived, coalesced droplet dimer can be broken down into the steps shown in Figure 1.12.

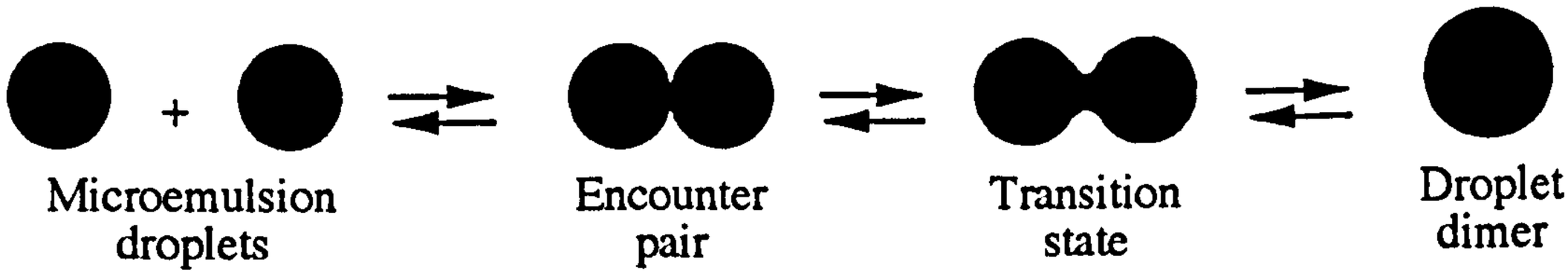

Figure 1.12

The droplets initially diffuse together to form a non-coalesced encounter pair which may proceed to form a transient droplet dimer by coalescence. Reversal of the process may occur at each stage with coalescence followed by re-separation leading to a "scrambling" of the components between the droplets. Based on investigations of a variety of microemulsion systems, the following observations are relevant here.

(i) The second order rate constant for the exchange of probe molecules between microemulsion droplets (k_c) is always slowest at temperatures closest to the *solubilisation* phase boundary (55). As discussed previously, this is where the droplet-droplet interactions are least attractive and where the curvature of the surfactant monolayer is closest to the *spontaneous* (i.e. most stable) curvature.

(ii) The second order rate constant k_c differs by approximately five orders of magnitude for different surfactant systems. The slowest rates to date have been observed for W/O microemulsions stabilised by AOT (50, 58).

The second order rate constant k_c can be expressed as

$$k_c = k_{dc} \exp(-E/RT) \qquad (1.11)$$

where k_{dc} is the rate constant in the absence of a significant energy barrier E to transient droplet dimer formation and is equal to the diffusion controlled limiting value. The energy barrier E is the free energy difference between the two original droplets and the highest free energy state reached in the course of the transient dimer formation (the transition state of the process). The energy E is a measure of the ability of a surfactant film to resist droplet coalescence and, as such, is expected to have some relevance to the stability of emulsions and foams. It is of interest to attempt to establish possible correlations between the magnitude of E and properties of the surfactant monolayer with the ultimate aim of being able to predict droplet dynamic properties for different surfactant structures.

In this section, some possible contributions to the magnitude of E are postulated. In order to do this it is necessary to assume a structure for the transition state. One possibility is that the transition state occurs between the non-coalesced encounter pair and the transient droplet dimer and has the hour-glass shape as shown above in Figure 1.12.

The energy of forming this transition state involves deforming the surfactant film in the region where the two droplets connect. One contributing factor to the magnitude of E might therefore be the energy required to bend the surfactant monolayer. The bending energy per unit area has previously been given by equation 1.9.

For two microemulsion droplets initially at their spontaneous curvature (and consequently at their natural radius r_o), the bending energy associated with the formation of the hour-glass-shaped transition state shown above is given approximately by

$$E_{bend} = 4 \pi r_1 r_2 [K/2 (1/r_1 + 1/r_2 - 2/r_0)^2 + \bar{K}(1/r_1 r_2 - 1/r_o^2)] \qquad (1.12)$$

where r_1 and r_2 are the principal radii of curvature in the "neck" region and are of opposite sign. If the bending energy dominates the free energy for the coalescence process, the exchange rate might be predicted from equation 1.12 to be accelerated as K, the monolayer bending rigidity and $\bar{K}$, the Gaussian curvature elastic modulus decrease and also as the spontaneous curvature tends to zero (i.e. $r_o \rightarrow \infty$).

Upon coalescence, the surface area of the transient droplet dimer produced is less than that of the two constituent droplets. Hence, droplet coalescence is expected to lead to a decrease in the area available to the surfactant monolayer. This area loss may be accommodated by compression of the surfactant monolayer or through "wrinkling" of the dimer surface. Alternatively, the surfactant may desorb from the droplet surface. The free energy cost for desorption (per mole of surfactant desorbed to form monomers in the continuous phase) is given by -RT ln(monomer activity in the continuous solvent). This approximates to -RT ln cμc if the activity coefficient of the surfactant is assumed to be unity. On the basis of this argument, desorption of surfactant, and consequently coalescence, may therefore be expected to be facilitated when the cμc is high.

As mentioned earlier, droplet coalescence rates are not generally determined directly. The techniques frequently used monitor the exchange of solubilised probe molecules between microemulsion aggregates. Fletcher *et al.* have used a stopped flow technique to measure the rate of exchange of probe molecules within water-in-heptane

and water-in-dodecane microemulsions stabilised by AOT (50). They investigated three different pairs of probe molecules and observed that, for each system, the exchange rate was independent of the probes used. The exchange rate of probes has also been determined using a technique of TRF for these two water-in-oil systems. Using this technique the rate constants appear to be approximately 30 and 90 times faster for heptane and dodecane respectively as the oil phase (49, 59). Since using the stopped flow technique the same exchange rate constant was obtained using three different pairs of probe molecules, it appears more likely that exchange in these cases occurs through droplet coalescence. The faster rate in the case of the TRF results may be a consequence of probe molecules exchanging between aggregates without coalescence e.g. through surfactant-probe complexes migrating through the continuous phase.

It is also of interest here to mention results obtained by Fletcher and Holzwarth on the aggregation kinetics of tetradecane-in-water microemulsions stabilised by $C_{12}E_5$ (51). Using a temperature jump technique they have determined rate constants for droplet aggregation i.e. for the formation of non-coalesced encounter pairs. At the solubilisation phase boundary, the rate constants were found to be approximately 100 times slower than the probe molecule exchange rate constants determined by TRF for heptane-in-water microemulsions of comparable size. Despite the change in the nature of the oil phase, it is clear that the results are not consistent with droplet coalescence being the only mechanism of probe exchange for this particular system. (For this to be the case, the overall exchange rate must be equal to or slower than the encounter pair formation rate). There appears therefore to be an appreciable energy barrier associated with the approach of the aggregates which decreases with increasing droplet size. These results suggest that the transition state to the overall microemulsion droplet coalescence process may occur in the step involving the formation of the non-coalesced droplet encounter pair (rather than in the subsequent coalescence step).

The above discussion has attempted to bring together possible factors which may have a bearing on the microemulsion coalescence rate in solution. These may include: (i) the spontaneous curvature of the surfactant monolayer; (ii) energy changes associated with the close approach of microemulsion droplets; (iii) the energy required to bend the surfactant monolayer; and (iv) the energy required to desorb surfactant from the droplet surface. In this thesis, kinetic studies have been performed in an attempt to find correlations that may exist between the above mentioned parameters and microemulsion droplet exchange rates.

1.2.7 Solubilisation of biopolymers in W/O microemulsions.

It is quite common in industry for emulsion based products to be stabilised by a mixture of low molar mass surfactants and polymeric material. An example of this in the food industry is margarine in which the W/O emulsion is stabilised by the presence of both monoglycerides and milk proteins (60). The protein may contribute to the overall stability by co-adsorbing at the oil-water interface together with surfactant molecules, or alternatively, stability may arise through its presence in the continuous phase of the emulsion. Some of these processes will be described in section 1.3.3.

It has been observed that proteins may be solubilised into the dispersed aqueous phase of W/O microemulsion aggregates (61). The location of the solubilised protein depends upon the competing interactions between itself and the dispersed phase, the continuous solvent and the surfactant monolayer. This has recently been discussed by Pileni (62). It is possible therefore, to observe protein adsorption behaviour at the surfactant stabilised oil-water interface through changes in the spontaneous curvature of the droplet surface.

The ability of water-in-oil microemulsions to solubilise proteins has led to a large number of investigations having been performed over the past fifteen years (63 - 66). A large proportion of these have been concerned with enzyme catalysed reactions within the dispersed phase of the microemulsion (61, 67, 68). The interest in these novel reaction media arises since it is observed that the rate and equilibrium position of such reactions may differ greatly from that observed in bulk solution (69).

Another area which has received a significant amount of interest is in the possible use of microemulsions as protein extraction/purification systems (70 - 72). It has been observed that proteins may be extracted from various protein mixtures using Winsor II systems. Selective extraction may be achieved through manipulation of the pH and salt concentration of the aqueous medium (27).

1.3 Unstable Oil - Water Mixtures : Macroemulsions.

1.3.1 Introduction to macroemulsions and the Hydrophile-Lipophile Balance.

Upon shaking an oil-water mixture containing surfactant, a macroemulsion may be produced in which either droplets of oil are dispersed in the continuous aqueous phase (O/W) or water droplets are dispersed in the apolar medium (W/O). This property of surfactant molecules of being able to stabilise dispersions of two normally immiscible liquids has been known for thousands of years. Indeed, one of the earliest reported macroemulsion preparations comes from ancient Greek literature in which in the second century, the Greek physician, Galen, produced an emulsion containing beeswax as the apolar phase (73). In the chemical industry today, macroemulsions represent one of the most important uses of surface-active molecules. Their wide range

of applications can be illustrated with the example of the surfactant Span 20, a hydrophobic sorbitan ester. In the food industry, this is employed in the stabilisation of fat crystals in chocolate production (74), whereas the same species is also used to stabilise ammonium nitrate emulsion explosives (75).

Prediction of the type of macroemulsion produced (O/W or W/O) when an oil + water + surfactant system is emulsified has been the subject of many investigations over the years. In the 1930's, Clayton emphasised the importance to this problem of considering the nature of a surfactant's hydrophilic and hydrophobic groups (76). This was later extended by Griffin who introduced a method of classifying nonionic surfactants according to the relative proportions of hydrophilic and lipophilic (hydrophobic) groups within the molecule (77, 78). This is the Hydrophile-Lipophile Balance (HLB).

Surfactants are assigned a number ranging from 0 - 20 which reflects the hydrophilicity/lipophilicity of the molecule. Surfactants with low HLB values (e.g. 1 - 7) exhibit a resultant lipophilic tendency and promote W/O macroemulsion formation. Conversely, those with higher HLB values are hydrophilic and produce O/W macroemulsions. This is effectively equivalent to Bancroft's rule which states that the phase in which the surfactant is more soluble tends to be the continuous phase of the macroemulsion produced (79).

The HLB number of a surfactant may be calculated according to empirical formulae based on the surfactant's molecular geometry. One of the simplest formulae of this kind is given below for polyoxyethylene type nonionic surfactants (80).

$$\text{HLB} = (\text{mole \% hydrophilic group}) / 5 \qquad (1.13)$$

Later, Davies and Rideal gave the HLB method a more quantitative basis by assigning numbers to specific molecular groups (81). The overall HLB for the surfactant was then given by a summation of the various group contributions within the molecule.

$$HLB = \Sigma(\text{hydrophilic group numbers}) - \Sigma(\text{lipophilic group numbers}) + 7 \qquad (1.14)$$

It has become rather evident however, that this method of emulsifier characterisation has serious limitations. HLB numbers are assigned to surfactants on the basis of their molecular structure alone without consideration of the prevailing conditions e.g. nature of the oil phase, temperature, salt concentration etc. It is well known that nonionic surfactants can change their solution behaviour from promoting O/W microemulsion formation at low temperatures, to W/O aggregate formation at elevated temperatures. Such factors might also therefore be predicted to affect the type of macroemulsion produced. This arises since it is generally observed that the type of microemulsion formed in a two phase oil-water system is the same as the type of macroemulsion produced when the two phases are mixed, i.e. a Winsor I O/W microemulsion system will produce a corresponding O/W macroemulsion (82, 83). This is shown schematically in Figure 1.13 below.

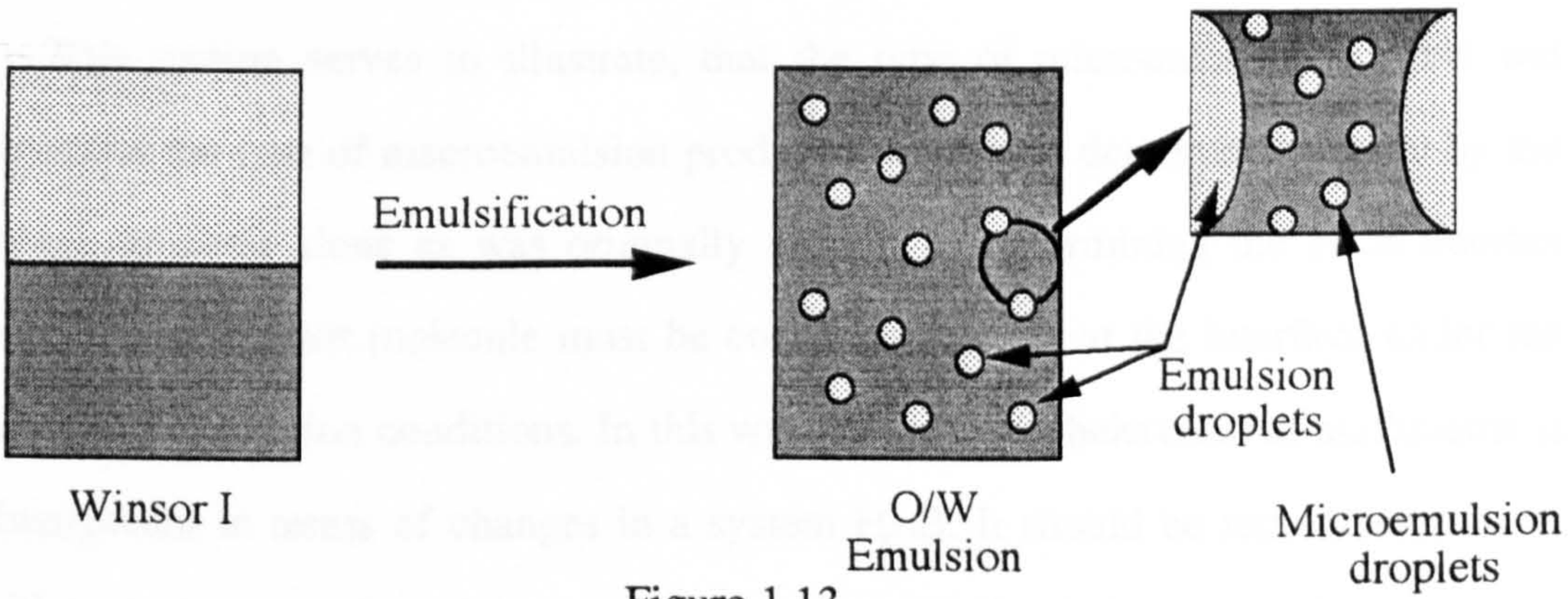

Figure 1.13

In the macroemulsion produced, the emulsion drops coexist in conjunction with microemulsion droplets. Since the emulsion monolayers are effectively flat in

comparison with microemulsion droplets, the reason for this equivalence between the type of macroemulsion formed and the type of microemulsion produced at equilibrium is at present unresolved. Clearly however, factors which affect the microemulsion phase behaviour will also directly affect the type of macroemulsion produced. It is far more appropriate therefore, to consider an *effective* HLB for a surfactant *in situ* within the monolayer under the influence of the solution conditions. This is often referred to as the system HLB (80).

If the system HLB in an oil + water + surfactant system is high, aggregates will form in the aqueous phase (and O/W macroemulsion formation will be promoted). Conversely, a low system HLB will favour water-in-oil aggregate formation (and W/O macroemulsion formation). The system HLB relates to microemulsion formation and therefore is only applicable to systems at surfactant concentrations in excess of the cμc. It is not related to the preference of the surfactant monomer for either the oil or water phases. This can be highlighted by the observation that monomers of the nonionic surfactant $C_{12}E_5$ at ambient temperature partition between water and heptane strongly in favour of the apolar phase, however, aggregate formation occurs in the water (42). The macroemulsion type follows the microemulsion type (not the monomer partitioning) and consequently an O/W emulsion is formed upon mixing the two phases.

This section serves to illustrate, that the type of microemulsion formed and consequently the type of macroemulsion produced, cannot be determined simply by the surfactant structure alone as was originally thought in determining the HLB number concept. The surfactant molecule must be considered *in situ* at the interface under the influence of the solution conditions. In this way, the solution behaviour of surfactants is best interpreted in terms of changes in a system HLB. It should be remembered here, that although the type of emulsion produced may be predicted through an interpretation in terms of HLB, no indication of the *kinetic stability* of the emulsion is obtained.

1.3.2 Macroemulsion breakdown mechanisms.

Macroemulsions are thermodynamically unstable and will eventually phase separate into two or more phases. Phase separation occurs by a variety of different processes as shown in Figure 1.14 and discussed below.

(1). Flocculation.

This is the process whereby individual droplets form clusters or flocs in the continuous phase of the emulsion. The initial droplet size however, is retained within the flocculated structure. If attractive interactions between droplets outweighs repulsive inter-droplet forces, flocculation may occur. Consequently, factors which effect the interactions between droplets will have a direct bearing upon the extent of flocculation observed. In the case of emulsions stabilised by polymers, flocculation may be induced if the polymer molecules adsorb to the surface of more than one droplet. This type of flocculation is known as *bridging flocculation* (84). Flocculation has also been observed to be induced by the presence of non-adsorbing polymer molecules (85) and micellar aggregates (86) in the continuous phase. This process is termed *depletion flocculation* (87, 88) and arises due to the expulsion of polymer (or aggregates) from the thin films of continuous phase separating approaching emulsion droplets. This will be discussed further in Chapter seven.

Since droplets within a floc retain their individuality they may be redispersed if a sufficient external force is applied. The process of flocculation is therefore reversible.

(2) Creaming/Sedimentation.

In general there exists a density difference between the two liquids constituting an emulsion. If the less dense liquid comprises the dispersed phase, then in time, droplets will accumulate at the top of the emulsion. This process is referred to as creaming and is commonly observed in oil-in-water emulsions. In the opposite case, in which the dispersed phase is the more dense liquid, the droplets will collect at the base

Figure 1.14

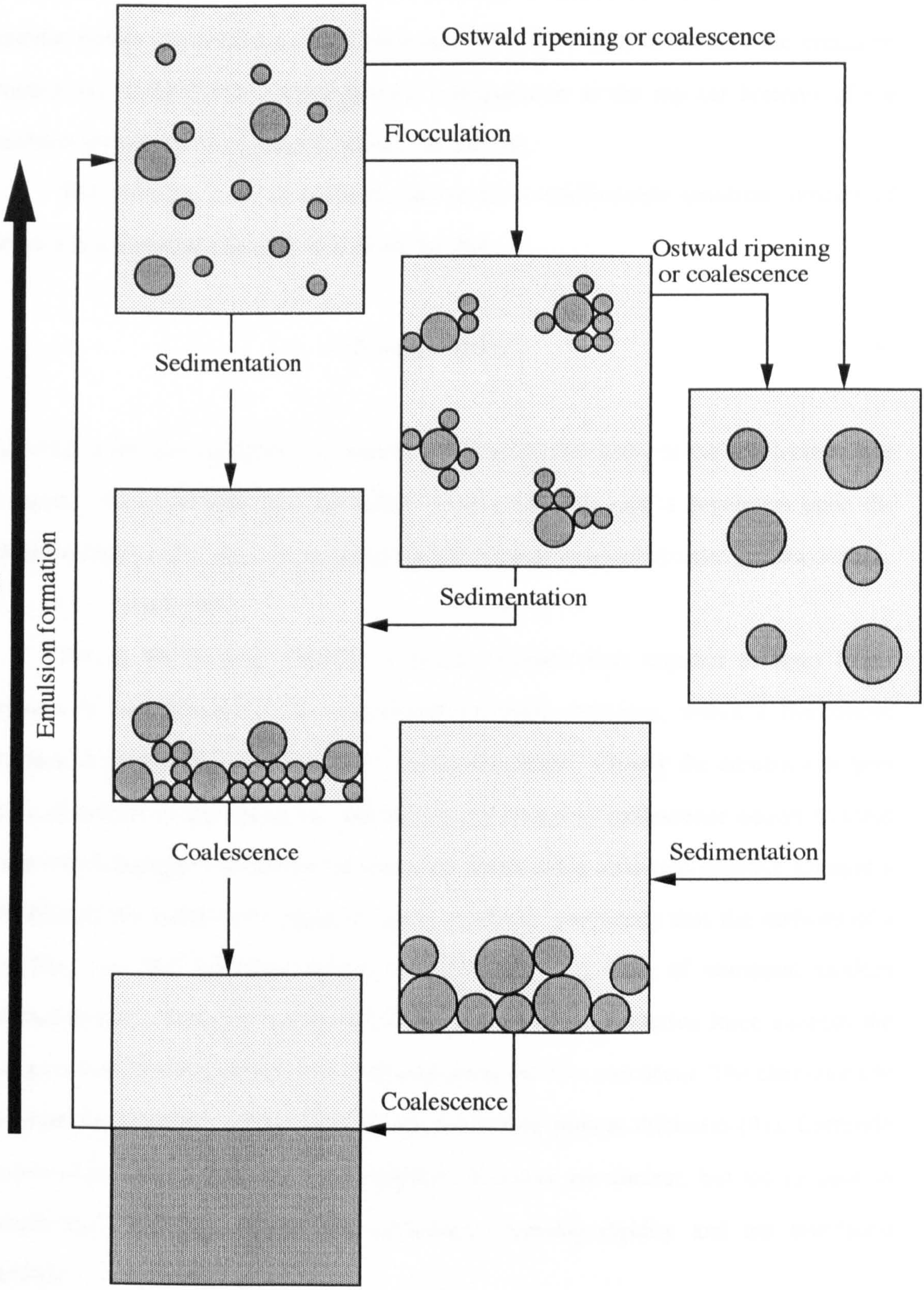
Ostwald ripening or coalescence
Flocculation
Ostwald ripening or coalescence
Sedimentation
Sedimentation
Sedimentation
Coalescence
Coalescence
Free energy
Emulsion formation
Two phase system

of the emulsion. This is termed sedimentation and is frequently observed in water-in-oil emulsions. Creaming or sedimentation of an emulsion produces a droplet concentration gradient within the emulsion. This increases with time until eventually the emulsion droplets are contained in a close-packed configuration at the top (or bottom) of the emulsion together with separated continuous solvent.

The velocity v of an isolated, spherical, nondeformable emulsion droplet of radius a in a liquid of viscosity η is given by (89)

$$v = (2 \Delta\rho\, g\, a^2)/(9\, \eta) \qquad (1.15)$$

where $\Delta\rho$ is the density difference between the two phases and g is the acceleration due to gravity. It can be seen that the sedimentation/creaming rate is dependent upon the emulsion droplet size and will be enhanced for systems in which droplet growth occurs.

(3) Coalescence.

This is the process whereby emulsion droplets fuse together to form larger droplets. It may proceed in a concentrated creamed emulsion, within a flocculated structure or upon collision of separate emulsion droplets. Clearly the emulsion droplet size distribution is not conserved and ultimately complete coalescence occurs to yield the two bulk liquids. The region between two approaching emulsion droplets contains a thin film of the continuous phase. It has been shown previously that the surfaces of a thin film (i.e. the emulsion droplet surfaces) are in a state of continual random fluctuation (90). If during a fluctuation, the change in the attractive force exceeds the change in the total repulsive force, then rupture of the film can occur. The characteristic thickness at which this occurs is known as the critical rupture thickness (91). Currently factors which may affect the critical rupture thickness are unclear, but are thought to include the interfacial tension, the monolayer bending rigidity and the interfacial rheology.

(4) Ostwald ripening.

So far, oil and water mixtures have been treated as being completely immiscible. In all cases however, there will exist some mutual solubility between the two phases. This may be sufficient to give rise to a process known as Ostwald ripening.

If the droplet size distribution within an emulsion is polydisperse, then there will exist an internal Laplace pressure difference between the small and large droplets. This will produce a thermodynamic driving force favouring the production of large droplets at the expense of smaller ones. This is described by equation 1.16 below (41)

$$\ln (C_{(a)}/C_{\infty}) = 2 \gamma V /(a R T) \qquad (1.16)$$

where $C_{(a)}$ is the solubility of a droplet of radius a, C_{∞} is the solubility of the bulk liquid, V is the molar volume of the liquid and γ is the interfacial tension. Molecules of the dispersed phase may then dissolve in the continuous phase and migrate from the small to the larger droplets. The rate at which Ostwald ripening occurs depends therefore on the solubility of the dispersed phase in the continuous solvent and the speed of diffusion of material dissolved in the continuous phase. An additional mechanism whereby material may exchange between emulsion droplets is through solubilisation into the interior of microemulsion aggregates present in the continuous phase of the emulsion. Ultimately, an emulsion of polydisperse droplet size may attain a state in which complete resolution of the two phases has occurred through Ostwald ripening.

In general, the four breakdown processes outlined above may occur simultaneously or in any order depicted in Figure 1.14. It is clearly evident that the rate at which each process proceeds is highly dependent upon the extent to which the other processes are operating. For example, the rate of creaming observed in an emulsion depends upon the degree of flocculation of the droplets and on their size, which is

dependent upon the rates of coalescence and Ostwald ripening within the emulsion. It is normally extremely difficult to resolve the rates at which these individual mechanisms occur within the overall emulsion breakdown process.

1.3.3 Emulsion stabilisation.

Stabilisation as applied to emulsion systems, refers to the resistance of an emulsion to the four breakdown mechanisms discussed above. Each of these processes may produce serious adverse effects in the desired properties of the emulsion. Some important factors which may directly influence the stability of an emulsion are discussed below.

(1) Physical nature of the interfacial film.

Since emulsion droplets are in a state of continual motion they may undergo frequent collisions. If the interfacial film surrounding two colliding droplets ruptures, coalescence will take place since this involves a decrease in the free energy of the system. The ability of the surfactant film to prevent rupture upon collision is therefore of prime importance in determining the stability of the emulsion. One physical property of a surfactant film which effects its resistance to rupture is its "mechanical strength". For maximum "mechanical strength", the surfactant interfacial film should be condensed, with strong lateral intermolecular forces. Pure surfactants often produce interfacial films that are not condensed and consequently exhibit poor "mechanical strength". For this reason a mixture of two or more surfactants are commonly employed (92). An example of this may be the anionic surfactant sodium dodecyl sulphate (SDS) and the addition of dodecanol. A mixed monolayer is produced in which the lateral interactions between adjacent SDS tails are increased through the presence of the long chain alcohol producing a more condensed film. In some cases, emulsion droplets may

be stabilised through the formation of liquid crystalline layers at the droplet surface (74). The film produced is highly viscous and exhibits a strong "mechanical stability" that may resist the coalescence of individual droplets. Additionally, the film provides a steric barrier (see later) that prevents the dispersed particles from approaching each other closely enough for van der Waals attractive forces to operate.

A further requirement for the production of an effective stabilising film, is that it should exhibit a high elasticity. When emulsion droplets collide (either with themselves or with the vessel wall) deformation of the stabilising film may occur. If the surface concentration of surfactant is not maintained the local interfacial tension at that point in the interface will increase. The tension gradient now existing at the surface of the droplet resists further deformation thus stabilising the system. If surfactant can rapidly re-adsorb to the "bare" surface the tension gradient will be relaxed in which case the interface will exhibit a low elasticity. This is known as the Gibbs-Marangoni effect. If the stabilising film around the droplets does not show an appreciable elasticity, the emulsion may be unstable and breakdown rapidly.

(2) Electrostatic stabilisation.

The presence of a charged droplet surface may arise for O/W emulsions through the dissociation of a surfactant's charged ionic head group or through the surface adsorption of ions. In solution, the charged droplet will be surrounded by a diffuse layer of ions of opposite charge to the surface such that electrical neutrality is conserved. This electrostatic arrangement is referred to as an electrical double layer (93). When two droplets approach each other in solution a certain separation is reached at which their electrical double layers start to overlap. If the double layer thickness is sufficiently large, closer approach will be prevented through repulsion and the droplets will be electrostatically stabilised. The thickness of the double layer is highly dependent upon the concentration of electrolyte in the system. If this is high, the double layer thickness is reduced and the emulsion droplets may approach sufficiently closely such that van der

Waals attraction between them dominates the overall interaction. In this case flocculation may be observed. The theory which describes particle stability in terms of electrical repulsion and van der Waals attraction is well characterised and is referred to as the DLVO theory after its pioneers Derjaguin and Landau (94) and Verwey and Overbeek (95).

(3) Stabilisation by Polymers.

If a polymeric material is sufficiently surface active it may adsorb at an emulsion droplet surface forming loops and tails which extend into the continuous phase. When two emulsion droplets approach sufficiently closely, the adsorbed material may start to interact. Generally the polymer-polymer interaction will be unfavourable since this results in a loss of configurational entropy of the polymer segments and consequently, repulsion between the two droplets will occur. This type of stabilisation is known as *steric stabilisation* (96). Due to the nature of the adsorbed polymeric film, it may also provide an appreciable "mechanical barrier" to droplet coalescence.

Non-adsorbing polymer can also increase the stability of an emulsion through a process known as *depletion stabilisation* (97). This is typically observed when reasonably high concentrations of polymer are present in the continuous phase of an emulsion. For two droplets to approach each other sufficiently closely such that flocculation may occur requires polymer molecules to be expelled from the intervening region between the droplets. If the continuous phase is a good solvent for the polymer then this will be energetically unfavourable since it will involve demixing of the polymer chains and solvent. This gives rise to an energy barrier to flocculation. At lower polymer concentrations however, this energy barrier is much reduced and flocculation may then become a thermodynamically favourable process. This is the origin of depletion flocculation which is discussed in detail in Chapter seven.

Non-adsorbing polymeric species may also stabilise emulsions through their influence on the bulk rheology. This is discussed below.

(4) Viscosity of the continuous phase.

An increase in the viscosity of the continuous phase will reduce the diffusion coefficient of the droplets and hence retard the rate of creaming/sedimentation (see equation 1.15), coalescence etc. This is a very simple but highly important factor in determining the overall emulsion stability. The viscosity of the continuous phase of an emulsion may be dramatically increased through the addition of polymers, e.g. polysaccharides. In some cases, a weak gel network may be formed producing a highly stable droplet dispersion.

1.4 Presentation of Thesis.

The aim of this thesis is to attempt to correlate equilibrium properties of microemulsion systems with the formation and stability of the corresponding macroemulsions. The work is mainly confined to the study of water-in-oil micro/macro-emulsions stabilised by nonionic surfactants. This thesis may be conveniently divided into two parts. The first part, Chapters three to six, is dedicated to a study of the equilibrium microemulsion properties of various water + oil + surfactant systems and in the second part, Chapters six and seven, the macroemulsion behaviour of these systems is reported.

Initially in Chapter two a description of the experimental techniques employed and the specification of the materials used throughout this work is given. In Chapter three, a brief study of the microemulsion phase behaviour of several commercial emulsifiers of the type used in foods is presented. Their behaviour is interpreted in terms of HLB ideas which are known to account for the behaviour of pure nonionic surfactants. In Chapter four, water-in-hydrocarbon microemulsions stabilised by $C_{12}E_4$

are characterised. These results are compared to those obtained with various concentrations of a medium chain length triglyceride as the oil phase in Chapter five. Chapter six addresses the possible relationship between the monolayer bending rigidity constant K, and the microemulsion exchange rate for three surfactant systems in which values for K have previously been reported. The latter part this chapter discusses the possible correlations between these findings and macroemulsion phase separation rates for the corresponding systems. In Chapter seven, macroemulsion phase separation rates of the surfactant systems described in Chapters four and five are presented. Two effects are described in detail. Firstly, the effect of added microemulsion droplets of differing size on macroemulsion stability. The results are interpreted in terms of a theoretical model of depletion flocculation. Secondly, the effect of the addition of triglyceride oils to the emulsions is investigated. The resultant changes in the emulsion stability are correlated with changes in the properties of the equilibrium microemulsion systems. Finally in Chapter eight, the main conclusions from this thesis are drawn together.

2. EXPERIMENTAL.

CHAPTER 2.

2.1. Methods.

2.1.1 Microemulsion phase boundary determination.

Two techniques were employed for determining the extent of the one phase microemulsion region. The first of these involved preparing a series of solutions containing different concentrations of surfactant in the continuous phase. These were thermostatted in the type of vessel shown in Figure 2.1. The vessels were designed so as to provide ease of addition of liquid with minimal loss of volatile solvents through evaporation. The silicone rubber septa showed no signs of swelling when immersed in the solvents under study for up to five hours and hence were assumed to be inert over the experimental time scale. To each vessel the required amount of dispersed phase was injected through the septum to produce a certain mole ratio of dispersed component to total surfactant, denoted R.

$$R = \frac{[\text{dispersed phase}]}{[\text{surfactant}]} \qquad (2.1)$$

The sealed vessels were placed in a thermostat and continuously stirred by a magnetic bar. The temperature of the samples was gradually changed (typically less than 0.1°C /min) and the temperatures corresponding to the two boundaries were detected visually as a transition from clear to cloudy or vice-versa. Boundary temperatures were observed to be independent of the direction from which they were approached (i.e. raising or lowering the temperature). The R value was then incremented by further addition of dispersed phase and the procedure repeated.

The second method for boundary determination was that of a one phase turbidity titration. Initially, the surfactant solution was thermostatted as before in the titration

Figure 2.1

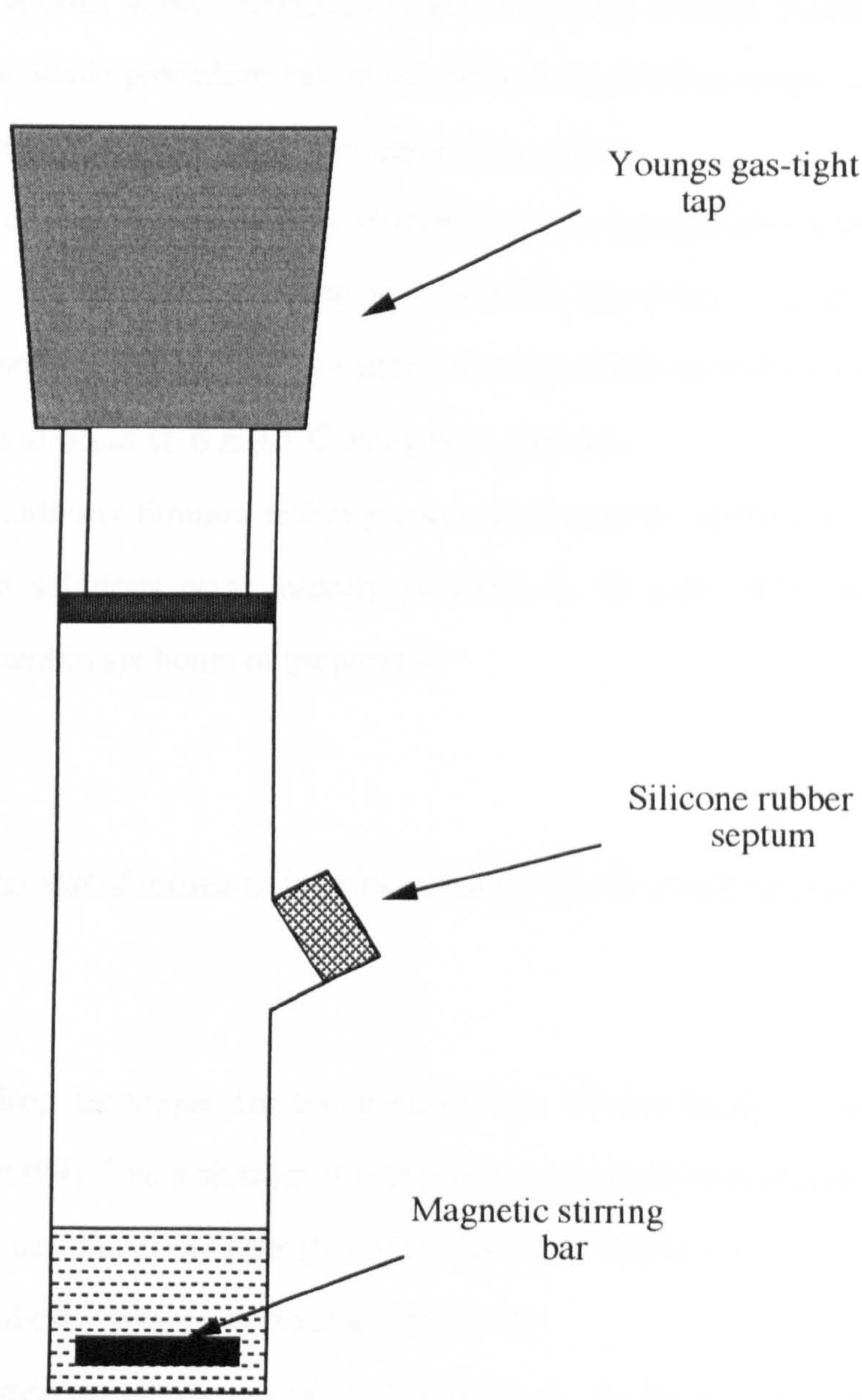
Youngs gas-tight
tap
Silicone rubber
septum
Magnetic stirring
bar

vessel. The dispersed phase was then added to the stirred solution through a microlitre syringe and the volume required to produce the first onset of turbidity was recorded. A known amount of concentrated surfactant solution was then injected until a one phase solution again resulted and the titration was repeated. In this way, a plot of the maximum solubilised volume versus surfactant concentration (at a single temperature) was obtained (98). The whole procedure had to be repeated at different temperatures to fully map out the position of the one phase microemulsion region.

The precision of the phase boundary determinations was typically better than ± 0.5°C. Results from the two methods were in reasonable agreement; e.g. the lower temperature phase boundary for heptane-in-water microemulsions stabilised by $C_{12}E_4$ (R = 15 ± 1) was found to occur at 6 ± 0.5°C using both methods.

The one phase turbidity titration technique was employed for protein-containing systems. Stock protein solutions were initially prepared in 50 mM buffer solution, stored on ice and used within six hours of preparation.

2.1.2 Measurement of oil-water interfacial tension by the spinning drop technique.

The spinning drop technique for the measurement of interfacial tension was developed by Vonnegut (99). The technique is particularly suitable for the measurement of very low values of interfacial tension (5 - 10^{-4} mN m^{-1}) where other techniques (e.g. Wilhelmy plate and drop volume techniques) fail (100).

The technique involves injecting a drop of liquid (e.g. oil phase) into a spinning capillary containing a second, more dense liquid (e.g. aqueous phase) as shown schematically in Figure 2.2. The centripetal force on the drop acts to elongate it along the axis of rotation whereas the interfacial tension force opposes this by a tendency to

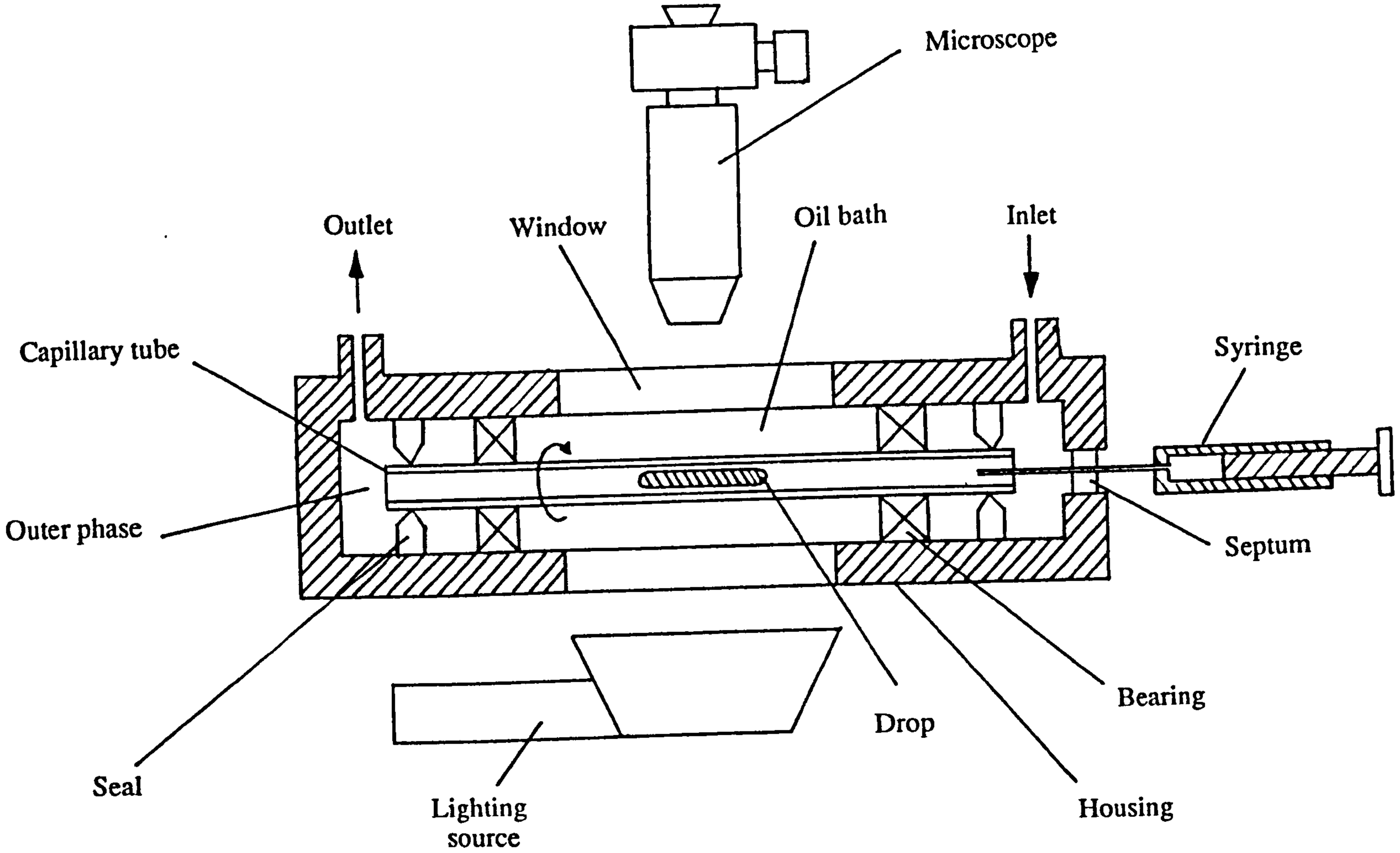
Microscope
Outlet
Window
Oil bath
Inlet
Capillary tube
Syringe
Outer phase
Septum
Bearing
Drop
Seal
Lighting source
Housing

Figure 2.2

minimise the oil-water interfacial area favouring a spherical drop shape. At equilibrium, a cylindrical shaped drop is generally obtained whose diameter is a function of the angular velocity of the spinning capillary, the interfacial tension and density difference between the two liquids. The full expression relating the shape of the drop to the interfacial tension is complex (99). However, by suitable choice of the drop volume injected and rotation speed of the capillary, it is generally possible to obtain drops whose length to width ratio exceeds about four. Under these conditions, the drop shape may be approximated as a cylinder with hemispherical caps. If the effects of gravity are ignored, the simple relationship below can be used to obtain the interfacial tension (99, 101).

$$\gamma = (d/2)^3 \omega^2 \Delta\rho/4 \qquad (2.2)$$

where d is the cylindrical drop diameter, ω is the angular velocity of the capillary in radians per second and $\Delta\rho$ is the density difference between the two liquids.

The tensiometers were supplied by Kruss (models site 02 and site 04). The rotating capillary containing the more dense liquid was thermostatted by circulating oil from a Lauda thermostat. Accurate determination of the capillary temperature was achieved through the use of an incorporated thermocouple. Typically the temperature was constant to within ± 0.5°C and a temperature range of between 12 - 50°C was obtainable. Effective droplet illumination was achieved by using a stroboscope in phase with the rotation of the capillary. A continuous light source was also used occasionally, but this generally produced poorer droplet contrast.

Operation of the tensiometer was fairly straight forward. The less dense oil phase was injected into one end of the rotating capillary through a septum and positioned in the field of view by inclination of the apparatus. The diameter of the drop was monitored until a stable equilibrium value was achieved. The time taken to

establish equilibrium was system dependent but generally ranged between 10 - 100 minutes.

The diameter of the drop was measured using a horizontally mounted microscope fitted with an eyepiece containing a graticule. The drop diameter was determined by aligning the upper edge of the drop with the zero graticule marking and coinciding the movable cross wires with the lower edge of the drop. The drop diameter was thus obtained in graticule scale units. Calibration factors for each eyepiece had previously been obtained by measuring the product $d^3\omega^2$ for a series of pre-equilibrated water-alcohol mixtures. Using reliable values of interfacial tensions and densities from the literature (102), the calibration factors were obtained from linear plots of $\gamma/\Delta\rho$ against $d^3\omega^2$ (103). These calibration factors were used in all calculations of tensions.

As is evident from equation 2.2, any error in reading the droplet diameter will result in a threefold percentage error in γ. For this reason the diameter was measured at a minimum of three positions along the droplet length and an average value taken. The maximum uncertainty in γ was estimated to be $\pm$ 10%.

2.1.3 Photon correlation spectroscopy.

Light scattering as a probe of colloidal dispersions has a long history with significant contributions from Tyndall, Maxwell, Rayleigh, Smoluchowski, Einstein and many others (104). However, it was not until the advent of the laser in 1961 that the technique of dynamic light scattering was developed. This technique exploits the coherence of the laser beam to yield information about the particles in a colloidal suspension (105). Over the past 15 years it has been extensively used for particle sizing and measurement of diffusion coefficients in microemulsion systems (106, 107).

If a dispersion of static colloidal particles is considered as forming a 3-dimensional array then, on illumination by a coherent light source, a characteristic, random diffraction or "speckle" pattern will be produced. Bright and dark areas will arise from constructive and destructive interference of the scattered light. In a real solution the particles are continually moving under Brownian motion and hence the diffraction pattern bright spots will move randomly. A detector positioned to register the intensity of a few of the bright spots will then yield a signal which fluctuates significantly about a mean value. (In conventional, static light scattering techniques, the detected area covers a large number of diffraction spots and the intensity fluctuations are of insignificant amplitude relative to the mean, time-averaged intensity and hence only the mean scattering intensity is obtained.) The characteristic frequency of these random intensity fluctuations contains information on the particle motion and hence its size. Small, fast moving particles produce high frequency fluctuations whereas larger, slower moving particles give lower frequencies. For the microemulsion particles studied in this work, the intensity fluctuations generally occur on a millisecond to microsecond time scale.

The apparatus, shown schematically in Figure 2.3, consists of the following components. The laser source illuminates the sample at the centre of a goniometer on which is mounted a sensitive photomultiplier. The signal from the photomultiplier is fed to a real-time, digital correlator which is, in turn, connected to a computer for subsequent particle size calculation The principles of this calculation are outlined below.

The digital correlator calculates the intensity autocorrelation function $G(\tau)$. The correlator is organised into a number of channels of time interval Δt which is set to be small relative to the characteristic period of an intensity fluctuation. The function $G(\tau)$ is obtained as the intensity in channel j (I_j) multiplied by the intensity in channel j+n (I_{j+n}) where $t = j\Delta t$ and $\tau = n\Delta t$. The function $G(\tau)$ (equivalent to $G(n)$) is collected and

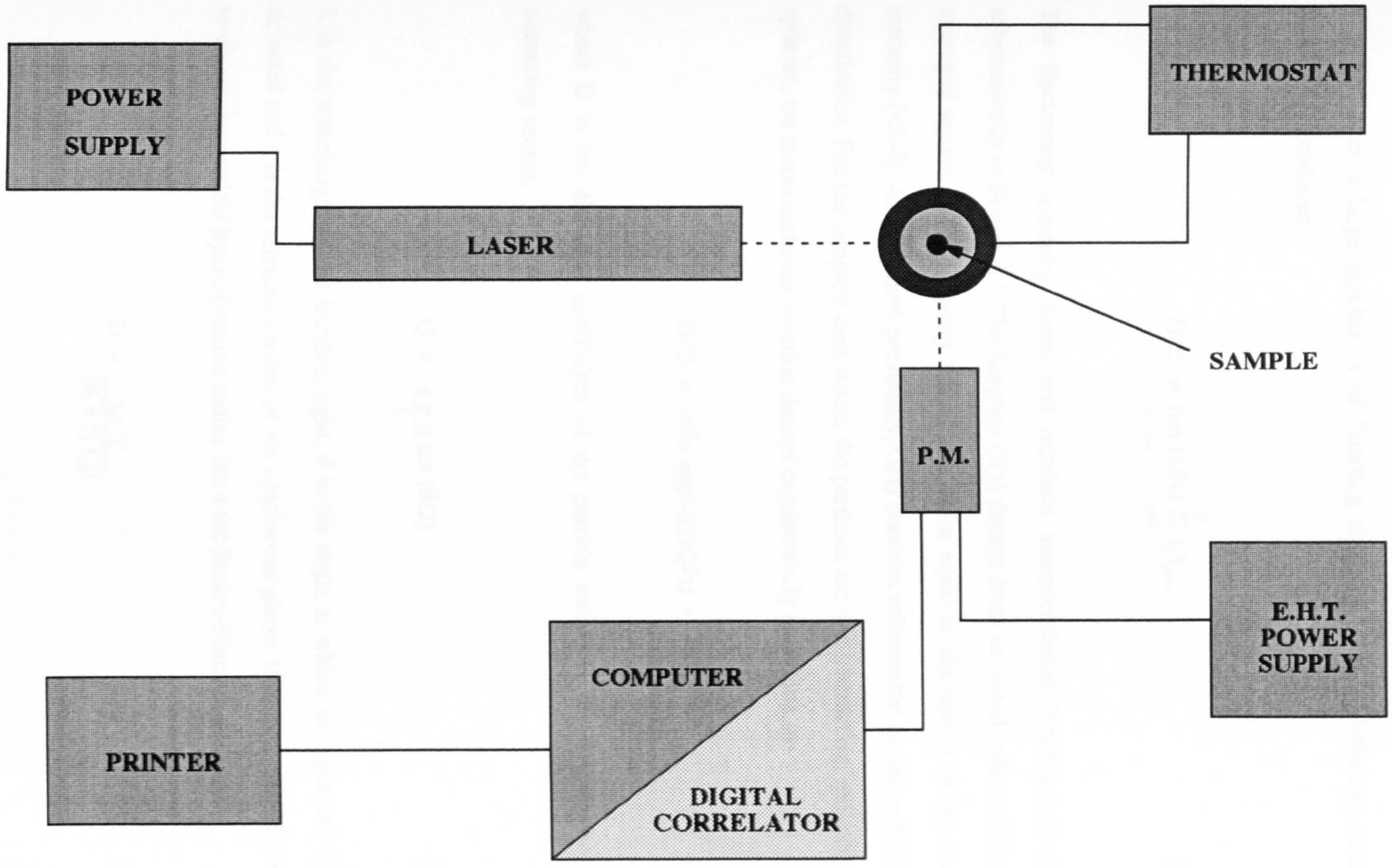
POWER SUPPLY
LASER
THERMOSTAT
SAMPLE
P.M.
E.H.T. POWER SUPPLY
COMPUTER
DIGITAL CORRELATOR
PRINTER

Figure 2.3

averaged over a large number N of "starting channels" j until sufficient statistical accuracy is produced.

$$G(\tau) = \lim_{N\to\infty} (1/N) \sum_{j=1}^{N} I_j I_{j+n} \qquad (2.3)$$

The fluctuating intensity signal and resultant autocorrelation function are shown schematically in Figure 2.4. The function $G(\tau)$ decays from an initial value of the time-averaged square of the intensity ($\langle I^2 \rangle$) to a value equal to the square of the average intensity ($\langle I \rangle^2$). As explained previously, $G(\tau)$ contains information on the particle size distribution. For the simplest case where the particles are non-interacting, monodisperse spheres, the autocorrelation function decays exponentially according to

$$G(\tau) = \langle I^2 \rangle \exp(-2DQ^2\tau) + \langle I \rangle^2 \qquad (2.4)$$

where D is the diffusion coefficient of the particle and Q is the magnitude of the scattering vector.

$$Q = \frac{4 \pi n}{\lambda} \sin(\theta/2) \qquad (2.5)$$

λ is the wavelength of the incident light, θ is the angle at which the scattered light is detected and n is the refractive index of the continuous phase. It is then a simple matter to obtain the particle hydrodynamic radius from the Stokes-Einstein equation

$$D = \frac{k_B T}{(6 \pi \eta r_H)} \qquad (2.6)$$

Figure 2.4

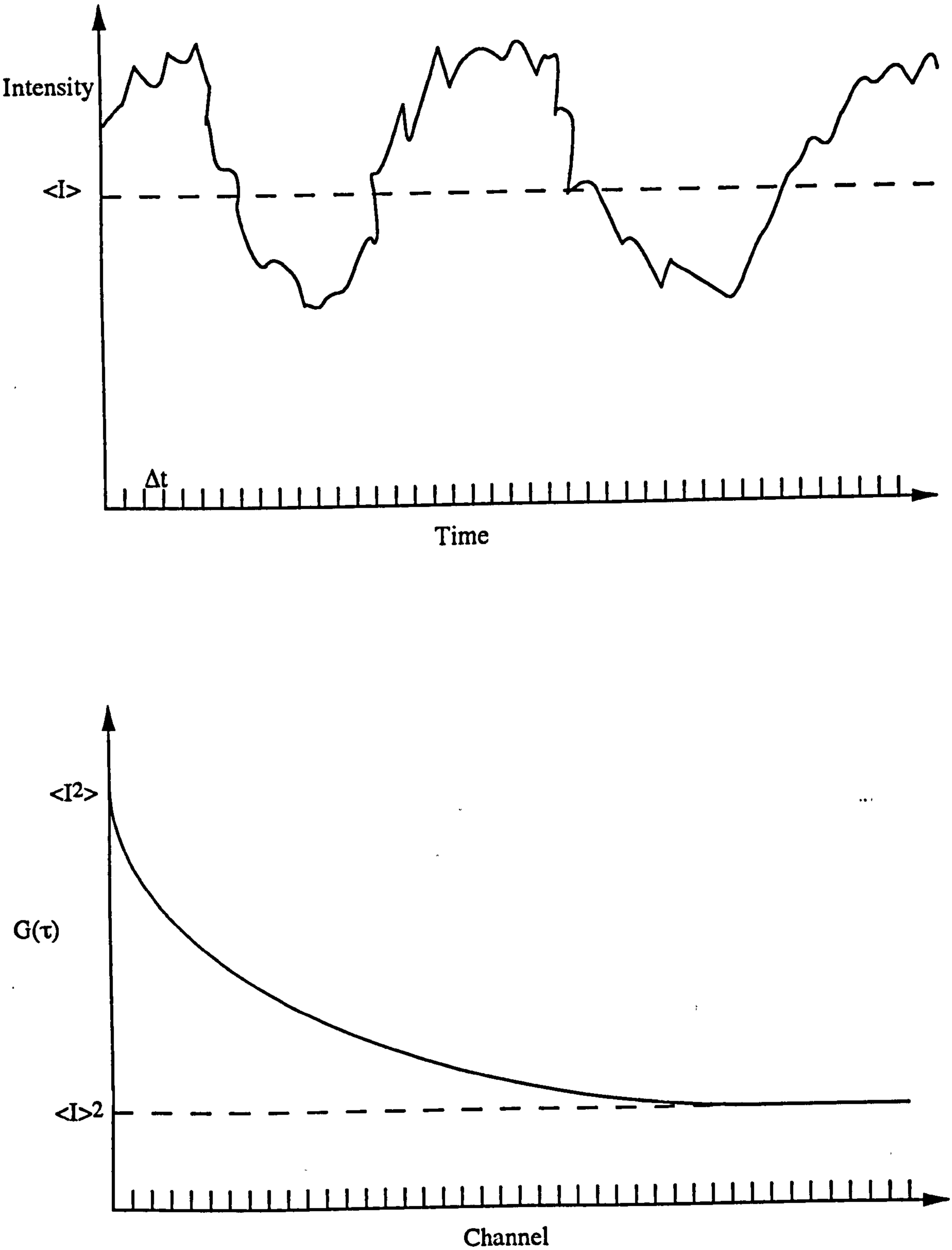

where k_B is Boltzmann's constant, T is the absolute temperature, η is the viscosity of the continuous solvent and r_H is the hydrodynamic radius of the particle.

If the particle size distribution is polydisperse, a non-exponential correlation function results. In this case a more detailed analysis is required. The observed decay may be described by an expansion of the type given by Koppel (108),

$$\ln G(\tau) = (\ln \langle I^2 \rangle - B\tau + (1/2!) \frac{\mu}{\bar{B}^2} (B\tau)^2 + \ldots) + \ln \langle I \rangle^2 \qquad (2.7)$$

where B is the mean decay constant ($2\bar{D}Q^2$) and μ/B^2 is the normalised variance. Samples investigated in this work displayed low values of this normalised variance (typically < 0.1) indicating the presence of aggregates with a low degree of polydispersity.

For the work described in this thesis, the experimental set-up was as follows. One phase microemulsion samples were contained in 1 cm path-length, stoppered fluorescence cuvettes (Hellma) and were positioned in a thermostatted, Malvern Instruments (PCS 100SM) goniometer. The temperature was regulated by a Malvern temperature controller (PCS 8) and an external Grant water circulating thermostat. Fluctuations in temperature were typically less than ± 0.1°C. A Spectra-Physics 15 mW He-Ne laser (λ = 632 nm) was incident on the sample and scattering was collected at 90° to the laser beam by a Malvern photomultiplier. Intensity variations were analysed by a Malvern digital correlator, model K7072 and the autocorrelation function displayed on the screen of the incorporated Commodore pet computer. The analysis of the autocorrelation function was performed using equation 2.7 and a hard copy of the results was obtained through the use of an online Commodore 4023 printer.

The solubilisation phase boundaries for one phase "made-up" microemulsion samples used in the PCS studies were generally found to be in agreement (± 0.5°C) with those previously determined from phase studies. Samples were thermostatted for a

minimum of 15 minutes prior to measurement to allow equilibration to the pre-selected temperature. Since the presence of dust can seriously perturb the autocorrelation function producing meaningless results, a rejection algorithm was implemented. Data was collected in one second "bursts". For each "burst", the routine calculated the normalised, time-averaged value of the measured scattered intensity from the total count of the scattered photons collected in that "burst". This value was compared with the average value calculated from the intensity at very long times (compared to the period of the fluctuations) as determined through the use of four delay channels. If the maximum fractional difference between these two values was outside a set value, the data of that "burst" was rejected. Otherwise, the data was collected and averaged. Setting of this rejection factor was most effectively performed by observing the build-up of the trace with time. Typically a 0.5% rejection level ensured dust particles did not significantly perturb the measurements.

Scattering was recorded until a smooth exponential decay was obtained without any irregularities. The samples were then checked for any signs of phase separation. Frequently, for very low intensity scattering solutions, a smooth decay trace could only be obtained after 2-3 days sampling. If any irregularities still remained the Malvern analysis software would only fit the first few channels up to the first aberration. This resulted in a high statistical uncertainty in the calculated radius. In these few cases the data were entered into a BBC curve fitting programme (109) and the best fit to a single exponential function calculated. This procedure was found to be more satisfactory for the case of very low scattering intensity samples.

2.1.4 Time-resolved fluorescence measurements.

Since the development of time-resolved fluorimeters in the early seventies they have been used extensively through out all three branches of chemistry, physics and biology. Within the field of colloidal chemistry detailed information has been obtained on various aspects of micellar (110 - 113) and microemulsion (48, 50, 53, 114, 115) behaviour. The technique as applied to surfactant colloidal systems, measures the fluorescence decay of probe molecules solubilised in the interior of microemulsion droplets. In the absence of fluorescence quenching molecules, the intensity decays exponentially. If quencher molecules are also present solubilised in the aggregates, the fluorescent life time of the fluorescent probe is reduced and the decay is described by a multi-exponential function. This arises from the summation of intensity decays of different lifetimes resulting from droplets containing different numbers of quencher molecules. Analysis of the non-exponential decay yields the average number of quenchers per aggregate and hence the number of aggregates. Information on the dynamics of exchange of probe molecules between aggregates on the microsecond - nanosecond time scale can also be obtained. Several good reviews on time resolved fluorimetry as applied to surfactant colloidal systems have been presented in the literature (116 - 118).

The apparatus is shown schematically in Figure 2.5. Thermostatted one phase microemulsion samples are excited with a very short pulse of light (~1 ns) from a spark gap lamp operating at a repetition rate of between 10^4 - 10^5 Hz. The excitation wavelength chosen is a compromise in an attempt to optimise the output intensity of the lamp and the maximum in the probes excitation spectrum. The fluorescent radiation is selected through use of optical filters and detected at 90° to the incident radiation by a sensitive photomultiplier. The pulse of light from the flashlamp is detected by the photomultiplier (P.M.1) which provides a start pulse for the time-to-amplitude converter

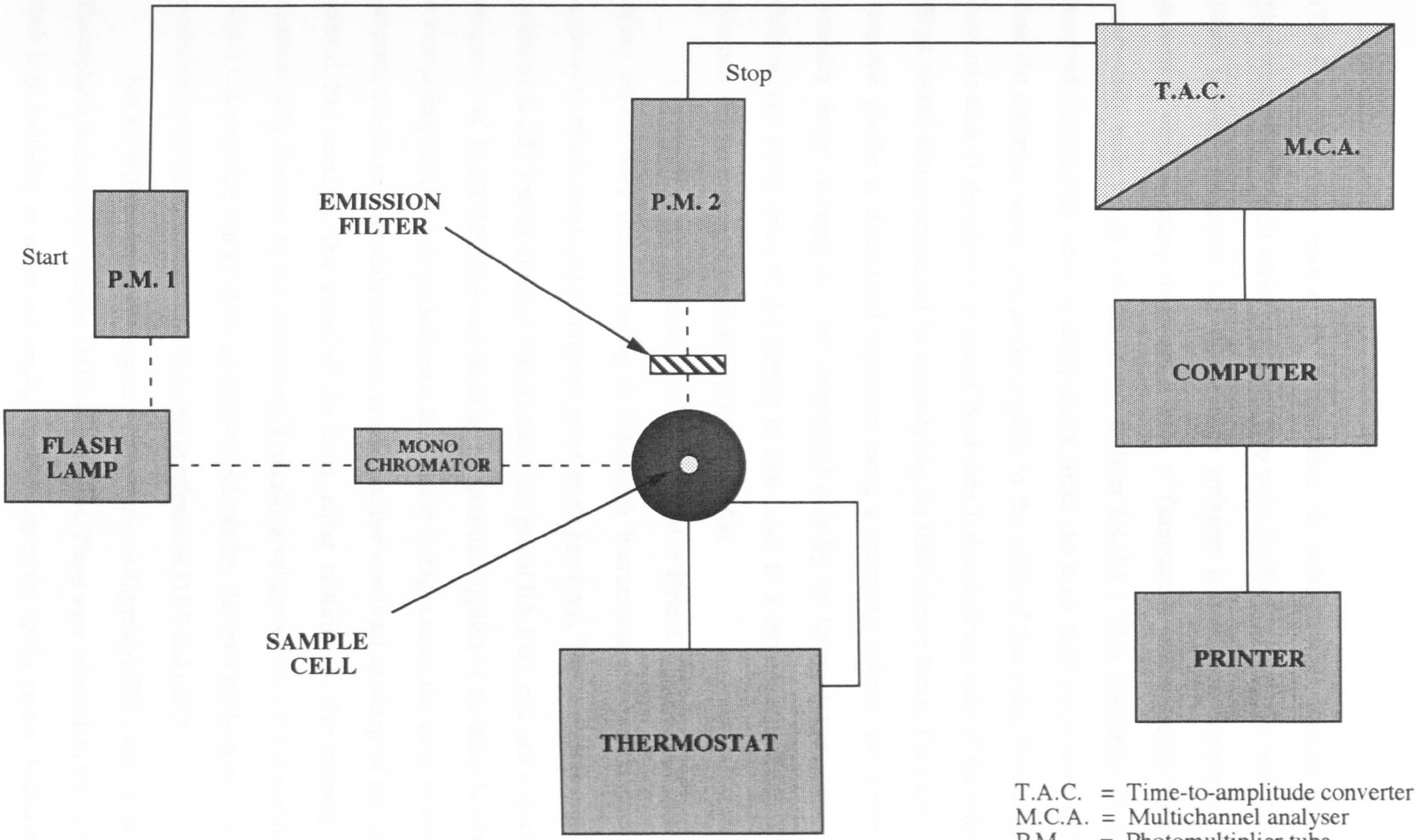

T.A.C. = Time-to-amplitude converter
M.C.A. = Multichannel analyser
P.M. = Photomultiplier tube

Figure 2.5

(T.A.C.). The first photon of fluorescence is subsequently detected by the photomultiplier (P.M.2) which provides a stop pulse for the T.A.C. In this way the time taken between excitation and fluorescence emission is accurately measured. This process is repeated many times and a trace of fluorescence intensity against time is continually built up on a multichannel analyser (M.C.A.). This represents the time-resolved fluorescence intensity decay curve. Since the lamp pulse exists over a finite time the observed decay is distorted slightly by the width of this pulse. Similarly, the response time of the photomultiplier ("dead-time"), despite being only of the order of 50 ps should also be accounted for on analysing the fluorescence decay. The instrument response profile is determined separately using a scattering solution for which the intensity decay characteristics are determined only by the instrument response. The fluorescence decay trace of the sample is then fitted to a convolution of the fitting function and the measured instrument response profile.

The experimental apparatus used is displayed in Plate 1. Fluorescence intensity decay curves were recorded using an Edinburgh Instruments 199 photon counting instrument which employed a thyratron gated spark gap lamp. The lamp was typically operated at 500 Torr of nitrogen with an electrode gap of 0.5 ± 0.1 mm and a sparking frequency of 30,000 Hz. The magnitude of the potential applied to the lamp is critical for obtaining stable running conditions. Insufficient voltage causes the lamp to misfire whereas excessive potentials produce an uncontrolled continual sparking of the lamp, termed free running. The status of the lamp, either misfiring or free running was electronically detected by the instrument. Typically a voltage of 3.3 kV was employed which just exceeded that at which the lamp would misfire. Reviews on the operation and optimisation of the instrument can be found in references (119) and (120).

For all W/O systems investigated, ruthenium tris-bipyridyl (RB) was chosen as fluorophore and methyl viologen (MV) as quencher. These were selected on the basis of their high solubility in water and negligible solubility in the apolar media. Additionally

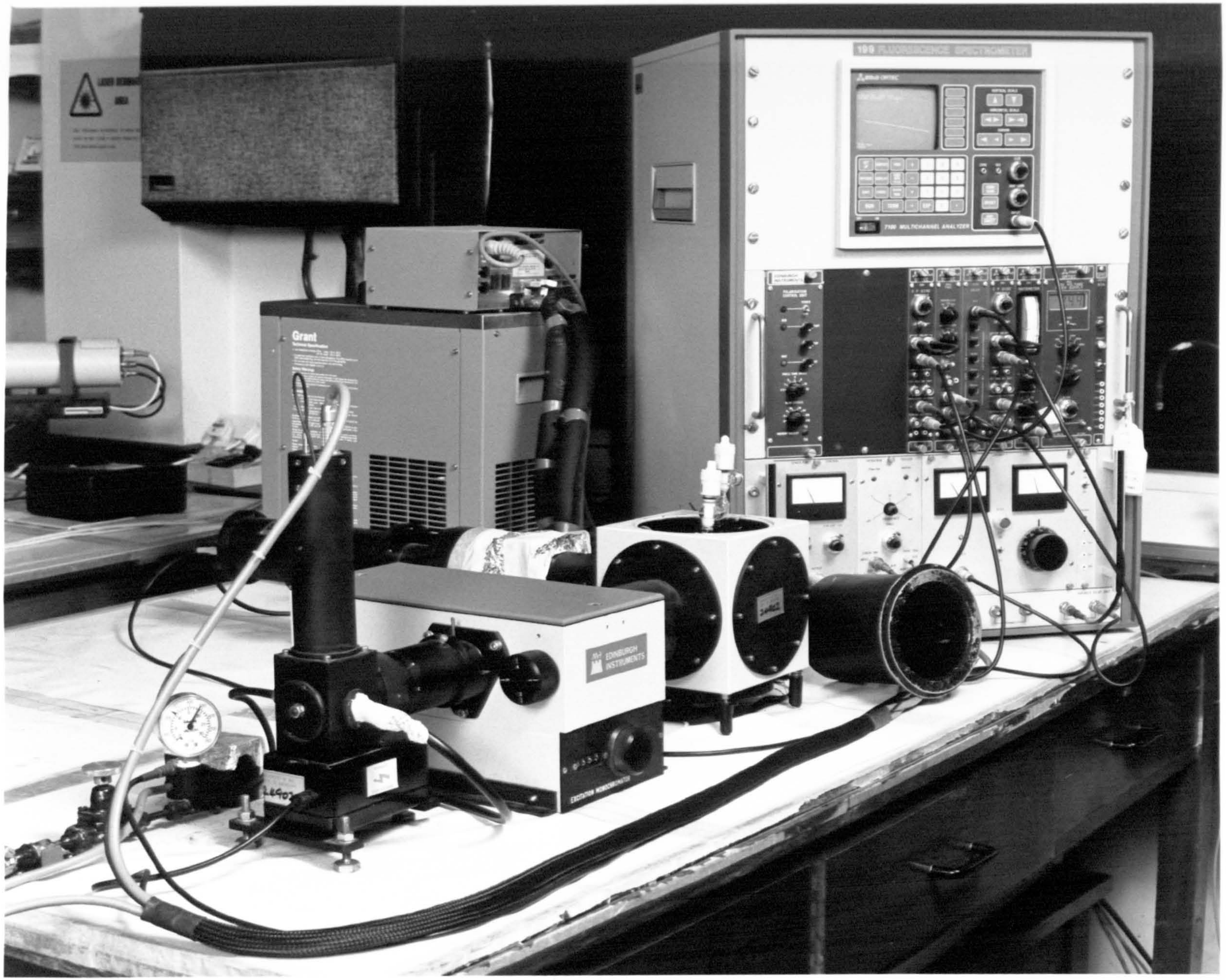
199 FLUORESCENCE SPECTROMETER
7100 MULTICHANNEL ANALYZER
Grant
EDINBURGH INSTRUMENTS
EXCITATION MONOCHROMATOR

Plate 1.

the fluorophore was chosen as it displays a long luminescence lifetime (0.58 μs at 25°C in water) (121). Samples were prepared by adding volumes of fluorescer and quencher from aqueous stock solutions to a solution of the oil containing the surfactant. The required volume of water was then added to give the desired final composition, R'_{water}. Typically, samples containing an average of 0, 1, and 2 quenchers per droplet were studied. Fluorophore concentrations were always less than 0.1 per droplet (on average). The one phase microemulsion sample was pipetted into the tubular arm of the fluorescence cuvette shown in Figure 2.6. Since oxygen is an efficient quencher of RB fluorescence (122), the samples were degassed via a minimum of 8 freeze-evacuate-thaw cycles using liquid nitrogen. The samples were then transferred into the quartz cuvettes through the use of the Youngs taps which allow transferral without the admission of air. Phase boundaries for each of the samples were determined and agreement was generally found to be within 1-2°C of previously determined boundary measurements. The degassed solutions were placed in the thermostatted spectrometer cell holder and allowed a minimum of 15 minutes to equilibrate to the pre-selected temperature which was controlled to within 0.2°C by an external water circulator.

Excitation was performed at 356 nm and fluorescent emission was selected using two long pass filters, supplied by Schott, which absorb light at wavelengths below 385 nm and 570 nm (Schott type GG 385, OG 570). Photon counting was started and continued until the peak channel registered approximately 10,000 counts. This typically took up to 30 minutes. The instrument response profile was then immediately determined by replacing the sample with a scattering solution containing colloidal silica (Ludox) and removing the emission filters. Sampling was again performed until 10,000 counts registered in the peak channel (typically < 2 minutes).

The fluorescence intensity decay curves were then computer fitted to a convolution of the theoretical function with the experimentally determined instrument response profile. The data analysis is described in more detail in Chapter 4.

Figure 2.6

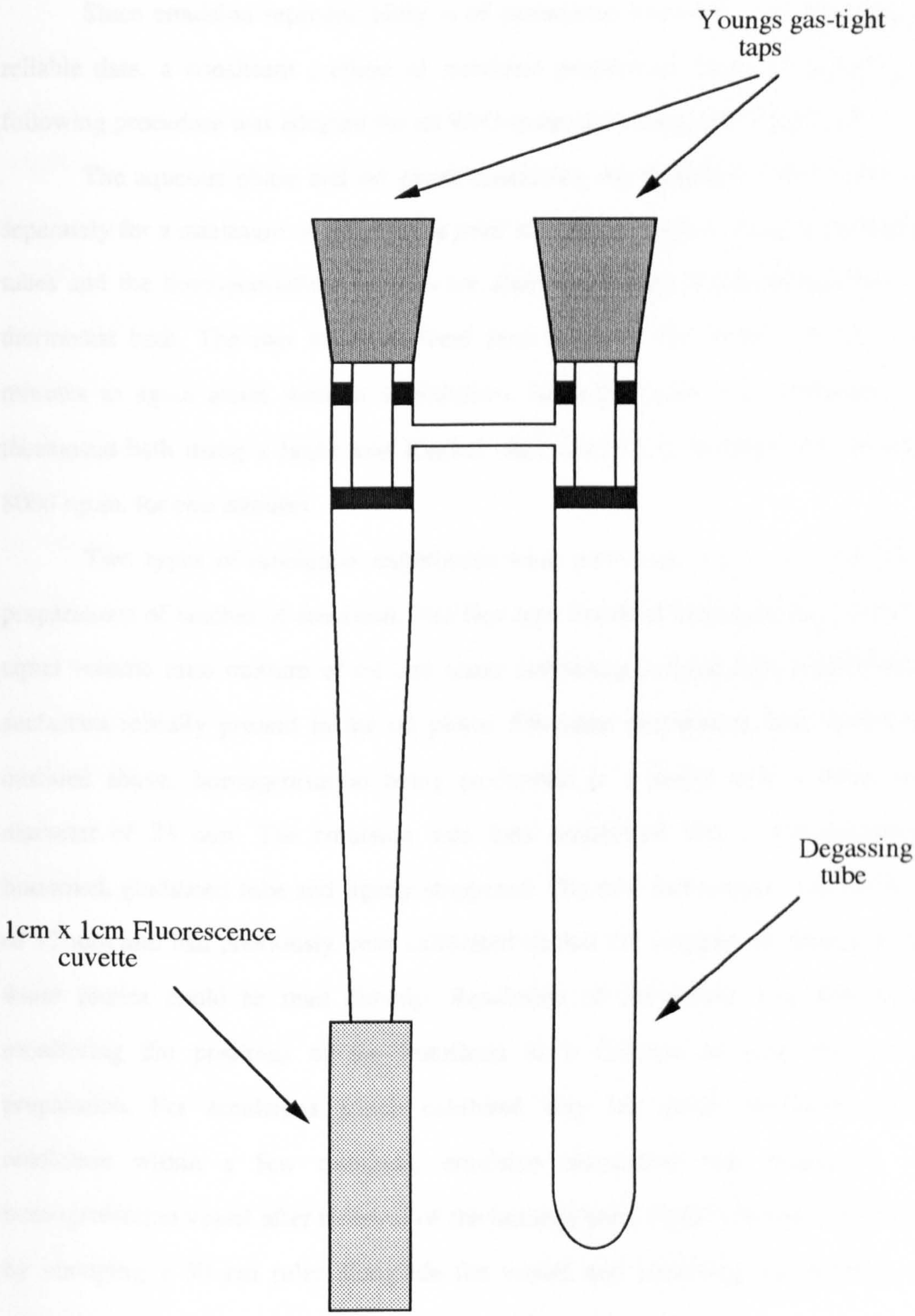
Youngs gas-tight taps
Degassing tube
1cm x 1cm Fluorescence cuvette

2.1.5 Emulsion experimentation.

Since emulsion reproducibility is of paramount importance for obtaining good reliable data, a consistent method of emulsion preparation must be employed. The following procedure was adopted for all W/O systems investigated in this work.

The aqueous phase and oil phase containing the surfactant were thermostatted separately for a minimum of 20 minutes prior to homogenisation. Each of the resolution tubes and the homogenisation vessel were also equilibrated at this temperature in the thermostat bath. The two solutions were then added to the vessel and allowed two minutes to again attain thermal equilibrium. Homogenisation was performed in the thermostat bath using a Janke and Kunkel ultra turrax T25 homogeniser operating at 8000 r.p.m. for two minutes.

Two types of resolution experiment were performed which involved different preparations of batches of emulsion. The first type involved homogenising 12 cm^3 of an equal volume ratio mixture of oil and water containing a fixed total concentration of surfactant initially present in the oil phase. Emulsion preparation was carried out as outlined above, homogenisation being performed in a vessel with a mean internal diameter of 23 mm. The emulsion was then transferred into a thermostatted, flat bottomed, graduated tube and tightly stoppered. The tube had a mean internal diameter of 15 mm and had previously been calibrated so that the volumes of separated oil and water phases could be read directly. Resolution of the phases was determined by monitoring the positions of the interfaces as a function of time after emulsion preparation. For emulsions which exhibited very fast phase resolution (complete resolution within a few minutes), emulsion breakdown was monitored in the homogenisation vessel after removal of the homogeniser. Phase volumes were recorded by clamping a 30 cm ruler alongside the vessel and observing the position of the

interfaces with time. Subsequently these readings were converted into volumes of the resolved phases.

The second type of resolution experiment performed involved adding small volumes of equilibrium microemulsion to portions of a stock emulsion. Initially 2 cm^3 samples of microemulsion of a fixed size but containing differing volume fractions of droplets were prepared and thermostatted at the experimental temperature. This temperature corresponded to the solubilisation boundary of the microemulsion samples. A large volume of a stock emulsion was prepared with a water to oil ratio of 3:2. Aliquots of this stock emulsion were then used to investigate the effect of added microemulsion droplets. The volume of added microemulsion was chosen such that an approximately equal phase volume ratio was maintained in each emulsion sample after addition of the microemulsion droplet solution. The mixing of the microemulsion with the emulsion was performed in the following way. Firstly, two separate 5 cm^3 portions of the emulsion were added to each tube. Secondly, the 2 cm^3 portions of microemulsion solution were then added to each tube in turn, stoppered, and given six inversions before immediately returning to the thermostat. This procedure was designed to allow complete mixing of the microemulsion sample with the emulsion such that the average emulsion droplet size was unchanged. Phase resolution was monitored as described above.

For emulsion resolution experiments performed in the presence of protein the latter technique described above was adopted. The aqueous phase in this case contained the protein in a 50 mM buffer solution. Following emulsification, 2 cm^3 of equilibrium microemulsion containing dispersed protein was added to each tube and resolution monitored.

Estimation of emulsion droplet sizes was performed at various stages during the resolution experiments. The technique used was that of optical microscopy. Small samples (< 0.2 cm^3) were carefully extracted from the middle of the emulsion with a

Pasteur pipette and spotted onto a clean microscope slide. A raised coverslip was positioned over the sample being bridged at either end by coverslip spacers (approximately 0.2 mm clearance). This prevented the droplets being compressed which could give rise to a possible erroneous size distribution. The slide was mounted on a Linkam (model C060) temperature controlled microscope stage and the droplets were viewed at 100 x magnification through a Nikon Labophot microscope. Photographs were taken with a top mounting Pentax 35mm S.L.R. camera operating in automatic mode. After comparison with a calibration graticule (National Physical Laboratory, model 034) viewed under the same conditions, a very approximate determination of the average emulsion drop size was possible.

2.1.6 Density measurements.

Absolute values of sample density were determined using a Paar DMA 55 densimeter thermostatted using a Haake F3 thermostat. Density values were obtained to ± 0.00001 g cm^{-3} over a range of temperatures. Calibration was performed at each temperature using values for the density of water and air taken from reference (123).

2.1.7 Viscosity measurements.

Kinematic viscosities were determined for the various alkanes and alkane/surfactant solutions using a selection of Ubbelohde viscometers of different capillary diameters. These were suspended vertically in a stirred, thermostatted water bath, the temperature of which was controlled to within 0.1°C. Each viscometer was calibrated by measuring the outflow times for pure water at each temperature. The

appropriate viscometer was chosen so as to give an outflow time for each sample in excess of 150 seconds. The uncertainty in the final viscosity was typically < 0.3%. Viscosities were obtained from the kinematic viscosities using measured density values or values from reference (123).

2.1.8 Measurement of refractive index.

Refractive index was determined as a function of temperature through the use of a thermostatted Abbe refractometer and sodium lamp. The precision of refractive index values (at λ = 589 nm, Sodium D line) determined in this way was estimated to be $\pm$ 0.0001.

2.1.9 Measurement of the conductivity of emulsions.

Conductivities of emulsions were measured with a Jenway PCM 3 conductivity meter. Samples were thermostatted in a water bath and continuously stirred using a magnetic bar. Since the purpose of this measurement was to determine the nature of the emulsion formed (i.e. W/O or O/W), conductivity values to within $\pm$ 30% were acceptable.

2.1.10 Analysis for water.

Water contents in one phase W/O microemulsion samples were determined by Karl Fischer titrations (124) using a Baird and Tatlock AF3 auto-titrator. Calibration of

the titrator using known volumes of water was performed immediately prior to use as the Karl Fischer reagent (B.D.H. improved) degraded slowly with time. For W/O microemulsion phase analysis, known volumes of the oil were injected rapidly into the titration vessel and a digital readout of the water content (in mg) was produced at the end of the titration. A minimum of three separate determinations were performed for each solution. Reproducibility between duplicate determinations was generally better than ± 2% or ± 0.2 mg water which ever was the greater. The calibration was re-checked at the end of a series of measurements.

2.1.11 Preparation of glassware.

All glassware was intially rinsed with tap water before immersing in concentrated chromic acid for a minimum of four hours. On removal, it was thoroughly washed in hot water followed by two final rinses in pure water. Drying was achieved using a laboratory oven operating at 65°C.

2.2 Materials.

2.2.1 Surfactants.

Table 2.1 lists the surfactants used in this study with their respective supplier and reported purity. Span 20, Tween 20 and Triodan 20 were commercial samples containing mixtures of several homologues. They were used as received. The predominant component of each sample is shown in Figure 2.7. It has been shown by high pressure liquid chromatography that Span 20 and Tween 20 samples typically contain only approximately 50% of the monoester shown with significant proportions of the di- and tri- esters (125).

The general structure of the pure polyoxyethylene alkyl ethers used in this work is also shown in Figure 2.7. Gas-liquid chromatographic analysis of the samples showed only a single peak in each case and measured cloud points were found to be in good agreement (within 0.2°C) with the best literature values as shown in Table 2.2. For these reasons the surfactants were used as received.

2.2.2 Hydrocarbons.

The series of hydrocarbons used in this work is shown in Table 2.3. Purities were generally in excess of 99% and an additional purification was achieved by passing each through a chromatographic alumina column (B.D.H., Brockmann grade 1) to remove traces of polar impurities. The long chain length triglyceride oil (LCT) investigated contained tri-cis-cis-linolein as the predominant species (126). It was marketed as a "pure" sunflower oil, containing no added preservatives or antioxidants. Samples were twice passed through alumina columns prior to use. The medium chain length triglyceride oil (MCT) was provided by Unilever (Colworth). It was stated as

Figure 2.7

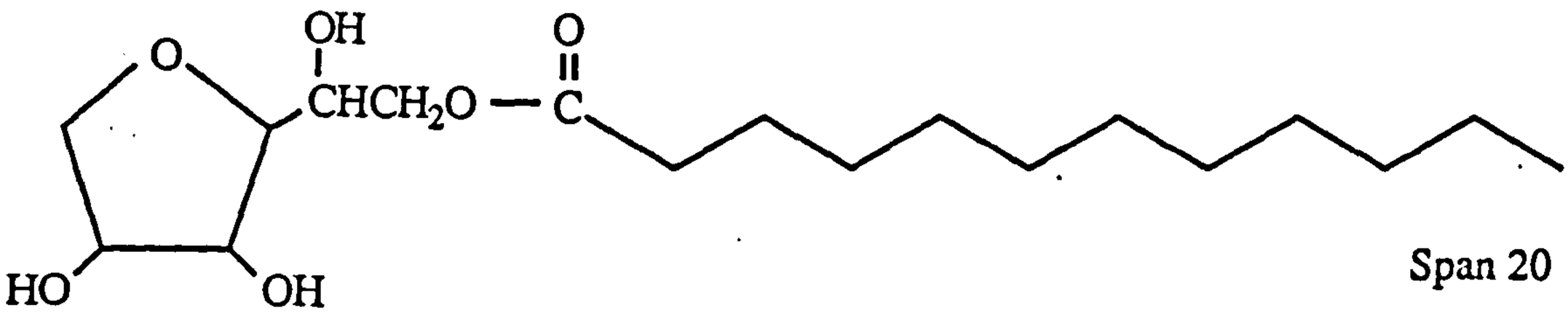

Span 20

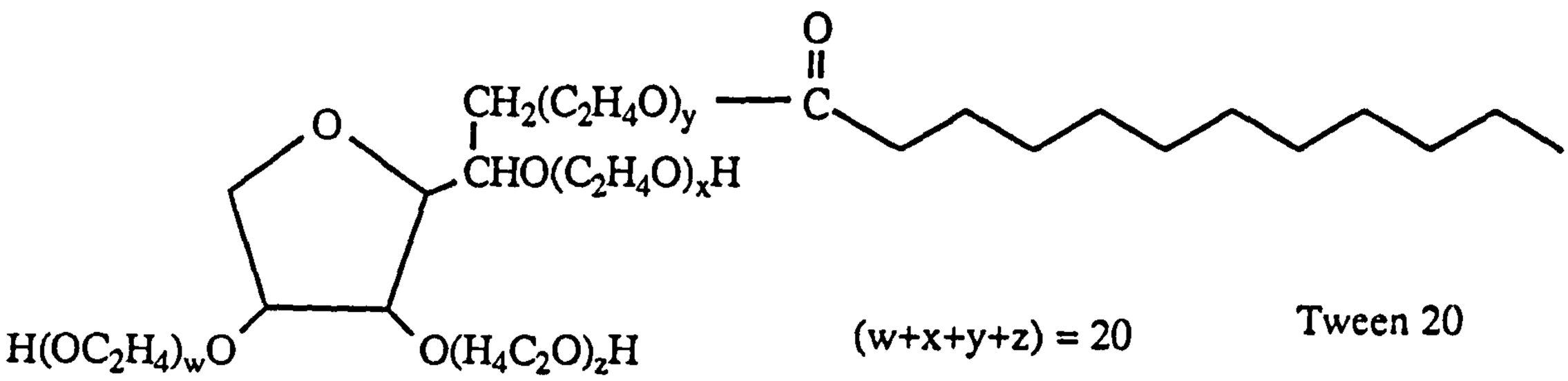

Tween 20

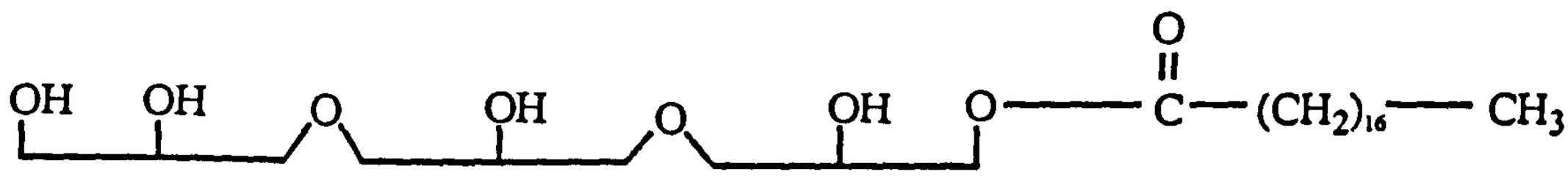

Triodan 20

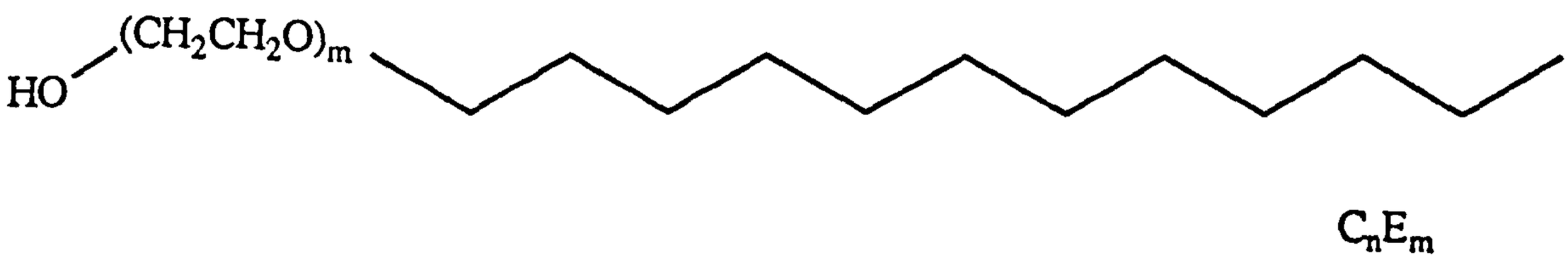

C_nE_m

containing esterified octanoic and decanoic acid in an approximate ratio 3:2. It contained no added antioxidants, preservatives or colourings and was also columned twice before use. Compositional analysis has previously been performed for this oil by Andrangui *et al.* (127). The following compositional results were found.

Chain length	Content /%
Hexanoic	3 max
Octanoic	50 - 65
Decanoic	30 - 45
Dodecanoic	5 max

2.2.3 Inorganic salts.

A list of inorganic salts used in this work is given in Table 2.4 along with the manufacturers specified purity. All were used as received.

2.2.4 Proteins.

The three proteins investigated are listed in Table 2.5 along with their purity and supplier. All three were used in 50 mM buffer solutions and these are listed in Table 2.6 along with their corresponding pH values. Also tabulated are the isoelectric point, relative molecular mass and tertiary structure of each protein.

2.2.5 Water.

Water used throughout this work was distilled, passed through an Elgastat ion-exchange column and finally passed through a Milli-Q reagent water system. Conductivity of the water was determined to be < 0.6 nS m^{-1}. The measured value of the air-water surface tension at 25°C of 71.9 ± 0.1 mN m^{-1} was in agreement with the best reported literature values (123, 128). This demonstrated the absence of surface active species which is of prime importance in this work.

Table 2.1

Name	Purity /%	Supplier
Span 20	unspecified	Sigma Chem. Co.
Tween 20	unspecified	Sigma Chem. Co.
Triodan 20	unspecified	Grindsted
C_8E_3	>98.0	Bachem Co.
$C_{10}E_4$	>98.0	Nikko Chem. Co.
$C_{12}E_4$	>98.0	Nikko Chem. Co.
$C_{12}E_5$	>98.0	Nikko Chem. Co.

Table 2.2

Surfactant	Conc /wt%	C.P.(expt) /°C	C.P.(lit) /°C (ref)
C_8E_3	1.0	11.6	11.8 (129)
$C_{10}E_4$	1.0	20.3	20.5 (129)
$C_{12}E_4$	0.5	6.8	7.0 (40)
"	1.0	6.6	6.6 (129)
$C_{12}E_5$	1.0	31.8	32.0 (129)

Table 2.3

Name	Purity /%	Supplier
Hexane	>99.5	Fluka
Heptane	>95.0	Fisons
Octane	>99.5	Fluka
Decane	>99.0	Fluka
MCT (miglyol 812)	unspecified	Dynamit Nobel
LCT (sunflower oil)	unspecified	Flora

Table 2.4

Name	Purity /%	Supplier
NaCl	99.9	B.D.H.
NaH_2PO_4	>99.0	B.D.H.
Na_2HPO_4	>99.0	B.D.H.
Glycine	>99.0	Sigma Chem. Co.
Methyl viologen	~98	Sigma Chem. Co.
$Ru(bipy)_3$	~98	Sigma Chem. Co.

Table 2.5

Name	Purity /%	Supplier
α-chymotrypsin (Bovine pancreas type II)	85-90	Sigma Chem. Co.
Bovine serum albumin (Fraction V)	96-99	Sigma Chem. Co.
Sodium caseinate	unspecified	Unilever (Colworth)

Table 2.6

	α-chymotrypsin	B.S.A.	Na caseinate
Type	Globular	Globular	Disordered
R.M.M.	24,800	67,000	~24,000
pI (ref)	8.2 (130)	4.7 (131)	~5.0 (132)
Buffer	Glycine	$HPO_4^{2-}/H_2PO_4^-$	$HPO_4^{2-}/H_2PO_4^-$
pH	9.0	7.0	7.0

3. SOLUBILISATION AND HLB

IDEAS FOR COMMERCIAL FOOD

EMULSIFIERS.

CHAPTER 3.

3.1 Introduction.

Emulsion formation and subsequent stability is strongly dependent upon the type of emulsifier that is employed. Ideally, emulsifiers should lower the interfacial tension between the two phases facilitating emulsion formation, and the adsorbed interfacial layer should inhibit the breakdown mechanisms previously discussed in Chapter 1. In the food industry, commonly used emulsifiers include proteins, polysaccharides and low molar mass nonionic surfactants such as monoglycerides and sorbitan esters (60). The low molar mass surfactants are used typically as complex mixtures of several homologues. Usually combinations of different types of emulsifiers are employed to obtain the desired degree of stability / instability in the final product.

As mentioned earlier, surfactants with low HLB values are effective in stabilising W/O emulsions whereas O/W emulsions are stabilised by surfactants with high HLB values. However, the type of emulsion produced has also been shown to be dramatically influenced by the nature of the solution conditions (133). For example, the nature of the oil phase, temperature, salt concentration, addition of cosurfactant and phase volume ratio can all individually or collectively alter the type of emulsion produced. This was interpreted in terms of a system HLB for the surfactant *in situ* within the total oil/water mixture. Changes in this system HLB value have been correlated with changes in microemulsion formation which, in turn, are related to changes in the spontaneous curvature of the surfactant monolayer as previously discussed in section 1.3.1 (134 - 137). Pure nonionic surfactants with low HLB values, have been shown to form small, W/O microemulsion aggregates of high negative spontaneous curvature. Similarly, those with high HLB values, form small, O/W aggregates of high positive spontaneous curvature. Combining two surfactants of contrasting HLB values enables microemulsion droplet size and hence solubilisation to

be maximised by varying the surfactant composition (138, 139). Similar results can also be achieved through varying the salinity of the aqueous phase, a maximum solubilisation being attained at a particular salt concentration (140, 141).

The objective of this study was to investigate whether the solubilisation behaviour of W/O microemulsions formed with commercial, low molar mass, nonionic surfactants of known HLB values, was consistent with that known for pure nonionic surfactant systems. To this end, the effect of mixing surfactants with low and high HLB values has been investigated, together with the effect of changing the salinity of the dispersed phase. The three commercial surfactants investigated are listed below with their corresponding HLB values (142).

Table 3.1

Surfactant	HLB
Triodan 20	7.1
Span 20	8.6
Tween 20	16.7

3.2 Effect of Hydrophilic - Lipophilic Surfactant Mole Ratio on the Solubilisation of Water in Heptane.

3.2.1 Effect of Tween 20 on the excess water solubilisation boundary formed with Span 20 and Triodan 20.

As was shown by Boyd *et al.* (92), mixtures of Spans and Tweens form mixed monolayers at the oil-water interface. Vincent and coworkers later extended these findings and demonstrated the formation of W/O microemulsions with an equimolar

mixture of Span 80 and Tween 80 in cyclohexane (143). The subsequent stability of the corresponding W/O macroemulsions was found to exceed that of those formed with either Span 80 or Tween 80 alone.

The effect of Span 20 : Tween 20 mole ratio on the position of maximum water solubilisation (i.e. the excess water solubilisation phase boundary) at 25°C in heptane is shown in Figure 3.1. The assumed molecular weights of Span 20 and Tween 20 are 346 and 1210 respectively which correspond to the predominant components of each surfactant mixture. R_{water} is defined here as the mole ratio of dispersed water to total surfactant in the system. As can be seen, Span 20 alone solubilises little water under these conditions, however, upon addition of Tween 20 into the system solubilisation is much enhanced. This effect is consistent with that expected for pure nonionic surfactants. Span 20 (a low HLB surfactant) solubilises little water which is consistent with the formation of small, highly negatively curved, W/O aggregates. Upon addition of Tween 20 to the system, the surfactant coadsorbs at the interface producing a mixed monolayer. The increase in solubilisation is consistent with the notion that the larger effective head group area of the Tween molecule produces a decrease in the preferred curvature of the monolayer and hence a larger microemulsion droplet size.

At the solubilisation boundary, if a significant fraction of the total surfactant concentration remains in the oil phase as monomers the R_{water} value will be expected to change with surfactant concentration. In such instances, if the total surfactant concentration is low the R_{water} value would be expected to be small. Since this is not observed in Figure 3.1 it can be presumed that the concentration of non-adsorbed lipophilic surfactant is probably less than approximately 50 mM.

Increasing the Tween content beyond that necessary for microemulsion formation produces a viscous, birefringent mixture which contains some separated liquid crystalline phase. Since the addition of Tween promotes a shift towards zero monolayer curvature, it appears likely that this phase is lamellar in structure.

Figure 3.1.

Effect of Tween 20 on the excess water solubilisation boundary for different initial Span 20 concentrations in heptane at 25.0°C.

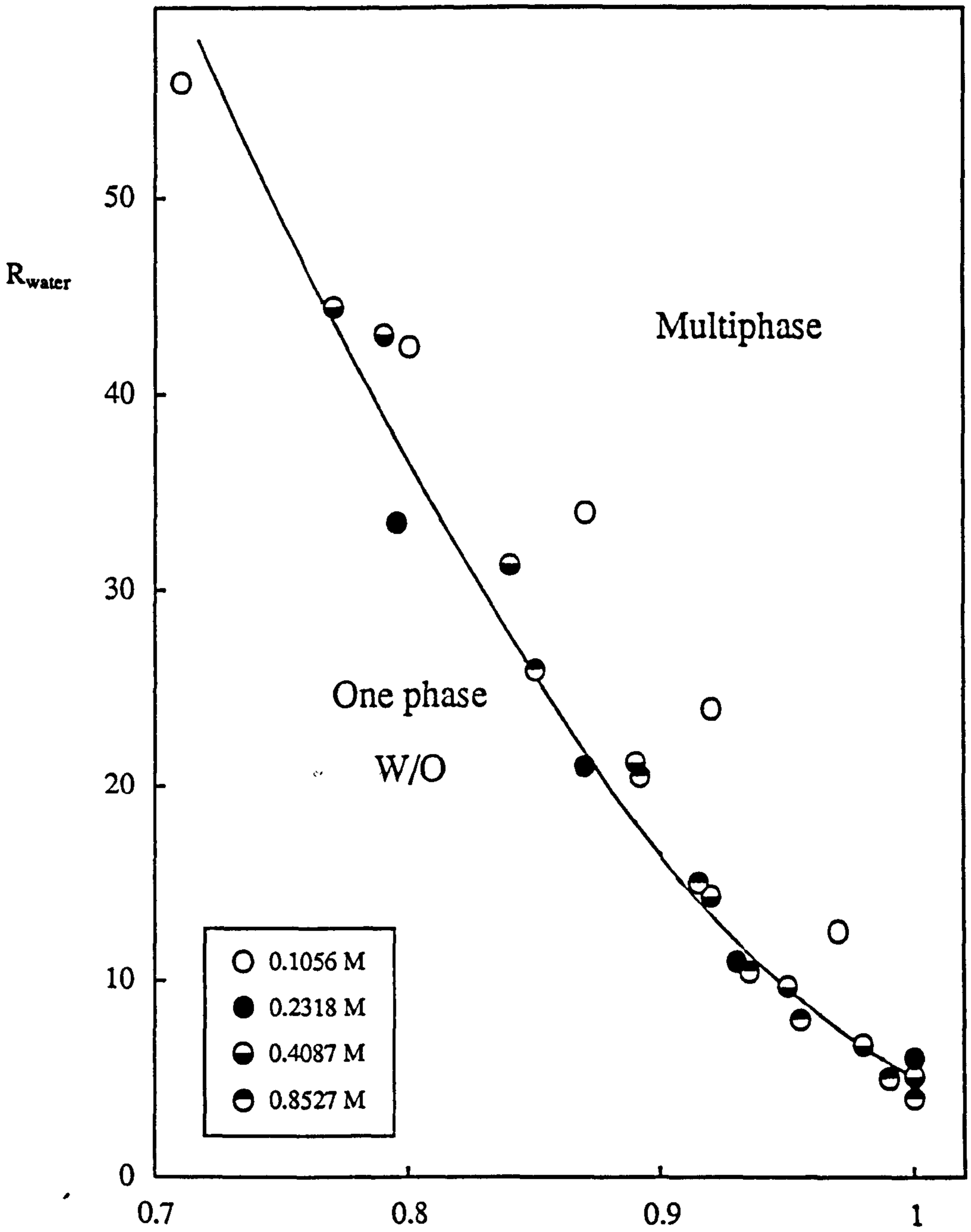

Figure 3.2 shows the similar solubilisation profile with Triodan 20 replacing Span 20. The assumed molecular weight of the lipophilic surfactant is 506. Changing the nature of the lipophilic surfactant has had little effect on the solubilisation curve. It is tempting to interpret this behaviour as indicating that the effective head group areas of both Span 20 and Triodan 20 are similar. However, since both surfactants are complex mixtures of mono-, di- and tri-esters the overall geometrical situation is likely to be more complicated.

3.2.2 Effect of SDS on the excess water solubilisation boundary formed with Span 20 and Triodan 20.

Figures 3.3 and 3.4 show the effects of SDS (a high HLB surfactant) on the solubilisation profile formed with the low HLB surfactants Span 20 and Triodan 20 respectively. It can be seen that for both systems the addition of SDS enhances solubilisation. Again, this is consistent with the SDS molecule coadsorbing at the interface forming a mixed monolayer as in the case of Tween 20. However, it is clear that a greater mole fraction of SDS is required to bring about an equivalent amount of solubilisation as that produced by Tween 20. This is consistent with the Tween molecule having either a larger effective head group area or a smaller effective tail group area than the SDS molecule.

A similar study was performed by Johnson and Shah (144) with Span 20 and the twin tailed, anionic surfactant di-ethylhexyl sodium sulphosuccinate (AOT). They found that stable one phase microemulsion regions could be produced in hexadecane with this surfactant system. A maximum water to total surfactant mole ratio of 50 could be obtained with a Span 20 mole fraction of 0.56. It appears therefore, that SDS in heptane and AOT in hexadecane have similar effects on the curvature of monolayers of Span 20.

Figure 3.2.

Effect of Tween 20 on the excess water solubilisation boundary for two initial Triodan 20 concentrations in heptane at 25.0°C.

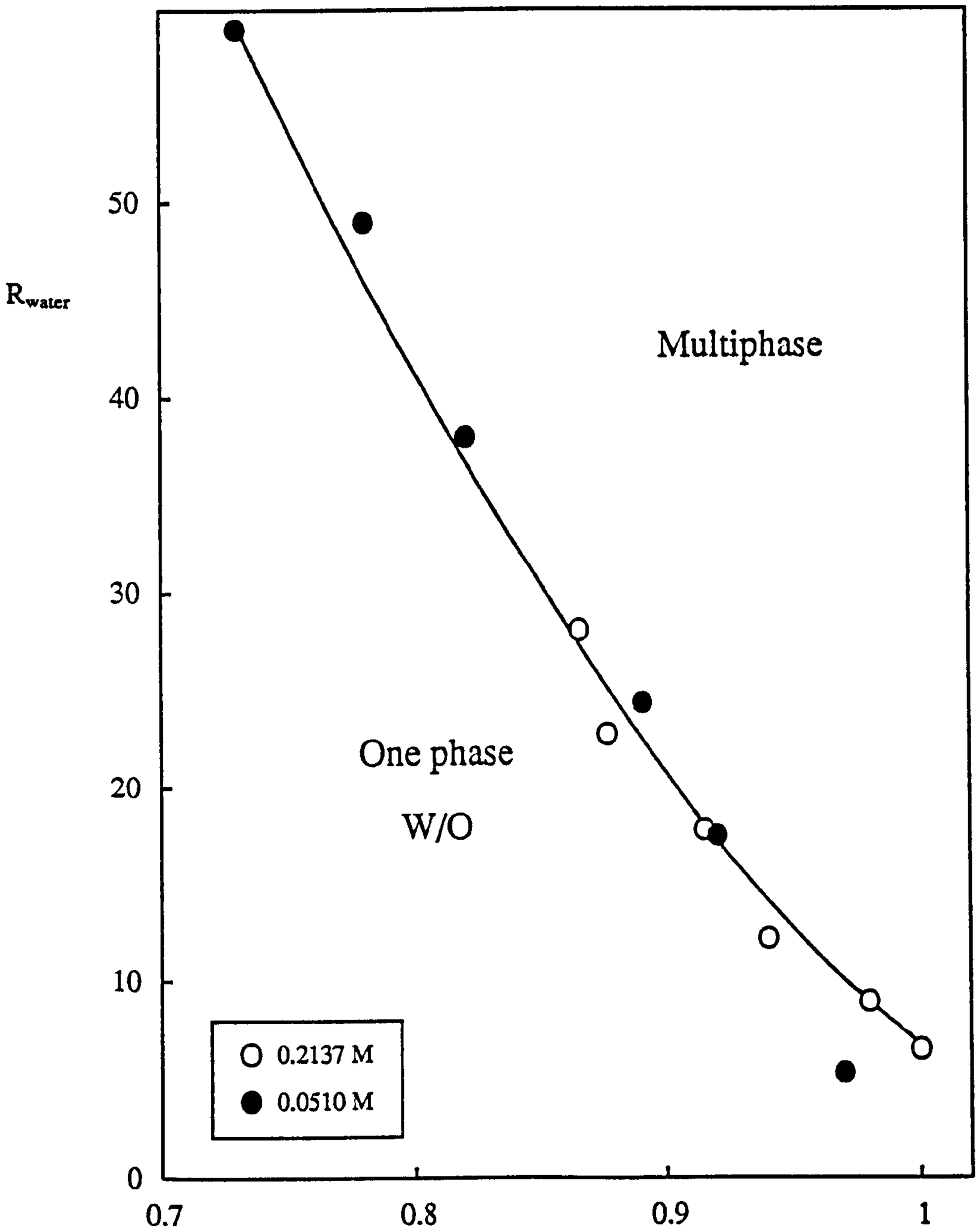

Figure 3.3.

Effect of Tween 20 and SDS on the excess water solubilisation phase boundary for 0.4 M Span 20 in heptane at 25.0°C.

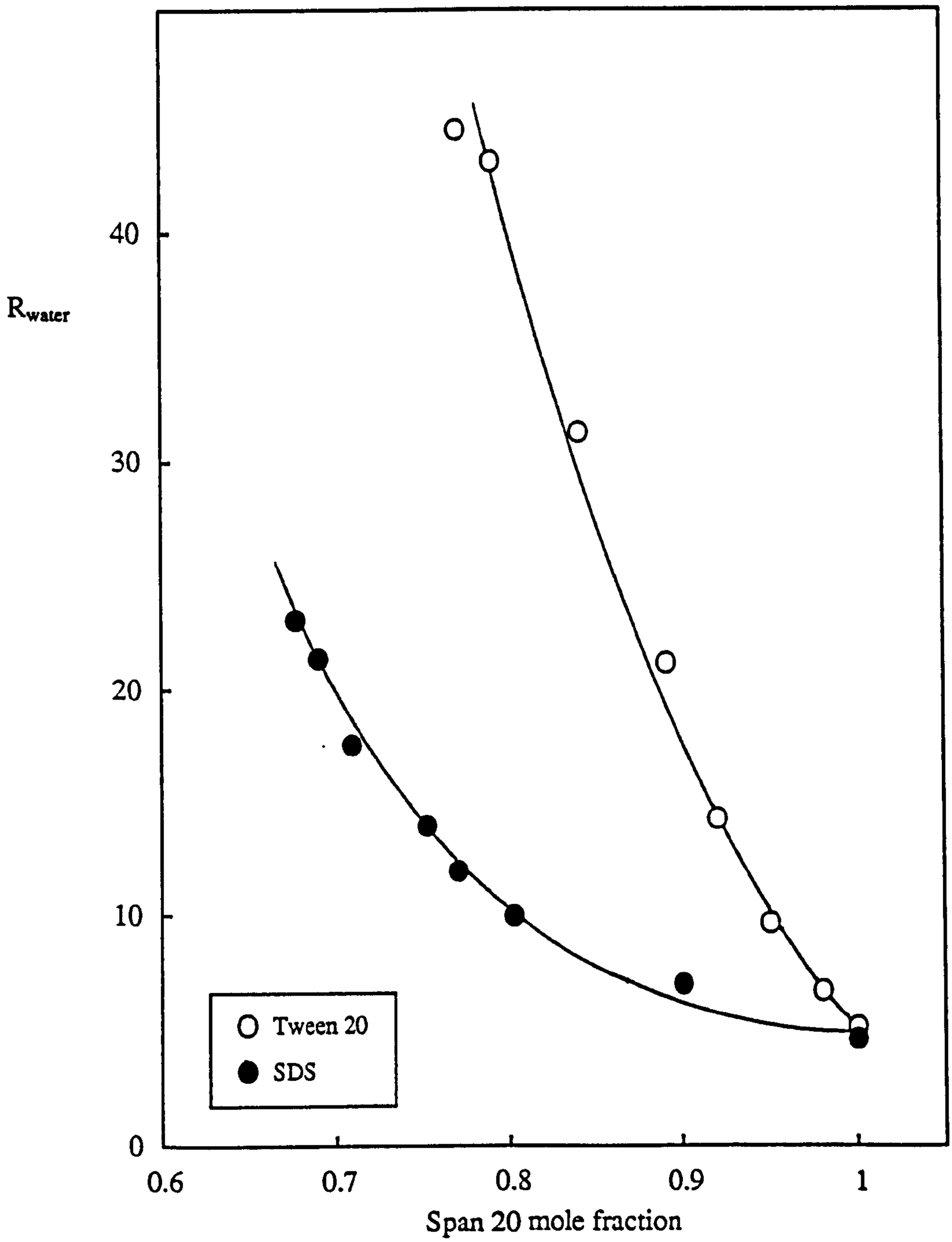

Figure 3.4.

Effect of Tween 20 and SDS on the excess water solubilisation boundary for 0.05 M Triodan 20 in heptane at 25.0°C.

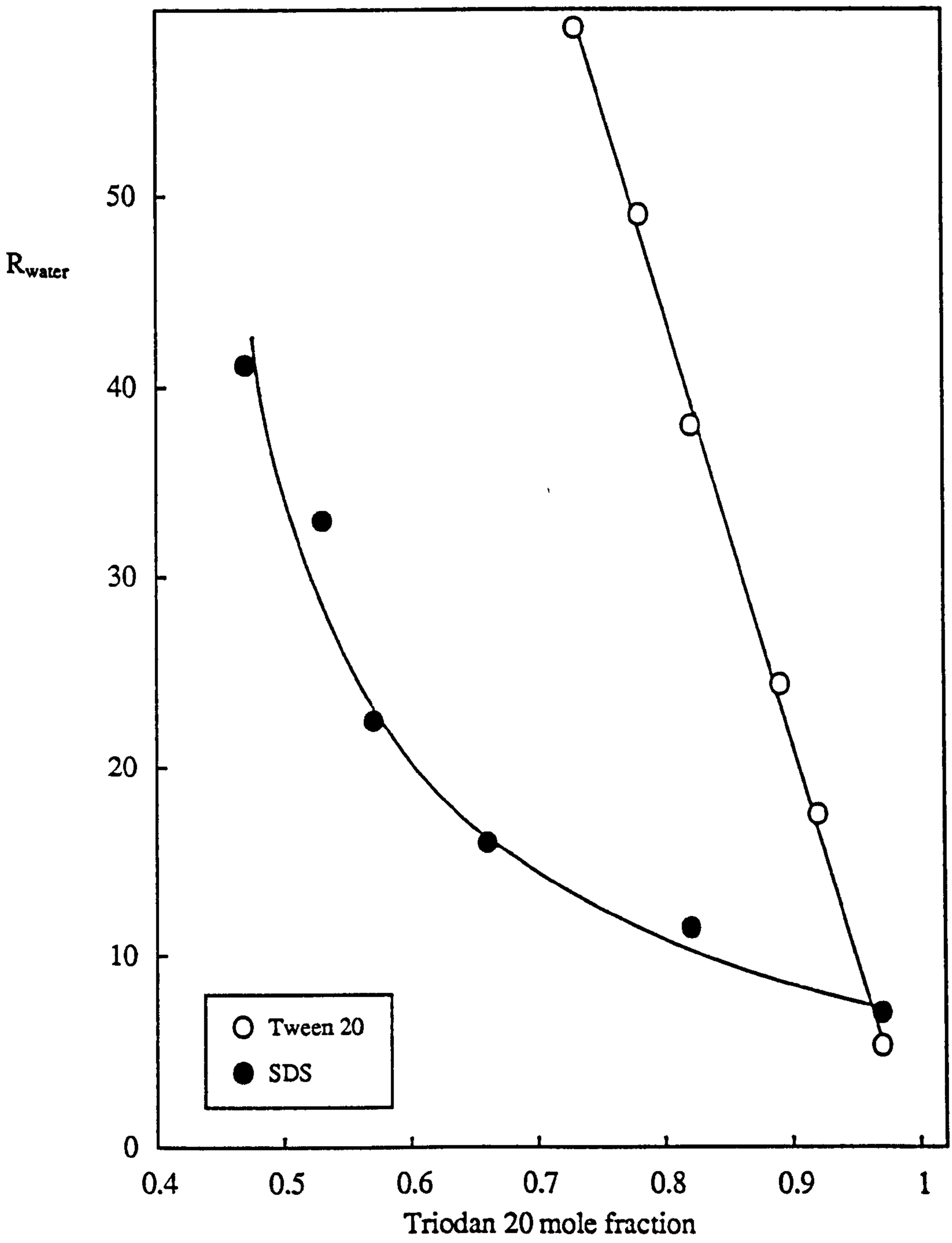

3.3 Effect of Aqueous Sodium Chloride on the Solubilisation Profile for Span 20 / Tween 20 Mixtures in Heptane at 25°C.

Determination of the phase boundary with 2 M sodium chloride as the aqueous phase dramatically shifts the solubilisation profile as can be seen in Figure 3.5. Span 20 alone solubilises negligible amounts of the aqueous phase and, to produce an equivalent solubilisation to that of pure water, large quantities of Tween 20 must be added in the case of the 2 M salt solution.

A shift in the solubilisation boundary to higher Tween contents for an increase in salt concentration, is consistent with the salt reducing the effective surfactant head group area or increasing the area occupied per surfactant tail at the interface. As discussed in the Introduction, salt addition is expected to reduce the effective head group area producing a shift towards more negative spontaneous curvature. This interpretation is consistent with larger concentrations of Tween 20 being required to bring about solubilisation.

3.4 Conclusions

It is clear from this brief study of commercial nonionic surfactants that these complex mixtures behave similarly, (at least with regard to water solubilisation) to pure nonionic surfactants described in the literature (138, 141, 145). However, commercial surfactant mixtures have severe disadvantages as systems for fundamental surfactant studies. Firstly, they are complex, poorly characterised mixtures. Secondly, equilibrium phase resolution of oil and water from emulsions containing these surfactant mixtures was extremely slow (typically taking longer than several weeks). Since these initial solubilisation studies did not indicate the behaviour of these mixtures to be peculiar or

Figure 3.5.

Effect of Tween 20 on the excess water solubilisation boundary, in the presence of 2.0 M NaCl solution for 0.4 M Span 20 in heptane at 25.0°C.

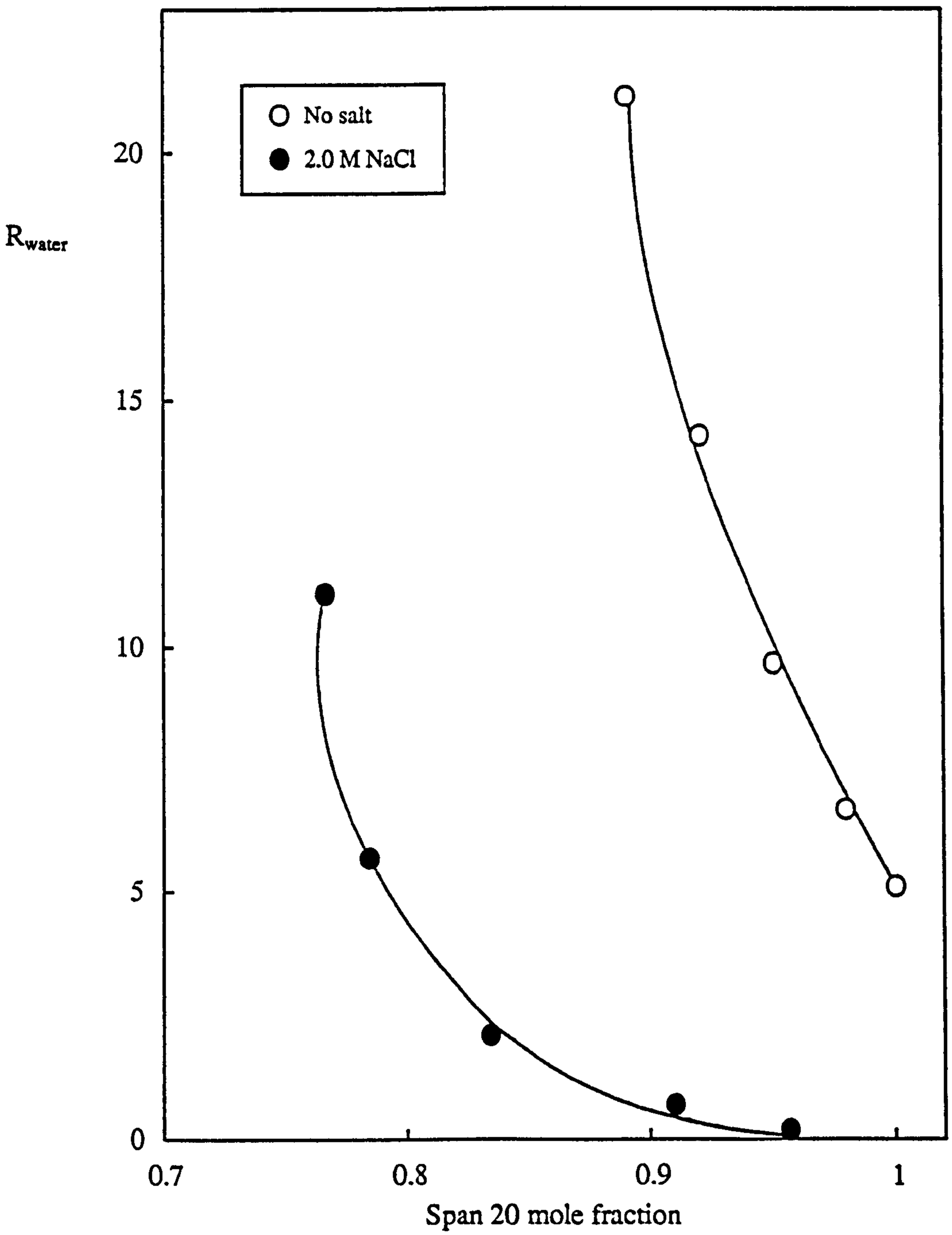

specific, it was decided to use the more amenable, pure nonionic surfactants of the type C_nE_m for all subsequent studies described in this thesis.

4. CHARACTERISATION OF MICROEMULSION SYSTEMS CONTAINING $C_{12}E_4$ + ALKANE + WATER.

CHAPTER 4.

4.1 Introduction.

There is continuing interest in the relationship between equilibrium microemulsion formation and macroemulsion stability (146). As discussed, factors which govern microemulsion properties may be expected to affect macroemulsion type and stability. The present approach of studying microemulsion phases allows the measurement of equilibrium properties of surfactant monolayers which are likely to be important in determining emulsion stability. Importantly, the surfactant is not considered in isolation; rather, the properties of the surfactant monolayer *in situ* at the interface between the relevant oil and water phases are determined.

In this chapter, the phase boundaries for microemulsions formed with the pure nonionic surfactant tetra-oxyethylene mono-n-dodecyl ether, $C_{12}E_4$ are presented. The effects of temperature, oil chain length and salt concentration are considered. An account of the solubilisation of protein into the dispersed aqueous phase of water-in-oil microemulsions is also presented. Subsequently, interfacial tensions and microemulsion droplet sizes are given from which an approximate estimation of the monolayer rigidity is made. The implications of this value are considered and results of a study of microemulsion dynamics are presented.

4.2 Microemulsion Phase Behaviour for $C_{12}E_4$ + Alkane + Water Systems as a Function of Temperature.

The phase behaviour of nonionic surfactants has previously been extensively investigated by various authors and it represents the fundamental starting point for most microemulsion studies (31, 34, 147).

Figures 4.1 and 4.2 show the extent of the single phase oil-in-water (O/W) and water-in-oil (W/O) microemulsion regions with respect to temperature for heptane as the oil phase. The amount of solubilised oil or water is expressed as the molar ratio of dispersed component to total surfactant.

R_{oil} = [alkane] / [surfactant] for O/W

R_{water} = [water] / [surfactant] for W/O

Single phase O/W microemulsion regions formed with nonionic surfactant, are bound at low temperatures by the solubilisation boundary at which separation of an excess oil phase occurs, and at higher temperatures by the cloud point curve at which a surfactant-rich phase separates. For W/O microemulsion regions, the solubilisation boundary forms the upper temperature boundary and corresponds to the separation of an excess aqueous phase, and the so-called "haze-point" curve marks the lower temperature boundary at which a surfactant-rich phase separates. The solubilisation curves are thought to be determined primarily by the spontaneous curvature of the surfactant monolayer (134), and the observed changes correspond to an increased tendency towards more negative curvature with increasing temperature. This result has been noted previously for other homologues in the C_nE_m series and is consistent with an interpretation in terms of a dehydration of the ethylene oxide head group or an increase in solvent penetration into the surfactant tail region on increasing temperature (29, 31, 148). The cloud and haze point boundaries are thought to be determined by increasing attractive interactions between microemulsion droplets on moving away from the solubilisation phase boundary (29, 134).

The position of the phase boundaries has been determined at different surfactant concentrations. For O/W microemulsions, the position of the excess oil solubilisation

Figure 4.1.

One phase O/W microemulsion stability region for $C_{12}E_4$ + heptane + water as a function of surfactant concentration in the aqueous phase.

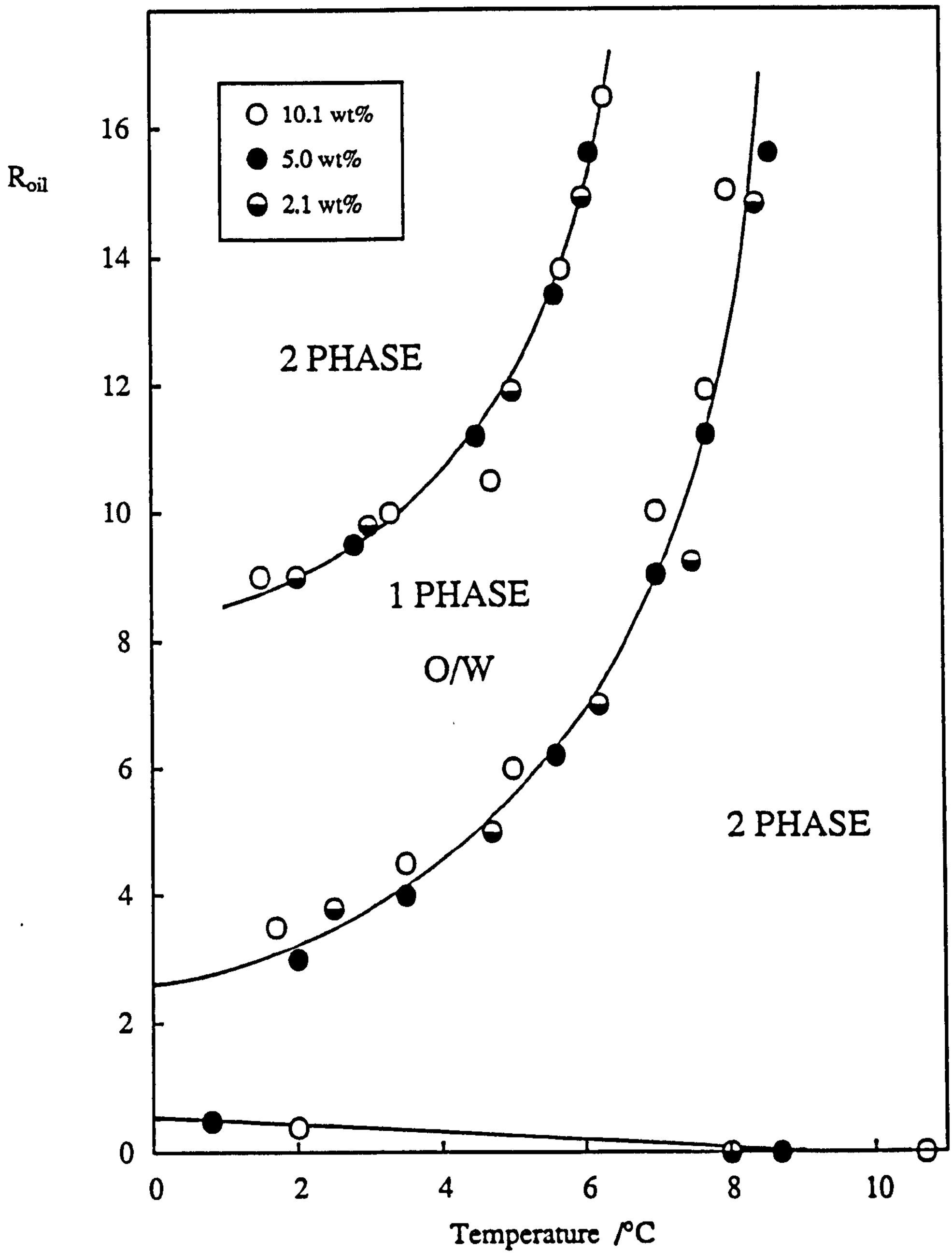

Figure 4.2.

One phase W/O microemulsion stability region for $C_{12}E_4$ + heptane + water as a function of surfactant concentration in the oil phase.

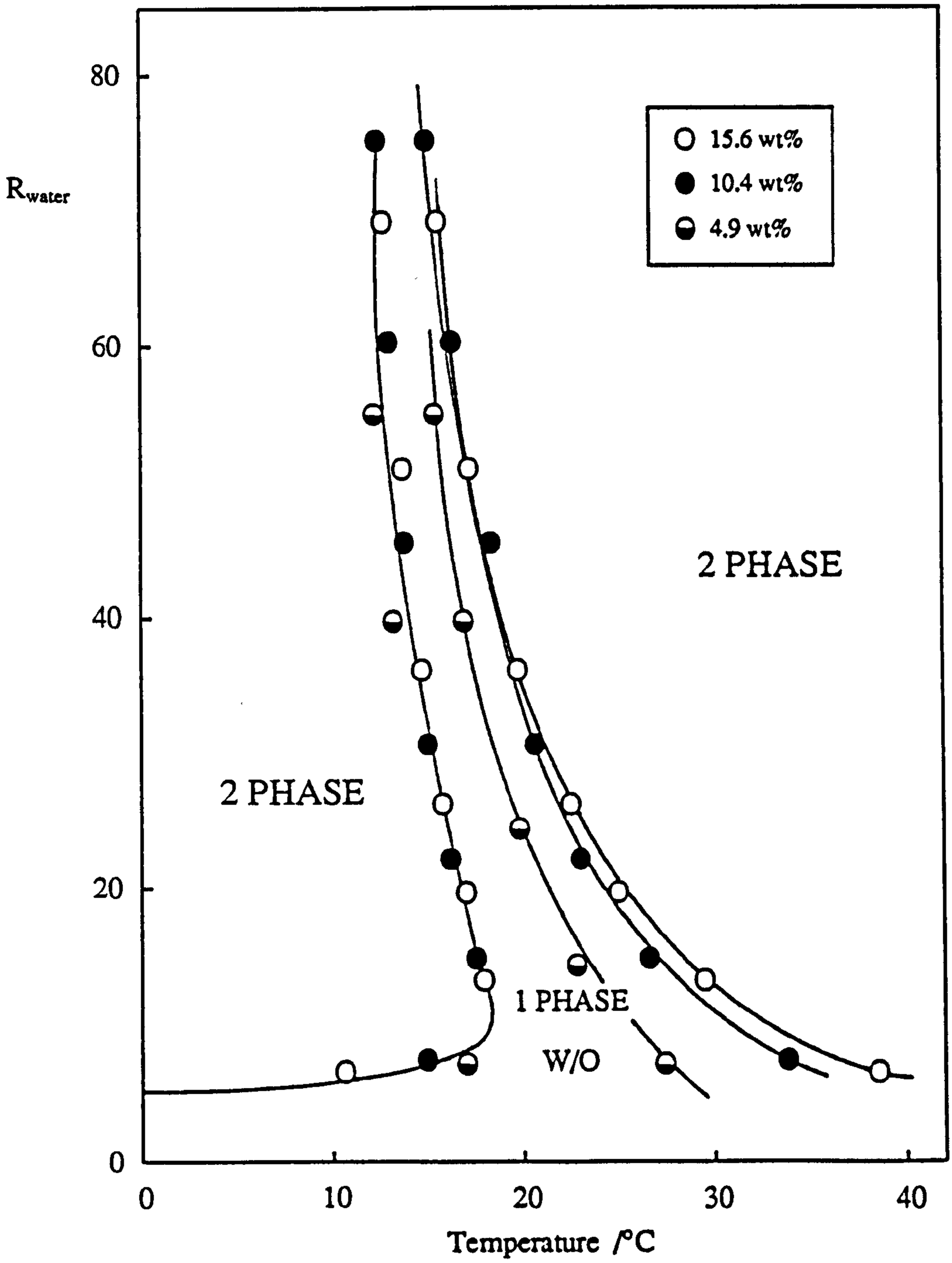

boundary appears to be independent of surfactant concentration (Figure 4.1). However, this is not the case for the corresponding W/O system (Figure 4.2). This arises from an appreciable concentration of the surfactant remaining in the oil as monomers not adsorbed at the microemulsion droplet surface (29, 98). Replotting the data as the maximum amount of solubilised dispersed phase as a function of surfactant concentration for a fixed temperature, highlights this phenomenon. Figures 4.3a and 4.3b show that, for both heptane and tetradecane as the continuous oil phase, a minimum concentration of surfactant in the oil is required before any significant amount of water is solubilised to form a W/O microemulsion. This minimum surfactant concentration (determined by the intercept on the abscissa) has previously been designated the *critical microemulsion concentration* (cμc) (29). The corresponding plots for the O/W microemulsions, Figures 4.4a and 4.4b, pass close to the origin as expected, since the critical micelle concentration in water (which is expected to be of a similar magnitude to the cμc in water) is known to be of the order of 10^{-3} wt% (9).

The slopes of these plots yield the molar ratio of dispersed component to surfactant within the microemulsion droplets (R'). For W/O microemulsions,

$$R'_{water} = [water] / ([surfactant] - c\mu c).$$

For O/W microemulsions,

$$R'_{oil} = [alkane] / ([surfactant] - c\mu c).$$

The latter is effectively equal to R_{oil} since the cμc is very low in this case.

Figures 4.5 and 4.6 show the variation of R' with temperature for O/W and W/O microemulsion systems with heptane as the oil. Similarly, the equivalent plots for tetradecane as the oil are shown in Figures 4.7 and 4.8. The advantage of this type of

Figure 4.3a.

Variation of the maximum extent of water solubilisation with $C_{12}E_4$ concentration in oil. Oil is heptane.

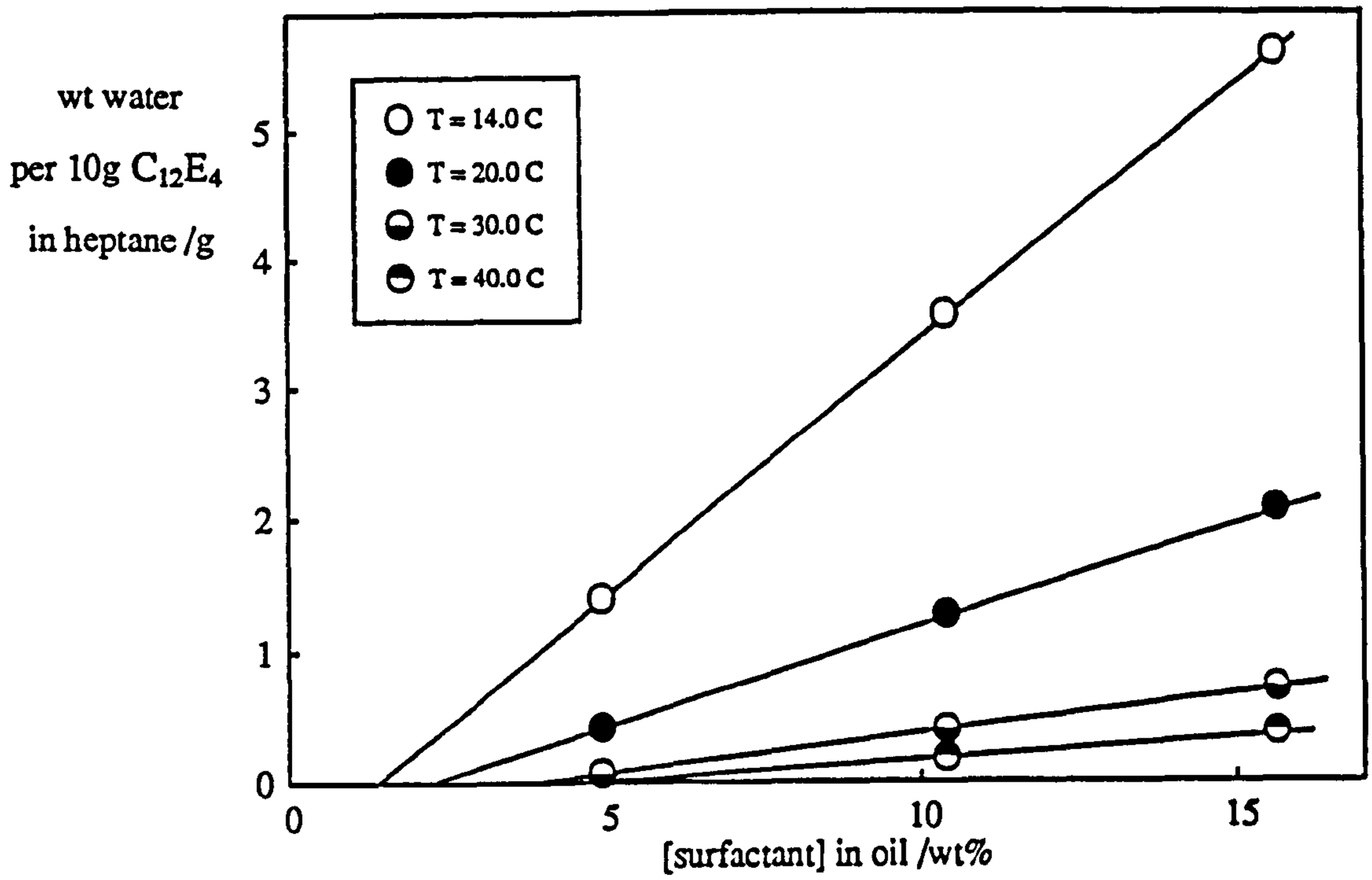

Figure 4.3b.

Oil is tetradacene.

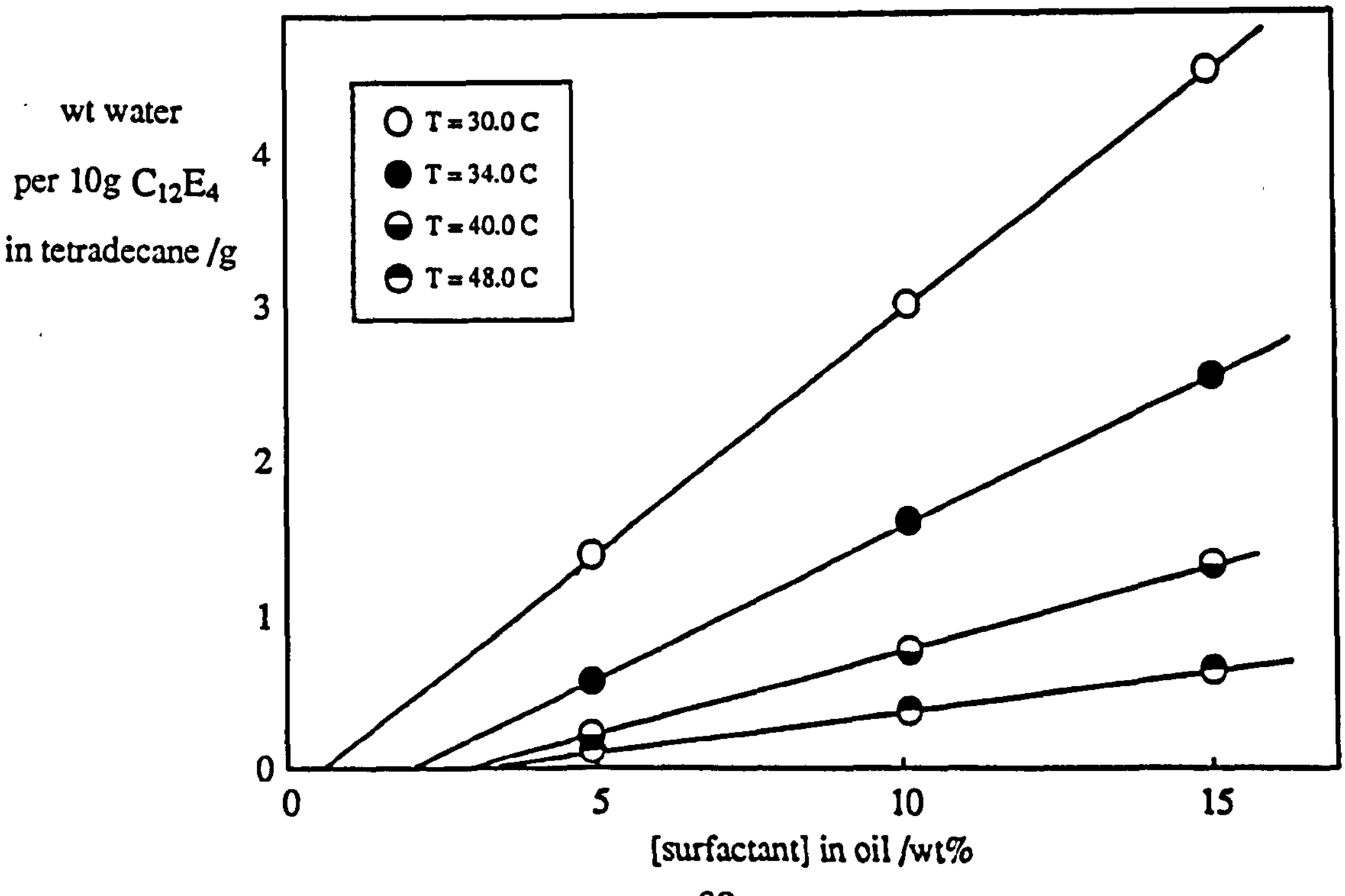

Figure 4.4a.

Variation of the maximum extent of oil solubilisation with aqueous $C_{12}E_4$ concentration. Oil is heptane.

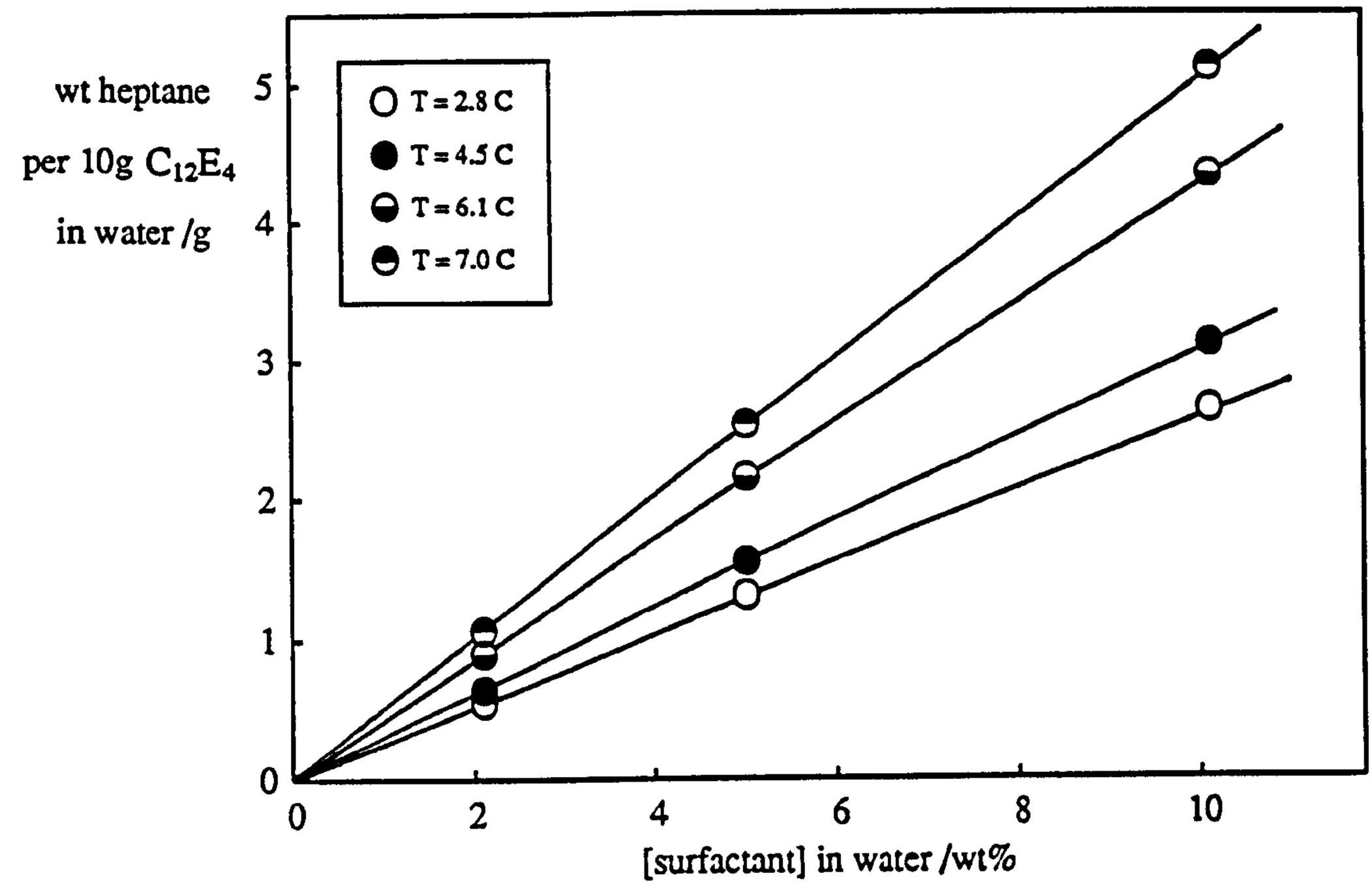

Figure 4.4b.

Oil is tetradecane.

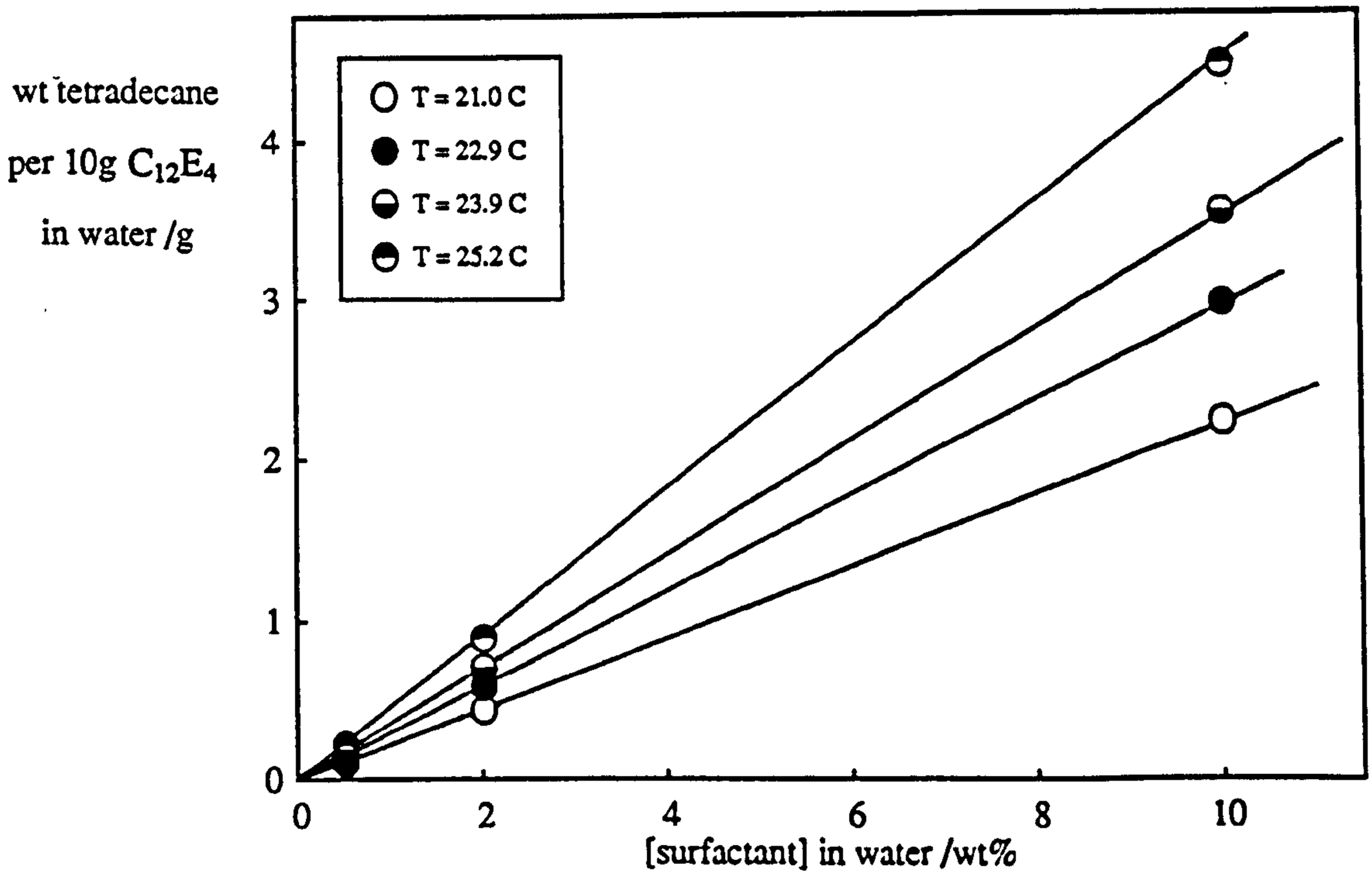

Figure 4.5.

One phase O/W microemulsion stability region for $C_{12}E_4$ + heptane + water. Filled points denote the excess oil solubilisation boundary, open points the cloud point boundary.

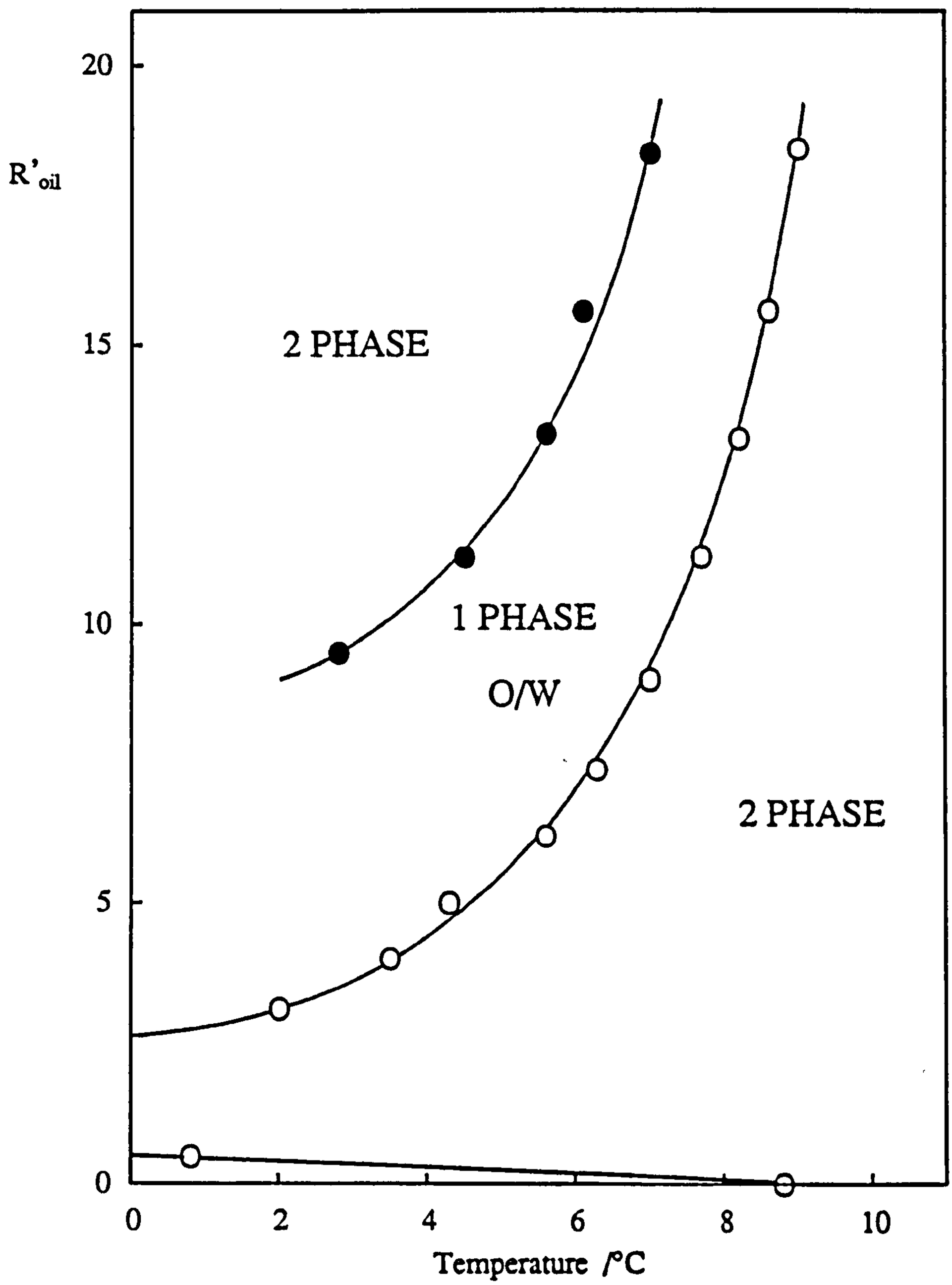

Figure 4.6.

One phase W/O microemulsion stability region for $C_{12}E_4$ + heptane + water. Filled points denote the excess water solubilisation boundary, open points the haze point boundary.

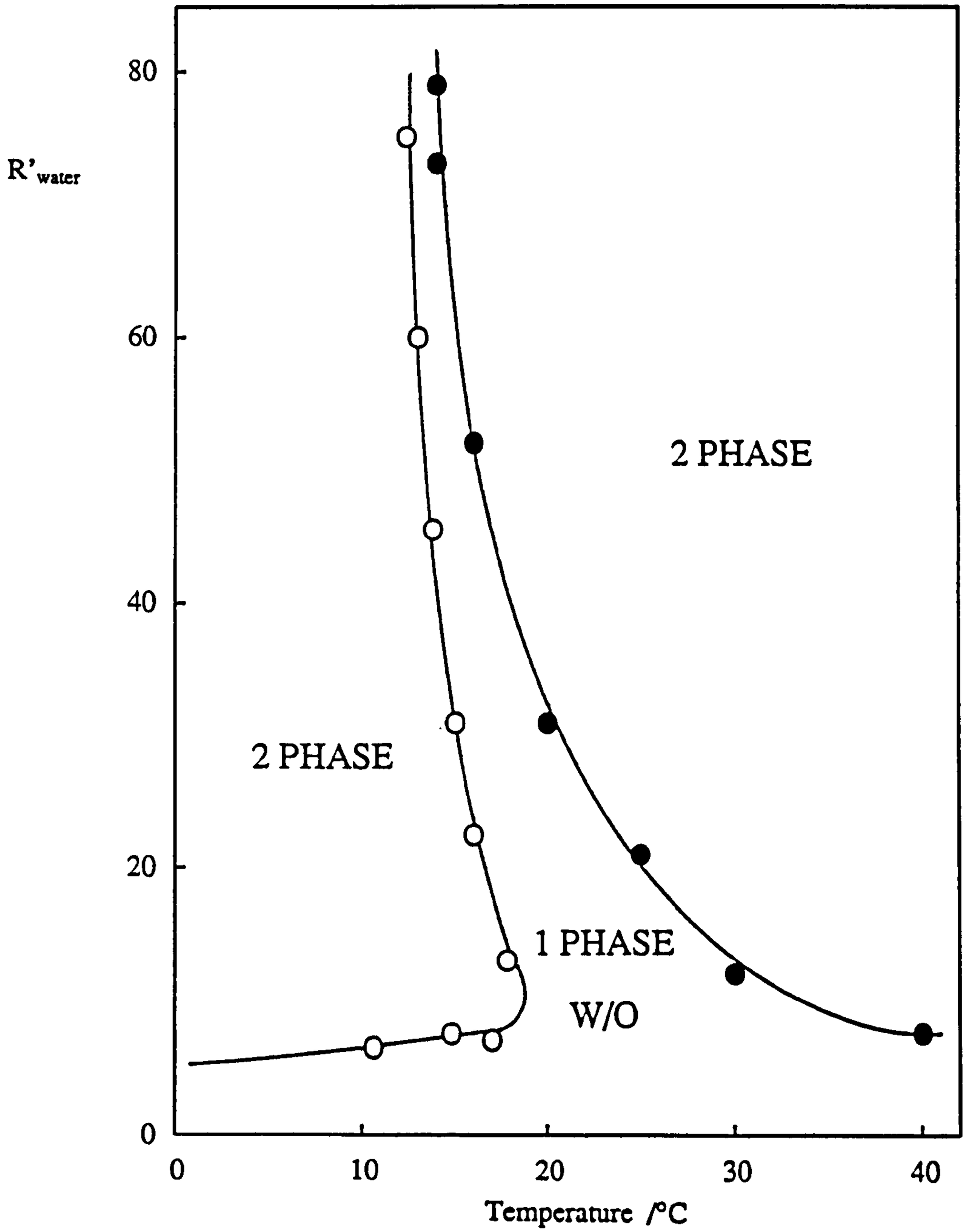

Figure 4.7.

One phase O/W microemulsion stability region for $C_{12}E_4$ + tetradecane + water. Filled points denote excess oil solubilisation boundary, open points the cloud point boundary.

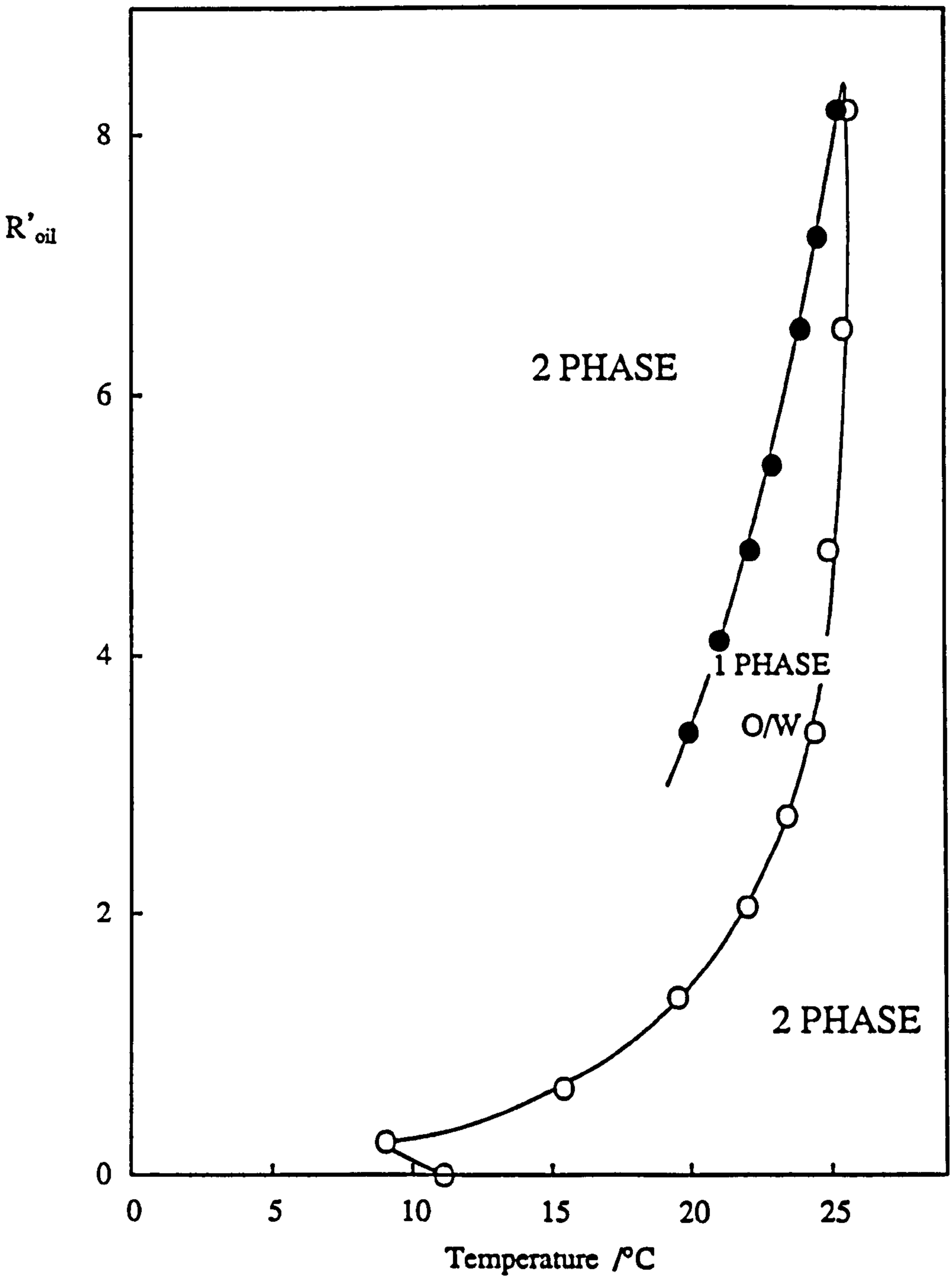

Figure 4.8.

One phase W/O microemulsion stability region for $C_{12}E_4$ + tetradecane + water. Filled points denote the excess water solubilisation boundary, open points the haze point boundary.

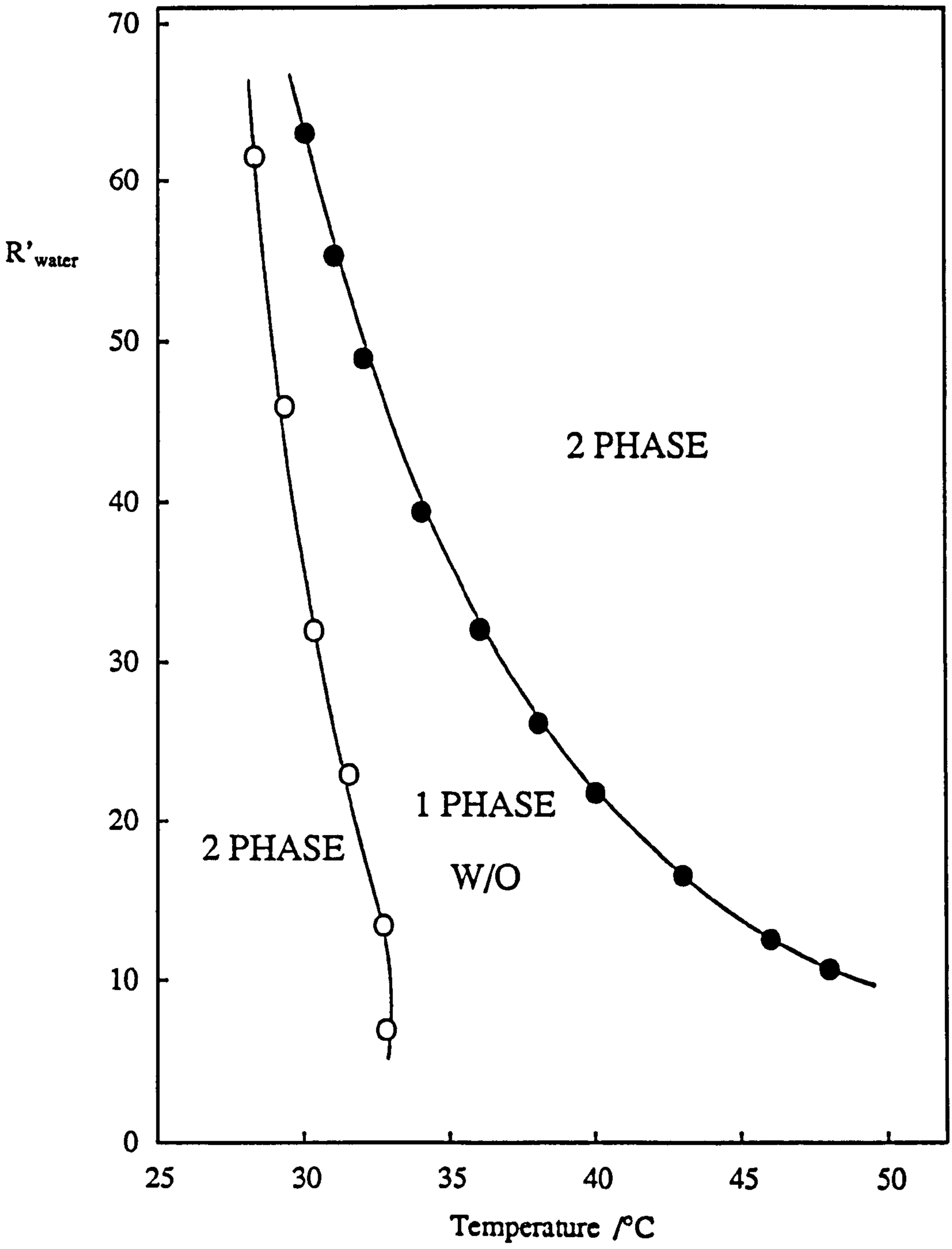

representation over that shown in Figures 4.1 and 4.2 is that the microemulsion droplet radius is proportional to R' (see equation 1.6) and so changes in the film curvature at the phase boundaries can be observed more clearly.

Substitution of heptane for tetradecane is seen to shift the temperature required for microemulsion formation to higher values. This is likely to be a consequence of a decreased penetration (i.e. reduced solvation) of the alkyl tail region of the surfactant monolayer by the longer chain alkane (149, 150).

The microemulsion aggregate type changes from O/W to W/O (or vice-versa) via a three phase region (Winsor III system). The extent of this three phase region is tabulated below in Table 4.1 for heptane and tetradecane as the oil phase. The values are seen to be in good agreement with previously determined results. The mid-point of this temperature range corresponds to the phase inversion temperature (PIT) of the corresponding macroemulsion (138). This is the temperature at which the emulsion type changes from O/W to W/O or vice-versa.

Table 4.1

Oil	Winsor III /°C	Lit. Winsor III (ref.) /°C
Heptane	10 - 12	10 - 12 (34)
Tetradecane	25 - 27	24 - 27 (34)

Values of the critical microemulsion concentration as a function of temperature are presented in Figure 4.9 and Table 4.2 for heptane and tetradecane as the oil phase. For heptane as the oil, the cμc was also determined by interfacial tension measurements. This value is plotted in Figure 4.9 and is seen to be in good agreement with those determined by the solubilisation plots.

Figure 4.9.

Critical microemulsion concentration versus temperature for W/O microemulsions formed with $C_{12}E_4$ in heptane and tetradecane. Half filled point determined by interfacial tension measurement for heptane as the oil phase.

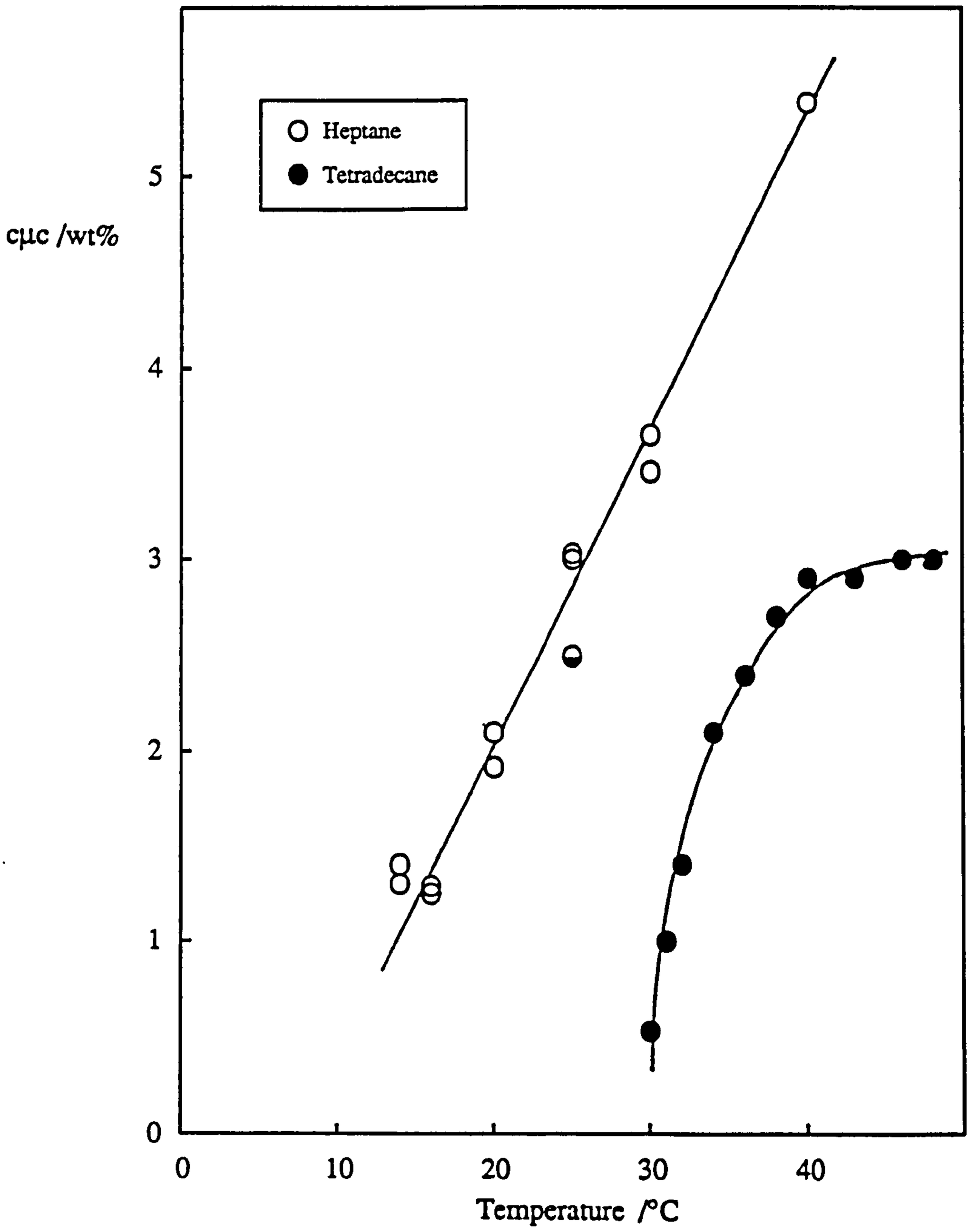

Table 4.2

Oil is heptane.		Oil is tetradecane.	
Temperature /°C	cμc /wt%	Temperature /°C	cμc /wt%
15	1.3 ± 0.3	30	0.5 ± 0.5
20	2.0 ± 0.3	32	1.4 ± 0.3
25	3.0 ± 0.4	34	2.1 ± 0.4
30	3.5 ± 0.4	38	2.7 ± 0.4
40	5.4 ± 0.8	40	2.9 ± 0.6

For both W/O systems it can be clearly seen that the cμc increases with increasing temperature, corresponding to the formation of lower R'_{water} values and hence smaller droplet sizes. This presumably arises from dehydration of the ethylene oxide head groups on increasing temperature. Another way of plotting the temperature variation of the cμc is shown in Figure 4.10. From the gradient, a value for the enthalpy of transfer of one mole of surfactant from the monomeric state in the oil, to the aggregated state may be calculated. Since aggregates of different sizes form at different temperatures, this enthalpy change is for transfer of surfactant monomer from oil to the temperature dependent, "preferred" curvature monolayer observed at the solubilisation phase boundary. The hydrophilic head group is transferred from an apolar environment to the preferred curvature monolayer where it is expected to be hydrated.

The calculated value for the enthalpy of transfer of a mole of monomers from heptane to the preferred curvature is -42 ± 10 kJ mol^{-1}. The corresponding value for tetradecane as oil phase is -52 ± 25 kJ mol^{-1}. Shinoda *et al.* have measured cμc values as a function of temperature for a range of nonionic surfactants in decane-water systems (151). Analysis of their data for $C_{12}E_4$ yields a value for the enthalpy of transfer of -37 ± 2 kJ mol^{-1}. They observed that the enthalpy change became more negative upon

Figure 4.10.

Variation of the critical microemulsion concentration of $C_{12}E_4$ in heptane and tetradecane with temperature.

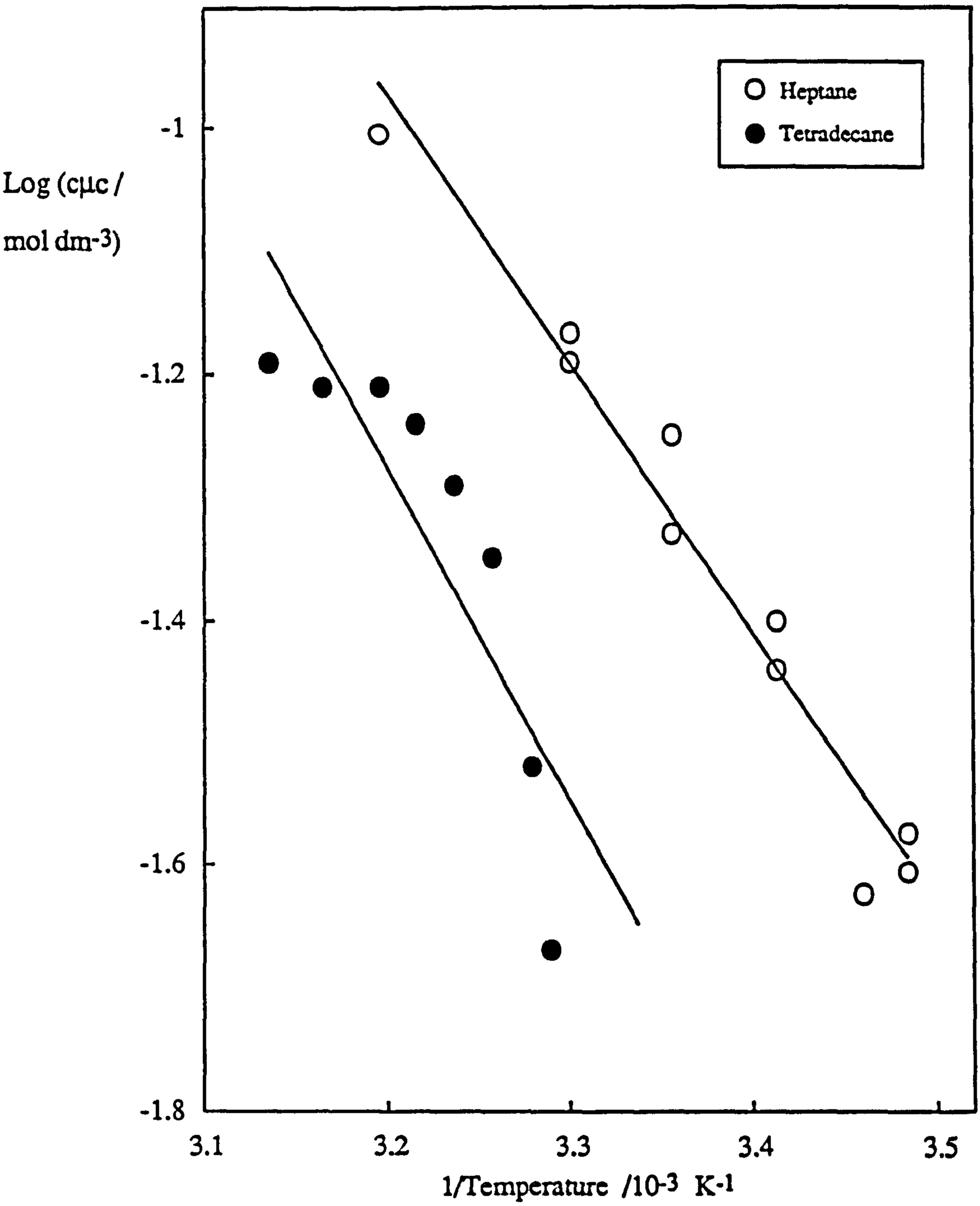

increasing the number of ethylene oxide units in the head group whereas variation of the alkyl chain length of the surfactant had little effect. The results here suggest that the enthalpy change becomes more negative with an increase in oil chain length. However, the experimental uncertainties in the values here are large and more accurate data is required to verify this.

4.3 Microemulsion Phase Behaviour for $C_{12}E_4$ + Alkane + Water Systems as a Function of Salt Concentration.

Figures 4.11a and 4.11b show the equivalent types of plot to those previously shown in Figures 4.3a and 4.3b for W/O microemulsions stabilised by $C_{12}E_4$. Maximum solubilisation of water is plotted as a function of surfactant concentration for different dispersed phase salt concentrations at a fixed temperature. It is clear that for both alkane systems, increasing the dispersed phase salt concentration reduces the maximum solubilisation capacity and increases the system cμc. The results for the two oils are summarised below in Table 4.3.

Table 4.3

Oil is heptane, T = 10.0°C.			Oil is tetradecane, T = 25.0°C.		
[NaCl] /M	R'_{water}	cμc /wt%	[NaCl] /M	R'_{water}	cμc /wt%
1.0	40	1.9 ± 0.3	1.0	52	1.7 ± 0.3
1.5	22	2.0 ± 0.4	1.5	28	2.8 ± 0.3
2.0	14	3.2 ± 0.4	2.0	18	4.1 ± 0.4

Addition of salt to the microemulsion system results in a shift towards more negative curvature of the surfactant film. As previously discussed this is thought to occur through a "salting-out" mechanism leading to a reduced effective head group area.

Figure 4.11a.

Variation of the maximum extent of water solubilisation at 10.0°C with $C_{12}E_4$ concentration in heptane, for various dispersed phase salt concentrations.

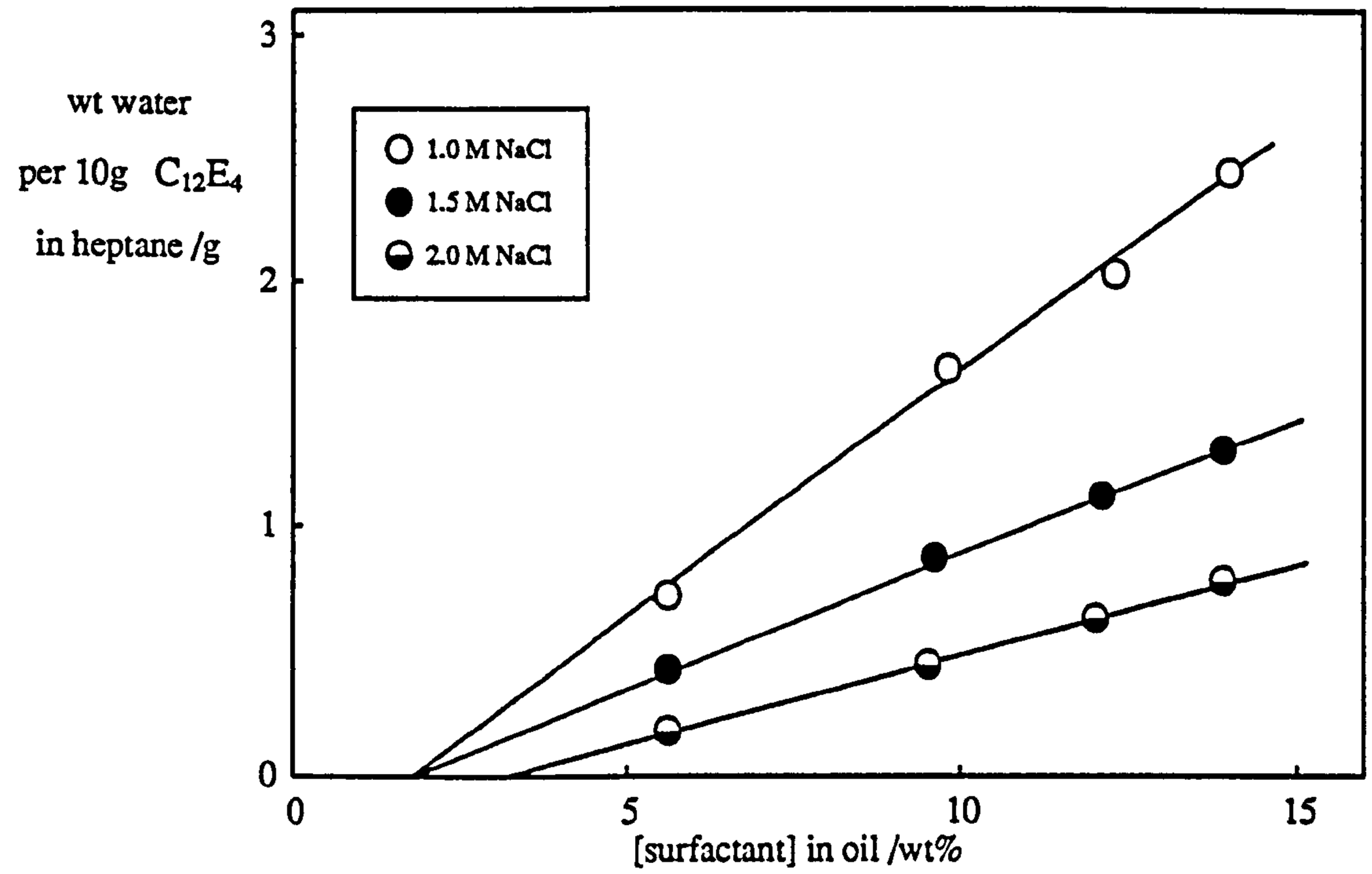

Figure 4.11b.

Variation of the maximum extent of water solubilisation at 25.0°C with $C_{12}E_4$ concentration in tetradecane, for various dispersed phase salt concentrations.

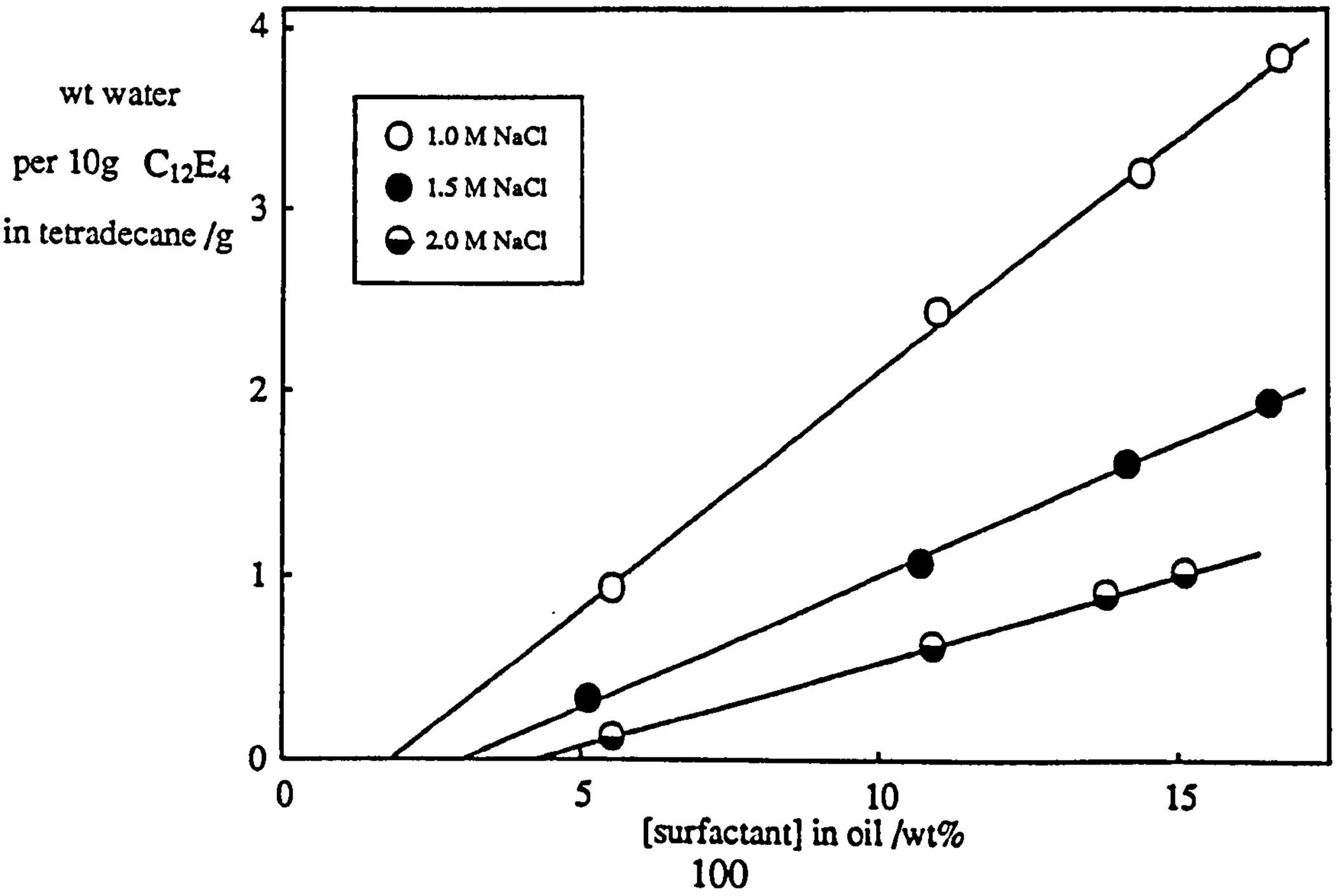

The effect of increasing salt concentration therefore parallels that of an increase in temperature.

Maximum water solubilisation values (R'_{water}) and critical microemulsion concentrations (cμc), have now been determined for W/O microemulsions stabilised by $C_{12}E_4$ in heptane and tetradecane, as a function of temperature and dispersed phase salt concentration. These variables act so as to modify the effective surfactant geometry. If the cμc is a function only of the droplet size (proportional to R'_{water}), a correlation between experimentally determined values of R'_{water} and cμc for each variable might be predicted. Figure 4.12 shows the variation of the cμc with R'_{water} (determined by temperature or salt variation) for microemulsions stabilised by $C_{12}E_4$ in heptane and tetradecane. It can be seen that the cμc values corresponding to a particular R'_{water} value are approximately the same, independent of how they were achieved. It appears therefore that the cμc is a function of the spontaneous curvature of the surfactant film and is independent of how the curvature is changed.

4.4 Effect of Solubilised Protein on the Excess Water Solubilisation Phase Boundary Formed with $C_{12}E_4$ + Heptane + Water.

The vast majority of food emulsions contain proteins which play a role in their stabilisation through adsorption at the oil-water interface. The interactions between adsorbed protein and low molar mass surfactant within the interface are paramount in determining the stability of the emulsion produced. For this reason extensive studies have previously been performed on the adsorption behaviour of proteins at oil-water and air-water interfaces in the presence and absence of low molar mass surfactants (152 - 154).

From W/O microemulsion studies, the effect of protein on the composition of the interfacial monolayer may be estimated through changes in the spontaneous

Figure 4.12.

Variation of the critical microemulsion concentration with the degree of solubilisation, R'_{water}, for W/O microemulsions formed with $C_{12}E_4$ in heptane and tetradecane.

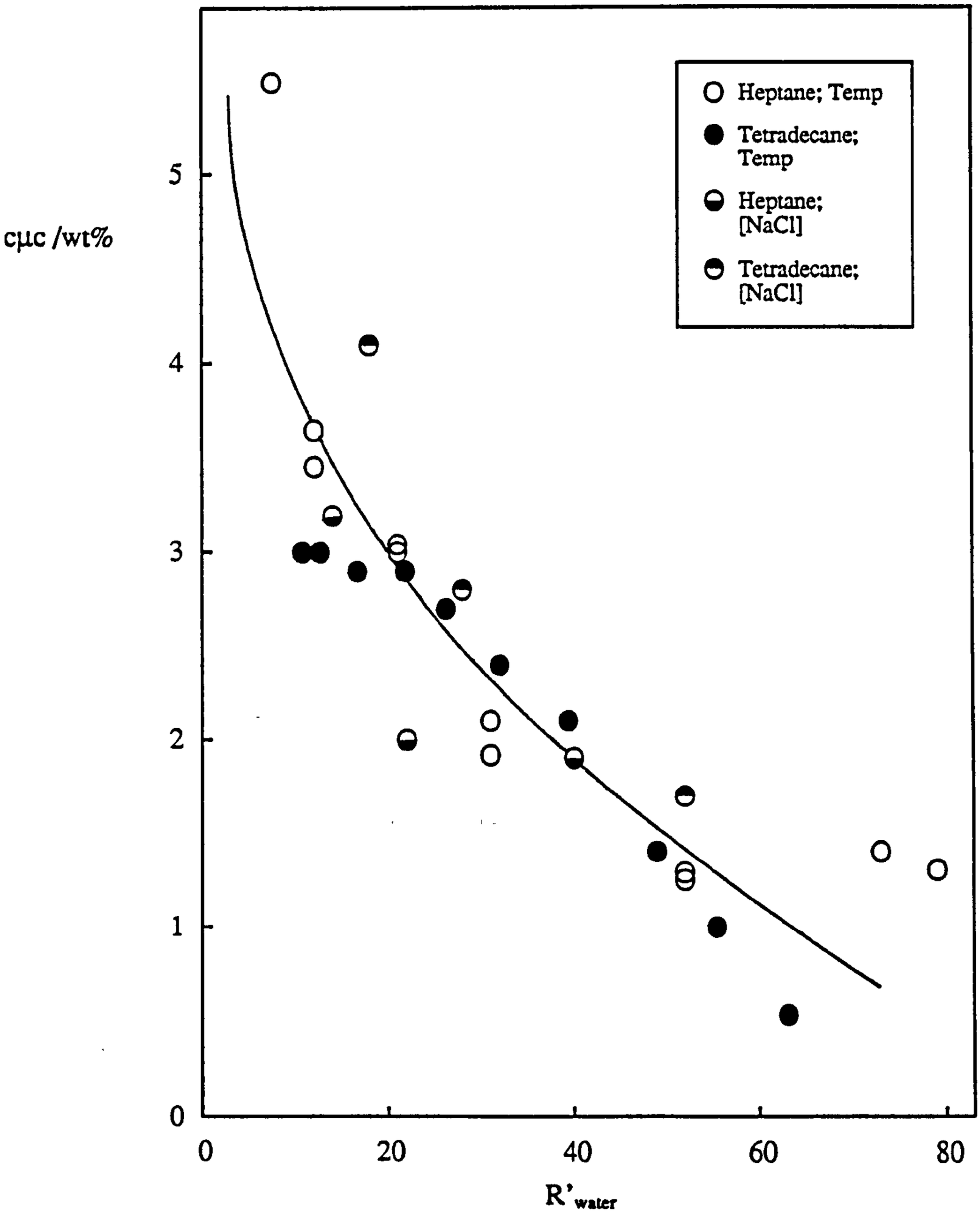

curvature of the surfactant film. Such changes may occur since solubilised proteins can occupy different locations within the microemulsion depending upon their interactions with the surfactant monolayer and the dispersed phase (62).

4.4.1 Solubilisation of α-chymotrypsin and BSA in the reversed micellar phase formed with $C_{12}E_4$ + heptane + water.

α-Chymotrypsin and BSA are both globular proteins which exhibit high solubility in water, forming clear, colourless solutions. Both proteins were used in 50 mM buffer solutions. α-Chymotrypsin was buffered in aqueous glycine at pH 9.0, and BSA in a sodium phosphate buffer at pH 7.0. Under these conditions both proteins exhibit a net negative charge (see Table 2.6). The size of the α-chymotrypsin molecule has previously been measured by X-ray crystallography to be 51 x 40 x 40 Å (155). The actual effective size in solution most surely exceeds this value due to solvation of its highly charged surface. The size of BSA in aqueous solution was found by electrical birefringence to be 140.9 x 41.6 x 41.6 Å (156).

The effect of each protein on the position of the solubilisation phase boundary for W/O microemulsions stabilised by $C_{12}E_4$ in heptane is shown in Figures 4.13a and 4.13b. Each data point has been derived from a plot of the type shown in Figure 4.3. It can be seen that solubilisation is little affected by incorporation of either protein into the dispersed phase. On increasing the protein concentration, solubilisation appears to decrease slightly compared to that of the aqueous buffer solution alone i.e. the solubilisation boundary is shifted to lower temperatures. This is consistent with the proteins having an effect similar to that of high concentrations of salt as previously discussed.

The calculated average number of protein molecules per microemulsion droplet (N) has been estimated using calculated values of the microemulsion core radius (r_c).

Figure 4.13a.

Effect of α-chymotrypsin concentration on the excess water solubilisation phase boundary formed with $C_{12}E_4$ in heptane. The protein is buffered at pH 9.0 in 50 mM glycine.

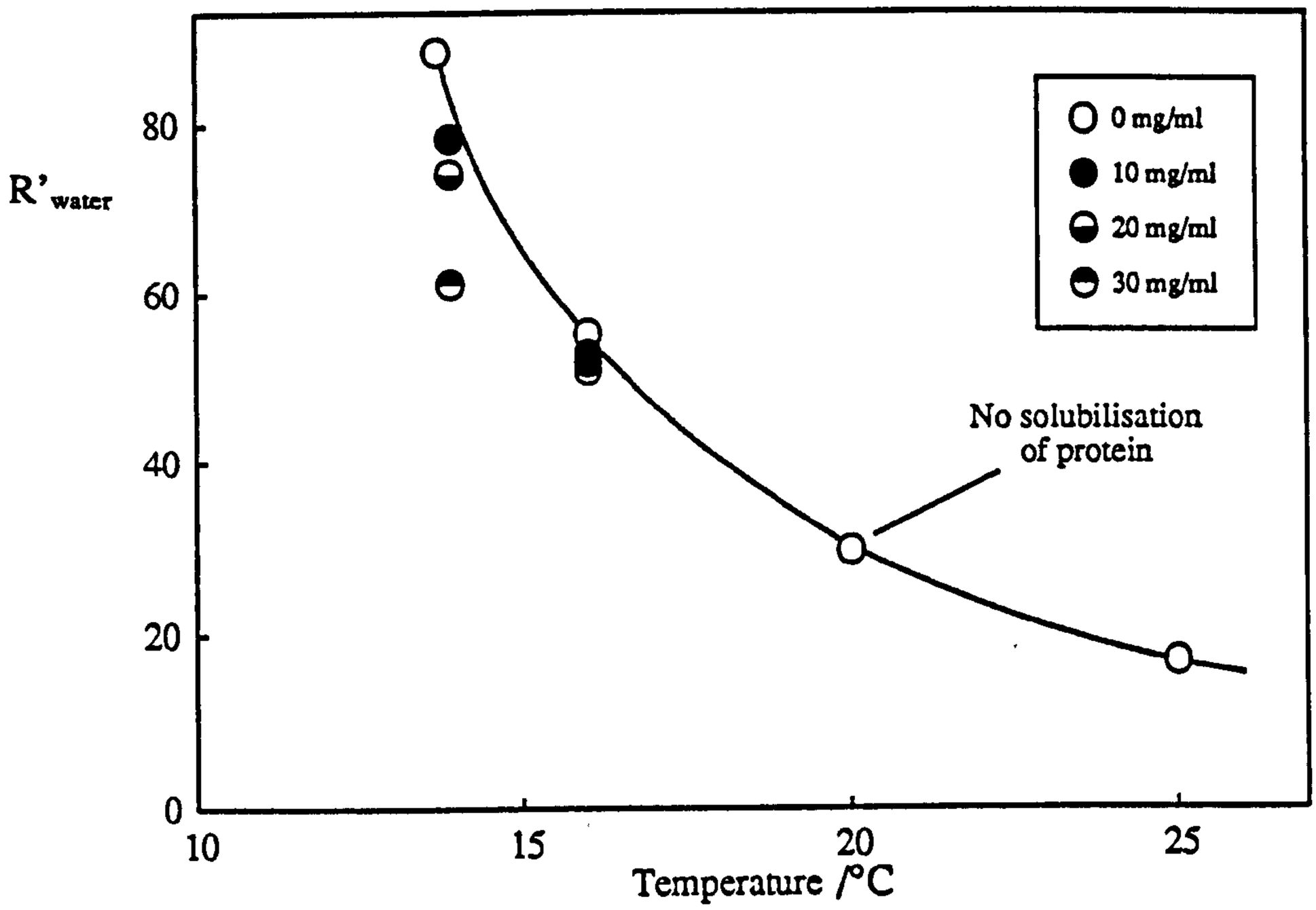

Figure 4.13b.

Effect of BSA concentration on the excess water solubilisation boundary. The protein is buffered at pH 7.0 in 50 mM sodium phosphate solution.

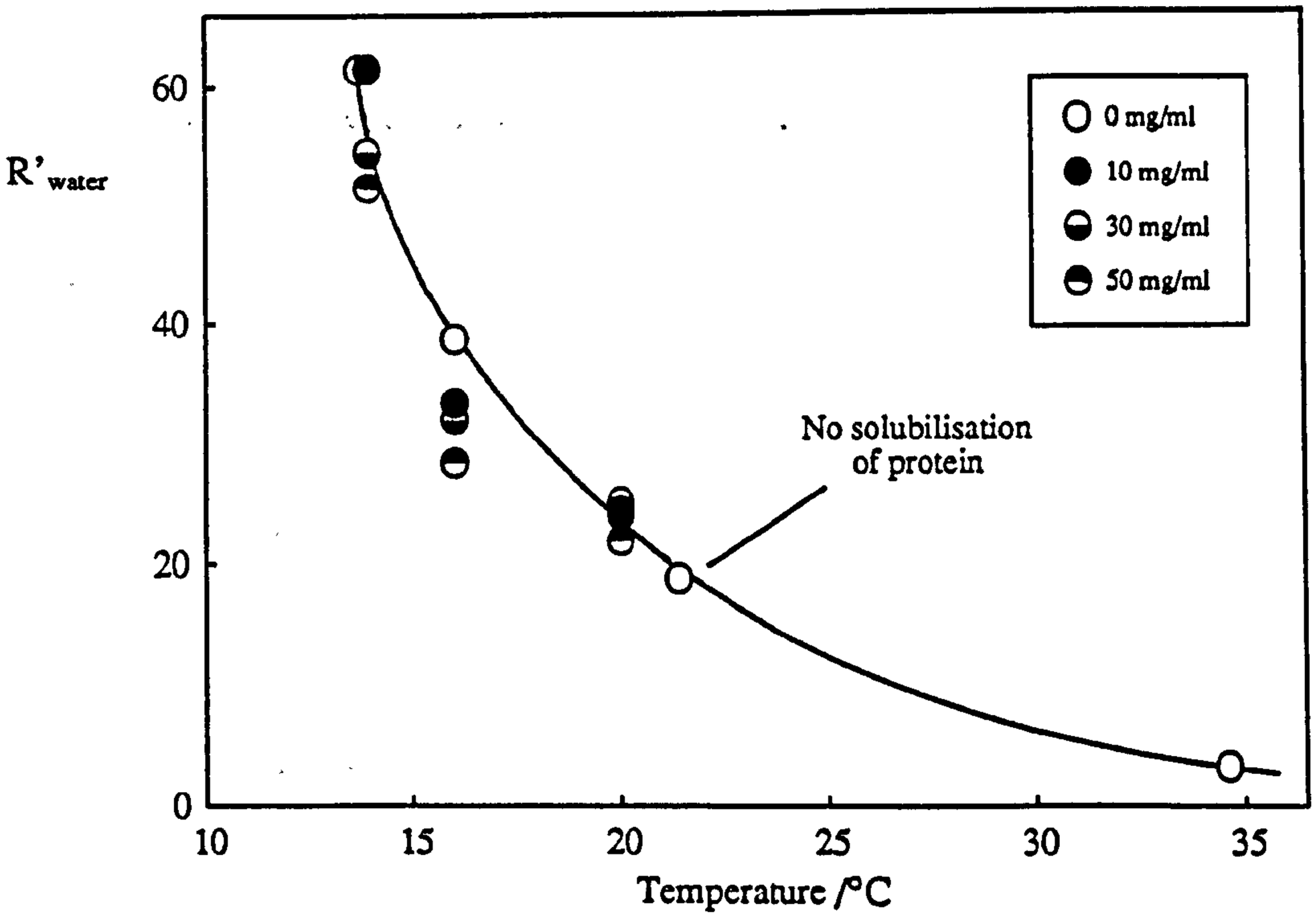

These are tabulated below in Table 4.4. This is not the maximum number of protein molecules that can be solubilised, merely the highest concentration investigated here. The protein concentrations in Table 4.4 are expressed in mg/ml.

Table 4.4

α-Chymotrypsin.

R'_{water}	[α-CT]	r_c /nm	N
61	30	17.0	15
52	30	14.6	11
30	0	8.4	0

BSA.

R'_{water}	[BSA]	r_c /nm	N
52	50	14.6	5.8
28	50	7.8	0.9
22	50	6.1	0.5
19	0	5.3	0

For both proteins a specific microemulsion composition is reached at which solubilisation of the lowest protein concentration tested is not possible. This occurs for α-chymotrypsin at 20°C which corresponds to $R'_{water} = 30$ for empty droplets formed by the buffer solution alone. At this point, solubilisation of a 5 mg/ml of protein solution was not possible. Similarly for BSA, solubilisation of a 10 mg/ml protein solution could not be achieved at 21.5°C which corresponds to $R'_{water} = 19$ in the "empty" system. Speculatively, these observations might be interpreted as indicating that the proteins occupy a position within the central core of "free" water in the microemulsion. The microemulsion size at which protein cannot be solubilised into the droplet presumably corresponds to the point at which the hydration requirements of both the protein and the surfactant hydrophilic head groups cannot be met by the small volume of dispersed water in the microemulsion core.

The effect of protein solubilisation on the critical microemulsion concentration is shown in Figures 4.14a and 4.14b for α-chymotrypsin and BSA respectively. It appears that both proteins have a negligible effect on the cμc. The deviations observed

Figure 4.14a.

Effect of α-chymotrypsin concentration on the critical microemulsion concentration of $C_{12}E_4$ in heptane.

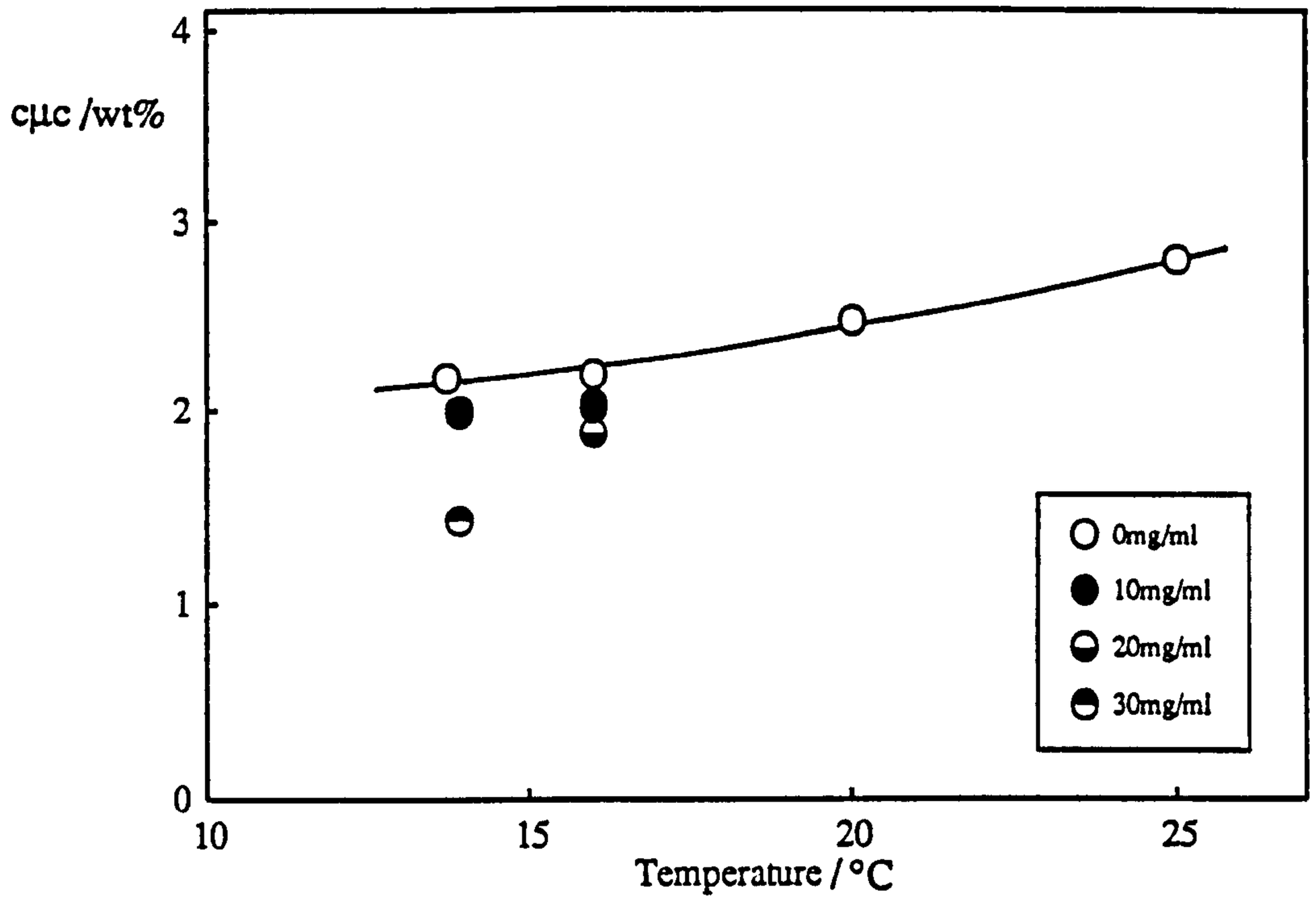

Figure 4.14b.

Effect of BSA concentration on the critical microemulsion concentration.

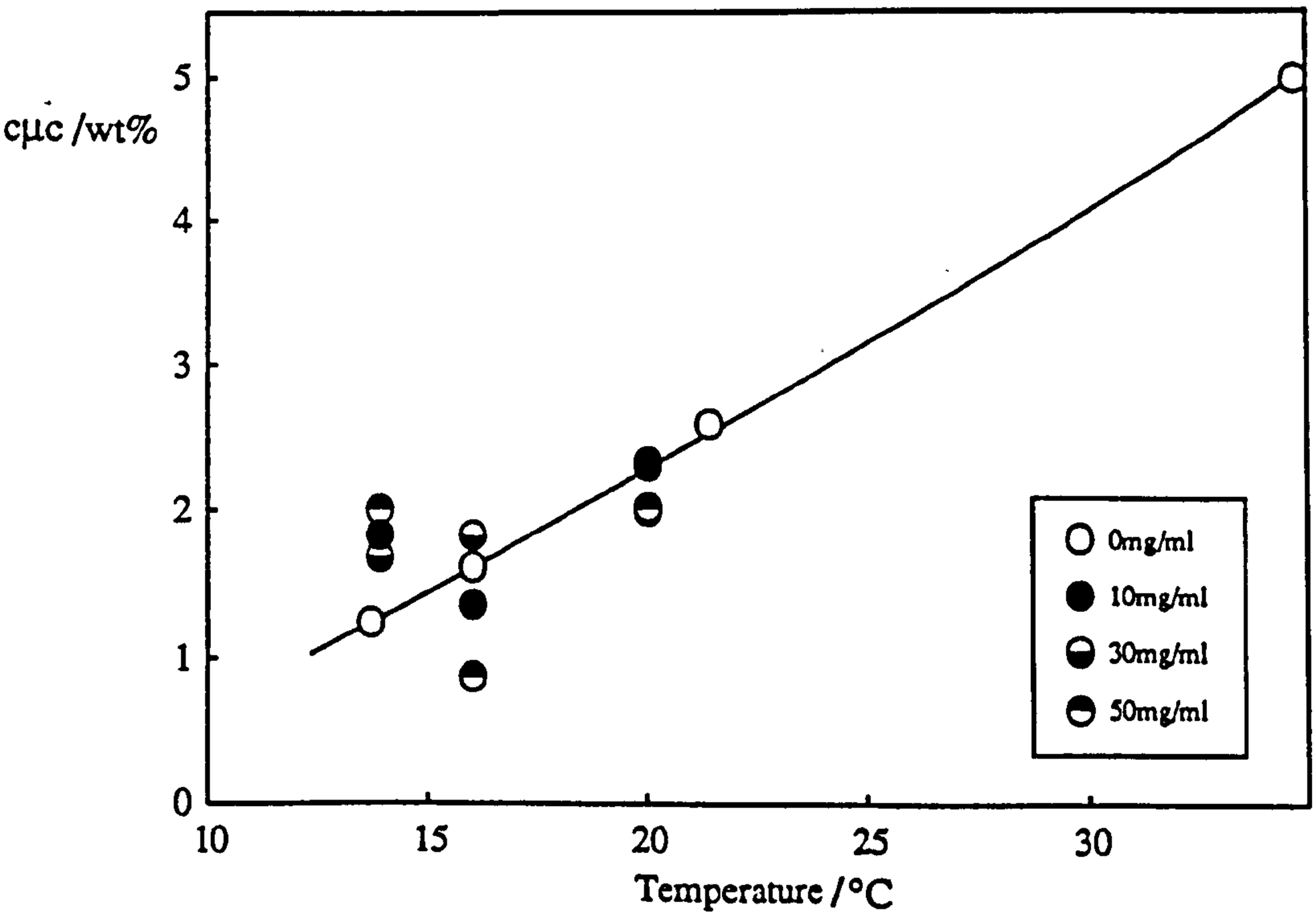

are within the experimental uncertainty for these systems. If the proteins exhibited an affinity for the surfactant monolayer the cμc might be expected to decrease. Since this is not observed, these results may indicate that the proteins are located within the water core of the aggregates.

4.4.2 Solubilisation of sodium caseinate.

Casein in milk occurs as a mixture of four main casein components, α_{S1}, β, α_{S2} and κ in the approximate proportions 4 : 4 : 1 : 1. These are held together in the form of polydisperse, proteinaceous colloidal particles called "casein micelles" (157). The size of these aggregates typically range between 50 and 300 nm. The widely used commercial emulsifier sodium caseinate is less aggregated than milk casein, but it has the same overall protein composition. Its exceptional emulsifying properties are attributed to a molecular structure which is highly disordered and substantially hydrophobic. A consequence of this hydrophobicity is its limited solubility in water (~2 mM at 20°C, measured). Aqueous solutions of sodium caseinate were prepared in 50 mM phosphate buffer at pH 7.0 by either continuously stirring the mixture for periods of up to two hours or by sonication. Phase boundary determinations for solutions prepared by either method were identical. Under the conditions employed the protein exhibits a net negative charge.

The effect of sodium caseinate on the position of the one phase upper temperature boundary for W/O microemulsions stabilised by $C_{12}E_4$ in heptane, is shown in Figure 4.15a. It appears that for all protein concentrations and temperatures investigated, the R'_{water} value remains approximately constant between 20 and 30 even when solubilisation of the buffer solution containing no protein reaches an R'_{water} value of 62. Solubilisation of 10 mg/ml sodium caseinate solution was not possible at a

Figure 4.15a.

Effect of sodium caseinate concentration on the excess water solubilisation phase boundary formed with $C_{12}E_4$ in heptane. The protein is buffered at pH 7.0 in 50 mM sodium phosphate solution.

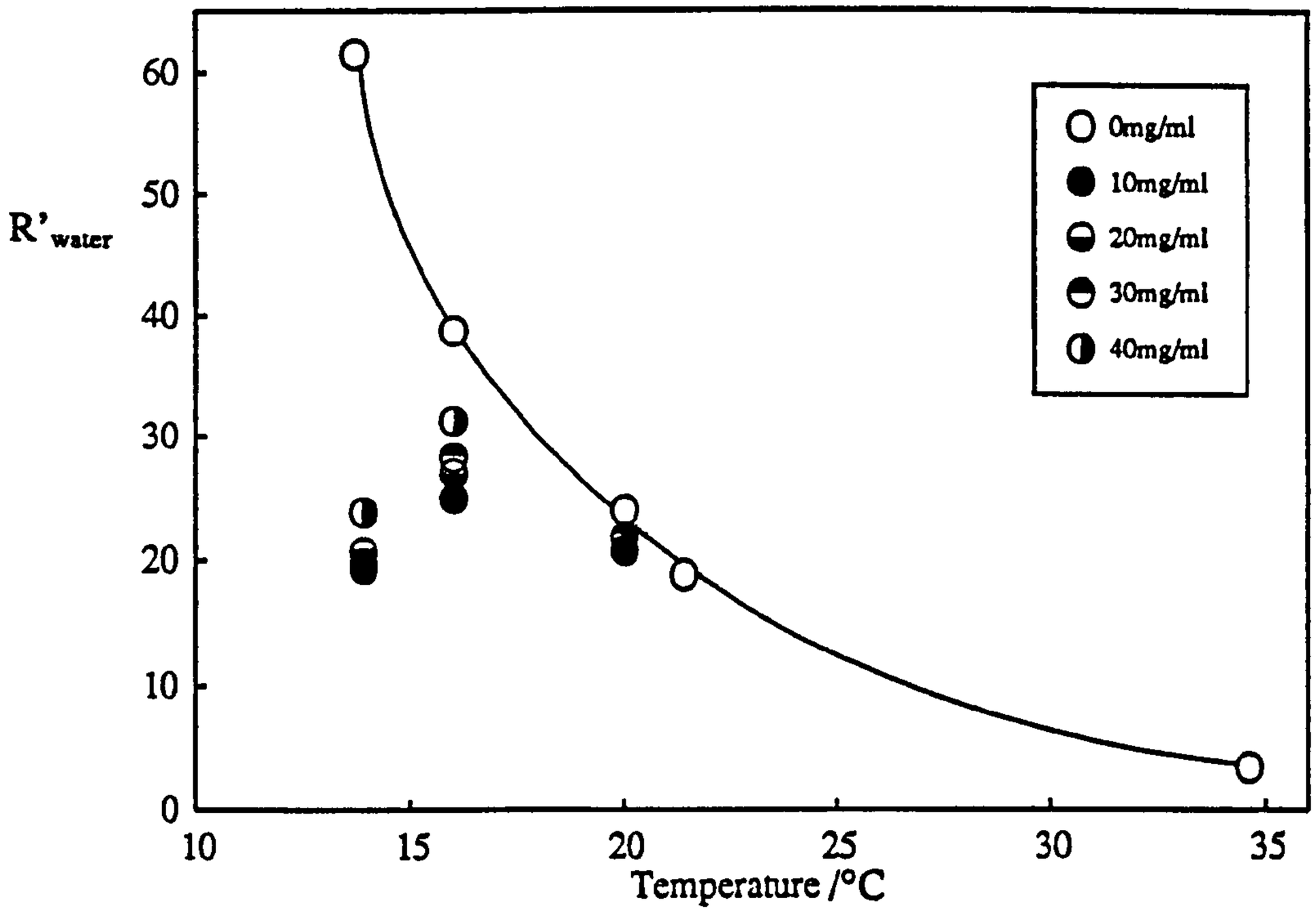

Figure 4.15b.

Effect of sodium caseinate on the critical microemulsion concentration.

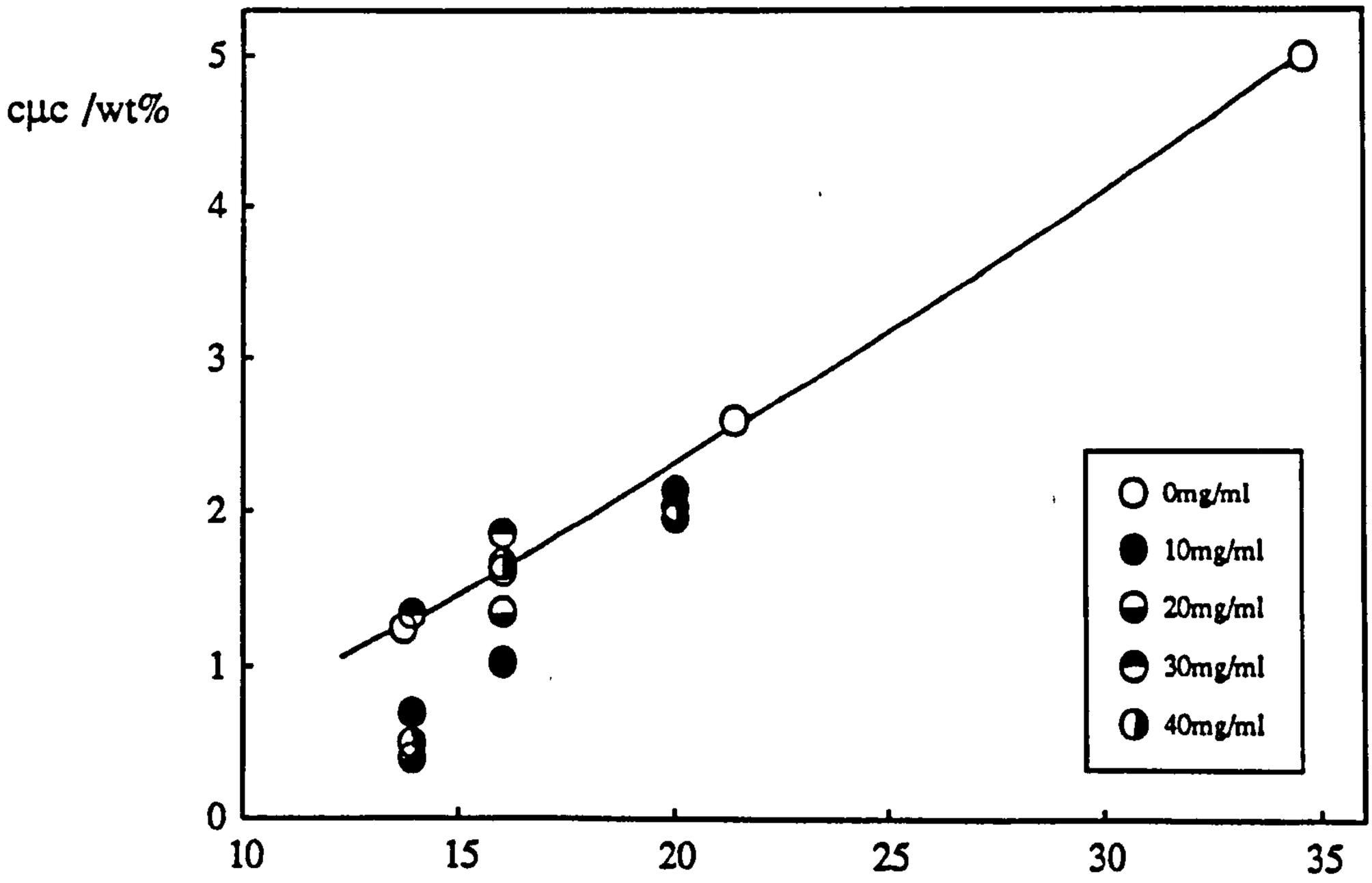

temperature of 21.5°C where the R'_{water} value for the "empty" droplet falls below about 20.

This interesting solubilisation behaviour may be due to the sodium caseinate in aqueous solution aggregating to form submicellar particles in equilibrium with free caseinate molecules as reported by Creamer and Berry (158). These aggregates may then be retained in the dispersed phase, forming microemulsion droplets around themselves which are only stable at water : surfactant ratios of 20 - 30. Since caseinate is not solubilised at lower R'_{water} values it appears that the presence of a water content in the microemulsion either greater or less than that required to solvate both the surfactant and the protein aggregate makes the system unstable.

The effect of sodium caseinate concentration on the critical microemulsion concentration is shown in Figure 4.15b. As was observed with the two previous proteins, no systematic variation with protein concentration is observed and the values are constant within the experimental error for this system.

4.5 Measurement of Microemulsion Droplet Sizes by Photon Correlation Spectroscopy.

4.5.1 W/O microemulsion droplets stabilised by $C_{12}E_4$ in heptane.

Photon correlation spectroscopy was used to determine the diffusion coefficients of microemulsion droplets. As described in section 2.1.3, the droplet hydrodynamic radius is calculated from the diffusion coefficient using equation 2.6. This value includes a contribution from any entrained solvent. Determination of the diffusion coefficient of a particle at a finite concentration, is an apparent value which is subject to the effects of inter-particle interactions. Measurements must therefore be extrapolated to

infinite dilution, where interactions can be neglected, in order to obtain the true diffusion coefficient (D_0) and consequently the true radius. It is important that such a dilution of the microemulsion samples is made in a way that the droplet composition does not change, i.e. W/O microemulsions must be diluted with oil containing the cμc of the surfactant.

As shown in Figure 4.16, the apparent diffusion coefficient (D) decreases upon moving away from the solubilisation phase boundary at 14.0°C. This may be due to either (i) an increase in microemulsion droplet size, (ii) an increase in attractive interaction between droplets, or (iii) both (i) and (ii). It will be shown later in section 4.7.2 that the droplet size is effectively constant as the one phase region is traversed in agreement with previously reported results (55). The effect on the apparent diffusion coefficient appears therefore to be one of increased droplet attraction as one moves away from the solubilisation boundary.

Microemulsion droplet sizes were determined for a range of R'_{water} values as a function of dispersed phase volume fraction at temperatures close to the solubilisation phase boundaries where interactions are expected to be weakest. Phase boundaries observed for these one phase "made up" microemulsion samples were found to be in agreement (± 0.5°C) with those previously determined. The results are shown in Figure 4.17 as the variation of apparent diffusion coefficient with droplet volume fraction. For all samples investigated a low degree of polydispersity was observed as evidenced by values of the normalised variance less than 0.1.

Cazabat and Langevin have shown that for small dispersed phase volume fractions the apparent diffusion coefficient varies with volume fraction (ϕ) according to (106).

$$D = D_0 (1 + \alpha \phi) \qquad (4.1)$$

Figure 4.16.

Variation of the apparent diffusion coefficient upon moving away from the excess water solubilisation phase boundary, for W/O microemulsions formed with 5.0 wt% $C_{12}E_4$ in heptane. R'_{water} = 65, cμc = 1.3 wt%.

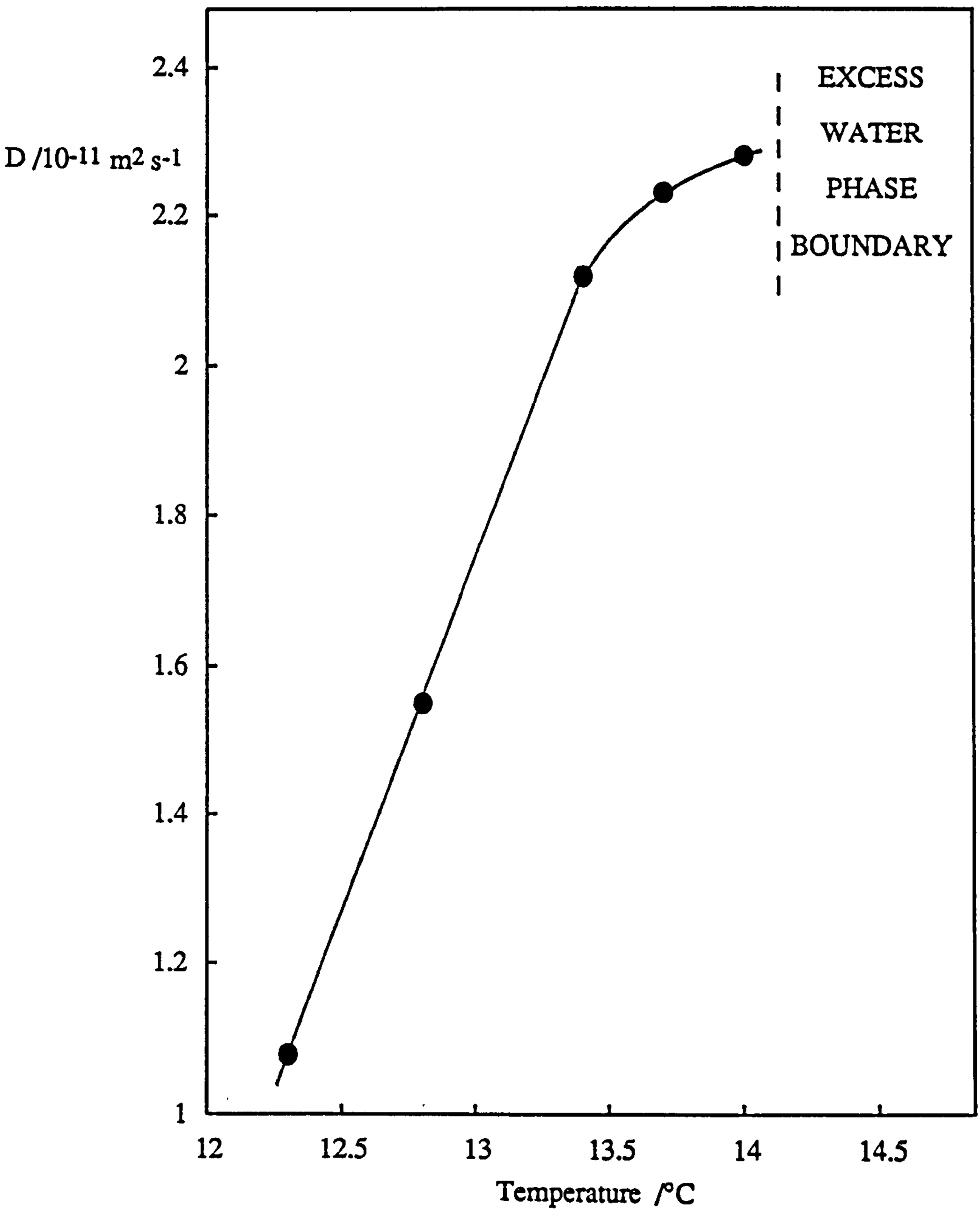

Figure 4.17.

Variation of the apparent diffusion coefficient with dispersed phase volume fraction, for water-in-heptane microemulsions stabilised by $C_{12}E_4$ at concentrations in excess of the cμc.

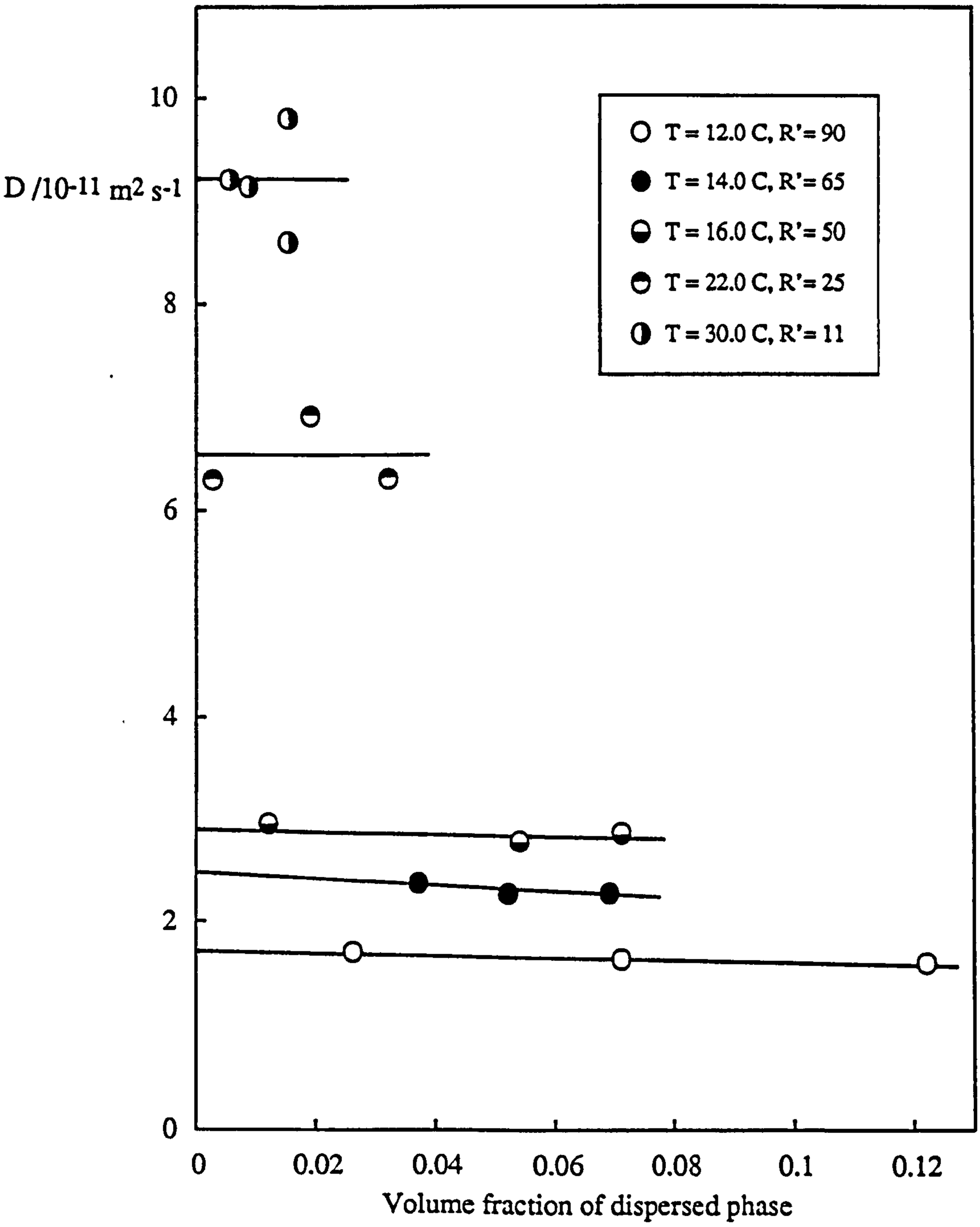

The constant α is the first virial coefficient of the diffusion coefficient. A value for α of 1.45 has been calculated for hard spheres (159) and negative values are expected for attractive interactions. The above equation has been applied to the results shown in Figure 4.17 and the values of α (together with the uncertainties) for various droplet compositions are given below in Table 4.5. Also tabulated are values for the true hydrodynamic radii calculated from the Stokes-Einstein relationship, using values of the diffusion coefficient extrapolated to infinite dilution. This corresponds to a surfactant concentration equal to the system cμc.

Table 4.5

R'_{water}	α	r_H/nm
90	-0.5 ± 1.5	26.5 ± 2.0
65	-1.4 ± 2.0	19.1 ± 1.5
50	-0.3 ± 1.5	17.0 ± 1.5
25	0 ± 7	8.1 ± 1.5
11	0 ± 12	6.6 ± 1.5

For all microemulsion droplet sizes investigated the concentration dependence of the diffusion coefficient is small at temperatures close to the solubilisation phase boundaries. Calculated values of α all appear to be the same within the error of their determination which indicates that the droplet interactions are approximately independent of the aggregate size. With the estimated uncertainties, this behaviour is consistent with that expected for dispersions of "ideal", non-interacting particles for which $\alpha = 0$.

As described previously in section 1.2.1, if the microemulsion droplets are assumed to be spherical and monodisperse, a linear relationship exists between the

microemulsion droplet hydrodynamic radius (r_H) and R'_{water}. This is given below for W/O microemulsion droplets.

$$r_H = \frac{3\, R'_{water}\, V_{molec}}{A_s} + \delta \qquad (4.2)$$

A_s is the area occupied by a single molecule of surfactant at the interface between the droplet core and the surfactant monolayer and v_{molec} is the molecular volume of the dispersed aqueous phase. The length δ is the thickness of the surfactant monolayer and contains a contribution from any entrapped solvent. It can be seen from Figure 4.18 that this geometrical relationship is consistent with the experimental results. The point at $R'_{water} = 15$ is derived from time-resolved fluorescence data assuming that two molecules of heptane solvate each surfactant tail group. The fitted data conforms to the empirical relationship

$$r_H/\text{nm} = 0.274\, R'_{water} + 2$$

which corresponds to an area occupied by the surfactant molecule of 0.32 ± 0.06 nm^2 and a surfactant film thickness of 2 ± 2 nm. The area A_s for W/O microemulsions is expected to be related to the surfactant hydrophilic head group area. A similar study on water-in-heptane microemulsions stabilised by the larger head group surfactant $C_{12}E_5$ gave a slightly larger value of A_s of 0.35 ± 0.06 nm^2 (29).

4.5.2. W/O microemulsion droplets stabilised by $C_{12}E_4$ in tetradecane.

As before, microemulsion droplet sizes were determined for a range of R'_{water} values at temperatures close to the excess water solubilisation phase boundary. The results are shown in Figure 4.19 as the variation of apparent diffusion coefficient with

Figure 4.18.

Hydrodynamic radii measured close to the solubilisation boundary versus R'_{water} for W/O microemulsions formed with $C_{12}E_4$ + heptane + water. Open point refers to a value derived from TRF data assuming two molecules of heptane per $C_{12}E_4$ solvation.

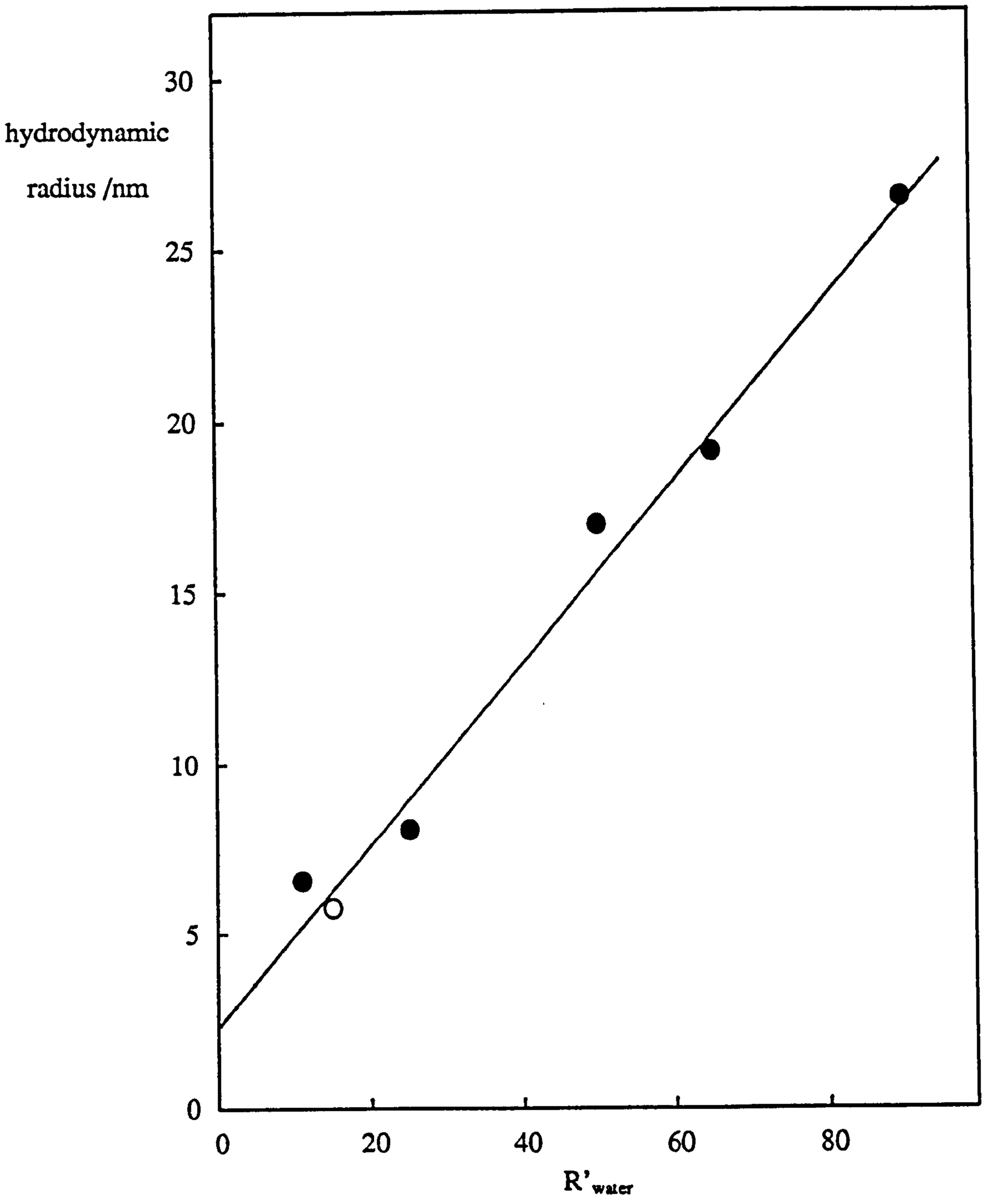

Figure 4.19.

Variation of the apparent diffusion coefficient with dispersed phase volume fraction, for water-in-tetradecane microemulsions stabilised by $C_{12}E_4$ at concentrations in excess of the cμc.

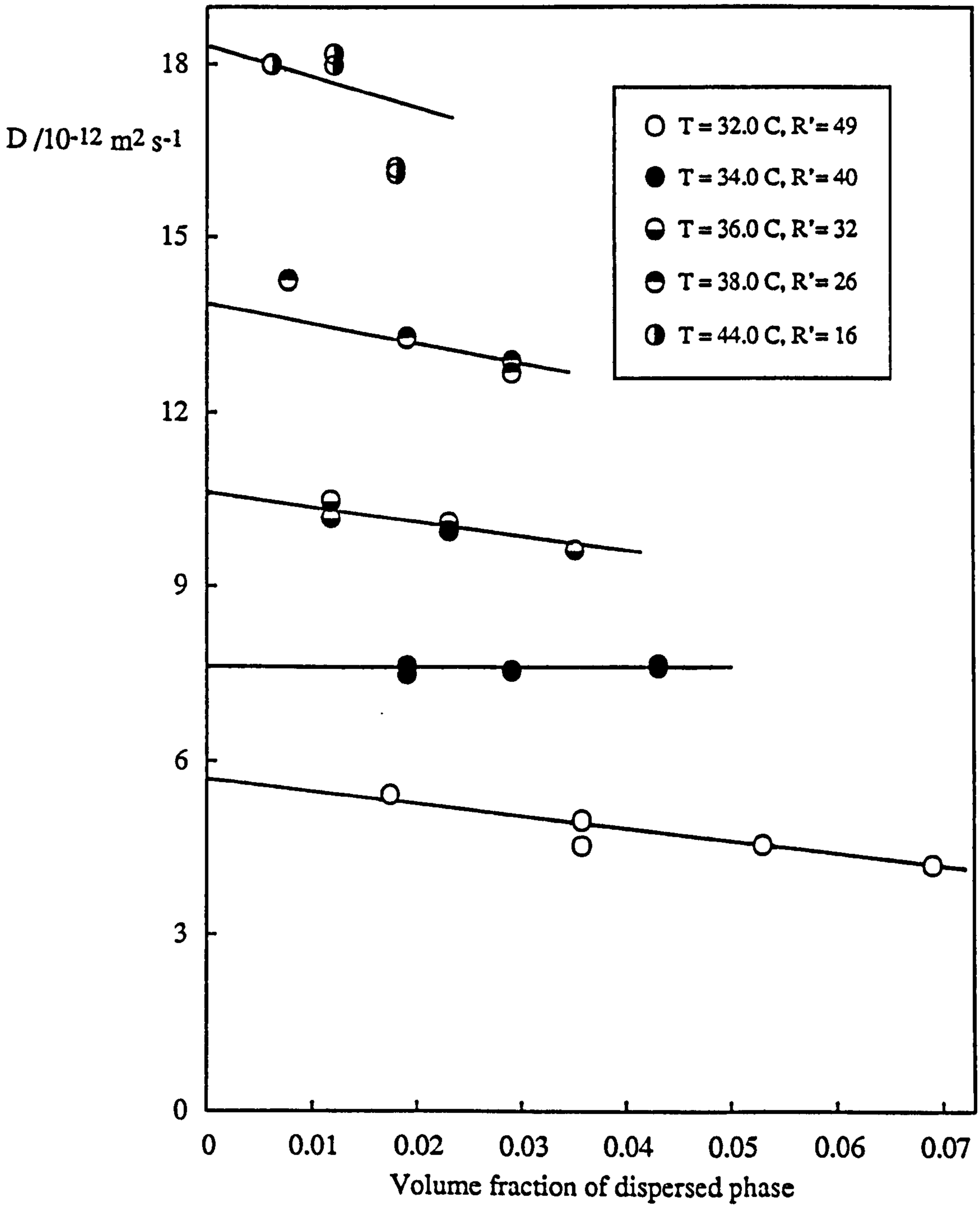

dispersed phase volume fraction. Table 4.6 shows the values of α together with the corresponding hydrodynamic radii for aggregates measured at infinite dilution.

Table 4.6

R'_{water}	α	r_H/nm
49	-4 ± 4	21.2 ± 3.0
40	0 ± 3	17.4 ± 2.0
32	-3 ± 3	12.8 ± 1.5
26	-4 ± 4	10.1 ± 1.5
16	-3 ± 10	8.3 ± 1.5

As for heptane as the oil, the diffusion coefficients show little sensitivity to the effects of droplet concentration and this is reflected in the small values of α. Again, the behaviour at these low droplet concentrations approximates to that expected for "ideal" particles.

The variation of the droplet size with R'_{water} is shown in Figure 4.20. The data is described by the following relationship.

$$r_H/nm = 0.345\, R'_{water} + 2.5$$

The area occupied per surfactant molecule at the interface between the droplet core and the surfactant monolayer is calculated to be 0.26 ± 0.06 nm^2 and the surfactant interfacial thickness to be 2.5 ± 2 nm. The estimated head group area for $C_{12}E_4$ within the curved W/O interface formed in tetradecane is slightly lower than for heptane although the difference between the values is of the same order of magnitude as the estimated uncertainties.

Figure 4.20.

Hydrodynamic radii measured close to the solubilisation boundary versus R'_{water} for W/O microemulsions formed with $C_{12}E_4$ + tetradecane + water.

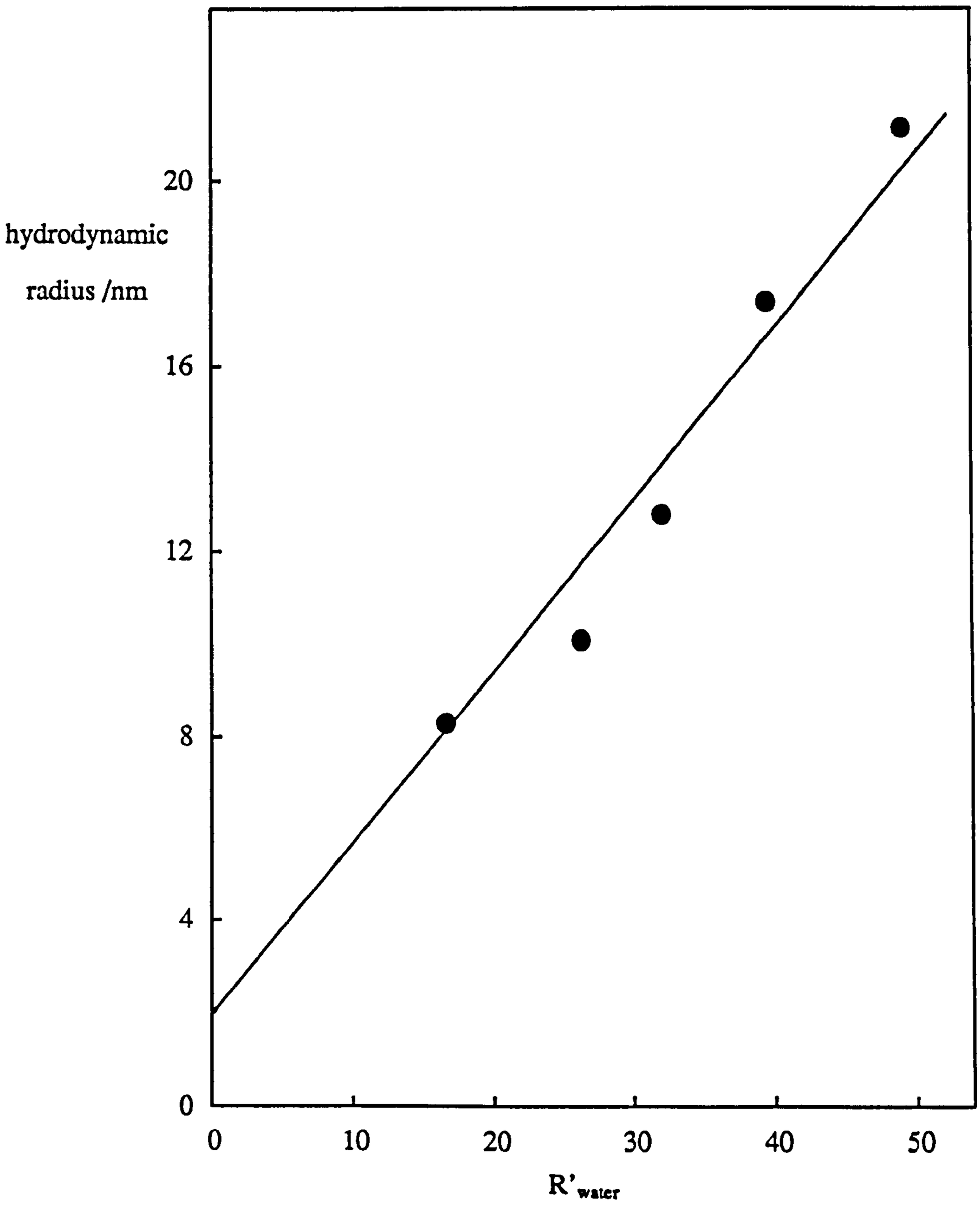

4.5.3 Effective surfactant head and tail areas within curved monolayers.

The variation of the maximum solubilisation for W/O aggregates with temperature has so far been rationalised in terms of variations in the effective areas of the surfactant head and tail groups. However, the light scattering results presented above show the dependence of the hydrodynamic radius on the droplet composition to be linear. Consequently, the effective area per surfactant head group remains constant in droplets of different sizes. If this is the case, then the observed changes in microemulsion solubilisation behaviour with temperature cannot be rationalised through variations in the effective head group area. Two extreme models may be used to interpret the solubilisation behaviour. The first of these is a model in which the effective surfactant head group area and the monolayer thickness remain constant and changes in the solubilisation behaviour arise from changes in the effective tail group area (model I). Alternatively, both the effective head and tail group areas may remain constant and changes in the monolayer thickness may result in changes in the degree of solubilisation (model II). These two models will be considered in turn.

Model I. Effective surfactant geometry within a curved monolayer - constant head group area and monolayer thickness.

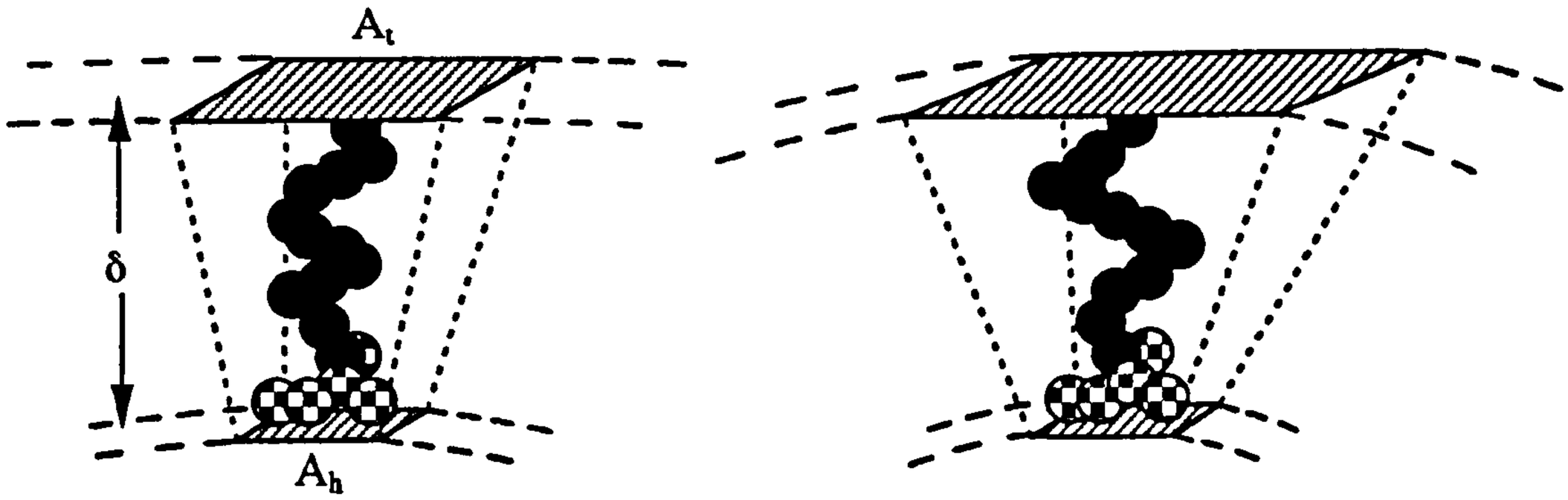

Low negative curvature
Low degree of oil penetration

High negative curvature
High degree of oil penetration

Figure 4.21

Using simple geometry, an expression can be derived relating the hydrodynamic radius to the effective head and tail areas. If the droplet is assumed to be spherical of radius r_H and interfacial thickness δ, then for a W/O droplet the head and tail group areas are given by

$$A_h = \frac{4 \pi (r_H - \delta)^2}{N_{agg}} \quad (4.3)$$

$$A_t = \frac{4 \pi r_H^2}{N_{agg}} \quad (4.4)$$

From equation 4.3 the radius of the core is given by

$$(r_H - \delta) = (A_h N_{agg}/4 \pi)^{1/2} \quad (4.5)$$

Substituting $N_{agg} = (4 \pi r_H^2/A_t)$ from equation 4.4 gives

$$(r_H - \delta) = r_H (A_h/A_t)^{1/2} \quad (4.6)$$

which reduces to

$$r_H = \frac{\delta}{[1 - (A_h/A_t)^{1/2}]} \quad (4.7)$$

Values for the effective tail group area have been calculated from this equation assuming A_h and δ remain constant at the values determined by light scattering measurements. Figures 4.22a and 4.22b show the variation of A_h and A_t with

Figure 4.22a.

Variation of the calculated effective tail group area with respect to temperature, for water-in-heptane microemulsion droplets stabilised by $C_{12}E_4$. The dashed line represents the variation of the measured head group area from PCS.

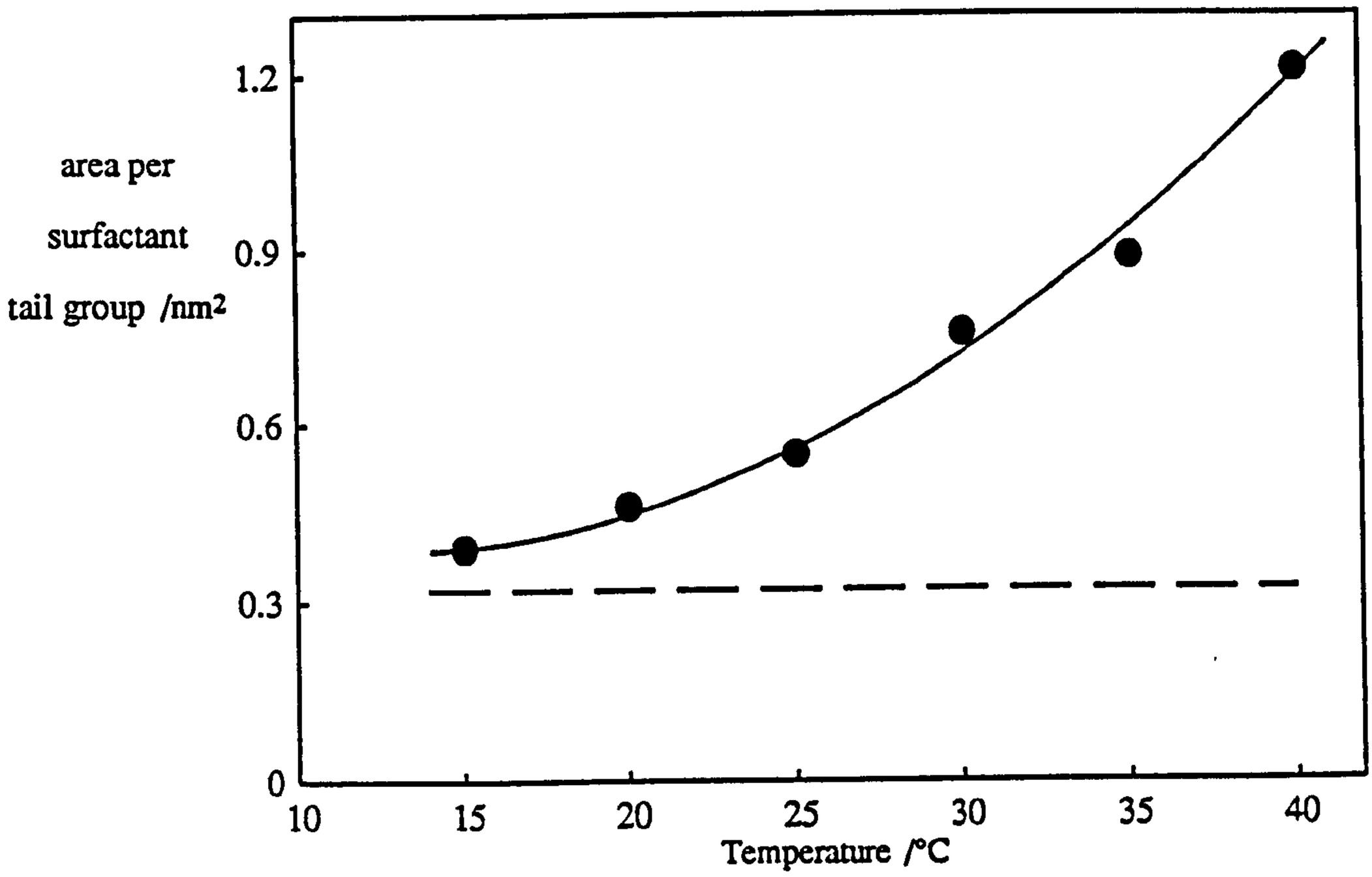

Figure 4.22b.

Water-in-tetradecane microemulsion droplets stabilised by $C_{12}E_4$.

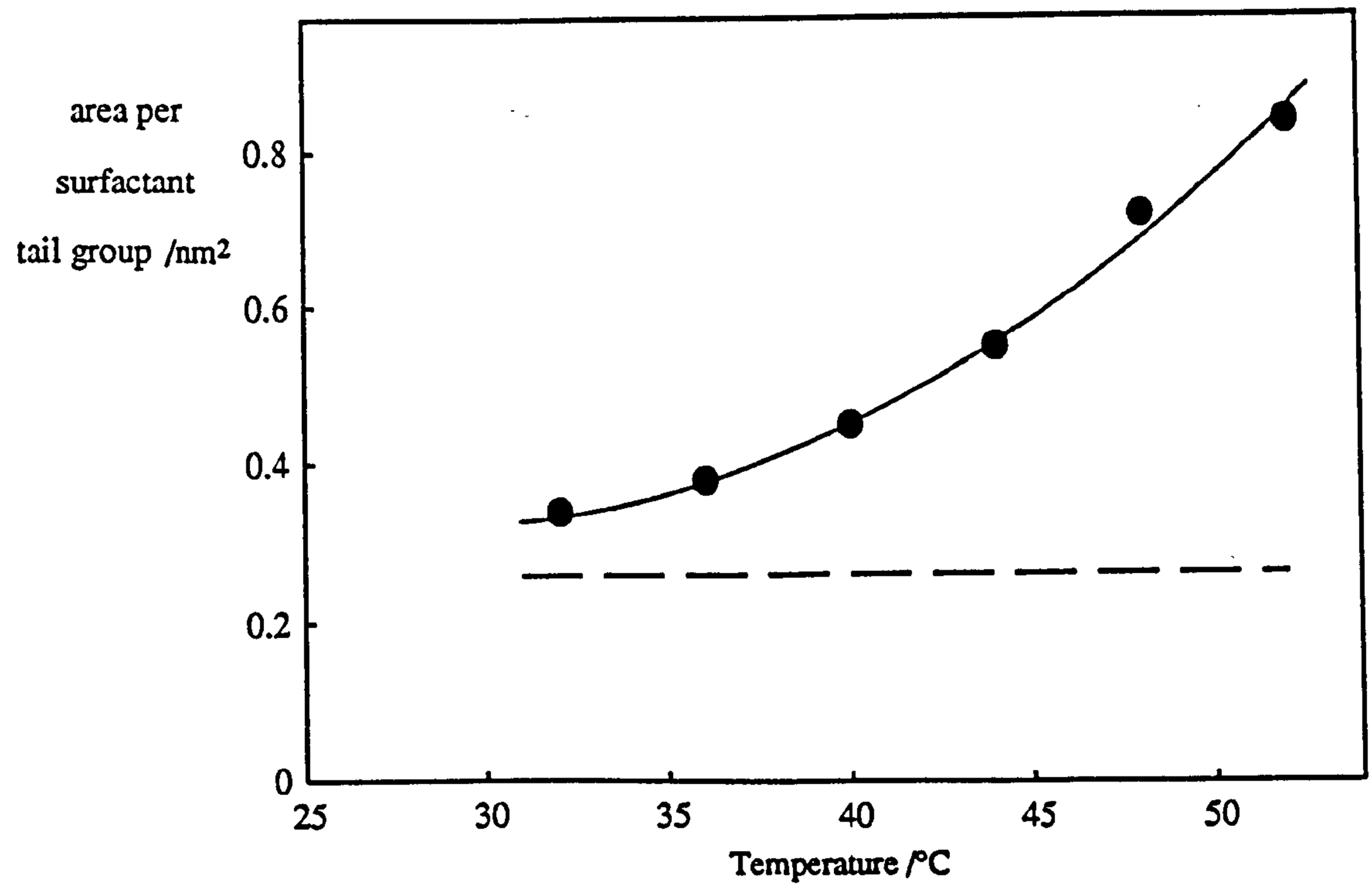

temperature for W/O microemulsion droplets at the solubilisation phase boundary for heptane and tetradecane as the oil phase. The data are tabulated below in Table 4.7.

Table 4.7

Oil is heptane. $A_h = 0.32\ nm^2$, $\delta = 2\ nm$			Oil is tetradecane. $A_h = 0.26\ nm^2$, $\delta = 2.5\ nm$		
Temp /°C	r_H /nm	A_t /nm^2	Temp /°C	r_H /nm	A_t /nm^2
15	18.9	0.39	32	19.3	0.34
20	10.7	0.46	36	13.9	0.38
25	7.6	0.55	40	10.0	0.45
30	5.1	0.76	44	7.6	0.55
35	4.5	0.89	48	6.0	0.72
40	3.7	1.21	52	5.4	0.84

From this model it is evident that the effective tail area must vary extensively to produce the required droplet size if it is assumed (from the linearity of the r_H v R'_{water} plots) that the head group area is constant. As expected, the ratio of the two effective areas tends to unity as the temperature corresponding to the start of the Winsor III region is approached. This corresponds to a situation in which the preferred net monolayer curvature is close to zero (37). From comparison of the plots for heptane and tetradecane as the oil phase it is clear that, at a constant temperature, the effective area per surfactant tail in heptane exceeds that in tetradecane. This is consistent with the notion that the shorter chain length alkane penetrates the surfactant tail region to a greater extent producing an increase in negative spontaneous curvature.

The second "limiting" model is one in which both the effective head and tail areas remain constant and the changes in the droplet size (i.e. the preferred monolayer

curvature) result from changes in the thickness of the monolayer. This possibility is illustrated below in Figure 4.23.

Model II. Effective surfactant geometry within a curved monolayer - constant head and tail group areas.

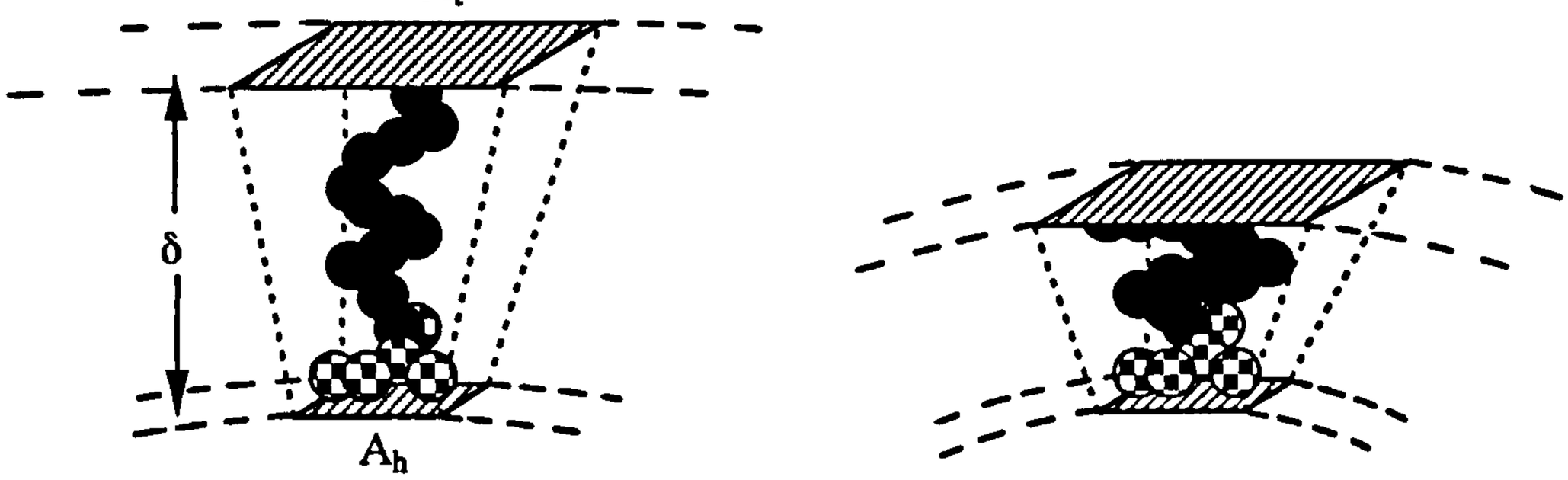

Low negative curvature
Expanded tail group conformation

High negative curvature
Contracted tail group conformation

Figure 4.23

A decrease in the monolayer thickness produces a shift towards more negative curvature i.e. smaller aggregates. The extent to which δ has to vary to produce the required range of droplet sizes is shown in Figures 4.24a, 4.24b and in Table 4.8 below for heptane and tetradecane as the oil phase.

Table 4.8

Oil is heptane. $A_h = 0.32\ nm^2$, $A_t = 0.46\ nm^2$			Oil is tetradecane. $A_h = 0.26\ nm^2$, $A_t = 0.37\ nm^2$		
Temp /°C	r_H /nm	δ /nm	Temp /°C	r_H /nm	δ /nm
15	18.9	3.14	32	19.3	3.12
20	10.7	1.78	36	13.9	2.25
25	7.6	1.26	40	10.0	1.62
30	5.1	0.85	44	7.6	1.23
35	4.5	0.75	48	6.0	0.97
40	3.7	0.61	52	5.4	0.87

Figure 4.24a.

Variation of the calculated interfacial thickness δ, with temperature, assuming A_h and A_t remain constant. For water-in-heptane microemulsion droplets stabilised by $C_{12}E_4$.

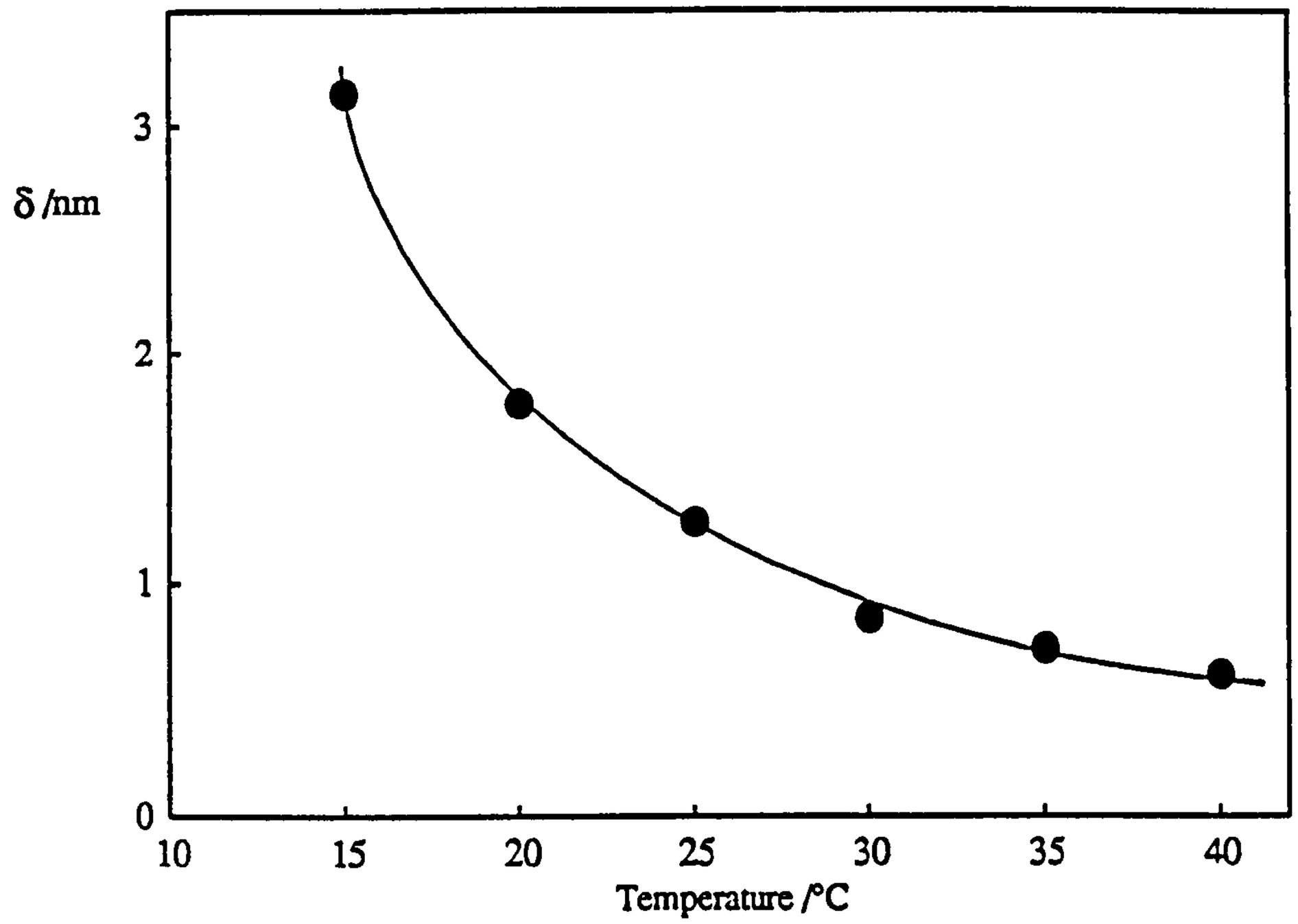

Figure 4.24b.

Water-in-tetradecane microemulsion droplets stabilised by $C_{12}E_4$.

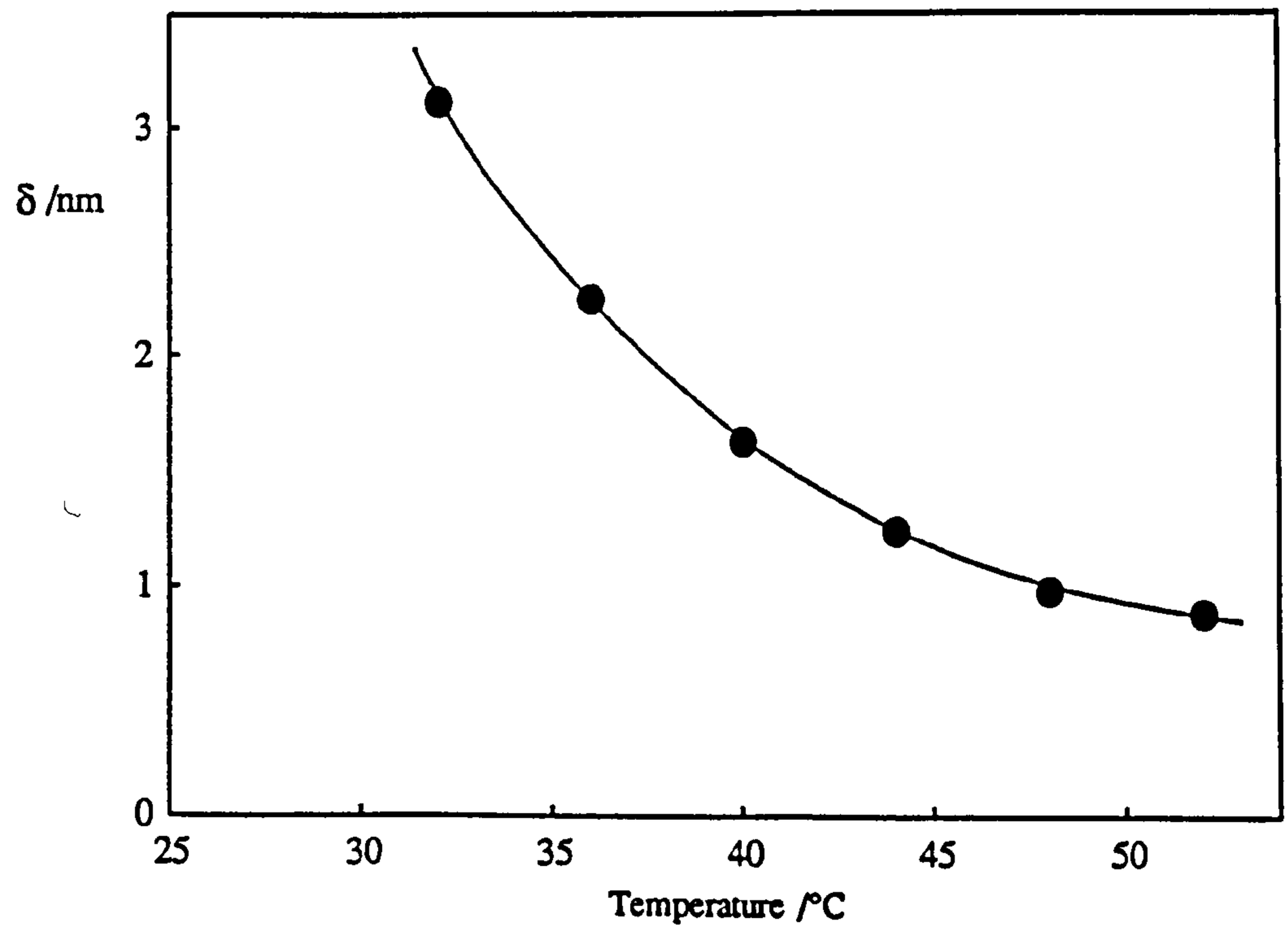

For heptane A_t was chosen to be 0.46 nm^2 and for tetradecane A_t = 0.37 nm^2. These estimates produced realistic values of δ for which the volume of the truncated pyramid did not fall below the unsolvated molecular volume of the surfactant molecule. Additionally, in both cases the monolayer thickness was always less than the all trans-length of the surfactant molecule (3.2 nm).

The actual process whereby the surfactant monolayer curvature changes with temperature may be intermediate between these two extreme models. The extent to which each may be occurring may be investigated by measuring the variation of δ with droplet size. This could be performed by small angle neutron scattering with selective deuteration.

4.5.4 Effect of solubilised α-chymotrypsin and BSA on the sizes of W/O microemulsions stabilised by $C_{12}E_4$ in heptane.

The effect of solubilised α-chymotrypsin and BSA on the excess water solubilisation boundary has previously been reported in section 4.4.1. With this information, microemulsion droplet sizes were measured for samples containing a dispersed phase protein concentration of 30 mg/ml. As in the phase boundary study, BSA was used in a 50 mM phosphate buffer solution at pH 7.0 and α-chymotrypsin in a 50 mM glycine solution at pH 9.0. The solubilisation boundaries for one phase "made-up" microemulsion samples were found to be in agreement (± 1.0°C) with those previously determined by the titration method.

Figures 4.25a and 4.25b show the variation of the apparent diffusion coefficient with dispersed phase volume fraction for droplets containing α-chymotrypsin and BSA respectively. For both systems, the apparent diffusion coefficient shows little sensitivity

Figure 4.25a.

Variation of the apparent diffusion coefficient with dispersed phase volume fraction, for water-in-heptane microemulsions stabilised by $C_{12}E_4$. The dispersed phase contains 30 mg/ml α-chymotrypsin in 50 mM glycine at pH 9.0.

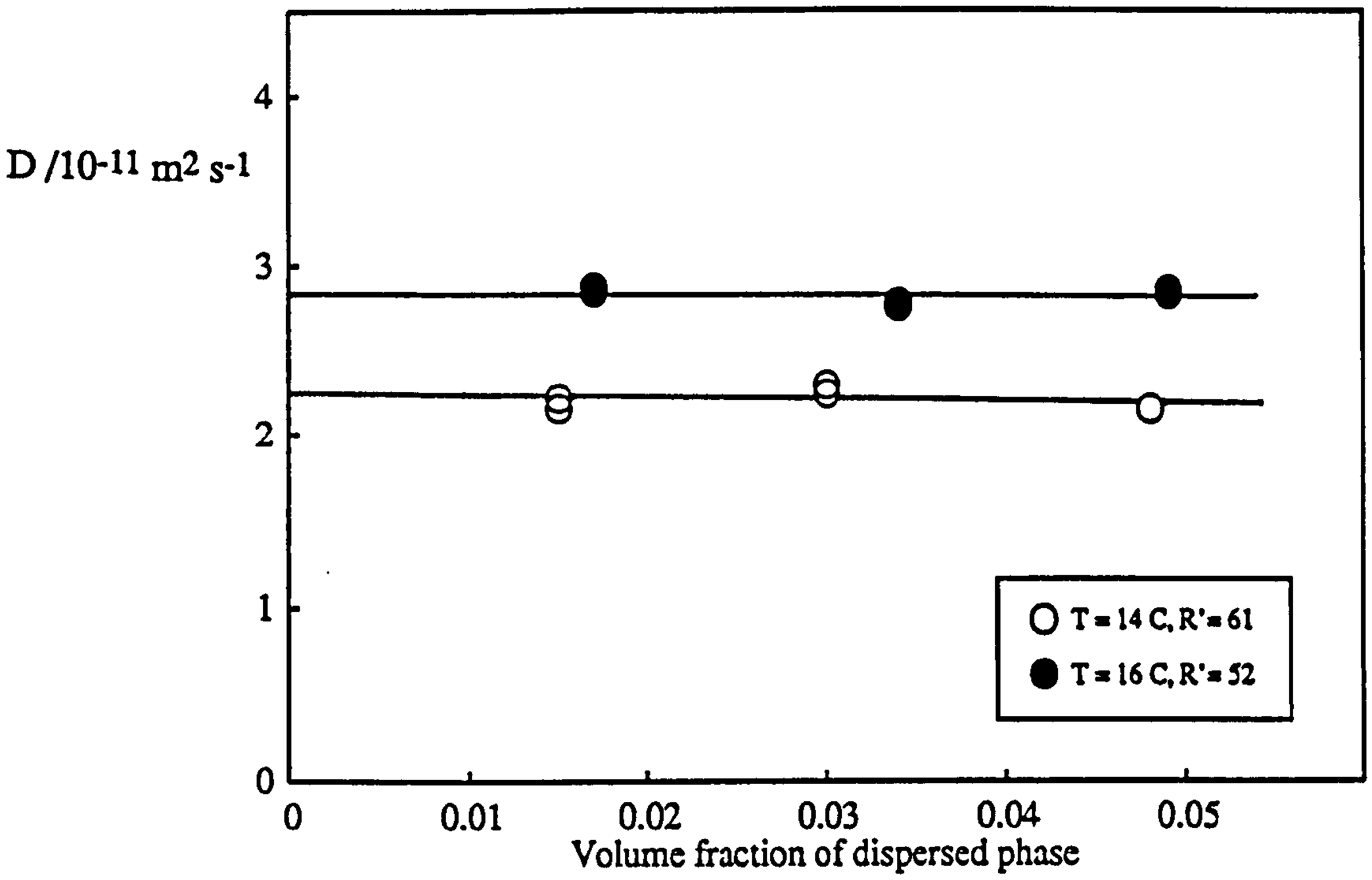

Figure 4.25b.

The dispersed phase contains 30 mg/ml BSA in 50 mM phosphate buffer at pH 7.0.

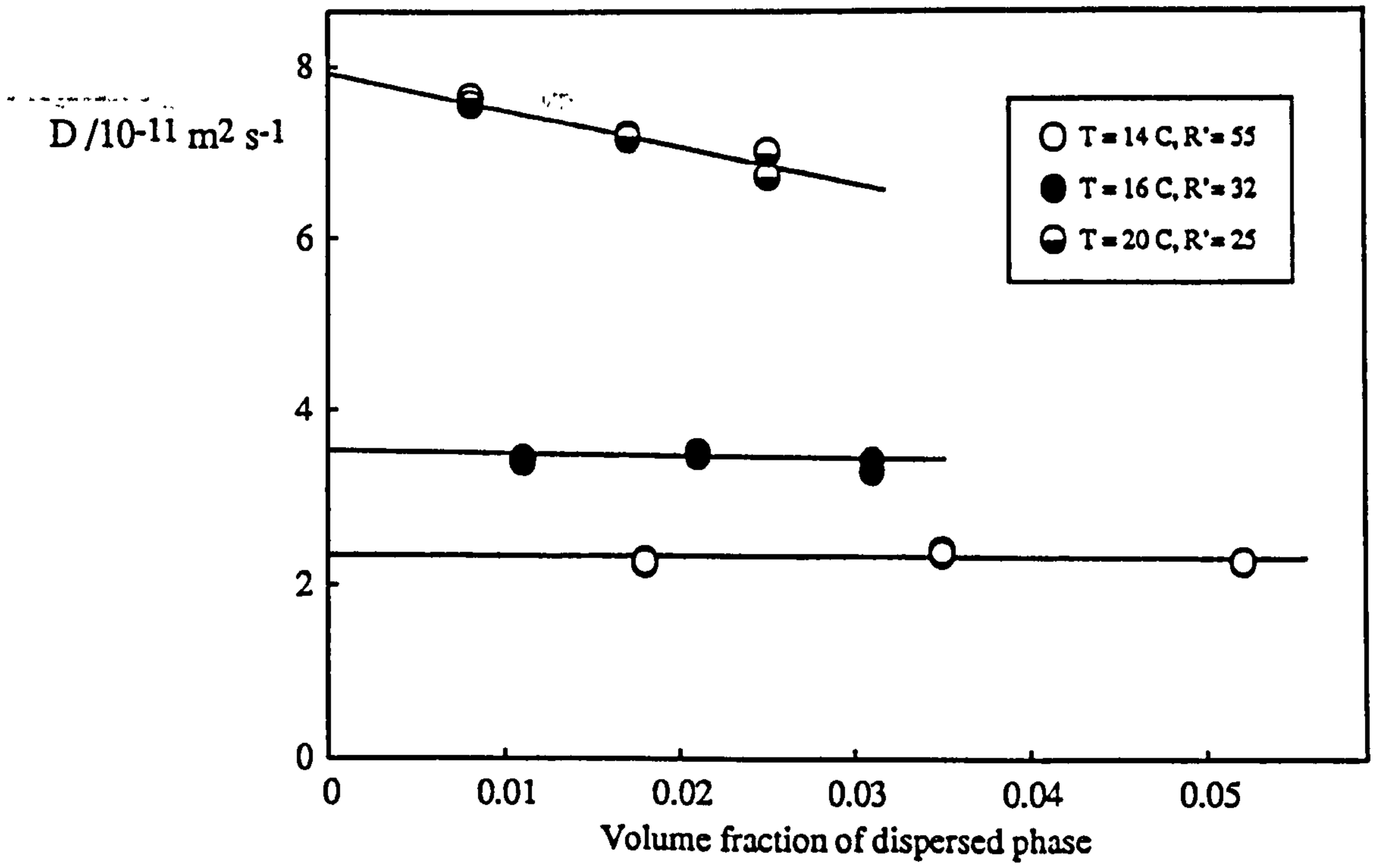

to the effect of droplet concentration and α values are zero within the errors as shown in Table 4.9.

Table 4.9

30 mg/ml α-Chymotrypsin.				30 mg/ml BSA.			
R'_{water}	α	r_H/nm	N	R'_{water}	α	r_H/nm	N
61	0 ± 2	20.7 ± 2.0	15	55	0 ± 2	19.7 ± 1.5	4.0
52	-0.5 ± 2	16.8 ± 1.5	11	32	-1 ± 3	13.8 ± 1.5	0.9
				25	-5 ± 10	6.5 ± 1.5	0.4

For these low protein concentrations, it appears that incorporation of the protein into the aggregate has no significant effect on the interactions between droplets. The aggregates again appear to behave "ideally". Also tabulated above are the true hydrodynamic radii of the droplets determined by extrapolation to infinite dilution and the calculated average number of proteins per droplet (N). Figure 4.26 compares values of the hydrodynamic radius for protein-containing aggregates with those formed with water alone as the dispersed phase.

Incorporation of α-chymotrypsin and BSA molecules into the microemulsion aggregates at these levels of occupancy has little effect on the droplet size. This is consistent with the proteins residing in the microemulsion droplets replacing their same volume of water. This is in agreement with the results of the phase boundary determinations in which it was observed that the position of the excess water solubilisation boundary was little effected by the incorporation of α-chymotrypsin and BSA into the dispersed phase.

Figure 4.26.

Hydrodynamic radii measured close to the solubilisation phase boundary versus R'_{water} for water-in-heptane microemulsions stabilised by $C_{12}E_4$. The composition of the dispersed phase is shown in the legend.

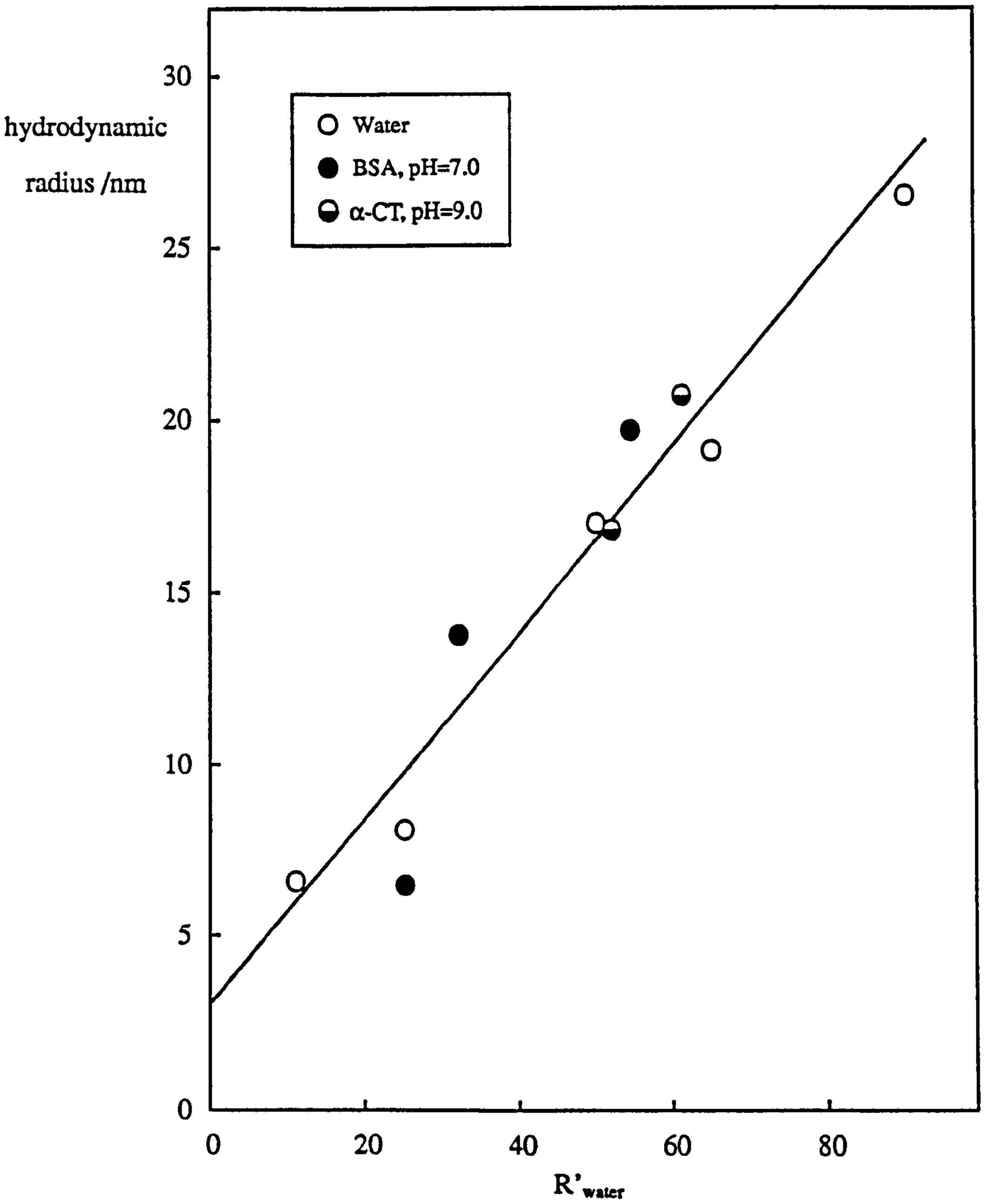

4.5.5 Effect of solubilised sodium caseinate on the sizes of W/O microemulsions stabilised by $C_{12}E_4$ in heptane.

As mentioned earlier, aqueous solutions of sodium caseinate contain protein aggregates which are typically in the size range of 50 - 300 nm. This was confirmed by the observation that a 1 mg/ml sodium caseinate solution indicated the presence of aggregates in this range with an approximate value for the normalised variance of 0.3. The aim of this study was to observe whether these protein aggregates were preserved when solubilised into the dispersed aqueous phase of W/O microemulsions.

One phase microemulsion samples containing different concentrations of sodium caseinate were prepared at various temperatures corresponding to positions on the excess water solubilisation boundary previously determined. Results from light scattering experiments on these samples indicated the presence of large aggregates in the range of 100 - 300 nm with a value for the normalised variance of 0.4. The samples showed no signs of phase separation during measurement. It seems likely therefore, that caseinate aggregates are retained solubilised in the aqueous cores of the microemulsion droplets. The large value for the variance indicates the polydisperse nature of these multiple aggregates.

4.6 Measurement of Interfacial Tensions Between Oil and Water Phases in the Presence of $C_{12}E_4$.

4.6.1 Post-cμc interfacial tension (γ_c) as a function of temperature.

It has been shown in the Introduction that the post-cμc interfacial tension can pass through a minimum value upon changing one of the solution variables

e.g. temperature, salt concentration etc. Interfacial tensions between the upper and lower phases of Winsor I, II and III systems have been measured as a function of temperature by the spinning drop technique for heptane and tetradecane as the oil phase.

For surfactant concentrations greater than the cμc in the oil, the interfacial tensions were observed to be independent of the surfactant concentration. Temperatures below about 12°C could not be achieved with the thermostat employed. Consequently interfacial tensions for heptane-in-water microemulsions, which form in this temperature range, could not be determined by this method. For tetradecane as the oil phase, the interfacial tensions corresponding to O/W microemulsion formation were observed to oscillate about mean values. This has previously been observed and discussed by Aveyard *et al.* (160). The values reported in Figure 4.27 consequently are mean values.

For the case of tetradecane as the oil phase it can be seen that, as the temperature is increased the tension falls to an ultralow value (~10^{-3} mN m^{-1}) and then rises. The left and right hand limbs of the tension minimum correspond to Winsor I and Winsor II systems in which the two phase compositions correspond to the solubilisation phase boundaries previously given (Figures 4.7 and 4.8). At temperatures close to the tension minimum a surfactant phase separates and the three phases coexist in equilibrium. This corresponds to the three phase Winsor III region. Separation of this surfactant phase allows the measurement of the tension between the excess oil and water phases and the minimum value is obtained at a temperature T^* (40). This temperature corresponds to the phase inversion temperature (PIT) of the corresponding macroemulsion (138). In this region the ratio of the effective head and tail group areas tends to unity and the net preferred curvature tends to zero. For tetradecane as the oil phase, T^* is shifted to higher temperatures as previously observed by phase boundary determinations. The depth of the tension minimum is also reduced in the case of tetradecane, consistent with the findings of previous authors (40, 161).

Figure 4.27.

Oil-water interfacial tension as a function of temperature for $C_{12}E_4$ in heptane and tetradecane at concentrations in excess of the cμc.

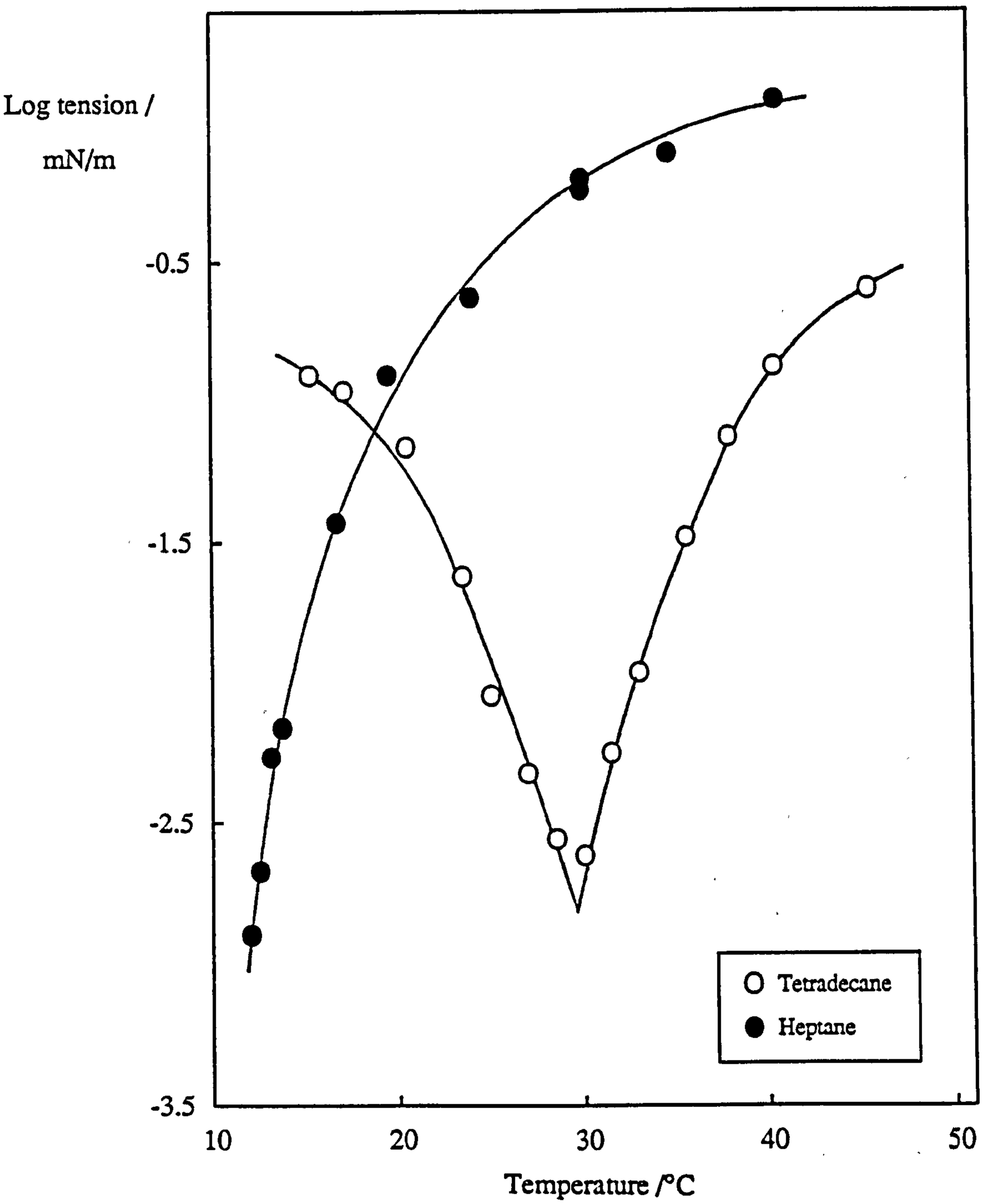

4.6.2 Correlation of γ_c with droplet size - Estimation of the monolayer rigidity.

As discussed in section 1.2.5, the post-cμc interfacial tension should scale with the droplet radius^{-2}. If the bending energy is assumed to dominate the free energy difference between the planar and curved interfaces, the constant of proportionality for this relationship can be shown to be $(2K+\bar{K})$. K is the monolayer rigidity constant, which is twice the energy required to bend a unit area of the film by a unit amount of curvature away from the spontaneous curvature, and $\bar{K}$ is the Gaussian curvature elastic modulus. This result is derived on the assumption that the film thickness is negligible in comparison with the radius. This condition is satisfied only for the larger microemulsion droplets studied here (of the order $r_H \geq 5\delta$). When the radius is taken as the droplet core radius plus half the thickness of the surfactant film, the experimental tension values scale very approximately with the droplet radius^{-2} for both heptane and tetradecane as the oil phase. This is shown in Figures 4.28a and 4.28b. The error bars indicate the estimated maximum errors in the droplet radii which arise from uncertainties in the temperatures of the solubilisation boundaries and from droplet size determinations. The deviations from the expected slope are of the same order of magnitude as the errors.

This analysis gives values of $(K+\bar{K}/2)$ of 1.0 ± 0.6 kT for heptane as the oil and 0.7 ± 0.7 kT for the tetradecane system. The two values are the same within the large errors of their determination and are both of the order of kT. This method clearly only provides a very approximate estimation of the monolayer rigidity since the errors associated with the values are of the same order of magnitude as the values themselves.

Previously, Aveyard *et al.* estimated values of $(K+\bar{K}/2)$ from this tension-size relationship for microemulsions stabilised by $C_{12}E_5$ (29). They obtained a value of 1.1 ± 0.5 kT for droplets produced with heptane as the oil phase, which was independent of the type of aggregate formed. For water-in-tetradecane microemulsions, they reported a value of 2.3 ± 0.9 kT. The difference between these two values is greater than for the

Figure 4.28a.

Variation of log tension with log radii for water-in-heptane microemulsions stabilised by $C_{12}E_4$. The solid line indicates the behaviour expected from equation (1.10).

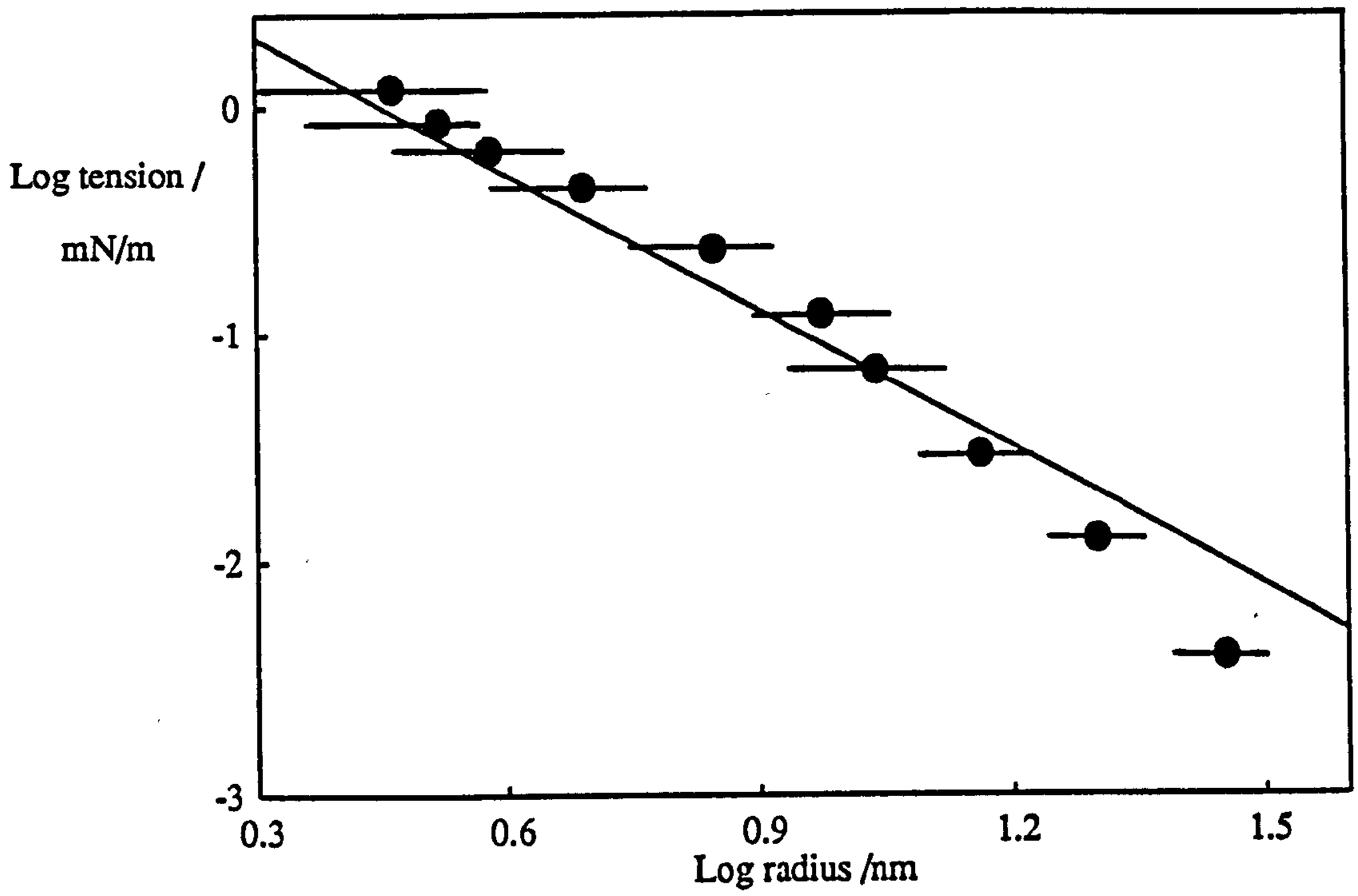

Figure 4.28b.

Water-in-tetradecane microemulsions stabilised by $C_{12}E_4$.

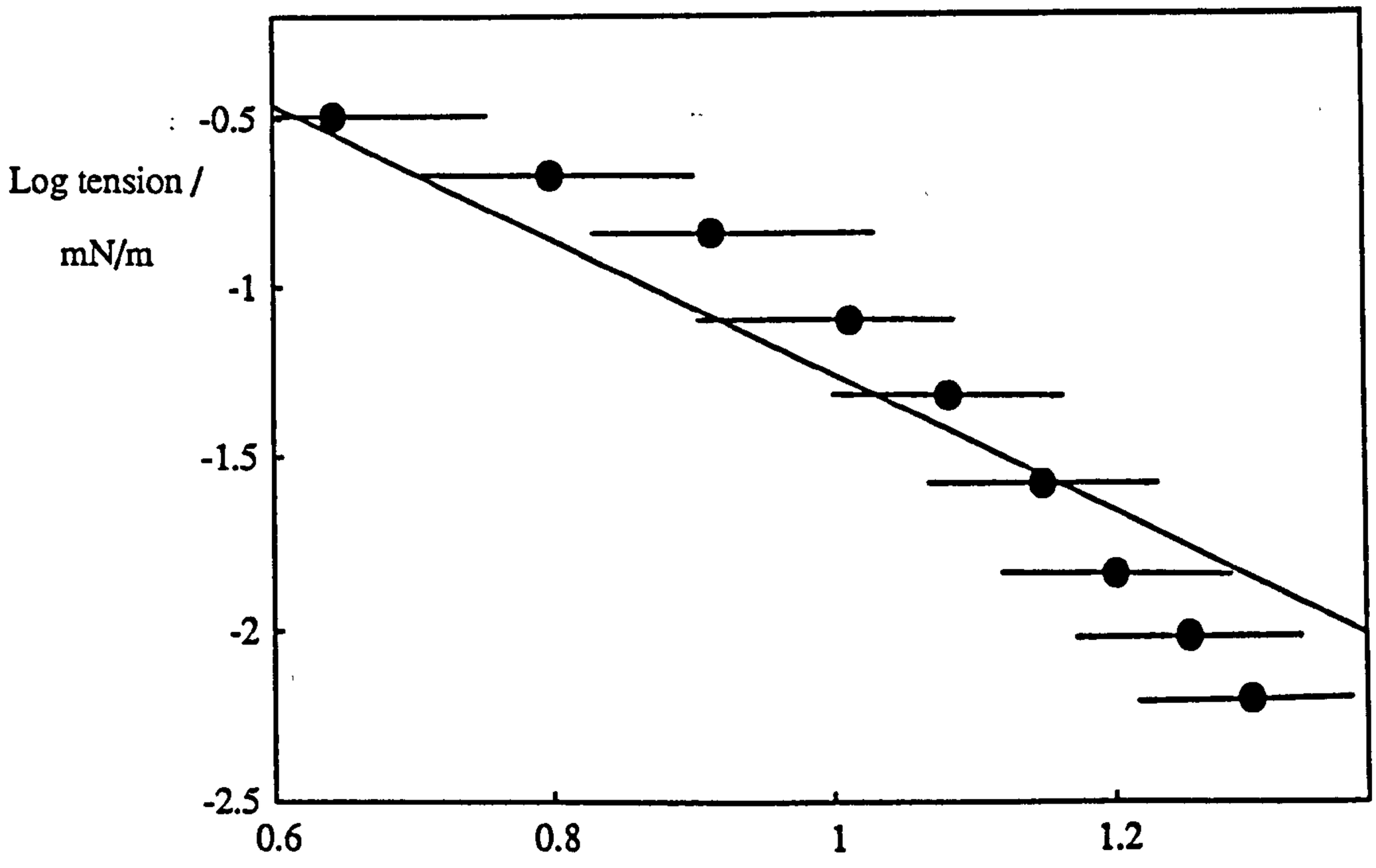

corresponding $C_{12}E_4$ systems. However, the values are again the same within their large reported errors.

Several methods have been developed for measuring directly monolayer rigidities. These include ellipsometry for the determination of flat monolayer rigidities (162), and electro-optical Kerr effect measurements (163) and neutron spin-echo determinations (164) for curved monolayers. These techniques provide a measure of K alone. To date they have mainly been applied to the study of ionic surfactant systems (46, 163, 165). One such study has been performed recently by Binks *et al.* (166). They have investigated the effect of changing the alkane chain length on K, as determined directly by ellipsometry, for the quaternary system AOT + alkane + water + salt at 20°C. They observed that for alkanes between heptane and tetradecane, K decreased with increasing alkane chain length. Lee *et al.* have also recently measured values of K by ellipsometry (167). They studied planar monolayers at oil-water interfaces formed with C_8E_3 + decane + water and $C_{10}E_4$ + octane + water. For C_8E_3 and $C_{10}E_8$ surfactant films they determined values of K of 0.35 kT and 0.76 kT respectively. These latter values were renormalised to a length scale of 7.5 Å by a procedure described in reference (168). These results are considered further in Chapter 6.

Caution must be exercised in comparing rigidities for different surfactant monolayers. Firstly, for the majority of the systems investigated to date, the uncertainties in the values of K are of the same order as the differences between different systems. Secondly, rigidities measured using different methods are not generally directly comparable since K is dependent upon the length scale of the observation used in the technique (169, 170). Thirdly, the rigidity values calculated from the tension-size relationship, contain contributions from both K and $\bar{K}$, whereas the more direct methods previously mentioned yield estimates of K alone. As yet, values for $\bar{K}$ have not been reported.

4.7 Time-Resolved Fluorescence Results for W/O Microemulsions Stabilised by $C_{12}E_4$ in Heptane.

4.7.1 Analysis of time-resolved fluorescence data.

The fluorescence intensity decay of a surfactant aggregate solution containing solubilised fluorescer (F) and quencher (Q) probe molecules is given by the following equation (171, 172)

$$I_t = I_0 \exp(-A_2 t - A_3 [1 - \exp(-A_4 t)]) \qquad (4.8)$$

where I_t and I_0 are the intensities at time t and zero, respectively. The three parameters A_2 - A_4 together with I_0, are obtained by computer fitting the experimental data to a convolution of equation 4.8 with the measured instrument response profile. If it is assumed that (i) the fluorescer and quencher probes are confined entirely within the surfactant aggregates, (ii) they are distributed randomly amongst the aggregates, and (iii) re-distribution of the probes between aggregates does not occur on the experimental time scale, then the three parameters A_2 - A_4 are given by

$$A_2 = k_0 \qquad (4.9)$$

$$A_3 = [Q]/[\text{aggregates}] \qquad (4.10)$$

$$A_4 = k_q \qquad (4.11)$$

where the rate constant k_q is the first order quenching rate constant for an aggregate containing a single quencher molecule. The rate constant k_0 is the fluorescence decay rate constant in the absence of quencher. This is obtained separately by measuring the

fluorescence intensity decay trace of the probe in a microemulsion sample containing no quencher. This trace is then fitted to a single exponential of the form

$$I_t = I_0 \exp(-k_0 t) \qquad (4.12)$$

The number of surfactant molecules per aggregate (N_{agg}) may be obtained from equation 4.13 below which takes account of the concentration of surfactant not involved in aggregate formation.

$$N_{agg} = ([\text{surfactant}] - c\mu c)/[\text{aggregates}] \qquad (4.13)$$

For systems where migration of the probes between aggregates occurs on the experimental time scale, the experimental intensity decay curves are still described by equation 4.8. However, equations 4.9 - 4.11 are now not valid. This situation is clearly indicated by the observation that A_2 is larger than k_0. For this case a particular mechanism of transfer must be assumed in order to determine the appropriate exchange rate constant from the parameters A_2 - A_4 (173).

For the W/O microemulsions studied here, ruthenium tris-bipyridyl (RB) and methyl viologen (MV) were used as fluorescer and quencher molecules respectively. Both species are positively charged and hence highly insoluble in the apolar medium. It is assumed therefore, that they are confined entirely within the W/O droplets. The assumed mechanism of inter-droplet exchange of these species is through a process involving the temporary coalescence of droplets followed by reseparation with a consequent "scrambling" of the components between the droplets (so called "fusion-fission" mechanism) (173). This process was illustrated previously in Figure 1.12. An alternative mechanism whereby a fragment of the aggregate breaks away and acts as a "carrier" for the probe is thought less likely. This would be associated with

nonspherical, polydisperse aggregates, whereas the microemulsion droplets formed with $C_{12}E_4$ in heptane have previously been shown to be consistent with monodisperse, spherical droplet formation. Quenching of RB fluorescence by a quencher in an adjacent but non-coalesced droplet (i.e. through the surfactant bilayer separating the two aggregates) is thought unlikely to occur at any significant rate. The quenching of RB fluorescence by MV in aqueous solution has previously been shown to occur by an electron-transfer mechanism (174). For quenching to occur through two non-coalesced droplets would involve the transfer of an electron through a surfactant bilayer of approximately 6 nm thickness which is considered unlikely.

It must be emphasised that the process of droplet exchange via a "fusion-fission" mechanism is purely an assumed possible pathway to interpret droplet dynamics. The real mechanism operating in solution may well be far more complicated than this simple picture. Recently, Johannsson *et al.*, investigating W/O microemulsions stabilised by AOT, observed that clusters of aggregates were produced at a temperature close to the haze point boundary and that exchange of probes occurred within these structures (175). They concluded that they could not confirm (on the basis of their measurements) that the process of exchange within a cluster was one of "fusion-fission" or whether some other exchange process was operative.

For the general case where the probe molecules exchange during the experimental time scale, Almgren *et al.* have shown the parameters A_2 - A_4 are given to a reasonable approximation, by the following expressions (173),

$$A_2 = k_q [x]_s + k_0 \qquad (4.14)$$

$$A_3 = n (1 - [x]_s/n)^2 \qquad (4.15)$$

$$A_4 = k_q/(1 - [x]_s/n) \qquad (4.16)$$

where n is the average number of quenchers per droplet and $[x]_s$ is the average number of quenchers in aggregates containing excited fluorescent probes in the steady-state phase of the decay. Equations 4.14, 4.15, 4.16 above are solved to yield the three unknowns n, k_q and $[x]_s$. The concentration of aggregates can be determined from the value of n since

$$[\text{aggregates}] = [\text{quencher}]/\, n \qquad (4.17)$$

which allows calculation of the droplet aggregation number using equation 4.13. The first order rate constant for droplet exchange via the "fusion-fission" mechanism, k_f, is obtained by calculating $[x]_s/n$ for the sample and determining the corresponding value of $k_f/\, k_q$ from Figure 4.29a, reference (173).

Good fits to the data were obtained using equation 4.8 with the reduced chi-squared (χ^2) being of the order of 1.5 or better. A typical fitted intensity curve is shown in Figure 4.29b with its corresponding residuals plot. For high surfactant concentrations (20 - 30 wt%) a slight aberration was often observed in the first few channels of the decay trace. This was found to be due to a small amount of a fluorescent impurity in the sample of $C_{12}E_4$. Different batches of the surfactant all contained this impurity. Fitting of intensity decay traces for these high surfactant concentration samples typically produced poor values of χ^2 (> 2.0). To overcome this problem, the intensity decay of a "blank microemulsion" was recorded, which apart from containing no fluorescer, was identical to the sample investigated. The blank was recorded under identical conditions to the sample. Its trace was then subtracted from the sample before fitting. In this way the fitting of the decay trace was much improved with χ^2 values of ~1.5. In some cases where the impurity peak was very slight, the sample decay trace was fitted starting two channels past the peak value. The parameters obtained through either method were the same within the error of their determination (~10%).

Figure 4.29a.

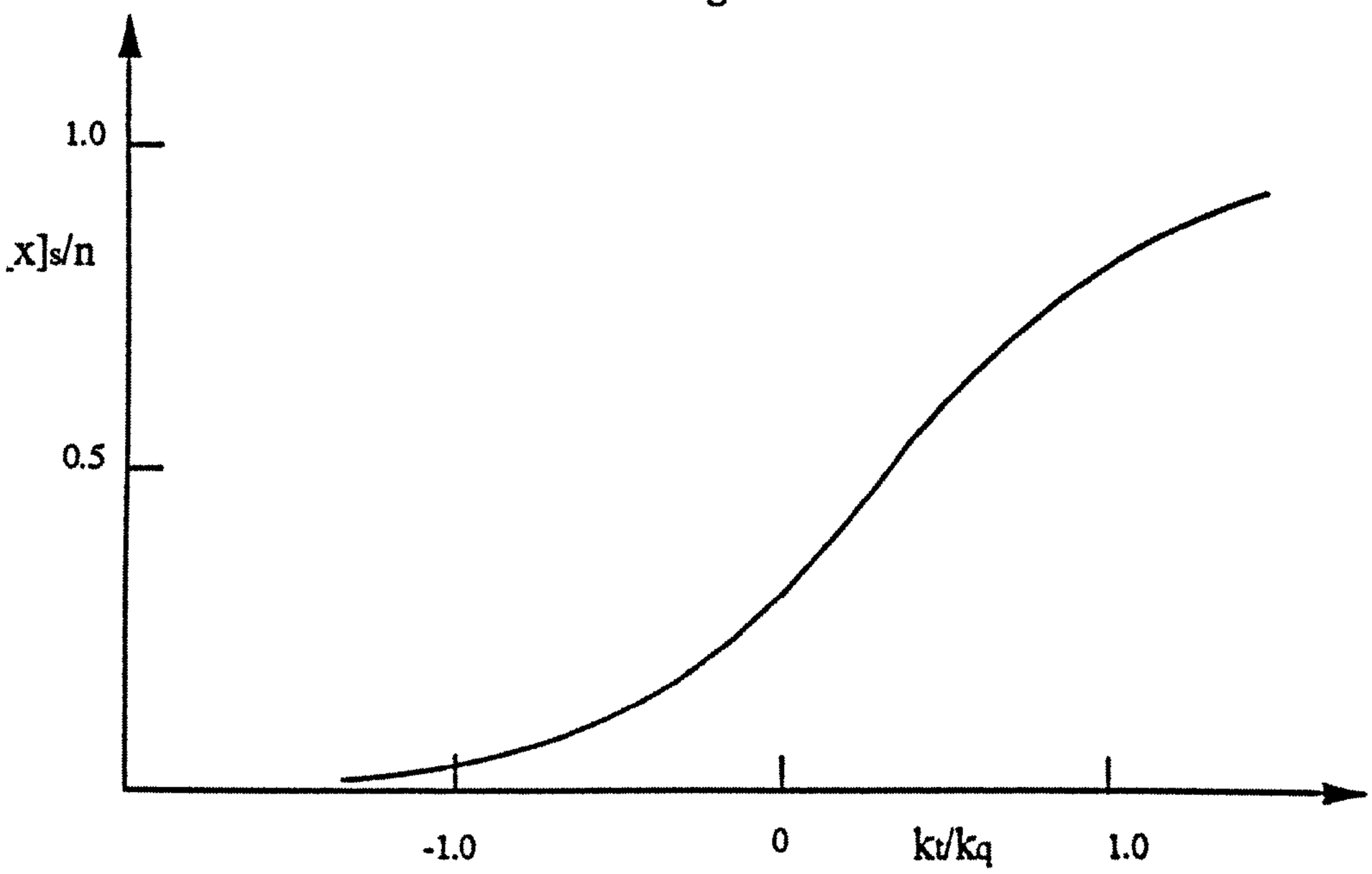

Figure 4.29b.

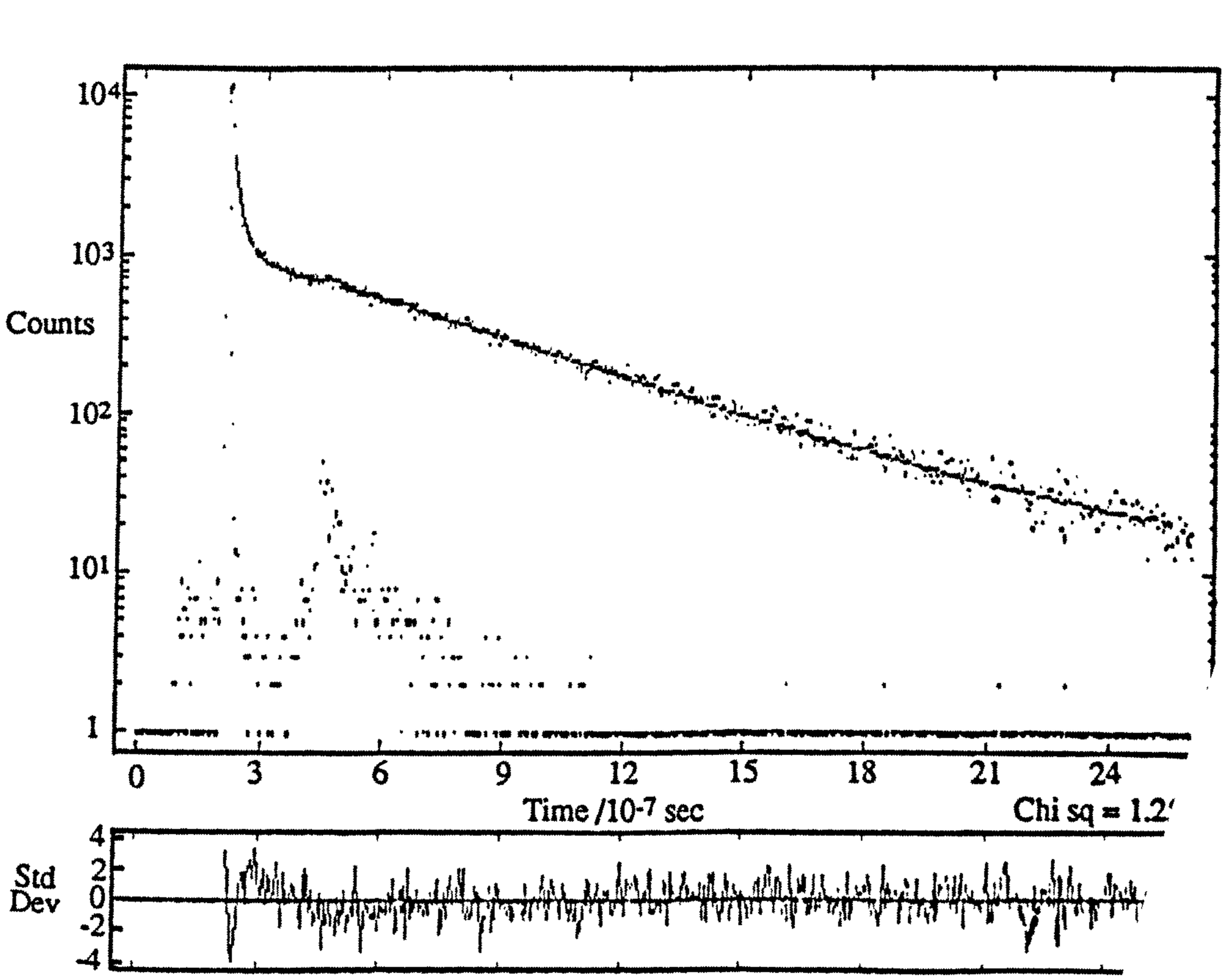

Typically samples containing an average of 0, 1 and 2 quenchers per droplet were studied at surfactant concentrations between 10 and 30 wt%. The incorporation of probe molecules into the dispersed phase of the droplets was found to shift the position of the phase boundaries by no more than 1 - 2°C. This indicated that the system was not perturbed to any large extent by the presence of the probes. A slight increase in temperature of 1 - 2°C for the position of the one phase microemulsion region was observed on increasing the surfactant concentration to 30 wt%.

4.7.2 Results for W/O microemulsions stabilised by $C_{12}E_4$ in heptane.

Microemulsion droplets of composition $R'_{water} = 15$ were studied as a function of temperature across the one phase stability region. The upper temperature limit, the excess water solubilisation boundary, occurs at approximately 28°C whereas the low temperature haze boundary is observed at 17°C. The critical microemulsion concentration for the system was previously determined at the solubilisation boundary to be 3.2 ± 0.4 wt%. At temperatures close to the solubilisation boundary, it has been shown by PCS that the droplets are close to spherical and interact only weakly. As the haze boundary is approached however, the apparent hydrodynamic radius increases. This was previously shown in Figure 4.16 as a decrease in the apparent diffusion coefficient.

Microemulsion droplet radii were calculated from the aggregation numbers determined by TRF according to the equation (55)

$$r = [(3/4\pi)\, N_{agg}(v_{surf} + R'_{water}\, v_{water})]^{1/3} \qquad (4.18)$$

where v_{surf} and v_{water} are the molecular volumes of the surfactant and dispersed water respectively. Radii calculated from this equation for the different surfactant

concentrations are shown in Figure 4.30 for temperatures across the one phase region. It can be seen that the droplet size remains constant on traversing the one phase region and that the measured size is independent of the droplet concentration. The average radius is seen to be 5.3 ± 0.4 nm which corresponds to an average aggregation number of 590 ± 120. This compares well with the value of 6 ± 2 nm for the hydrodynamic radius determined previously by PCS. Since the values derived from TRF data do not take into account solvation of the surfactant tail region they might be expected to be smaller than those determined by light scattering measurements. However, no significant difference is observed between the two values due to the large uncertainty in the PCS determined values caused by the low scattering intensity of these systems. As previously mentioned, TRF results are independent of assumptions concerning inter-droplet interactions. The increase in the apparent hydrodynamic radius observed by PCS on moving towards the haze curve, therefore, is not due to an increase in droplet size and must be a consequence of an increasing attraction between aggregates.

The quenching rate of RB by MV in bulk aqueous solution is close to the diffusion controlled limit expected for species of the same type of charge (174). The first order quenching rate constant (k_q) for quenching within a microemulsion aggregate is therefore a measure of the time taken for the fluorescer and quencher probes to diffuse together within the aggregate. If it is assumed that the probes do not interact with the surfactant monolayer and display normal diffusion behaviour, the following relationship between k_q and the microviscosity experienced by the probe molecules in the droplet, η_m, has previously been derived (48).

$$k_q = \frac{8\,R\,T}{(3\,\eta_m\,V\,N_A)} \qquad (4.19)$$

The microemulsion droplet volume V, is the volume which is accessible to the probe molecules and is taken to be equal to ($N_{agg}\ R'_{water}\ v_{water}$), where v_{water} as before is the

Figure 4.30.

Variation of microemulsion droplet radii (unsolvated) across the one phase stability region for $R'_{water} = 15$ W/O microemulsion droplets stabilised by $C_{12}E_4$ in heptane.

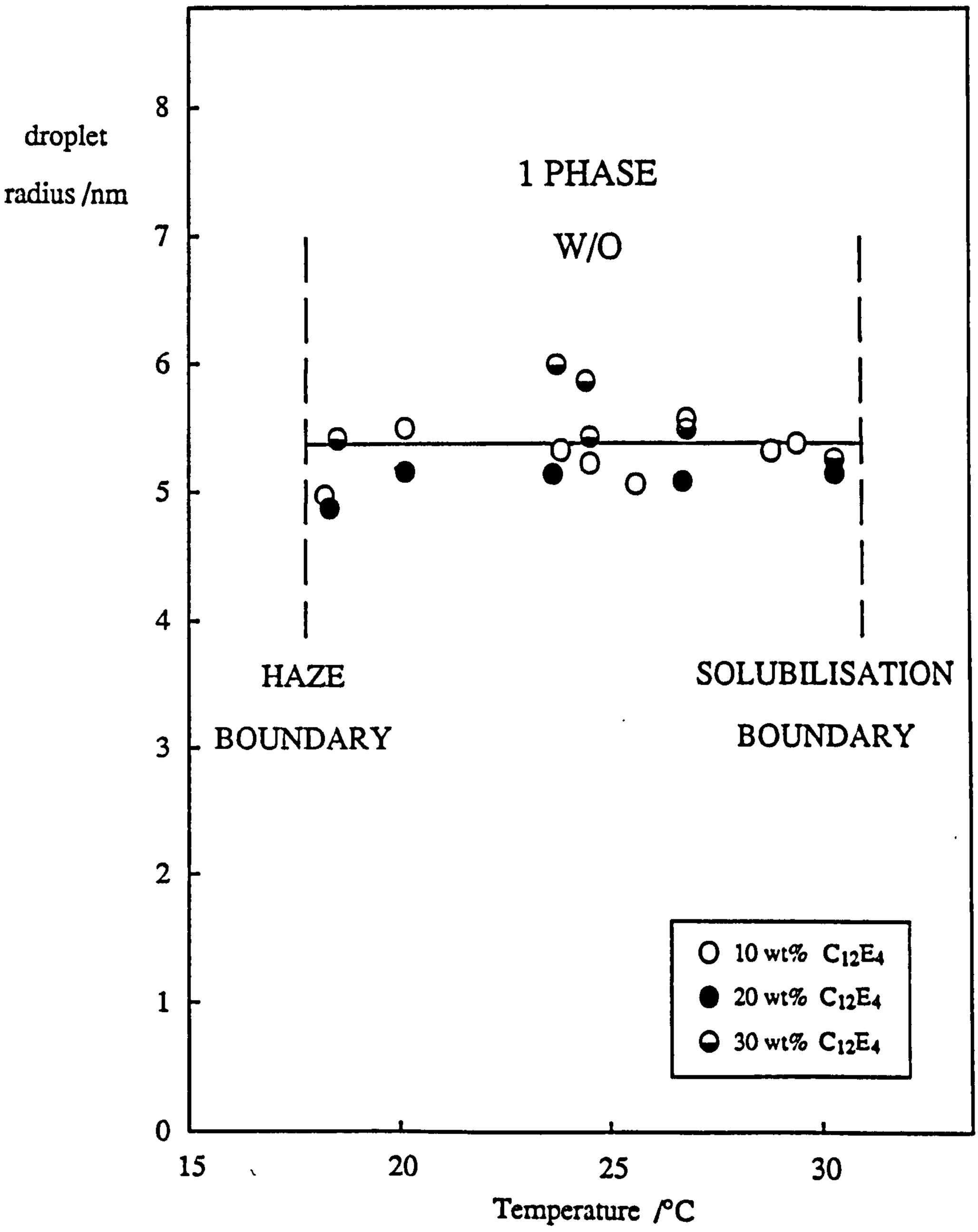

molecular volume of water. N_A is Avogadro's constant, and R and T have their usual significance. Values of (k_q N_{agg} R'_{water}), predicted by equation 4.19 to be proportional to $1/\eta_m$, are shown in Figure 4.31 as an Arrhenius type plot. The dashed line shows the expected behaviour if η_m is equated with the bulk viscosity of water. The experimental points are seen to be about 10 times lower than the calculated values. This indicates that the apparent microviscosity experienced by the probes within the water droplets is about 10 times that of bulk water (i.e. approximately 10 cP).

Variation of the first order unquenched fluorescence decay rate constant k_0 with temperature is shown in Figure 4.32. The values are effectively independent of the surfactant concentration and increase with increasing temperature. The data are seen to be indistinguishable from the results obtained in bulk water. The photophysical behaviour of RB has a complex dependence on solvent properties (176). However, results consistent with those obtained in bulk water presumably indicate that the probe experiences a "water-like" microenvironment.

Values of the first order rate constant k_t for exchange of probe molecules between microemulsion droplets via a "fusion-fission" mechanism, are shown in Figure 4.33 as a function of droplet concentration. The values are seen to be approximately proportional to the droplet concentration within the estimated uncertainties of their measurement. The second order exchange rate constants (k_c) corresponding to different temperatures within the one phase region are obtained from the slopes. These are displayed in Figure 4.34 in an Arrhenius type plot.

It is clear that the exchange rate constant *increases* with *decreasing* temperature, i.e. droplet coalescence is slowest at the high temperature excess water solubilisation phase boundary. This unusual behaviour implies that the energy barrier to coalescence decreases as the haze boundary is approached. A similar observation has been made for W/O microemulsions stabilised by $C_{12}E_5$ in heptane and tetradecane (55). For ionic surfactant systems, W/O microemulsion regions are bound at low temperatures by the

Figure 4.31.

Log (k_q N_{agg} R'_{water}) versus 1/temperature for R'_{water} = 15 W/O microemulsion droplets stabilised by $C_{12}E_4$ in heptane. The dashed line indicates the values calculated for a microviscosity equal to that of bulk water.

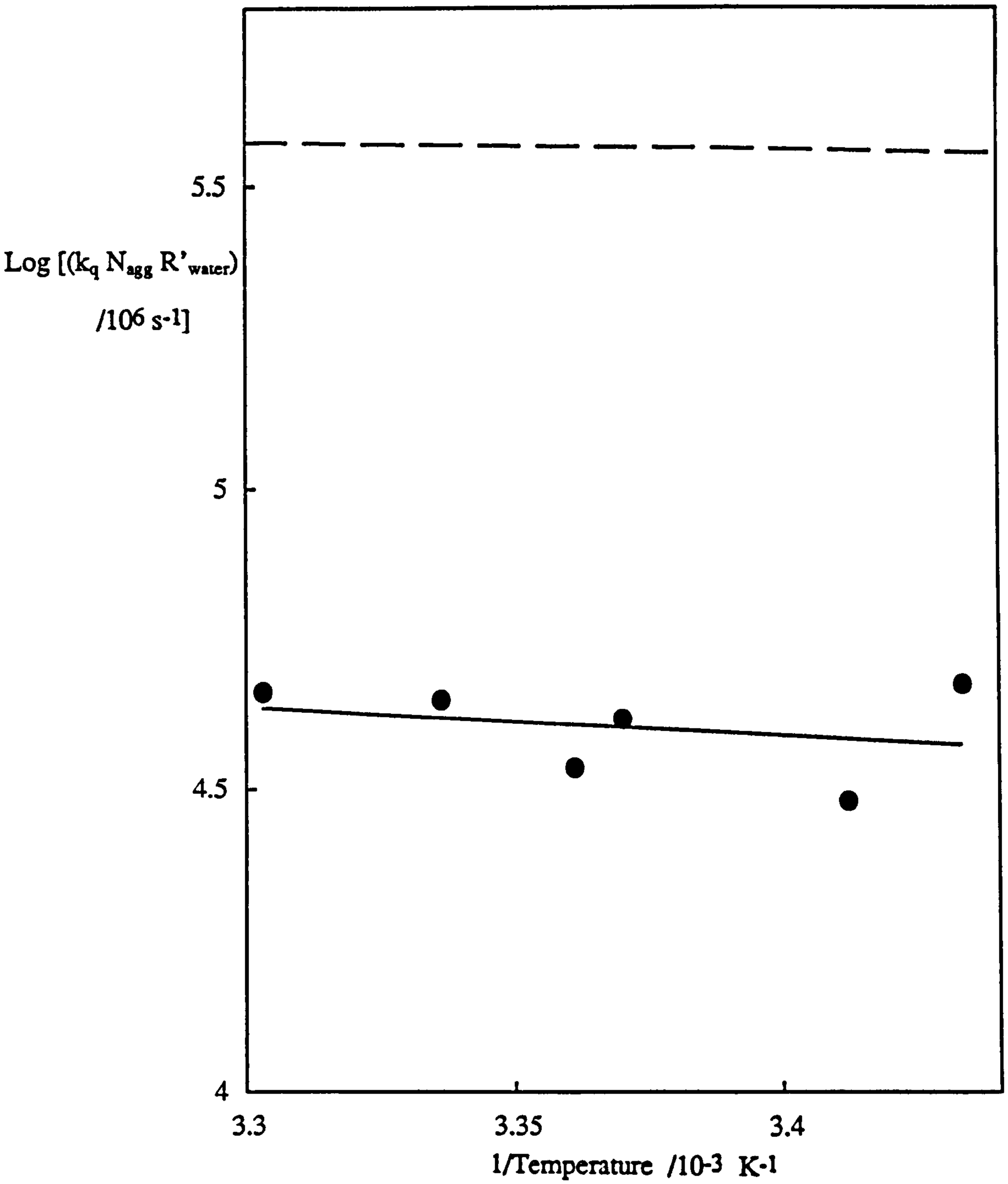

Figure 4.32.

Variation of the unquenched fluorescence decay rate constant k_o for RB in $R'_{water} = 15$ W/O microemulsion droplets stabilised by $C_{12}E_4$ in heptane. The dashed line indicates the behaviour in water (121).

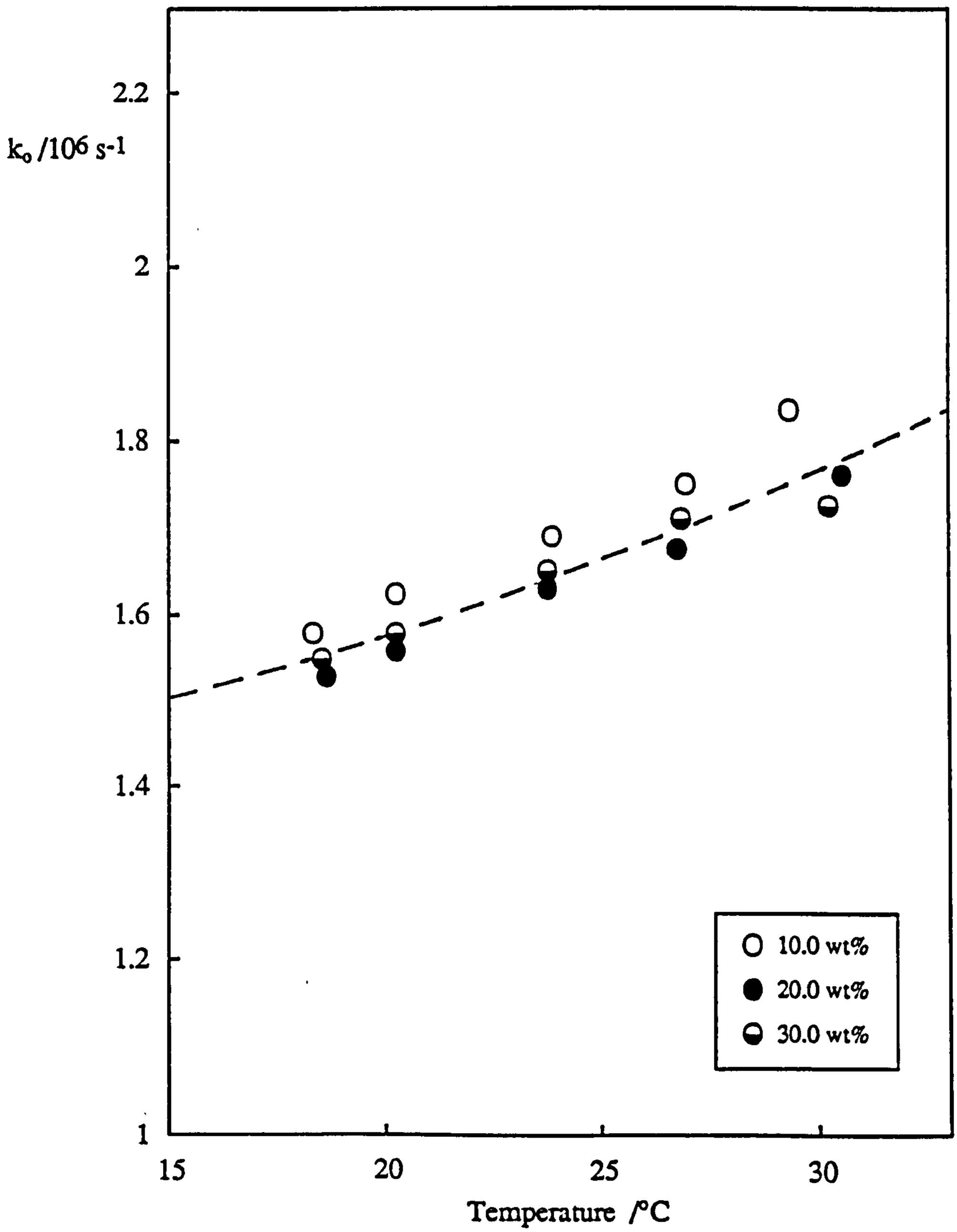

Figure 4.33.

First order exchange rate constant (k_t) versus droplet concentration for $R'_{water} = 15$ water-in-heptane microemulsions stabilised by $C_{12}E_4$. The temperatures correspond to positions within the one phase stability region.

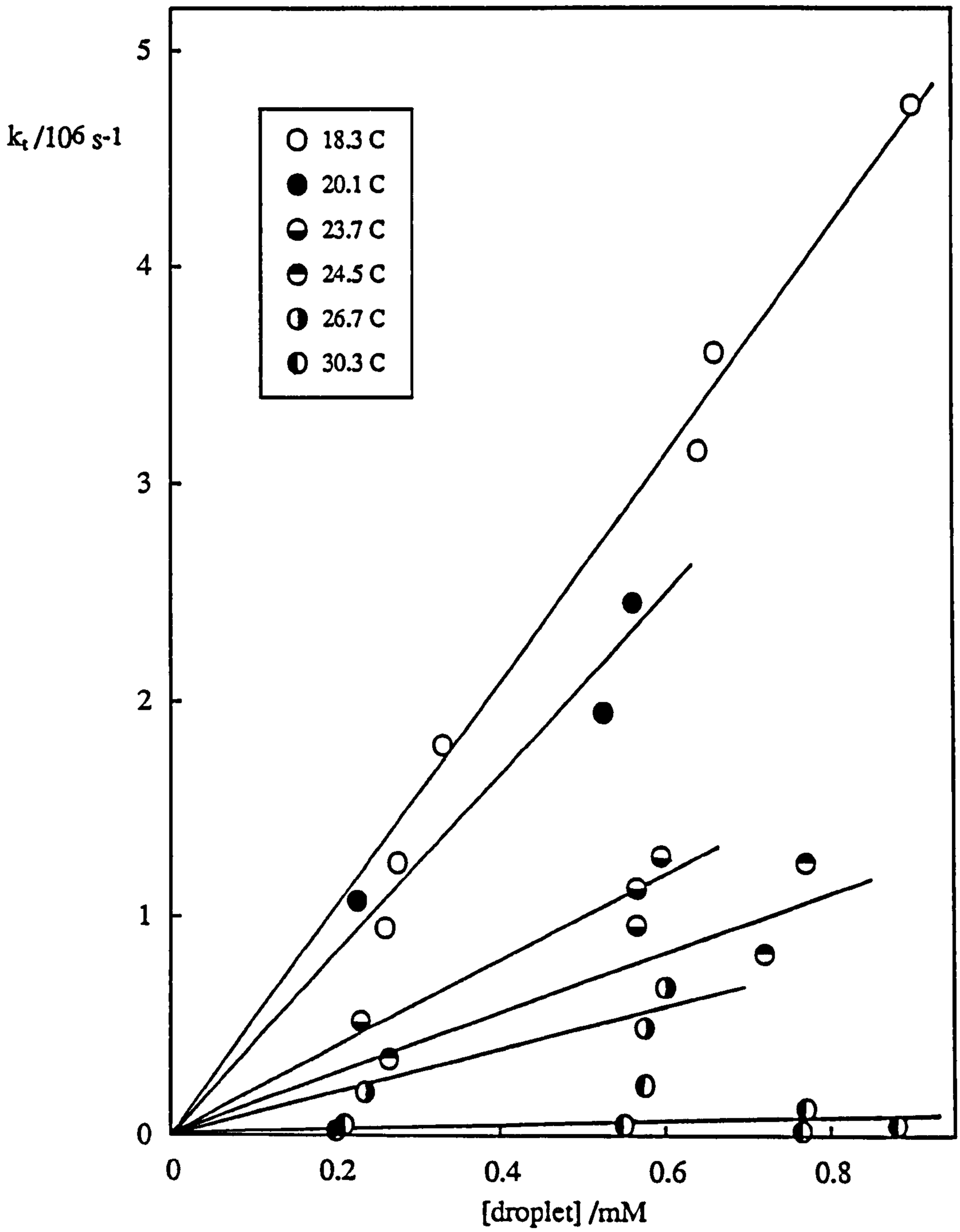

Figure 4.34.

Arrhenius plot of the second order exchange rate constant versus temperature for $R'_{water} = 15$ W/O microemulsion droplets stabilised by $C_{12}E_4$ in heptane. The dashed line indicates the behaviour expected for a diffusion-controlled rate constant.

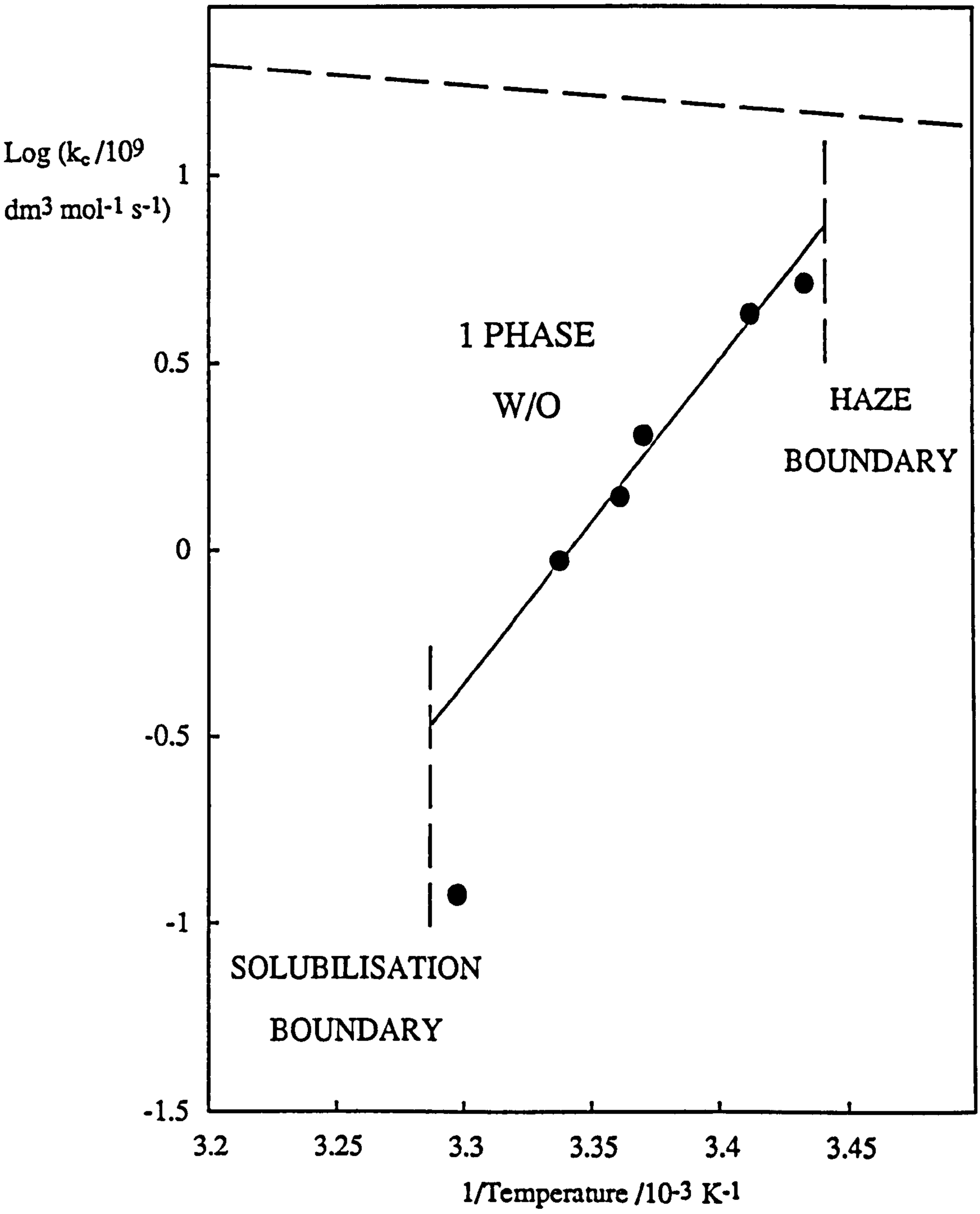

excess water solubilisation boundary with the haze curve now forming the upper temperature boundary. Exchange rates previously measured for these systems indicate that the slowest rate is again obtained at the solubilisation boundary which this time occurs at low temperatures (52, 54). It appears therefore that the exchange rate is always slowest at the solubilisation phase boundary irrespective of whether this forms the upper or lower temperature limit.

The dashed line indicates the variation of the diffusion controlled rate constant k_{dc} predicted for equal-sized spheres having no energy barrier to coalescence. This is calculated from the Smoluchowski equation (47)

$$k_{dc} = \frac{8\,R\,T}{3\,\eta} \qquad (4.20)$$

where η is the viscosity of the continuous solvent. The exchange rate constant tends to the diffusion controlled value at temperatures close to the haze curve phase boundary.

4.7.3 Some possible factors affecting the microemulsion exchange rate.

According to the "fusion-fission" mechanism, the exchange rate constant k_e should become larger for factors which increase the "stickiness" between the droplets upon collision, thereby enhancing the formation of encounter pairs. It has been shown earlier that the inter-droplet interactions are weakest at the solubilisation boundary and become progressively more attractive as the haze curve is approached. These changing interactions may well be one of the important factors which give rise to the observed temperature dependence. The exchange is also accelerated by factors which reduce the energy cost of forming the transition state. In order to postulate what these factors may be, it is necessary to assume a transition state for the exchange process. One possibility is that the transition state occurs between the non-coalesced encounter pair and the

transient droplet dimer and has an "hour glass" shape as previously shown in Figure 1.12. This involves the formation of regions of highly curved surfactant monolayer. The formation of this transition state may therefore be expected to be dependent upon the rigidity of the surfactant monolayer. Recently, Safinya *et al.* predicted the rigidity constant K to increase in proportion to the cube of the monolayer thickness (177). This increase might be expected to produce a decrease in the exchange rate. In Chapter 6 the effect of the length of the surfactant molecule on the exchange rate is considered for three surfactant systems where K has been determined directly by ellipsometry. An additional parameter which might be important in determining the energy barrier to coalescence is the system cμc (55). As discussed previously in section 1.2.6, formation of the transient droplet dimer involves a reduction in the area available to the surfactant molecule. This may be accommodated by desorption of surfactant from the droplet surface. Desorption of surfactant and consequently exchange via the "fusion-fission" mechanism, may therefore be expected to be facilitated when the cμc is high.

From the limited data reported in the literature, it is of interest to compare values of the exchange rate constant for different W/O microemulsion systems with their corresponding rigidity parameters and cμc values. The problem arises however, of how to compare exchange rate constants between different systems. Several methods of comparison are possible. Here (and in all subsequent comparisons in this thesis), the rate constants have been compared at the same R'_{water} value at temperatures close to the solubilisation phase boundaries. This appears to be the best method of comparing different systems since the exchange rates are maximally sensitive to system changes at this phase boundary. Additionally, attraction between droplets is a minimum at the solubilisation phase boundary and consequently the degree of clustering is also a minimum. The exchange of probes may then be best represented by the "fusion-fission" mechanism. Table 4.10 tabulates the exchange rate constants at the solubilisation phase boundary, rigidity parameters and cμc values for three different W/O microemulsion

systems. The values are compared to those obtained for water-in-heptane microemulsions stabilised by $C_{12}E_4$. The droplet sizes in all cases are within the range 5.5 ± 0.5 nm.

Table 4.10

Surfactant system	Log (k_{dc}/k_c)	$(K+\bar{K}/2)$ /kT	cμc /mol dm^{-3}
DTAC + Cyclohexane + Butanol	0.48 (52)	0.1 - 0.8 (52)	0.3 - 1.0 (52)
$C_{12}E_5$ + Heptane	1.30 (55)	1.1 ± 0.5 (29)	~0.08 (29)
$C_{12}E_4$ + Heptane	1.60 ± 0.3	1.0 ± 0.6	0.06 ± 0.01
AOT + Heptane	4.30* (50)	1.4 ± 0.3 (52)	~10^{-3}-10^{-4} (178)

* result from stopped flow data

The second order exchange rate constant k_c is expressed as a ratio to the diffusion controlled rate constant to allow comparison of systems of different viscosities. The values of $(K+\bar{K}/2)$ quoted were all obtained through the tension-size relationship. Values of the rigidity parameter for the DTAC /cyclohexane system were dependent upon the concentration of butanol present in the interface. Low values of $(K+\bar{K}/2)$ were observed for high butanol to DTAC mole ratios (between 5 and 10). From this limited data, it appears as though the lower rigidity system gives the fastest exchange rate at the solubilisation phase boundary. It should be remembered however, that the approximations and uncertainties in the calculated rigidity parameters are of comparable magnitudes to the differences between the systems. Also the magnitude and sign of the Gaussian curvature elastic modulus, $\bar{K}$, is unknown in each of these systems.

The exchange rate constants appear to also correlate with the measured values of the surfactant cμc in the oil. As predicted, the exchange rate is faster when the free energy required to desorb a molecule of surfactant from the interface is low, i.e. cμc is

high. For the DTAC /cyclohexane system, the oil phase contains high concentrations (between 0.3 and 1.0 mol dm^{-3}) of non-adsorbed butanol. The corresponding free energy required to desorb a molecule of butanol from the interface is therefore very low.

4.8 Conclusions.

From this study of the equilibrium properties of microemulsions stabilised by the nonionic surfactant $C_{12}E_4$, the main conclusions are listed below.

(1). The critical microemulsion concentration increases with temperature. For heptane and tetradecane as the oil phase, the enthalpies of transfer of one mole of monomers to the aggregated state are -42 ± 10 kJ mol^{-1} and -52 ± 25 kJ mol^{-1}. The cμc also increases with increasing salt concentration and an approximate correlation is seen to exist between R'_{water} and the cμc.

(2). Incorporation of α-chymotrypsin and BSA into the dispersed aqueous phase of W/O microemulsions has little effect on the position of the solubilisation phase boundary, the cμc or the droplet size. Sodium caseinate however, appears to be solubilised as proteinaceous aggregates which are only stable at water : surfactant mole ratios of between 20 and 30. These multiple aggregates are polydisperse, with sizes in the range of 100 - 300 nm.

(3). Water-in-oil aggregates at temperatures close to the solubilisation phase boundary behave ideally and the droplet size, extrapolated to infinite dilution, is directly proportional to R'_{water}. The area per surfactant head group at the droplet surface is effectively constant with increasing droplet size at 0.32 ± 0.06 nm^2 and 0.26 ± 0.06 nm^2 for heptane and tetradecane respectively. Changes in the monolayer curvature with temperature are consistent with two models in which either; (i) the effective head group area and the surfactant monolayer thickness remain constant and the effective area per

surfactant tail changes, or, (ii) both the effective head and tail group areas remain constant and the surfactant monolayer thickness changes.

(4). The post-cμc interfacial tensions pass through minimum values at temperatures which coincide with maximum dispersed phase solubilisation. The tension scales approximately with the radius^{-2} which enables a very approximate estimation of the monolayer rigidity parameter (K+K/2) to be made. For both heptane and tetradecane as the oil phase this value is of the order of kT.

(5). Using a technique of time-resolved fluorimetry it is shown that for a constant R'_{water} value, the microemulsion droplet size remains constant as the one phase microemulsion region is traversed. The viscosity of the dispersed aqueous phase appears to be of the order of ten times that of bulk water i.e. ~10 cP. The rate of exchange of fluorescer and quencher probes between microemulsion droplets is slowest at the high temperature, solubilisation phase boundary. Comparison of the exchange rates for different systems appear to suggest that the rate is enhanced for systems exhibiting a high cμc and a low monolayer rigidity.

5. CHARACTERISATION OF W/O MICROEMULSIONS FORMED WITH $C_{12}E_4$ + TRIGLYCERIDE / ALKANE + WATER.

CHAPTER 5.

5.1 Introduction to Triglycerides.

Triglycerides or triacyl glycerols, are the final esterified products of the reaction between glycerol and a carboxylic acid.

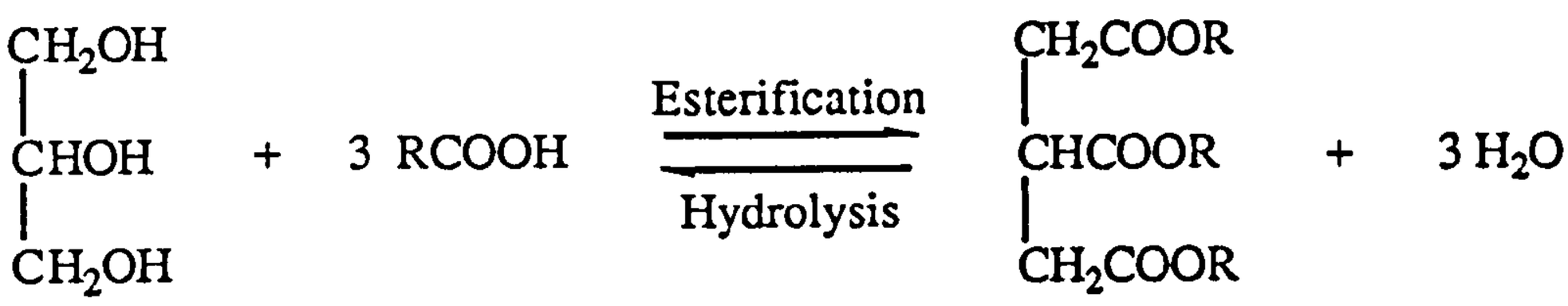

They are the basic constituents of all animal and vegetable fats and are therefore of major industrial importance. For example, in the food industry, triglycerides are the principal components of the oil phase in emulsions and oil based foods. In the field of detergency they make up more than 30% of common laundry soils, and in the cosmetics industry they are used extensively in product formulation.

Their physical properties are highly dependent upon the length and degree of unsaturation of the esterified group. Short chain length triglycerides, e.g. triacetin and tripropionin, are soluble in water and form aggregates above a certain concentration (179). However, upon increasing the chain length the solubility is dramatically reduced e.g. tricaproin, solubility = 1.17 x 10^{-6} moles dm^{-3} (180), and aggregate formation is prevented.

To date, only a limited amount of information has been accumulated relating to the role of triglyceride oils in microemulsion (181 - 184) and macroemulsion (127, 185) systems. Mori *et al.* investigated the O/W microemulsion phase boundaries for a series of pure nonionic surfactants with an oil phase consisting of the pure triglyceride triolein (183). In relation to detergency, they observed a maximum in the solubilisation of the oil from polyester-cotton fabrics at temperatures corresponding to the phase inversion temperatures for each system. Similar solubilisation experiments with triolein/hexadecane mixtures showed that the mixtures were solubilised to a greater

extent than the pure triolein alone. Also, a degree of preferential solubilisation of the hydrocarbon from the mixture was noted. A very narrow four phase region was also seen to exist for these mixed oil systems which consisted of water, oil and two different surfactant-rich phases (D and D'). Kunieda *et al.* observed a similar four phase region for systems containing $C_{12}E_4$, water and mixtures of hexadecane and a short chain triglyceride (181, 182). This was thought to be a consequence of the overlapping of the two, three phase regions separately formed in the three component mixtures where hexadecane and triglyceride alone form the oil phase. The D phase was thought to be bicontinuous in structure whereas the D' phase was postulated to be associated with large disc-like micelles.

In the study reported here, the effects of medium and long chain length triglycerides on the phase behaviour of W/O microemulsions stabilised by $C_{12}E_4$ are presented. Interfacial tensions and microemulsion droplet sizes are reported and compared with the values for heptane alone as the oil phase. Finally, the results from a study of microemulsion dynamics are presented and discussed in terms of factors which may affect the exchange rate.

5.2 W/O Microemulsion Phase Boundaries for $C_{12}E_4$ + Triglyceride / Heptane + Water Systems.

The positions of the excess water solubilisation phase boundaries were determined by the method of a single phase titration (previously described in section 2.1.1). The maximum amount of solubilised water is shown as a function of surfactant concentration in Figure 5.1a. The oil phase contains 50% v/v MCT in heptane. (In this thesis all oil phase compositions of the heptane/triglyceride mixtures are specified as percentages by volume of triglyceride in the total oil phase volumes). Figure 5.1b shows

Figure 5.1a.

Variation of the maximum extent of water solubilisation with $C_{12}E_4$ concentration in 50% MCT as a function of temperature.

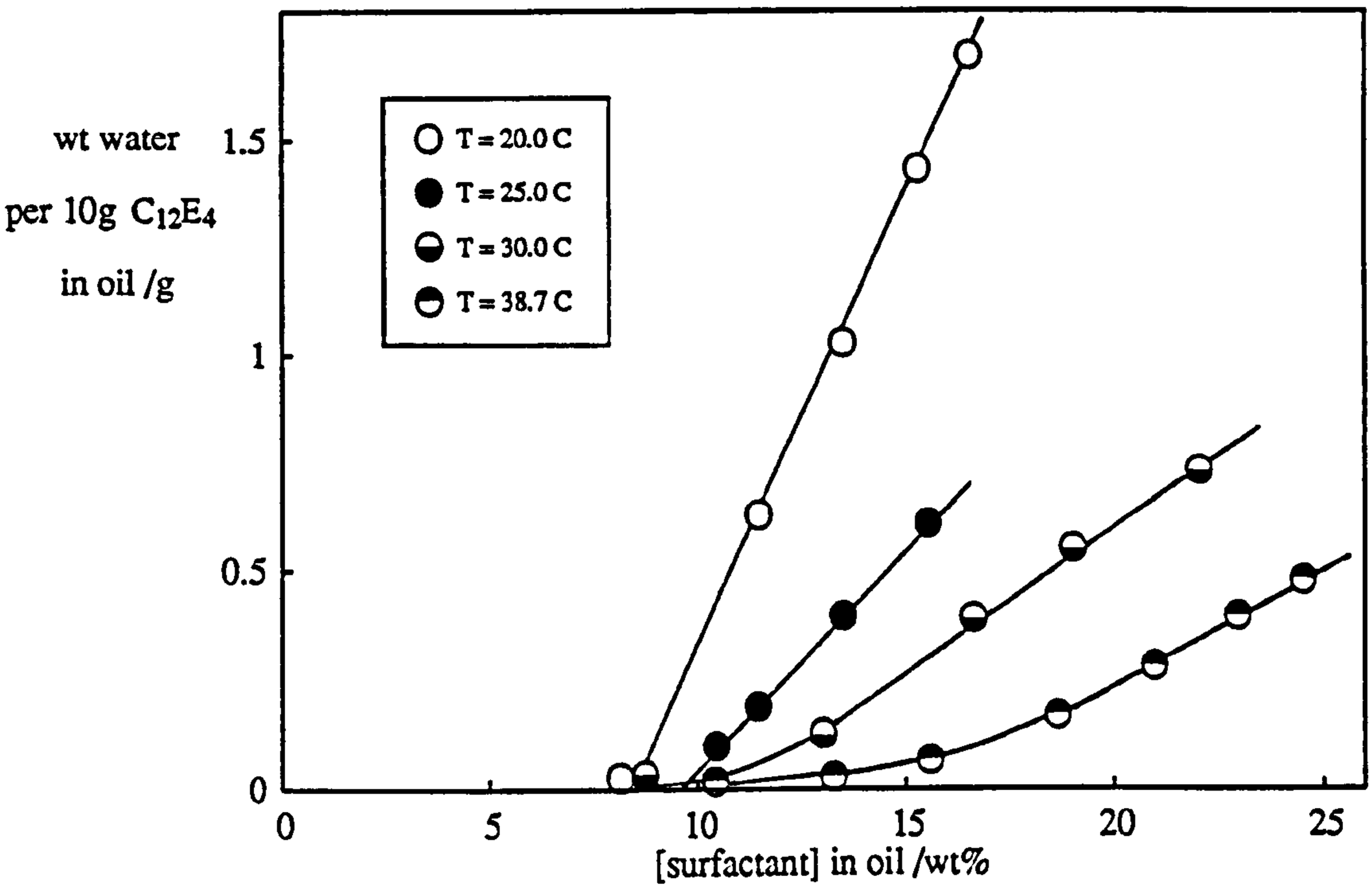

Figure 5.1b.

Solubilisation data for oil phases containing different concentrations of MCT.

Temperature = 30°C except for 75% MCT which was performed at 33°C.

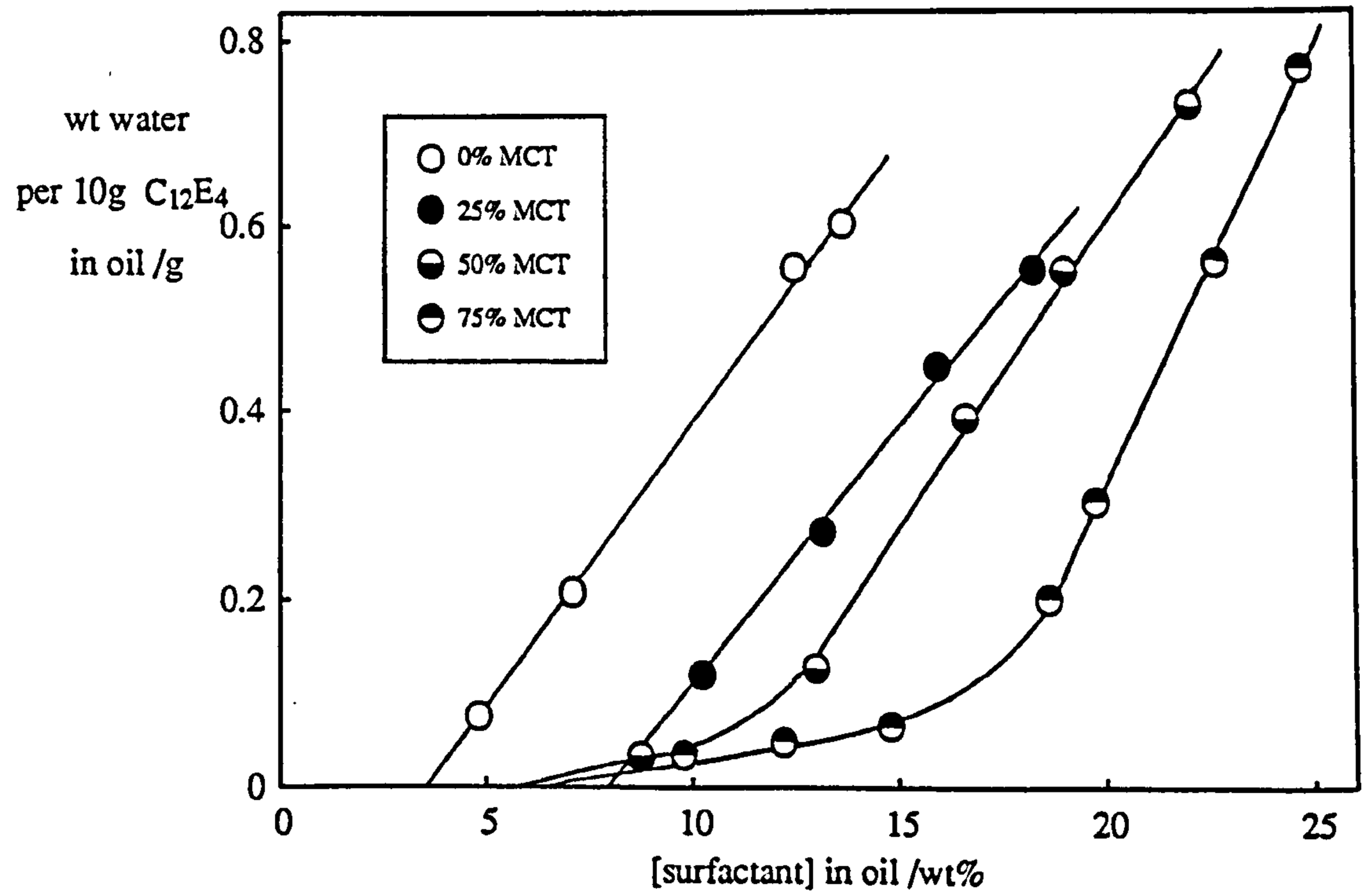

the effect of increasing the concentration of MCT in the oil phase on the maximum solubilisation of water at a constant temperature. Deviations from linearity are observed at low water uptakes for systems containing 50% or more MCT at temperatures in excess of 30°C. These deviations cannot be accounted for by the solubility of water in the triglyceride since this was found to be negligible (~0.04 wt% at 30°C, in agreement with related systems previously reported (186)). It is possible that water is associated with pre-cμc aggregates which are precursors of "true" microemulsion droplets. Alternatively, the deviations may be due to hydrolysis of the triglyceride. The carboxylic acid produced may act as a cosurfactant producing mixed aggregates with the $C_{12}E_4$ molecules. Hydrolysis is expected to be accelerated at higher temperatures and this may explain why this effect is more apparent at elevated temperatures.

As before, the mole ratio of water to surfactant within each aggregate (R'_{water}) is obtained from the gradients of these plots and the critical microemulsion concentration from the intercepts on the abscissa. For the triglyceride systems displaying deviations from linearity, the cμc was determined by extrapolating the linear portion of the data to the abscissa. Figure 5.2 shows the variation of R'_{water} with temperature for different concentrations of MCT in the oil phase. As the MCT concentration increases to 50 and 75%, the maximum degree of solubilisation dramatically decreases and the one phase region is shifted to higher temperatures. The position of the excess water solubilisation boundary for MCT alone as the oil phase is presumably shifted to higher temperatures and the maximum water solubilisation reduced. Temperatures greater than 40°C were not investigated to minimise possible degradation of the surfactant and triglyceride.

It is interesting to observe from Figure 5.2, that when the oil phase contains 25% MCT the excess water solubilisation boundary appears to be depressed slightly to lower temperatures. This was investigated further by determining the maximum water solubilisation at a fixed temperature, 14°C, as a function of MCT concentration in the oil phase. The results are shown in Figure 5.3a. In the absence of triglyceride, an R'_{water}

Figure 5.2.

Variation of the excess water solubilisation boundary with temperature for W/O microemulsions formed with $C_{12}E_4$ in heptane containing various MCT volume fractions. The horizontal lines denote maximum solubilisation.

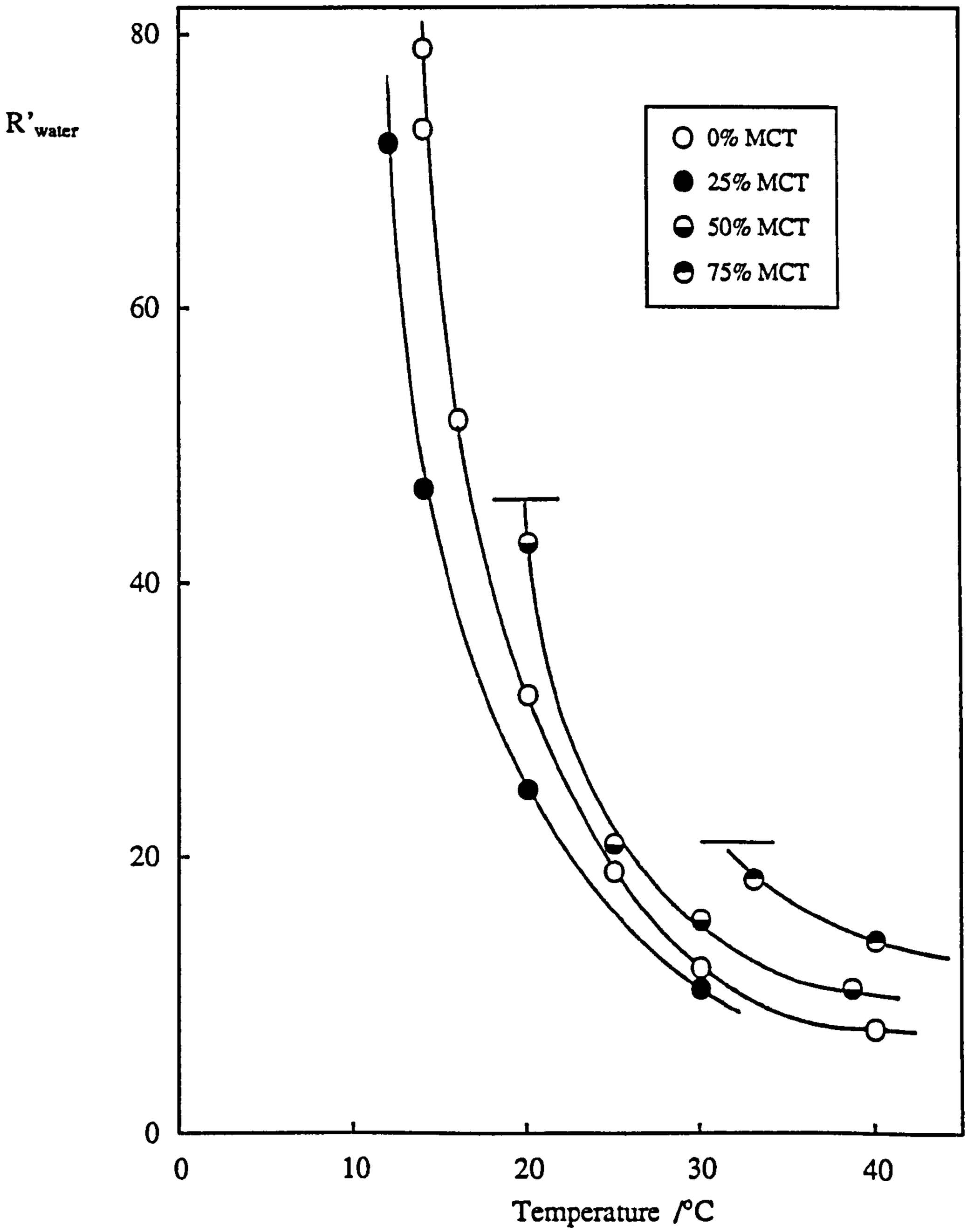

Figure 5.3a.

Variation of the maximum extent of water solubilisation at 14.0°C with volume fraction of MCT in heptane, for W/O microemulsions stabilised by $C_{12}E_4$.

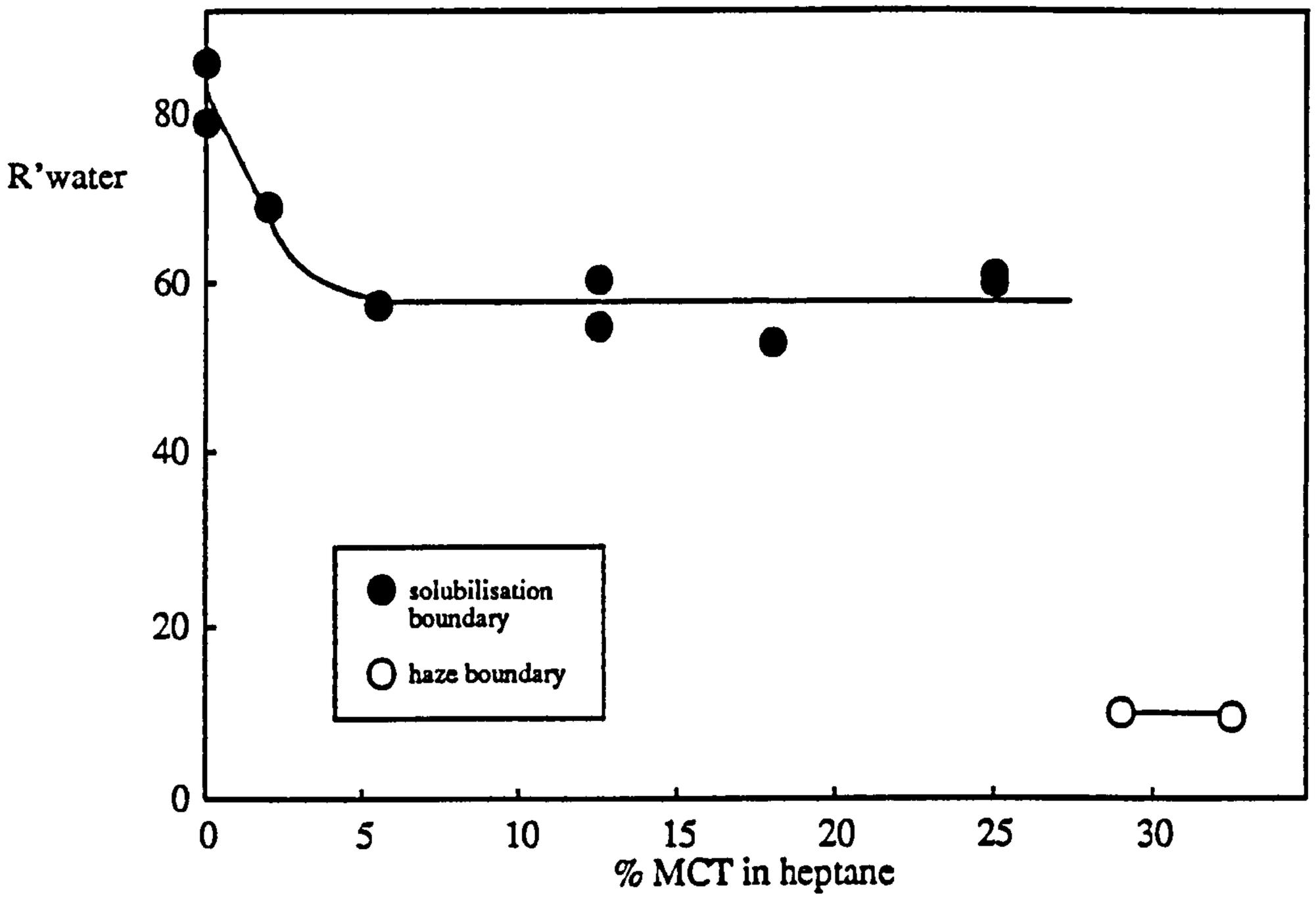

Figure 5.3b.

Variation of the critical microemulsion concentration with MCT concentration at 14.0°C.

value of 82 ± 7 is obtained. Upon addition of only 5% MCT to the oil phase the R'_{water} value drops to 58 ± 7. Further addition of MCT up to 25% has little effect on the degree of maximum solubilisation. It appears therefore, that for concentrations of MCT in the oil phase between 5 and 25%, a constant, preferred monolayer curvature is adopted. As seen in Figure 5.2 increasing the triglyceride concentration beyond 25% results in the shifting of the solubilisation phase boundary to higher temperatures. Low concentration of MCT (< 25%) therefore produce a shift towards more negative spontaneous curvature. This may indicate a preference of the triglyceride for the tail region of the surfactant monolayer producing an increase in the effective area per surfactant tail group. At higher MCT concentrations the opposite effect is observed and a shift towards more positive spontaneous curvature occurs. This is consistent with a reduced penetration of the triglyceride into the surfactant tail region. The reason for this changing behaviour with MCT concentration is at present unclear. Kunieda *et al.* observed similar behaviour upon varying the concentration of the short chain length triglyceride 1,2,3,-propanetriyl tris (2-ethylhexanoate) (TEH) in hexadecane (181). However, Mori *et al.* observed that the phase inversion temperatures of emulsions prepared with triolein/decane and triolein/hexadecane as the oil phase were relatively independent of triglyceride concentration up to 20 and 25% respectively (183). This may be a consequence of the bulkier long chain length triglyceride molecule being unable to penetrate into the alkyl tail region of the surfactant monolayer. Higher concentrations were observed to produce an increase in the PIT consistent with the findings of this work and that of Kunieda *et al.* From this study it appears that medium chain length triglycerides are one of the few variables that can change the monolayer curvature in opposite directions depending upon their concentration.

Figure 5.3b shows the variation of the critical microemulsion concentration with MCT concentration in the oil. This will be discussed later (p. 160).

The stability region for W/O microemulsions formed in 50% MCT is compared with that for aggregates formed in 50% of a commercial long chain triglyceride (sunflower oil), LCT, in Figure 5.4. The maximum degree of solubilisation is greatly reduced and the stability region shifted to higher temperatures in the case of the longer chain length triglyceride.

Several of the critical microemulsion concentrations determined from the solubilisation data for concentrations of triglyceride between 0 and 75% were also checked by interfacial tension measurements. These are shown in Figures 5.5a-d. Variation of the cμc with temperature for various concentrations of triglyceride in the oil phase is shown in Figure 5.6. It can be seen that the values determined from interfacial tension measurements are in reasonable agreement with those determined from the solubilisation plots. The cμc is seen to increase dramatically with increasing concentration of triglyceride. This is also demonstrated in Figure 5.3b, in which the temperature is held constant at 14.0°C. Concentrations in excess of 20 wt% non-adsorbed surfactant may be present in some systems containing high volume fractions of the polar oil. Previously, high solubilities of $C_{12}E_4$ in mixed triglyceride / alkane oils have been observed by Kunieda (182). However, quantitative measurements of cμc values were not performed.

The enthalpy of transfer of a mole of surfactant monomers from the oil phase containing 50% MCT to the aggregated state has been calculated from Figure 5.7 to be -26 ± 5 kJ mol^{-1}. This is significantly less than the value of -42 ± 10 kJ mol^{-1} determined for heptane alone as the oil phase and presumably reflects the increased affinity of the surfactant for the oil. The transfer enthalpies for 25% and 75% MCT (-26 ± 6 and -19 ± 8 kJ mol^{-1} respectively) suggest there is a slight trend to lower values with increasing MCT concentration i.e. as the oil mixture becomes more polar. The value for 50% LCT (-29 ± 7 kJ mol^{-1}) is higher than for the corresponding MCT mixture, consistent with the more apolar character of the LCT.

Figure 5.4.

One phase W/O stability regions for microemulsions formed with $C_{12}E_4$ in heptane in the presence of 50% by volume of the stated triglyceride.

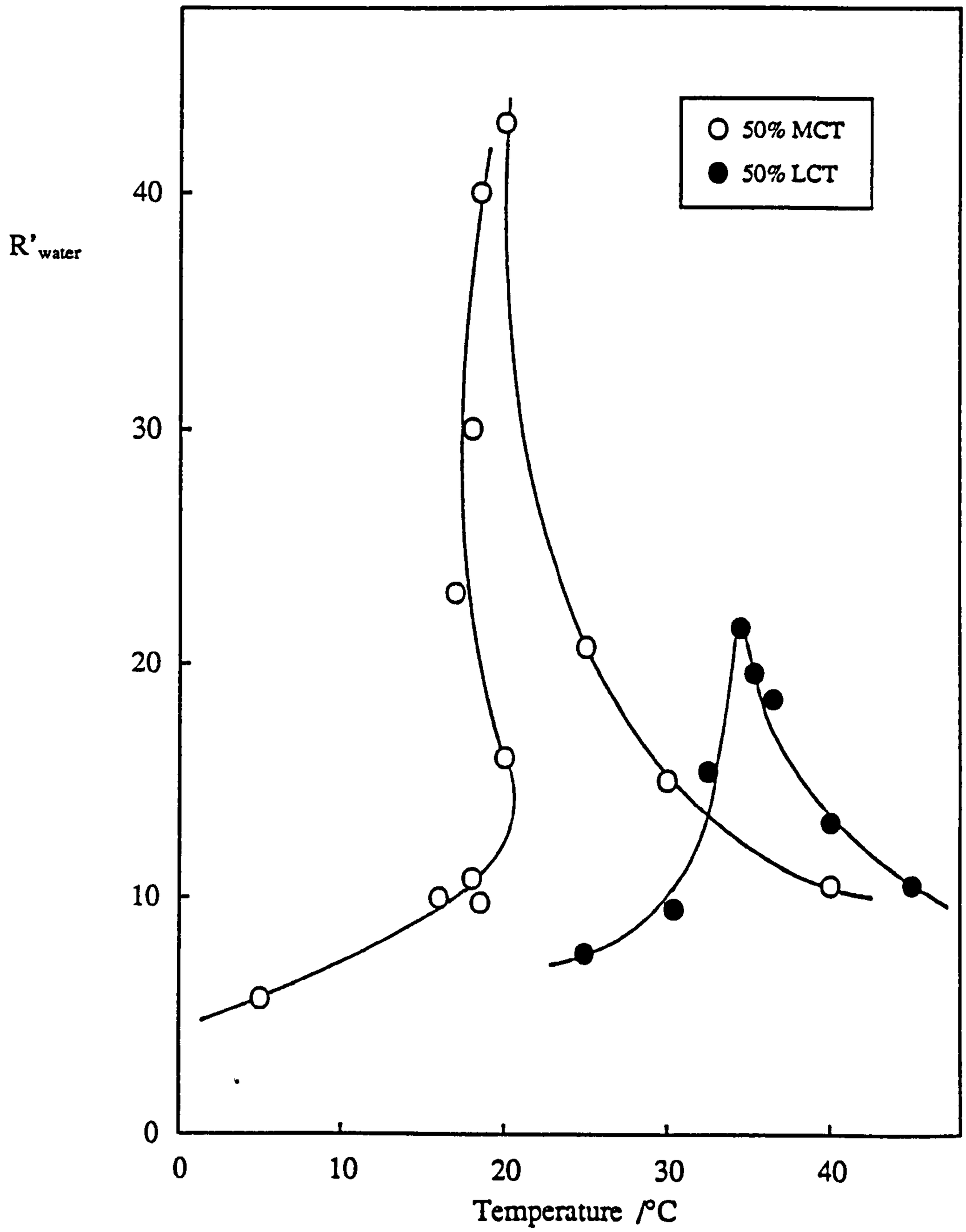

Figure 5.5.

Critical microemulsion concentration determinations by interfacial tension measurements, for $C_{12}E_4$ in heptane containing different volume fractions of MCT and LCT.

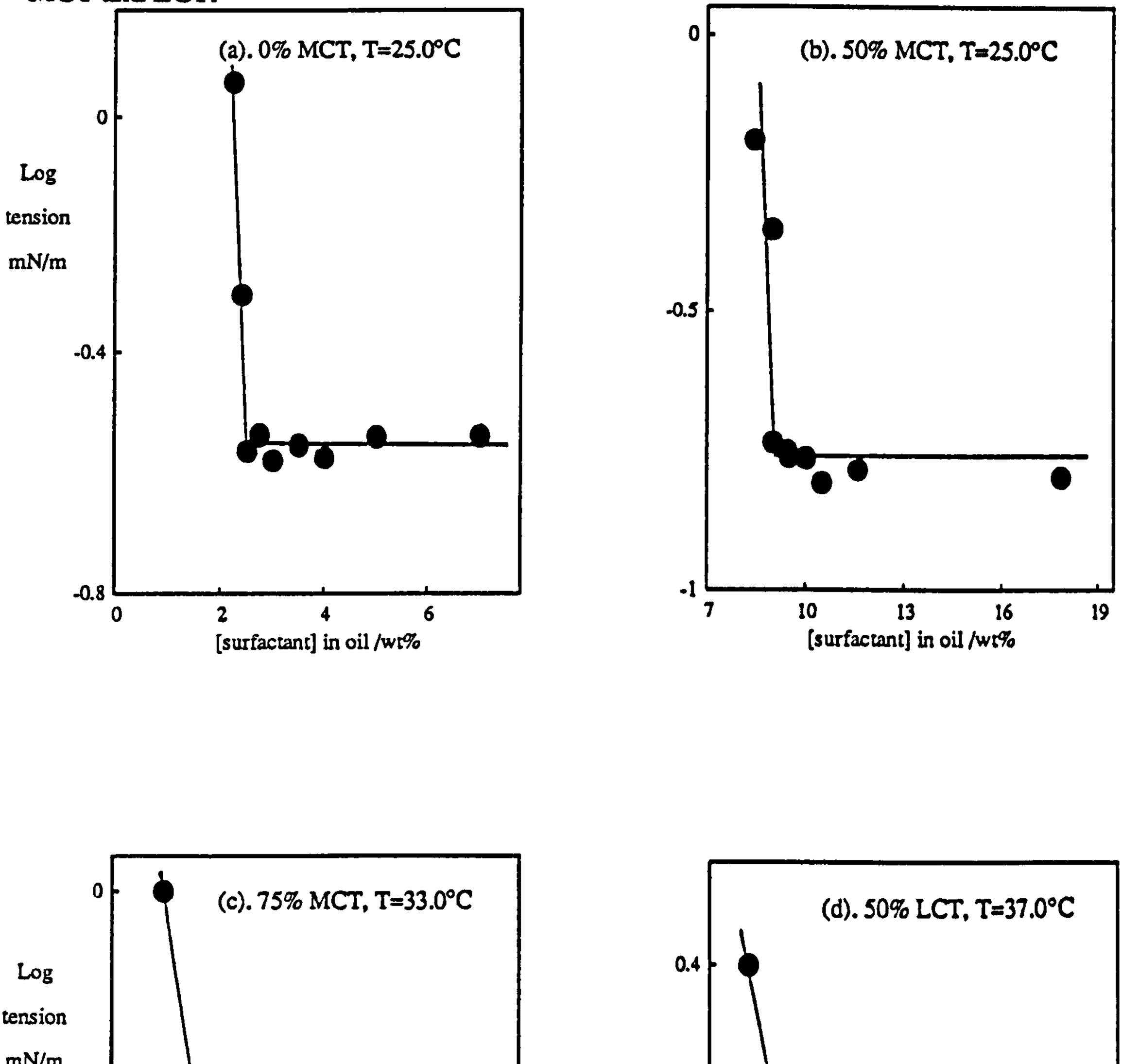

Figure 5.6.

Variation of the critical microemulsion concentration with temperature for W/O microemulsions stabilised by $C_{12}E_4$ in heptane at various volume fractions of triglyceride. The crosses were determined by interfacial tension measurements.

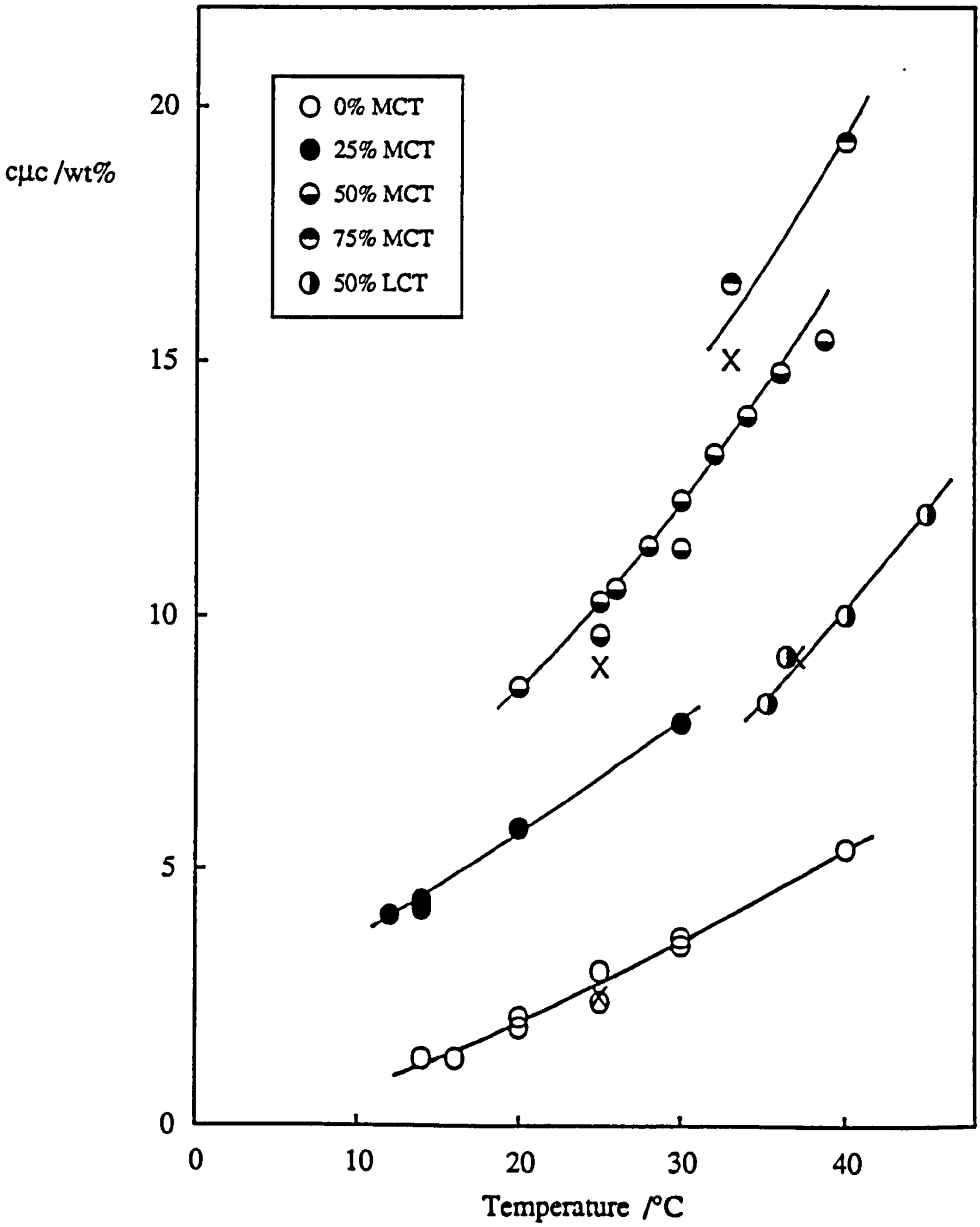

Figure 5.7.

Variation of the critical microemulsion concentration of $C_{12}E_4$ in 50% MCT with temperature.

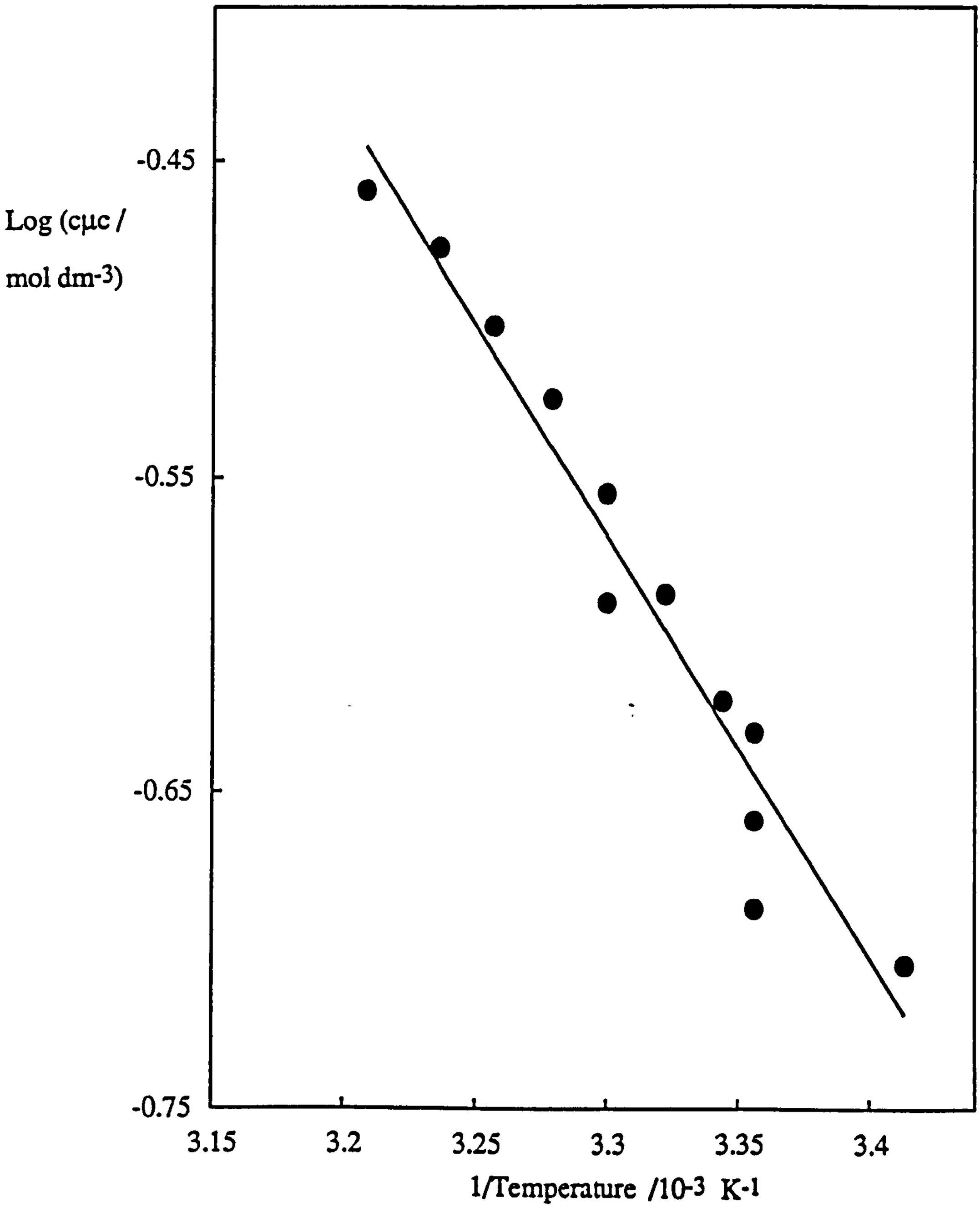

The progression of microemulsion phases observed as a function of temperature was investigated for an oil phase containing 50% MCT. The procedure adopted was as follows. Stoppered tubes containing surfactant and an equal phase volume ratio of oil and water were shaken and thermostatted at different temperatures. The surfactant concentration was fixed and in excess of the cμc corresponding to the highest temperature investigated. Once equilibrium had been attained the phases present were determined visually.

For all temperatures greater than 20°C a Winsor II system was produced at equilibrium. Similarly, temperatures below 18°C yielded the corresponding Winsor I system. Between these two temperatures a three phase Winsor III system was observed. The expected equivalence between this microemulsion phase inversion region and the macroemulsion phase inversion temperature was investigated by measuring the conductivity of the corresponding emulsion as a function of temperature. To produce a significant change in the conductivity, 0.05 M sodium chloride was used as the aqueous phase. Since nonionics are relatively insensitive to low concentrations of salt (40), the presence of this small concentration was assumed to have a negligible effect on the phase inversion temperature. The variation of the emulsion conductivity with temperature is shown in Figure 5.8a. The temperature at which the conductivity changes abruptly corresponds to the phase inversion temperature of the macroemulsion. This occurs around 20°C and is in reasonable agreement with the temperature range for inversion of the corresponding microemulsion system. Figure 5.8b shows the PIT determination for an emulsion prepared with heptane alone as the oil phase. The phase inversion temperature is in reasonable agreement with the microemulsion results tabulated in Table 4.1.

Figure 5.8a.

Conductivity as a function of temperature for emulsions prepared with $C_{12}E_4$ in 50% MCT. The aqueous phase contains 0.05 M NaCl.

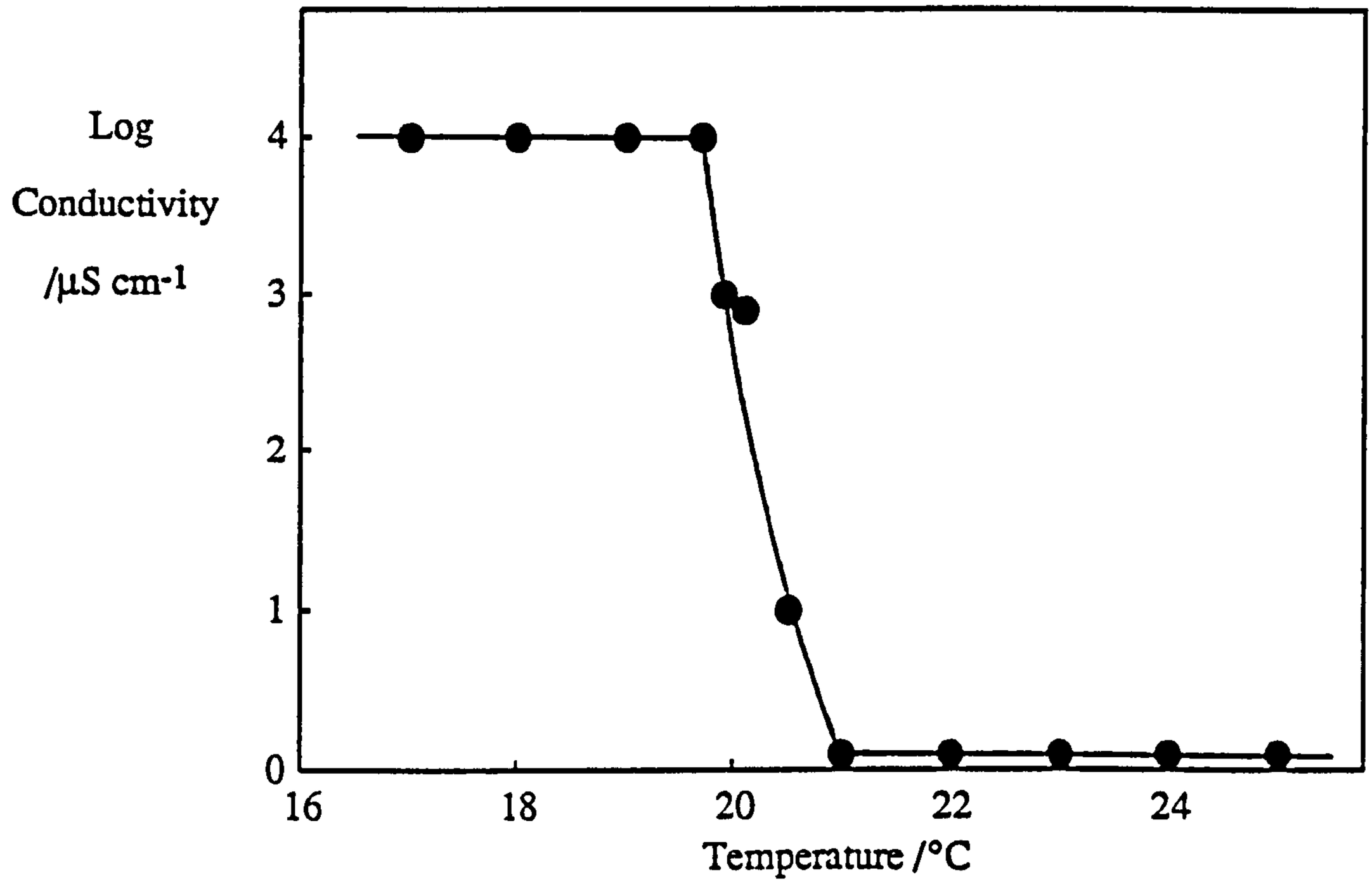

Figure 5.8b.

Conductivity as a function of temperature for emulsions prepared with $C_{12}E_4$ in heptane. The aqueous phase contains 0.05 M NaCl.

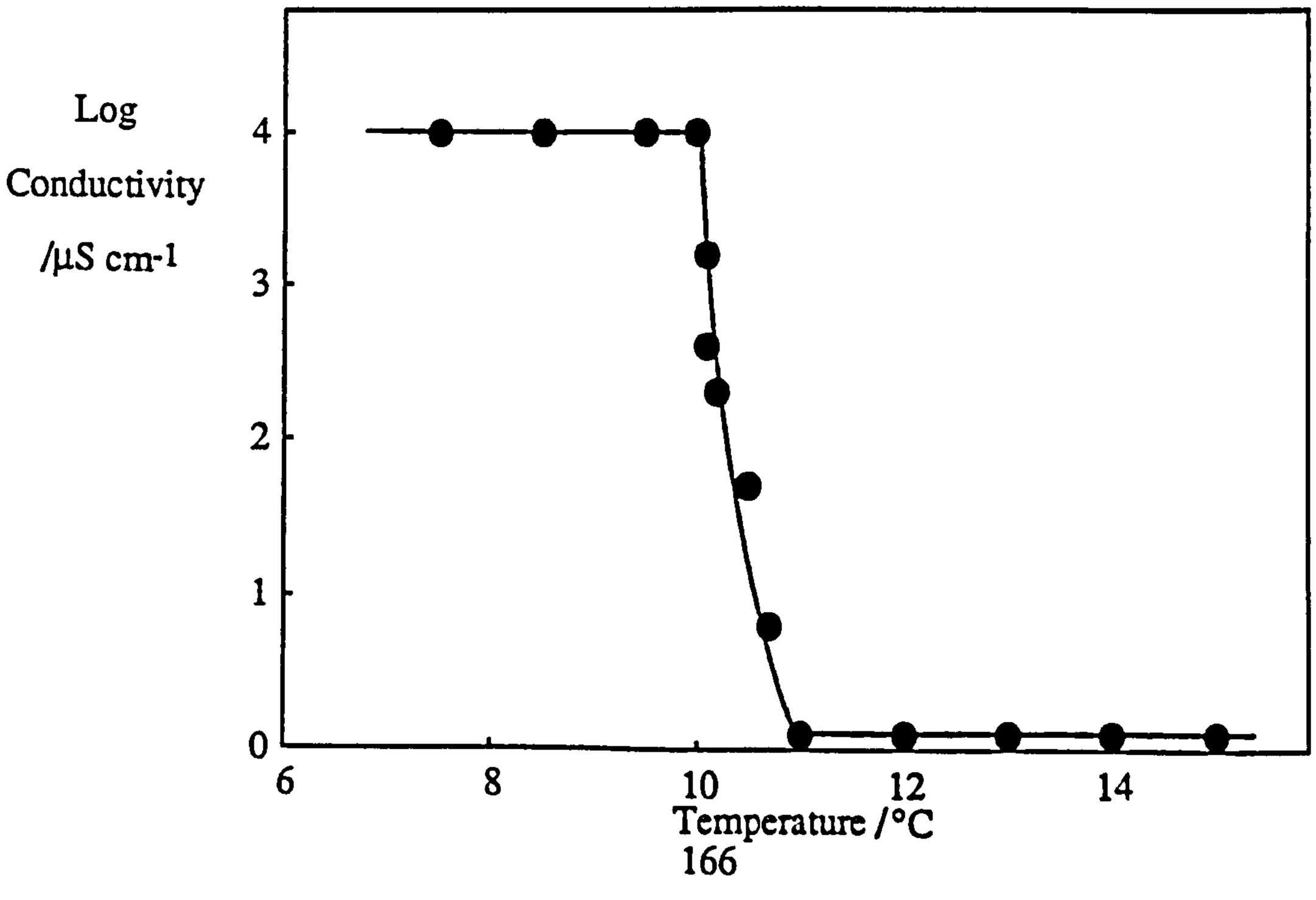

5.3 Measurement of Microemulsion Droplet Sizes by Photon Correlation Spectroscopy for 50% MCT in the Oil Phase.

One phase microemulsion samples were prepared with 50% MCT as the oil phase. Phase boundaries for these "made-up" microemulsions were in agreement (± 1°C) with the results determined from the solubilisation data. The variation of the apparent diffusion coefficient with volume fraction of the dispersed phase is shown in Figure 5.9 for temperatures close to the solubilisation phase boundaries. The plots are similar to those previously presented for heptane alone as the oil phase (Figure 4.17). Values for the coefficient α (see equation 4.1) (106) and hydrodynamic radii obtained by extrapolation to infinite dilution, are tabulated below in Table 5.1.

Table 5.1

R'_{water}	α	r_H/nm
43	-1 ± 3	13.3 ± 1.5
29	-6 ± 6	8.5 ± 1.0
18	-8 ± 8	6.7 ± 1.5
15	-10 ± 10	4.3 ± 1.5

Values for the normalised variance of the hydrodynamic radius were typically less than about 0.1 indicating a low degree of polydispersity in the samples.

The apparent diffusion coefficient of microemulsion droplets investigated at temperatures close to their solubilisation phase boundaries appears to be only slightly dependent upon the droplet concentration. Moving away from this boundary towards the haze curve however, causes the diffusion coefficient to dramatically decrease as was observed for the case of heptane alone as the oil phase. This has previously been shown to be a consequence of increasing attraction between the microemulsion droplets

Figure 5.9.

Variation of the apparent diffusion coefficient with dispersed phase volume fraction, for W/O microemulsions stabilised by $C_{12}E_4$. The oil is 50% MCT.

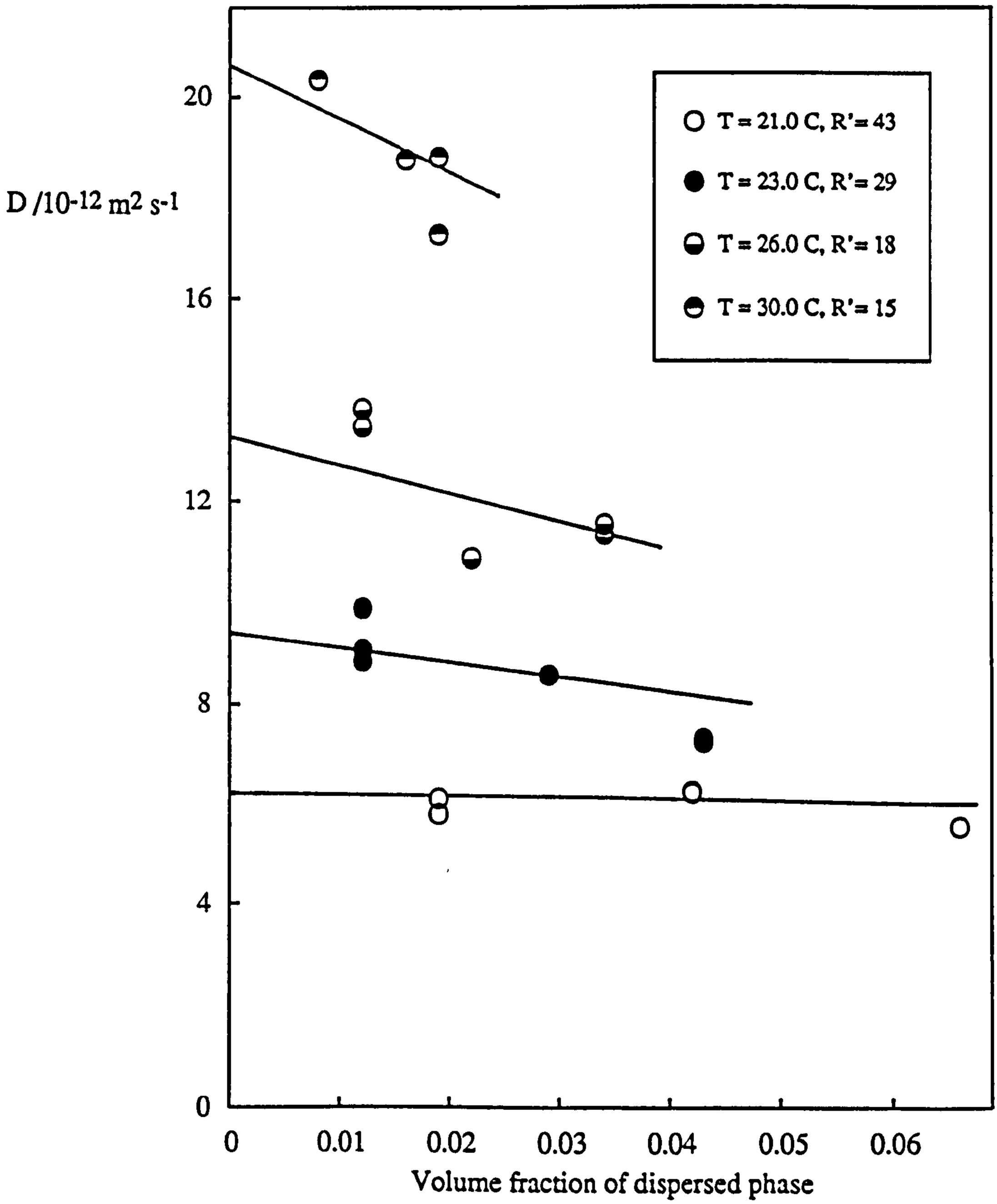

(section 4.7.2). The calculated values of α at the solubilisation phase boundary, despite the large errors, are slightly negative indicating the presence of attractive interactions between the droplets.

The hydrodynamic radius as a function of R'_{water} is compared with that obtained for heptane as the oil phase in Figure 5.10. The point at $R'_{water} = 15$ was derived from time-resolved fluorescence data assuming that a molecule of MCT and heptane solvate each surfactant tail group. Aggregates formed in the presence of 50% MCT appear to be consistently slightly smaller than those formed in heptane alone. However, the small differences between the two sets of data are of the order of the errors in their determination. The data conforms to the following empirical relationship.

$$r_H\,/\text{nm} = 0.270\,R'_{water} + 1.5$$

The intercept corresponds to a surfactant film thickness of 1.5 ± 2 nm. The value of the area occupied by the surfactant molecule at the interface between the droplet core and the surfactant monolayer is calculated to be 0.33 ± 0.05 nm^2. This value is virtually equal to that determined for heptane alone as the oil phase (0.32 ± 0.06 nm^2). It appears therefore, that the incorporation of 50% MCT into the oil phase has a negligible effect on the head group region of the surfactant monolayer. This suggests that the observed solubilisation differences between the two oils is may be due to a decreased penetration into the alkyl tail region of the surfactant monolayer by the bulky triglyceride molecule.

Figure 5.10.

Hydrodynamic radii measured close to the solubilisation boundary versus R'_{water} for W/O microemulsions stabilised by $C_{12}E_4$ in 50% MCT. Open point refers to a value derived from TRF data and the dashed line represents results for heptane.

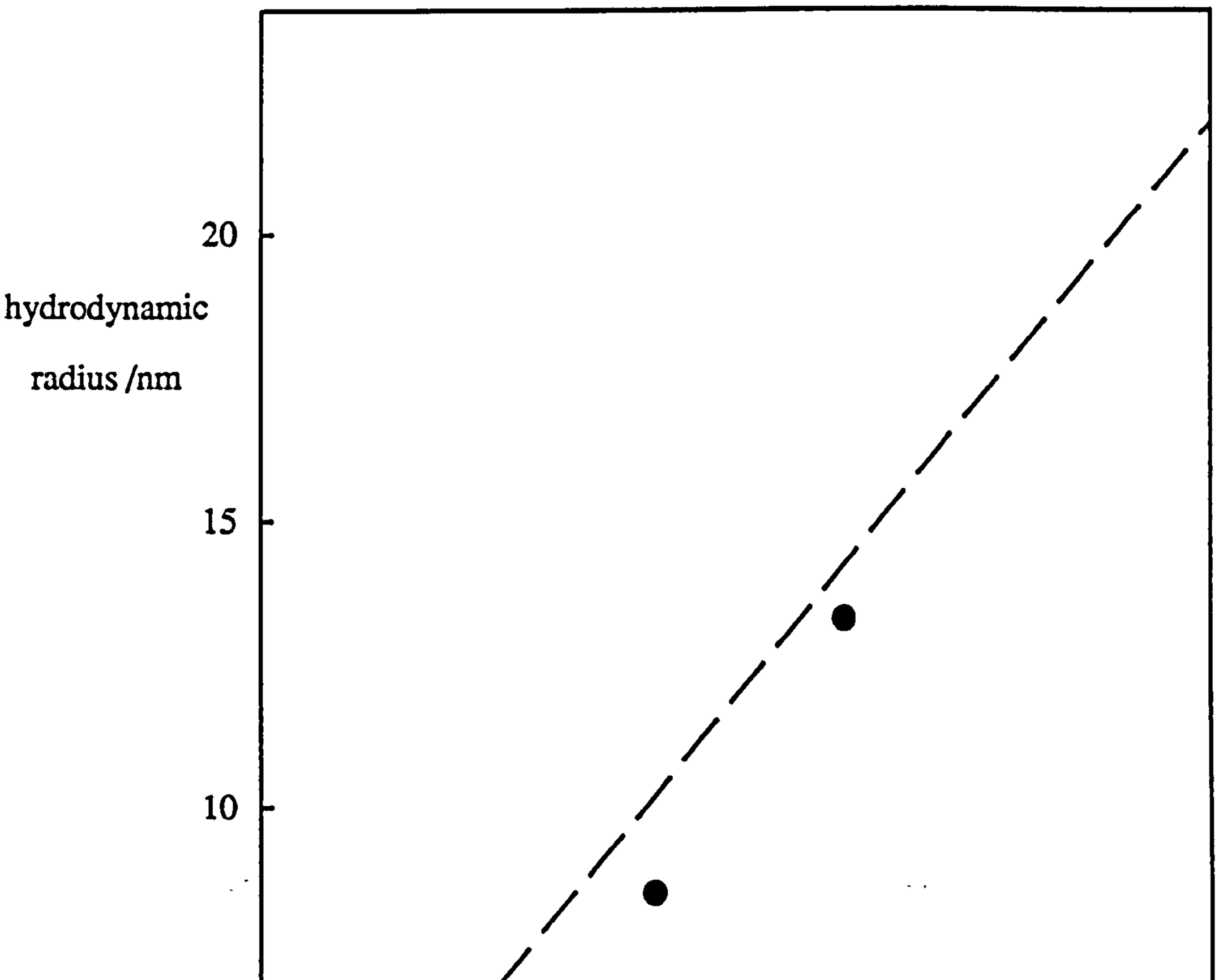

5.4 Measurement of the Post-cμc Interfacial Tension Between Water and Triglyceride / Heptane Mixtures as a Function of Temperature.

Interfacial tension measurements were made using the spinning drop technique as described previously in section 2.1.2. The time taken for the oil droplets to reach equilibrium was dependent upon the concentration of MCT in the oil phase. Generally longer equilibration times (30 - 60 minutes) were required for high MCT concentrations. This is consistent with the findings of Mori *et al.* who investigated oil-water interfacial tensions for a mixed oil containing triolein / hexadecane in the presence of $C_{12}E_4$ (183).

Figure 5.11 shows the variation of the oil-water interfacial tension with temperature for various MCT concentrations. The interfacial tensions for the low temperature side of the minimum (corresponding to the formation of oil-in-water aggregates) for 50% and 75% MCT, were thought to be unreliable since the drops were observed to slowly contract over a period of 1-2 hours. Consequently, these tension values have not been reported. This may be due to the preferential solubilisation of heptane into the interior of the aggregates formed in the aqueous phase. The oil drop in the capillary would then become more concentrated with the triglyceride resulting in an increase in the cμc. If significant concentrations of heptane are solubilised, the cμc may reach a value that exceeds the concentration of surfactant present in the oil phase. Saturation coverage of the interface may then not be maintained and the drop would contract. Mori *et al.* have observed a preferential solubilisation of the hydrocarbons decane and hexadecane over the triglyceride triolein in their studies of oil removal from fabrics (183). For 50% and 75% MCT the vertical lines denote the points at which the drops became coated with a surfactant phase. The three phases coexisted in equilibrium which corresponds to the start of the Winsor III regions. The minimum tension determined for each system corresponds to the point at which the drops break up. From

Figure 5.11.

Oil-water interfacial tension as a function of temperature for $C_{12}E_4$ in heptane containing various MCT volume fractions, at concentrations in excess of the cμc. The vertical lines denote the approximate start of the 3 phase regions.

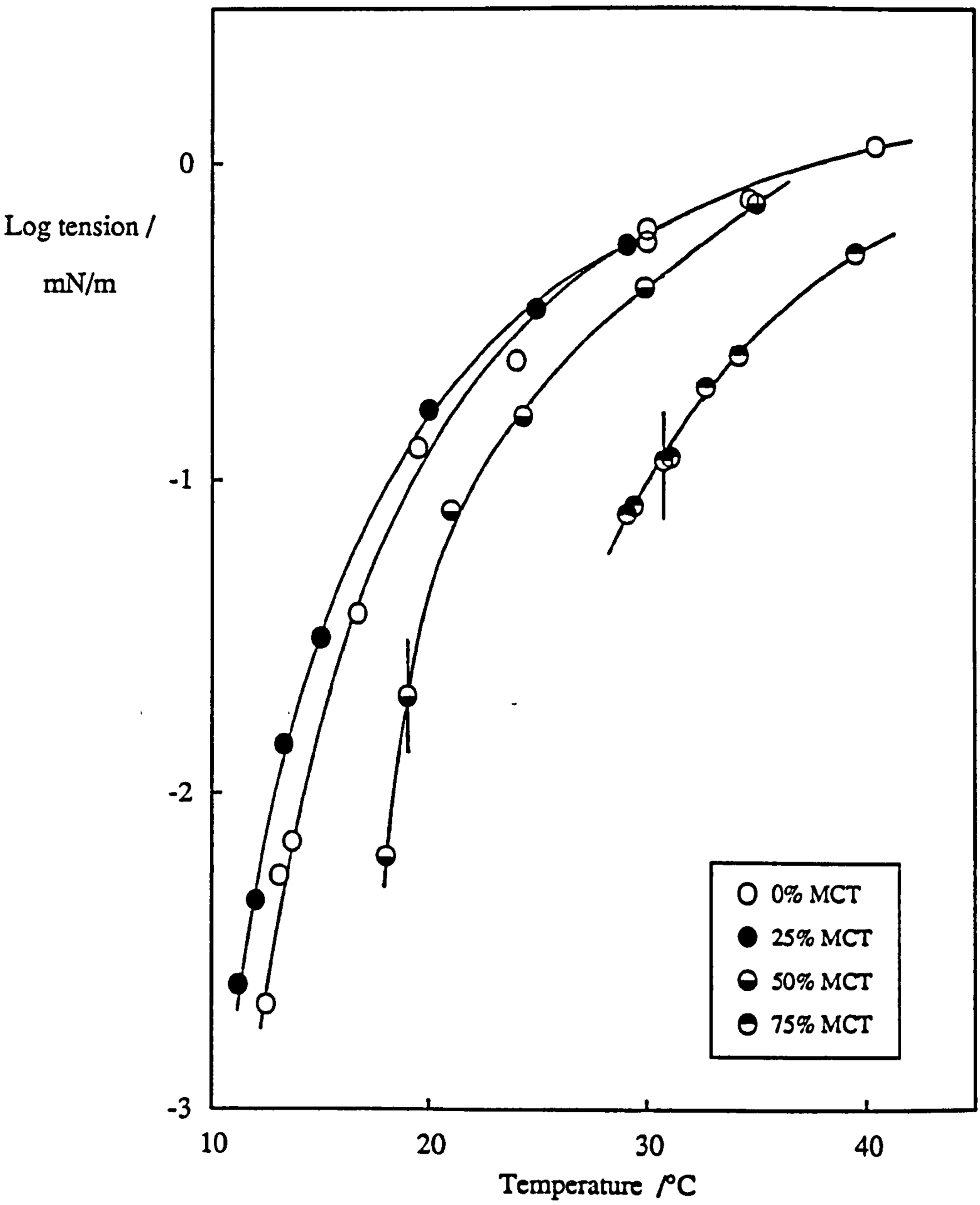

comparison of Figure 5.11 with Figure 5.2 it is evident that an inverse relationship exists between the interfacial tension and R'_{water}.

Using the tension-size relationship previously discussed in section 1.2.5, the monolayer rigidity parameter ($K+\bar{K}/2$) has been estimated for the 50% MCT system. From Figure 5.12 it can be seen that the droplet size scales approximately with radius^{-2} as expected from equation 1.10 and the results are similar to those obtained with heptane as the oil phase. The calculated values of ($K+\bar{K}/2$) for 50% MCT (0.9 ± 0.6 kT) and heptane alone (1.0 ± 0.6 kT) are both of the order of kT.

5.5 Time-Resolved Fluorescence Results for W/O Microemulsions Stabilised by $C_{12}E_4$ in 50% MCT.

As discussed previously, a correlation may be expected to exist between the microemulsion exchange rate, the monolayer rigidity and the ease of surfactant desorption as reflected by the cμc. Increasing the monolayer rigidity or decreasing the cμc is expected to reduce the exchange rate. From microemulsion phase studies in 50% MCT it has been shown that, at a fixed droplet composition, the cμc exceeds that of the corresponding heptane system. Approximate estimates for the monolayer rigidities for the two systems were seen to be very similar within their large determined errors. The exchange rates at the solubilisation phase boundary might be predicted therefore, to be influenced primarily by the differences in the ease of desorption of surfactant monomer from the droplet surface.

Microemulsion droplets of composition $R'_{water} = 15$ were studied as a function of temperature across the one phase stability region. The excess water solubilisation boundary, which forms the upper temperature limit, occurred at approximately 32°C and the lower temperature haze boundary at 20°C. The critical microemulsion

Figure 5.12.

Variation of log tension with log radii for W/O microemulsions formed with $C_{12}E_4$ in 50% MCT and in 100% heptane. The solid line indicates the behaviour expected from equation (1.10) in the text with $(K+\bar{K}/2)$ equal to 1 kT.

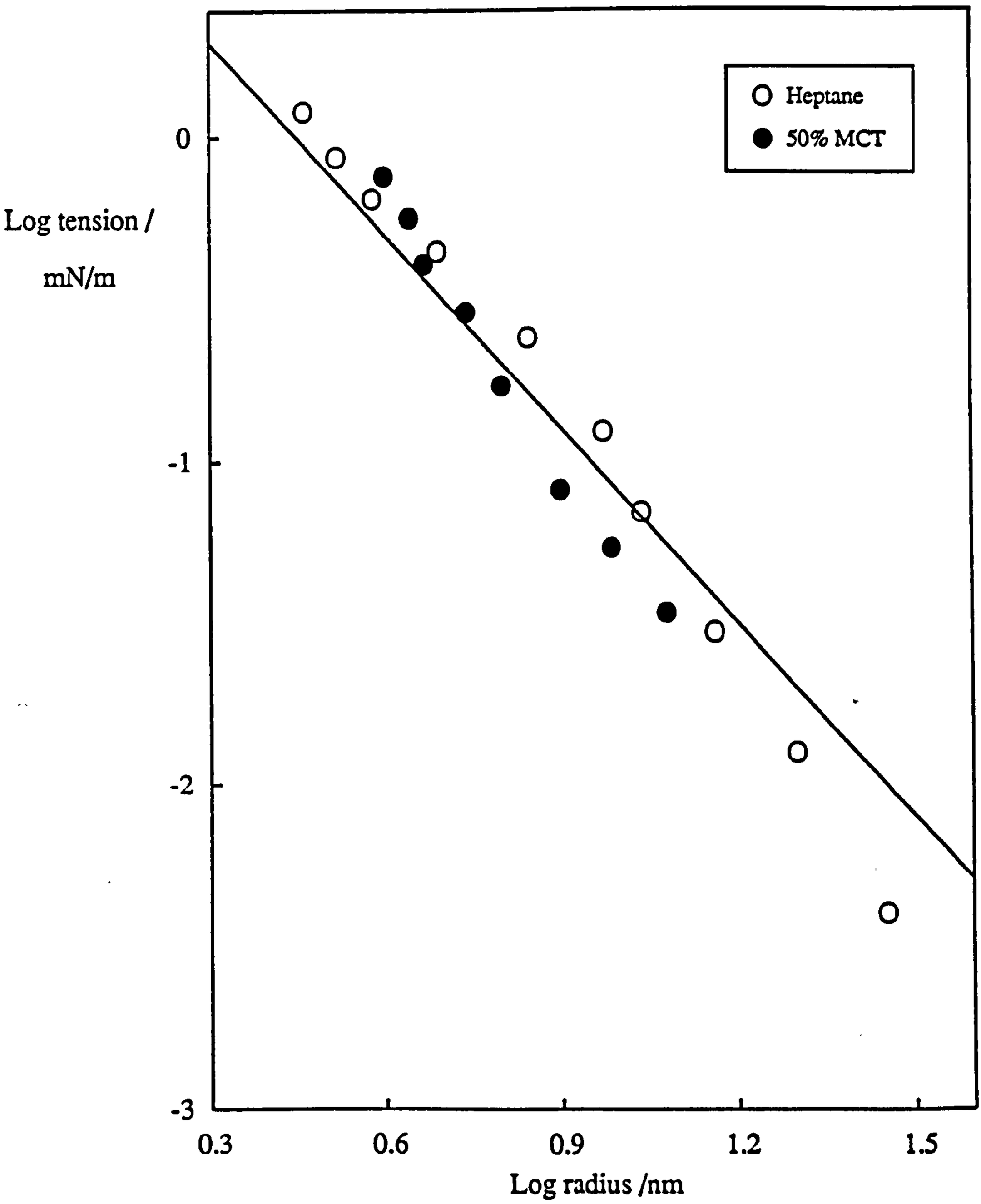

concentration for this system was determined to be 13 ± 1 wt%. As in the previous study, ruthenium tris-bipyridyl (RB) and methyl viologen (MV) were chosen as fluorescer and quencher respectively. These were assumed to be completely located within the water pool of the microemulsion. Samples were studied at surfactant concentrations between 20 and 40 wt% at average quencher concentrations of between 0 and 2 per droplet. The temperature of the one phase stability region was shifted by 2 - 3°C to higher temperatures upon increasing the surfactant concentration from 20 - 40 wt%. This is presumably due to an increased interaction between aggregates at these higher concentrations. As previously reported, the surfactant was observed to contain a small amount of a fluorescent impurity. A further fluorescent impurity was also seen to exist in the batch of triglyceride oil. These perturbed the first few channels of the decay trace producing poor values of the fitting parameter χ^2 (> 2.5). As before, this was overcome by recording the trace of a "blank microemulsion" and subtracting this from the sample decay profile before fitting. In this way the fitting was much improved as evidenced by χ^2 values of ~1.5. The experimental technique and analysis is described in more detail in sections 2.1.4 and 4.7.1.

Figure 5.13 shows the variation of the microemulsion radii, as calculated from equation 4.18 (assuming no solvation), with temperature across the one phase stability region. For 30 and 40 wt% $C_{12}E_4$ the size is seen to remain approximately constant and independent of the droplet concentration. In the case of 20 wt% $C_{12}E_4$ however, a slight decrease in radius is apparent as the haze boundary is approached. This may indicate that the cμc decreases significantly from its value of 13 wt% at the solubilisation boundary as the haze boundary is approached. Changes in the cμc are expected to be detected most sensitively when the cμc is high and the concentration of microemulsified surfactant is low. Recent results appear to suggest that the cμc may well be substantially lower at the haze boundary (187). The average value for the radius is 4.8 ± 0.5 nm which corresponds to an aggregation number of 440 ± 120. Previously determined

Figure 5.13.

Variation of microemulsion droplet radii (unsolvated) across the one phase stability region for R'_{water} = 15 W/O microemulsion droplets stabilised by $C_{12}E_4$ in 50% MCT.

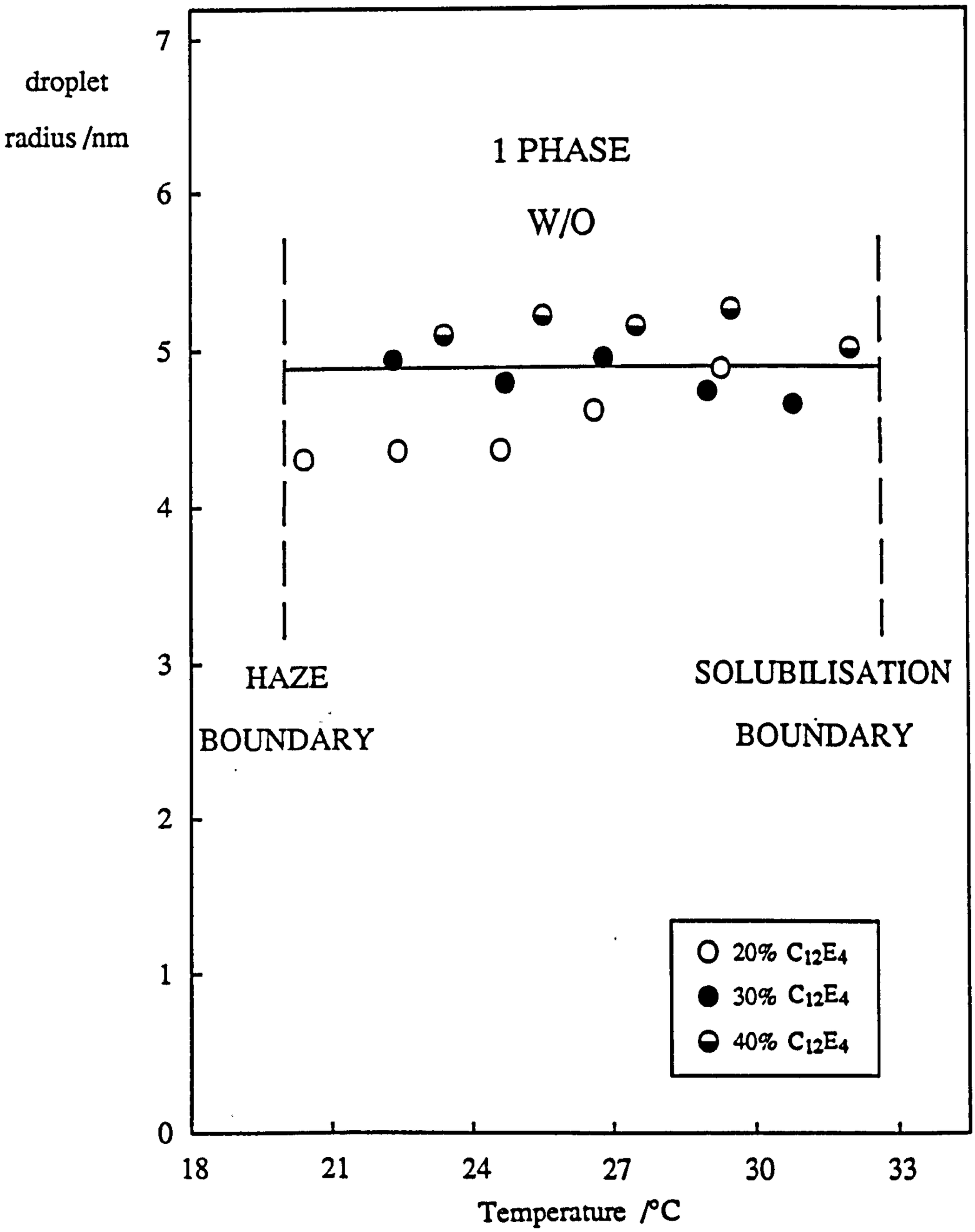

values for the droplet radius and aggregation number of R'_{water} = 15 aggregates formed in heptane alone as the oil phase are 5.3 ± 0.4 nm and 590 ± 120 respectively. It appears therefore that the aggregate size in the presence of 50% MCT is slightly lower than that in heptane. This is consistent with the findings from PCS for these systems.

It has been shown previously in section 4.7.2 (equation 4.19) that if the probes are assumed to show no interaction with the surfactant monolayer and to display normal diffusion behaviour, then the product ($k_q N_{agg} R'_{water}$) is expected to be proportional to $1/\eta_m$. N_{agg} is the aggregation number of the droplet, k_q is the first order quenching rate constant and η_m is the microviscosity experienced by the probe. The variation of ($k_q N_{agg} R'_{water}$) with temperature is shown in an Arrhenius type plot in Figure 5.14. The dashed line indicates the behaviour expected if η_m is equated with the bulk viscosity of water. The results are similar to those previously presented for heptane and indicate an apparent microviscosity about ten times that of bulk water.

Variation of the first order unquenched fluorescence decay rate constant k_o with temperature across the one phase region is shown in Figure 5.15. The values are seen to be only slightly different from those obtained in bulk water (121) and are similar to previous observations for heptane as the oil phase. This suggests that the probe is located within a "water-like" micro-environment within the droplet.

Values of the first order exchange rate constant k_t calculated assuming a mechanism of "fusion-fission", are shown in Figure 5.16 as a function of droplet concentration. The values are seen to be approximately proportional to the droplet concentration within their estimated uncertainties. The scatter of the points is increased compared to the results previously presented for heptane. This may be a consequence of the increased fluorescent impurities for these microemulsion samples arising from the additional impurity in the triglyceride. The second order exchange rate constants k_c, corresponding to the different temperatures within the one phase region are obtained from the slopes. These are displayed in Figure 5.17 in an Arrhenius type plot.

Figure 5.14.

Log (k_q N_{agg} R'_{water}) versus 1/temperature for R'_{water} = 15 W/O microemulsion droplets stabilised by $C_{12}E_4$ in 50% MCT. The dashed line indicates the values calculated for a microviscosity equal to that of bulk water.

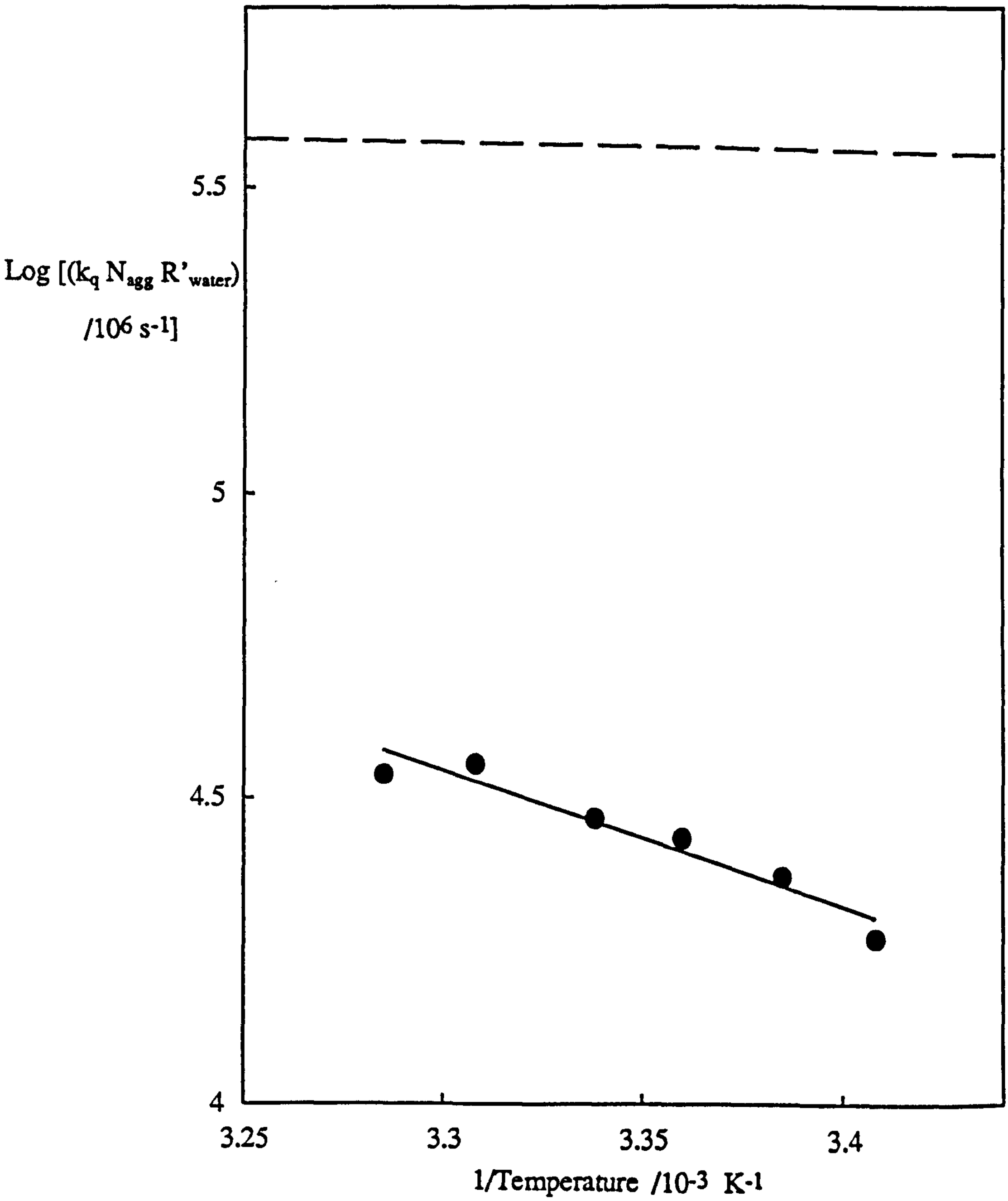

Figure 5.15.

Variation of the unquenched fluorescence decay rate constant k_o for RB in R'_{water} = 15 W/O microemulsion droplets stabilised by $C_{12}E_4$ in 50% MCT. The dashed line indicates the behaviour in water (121).

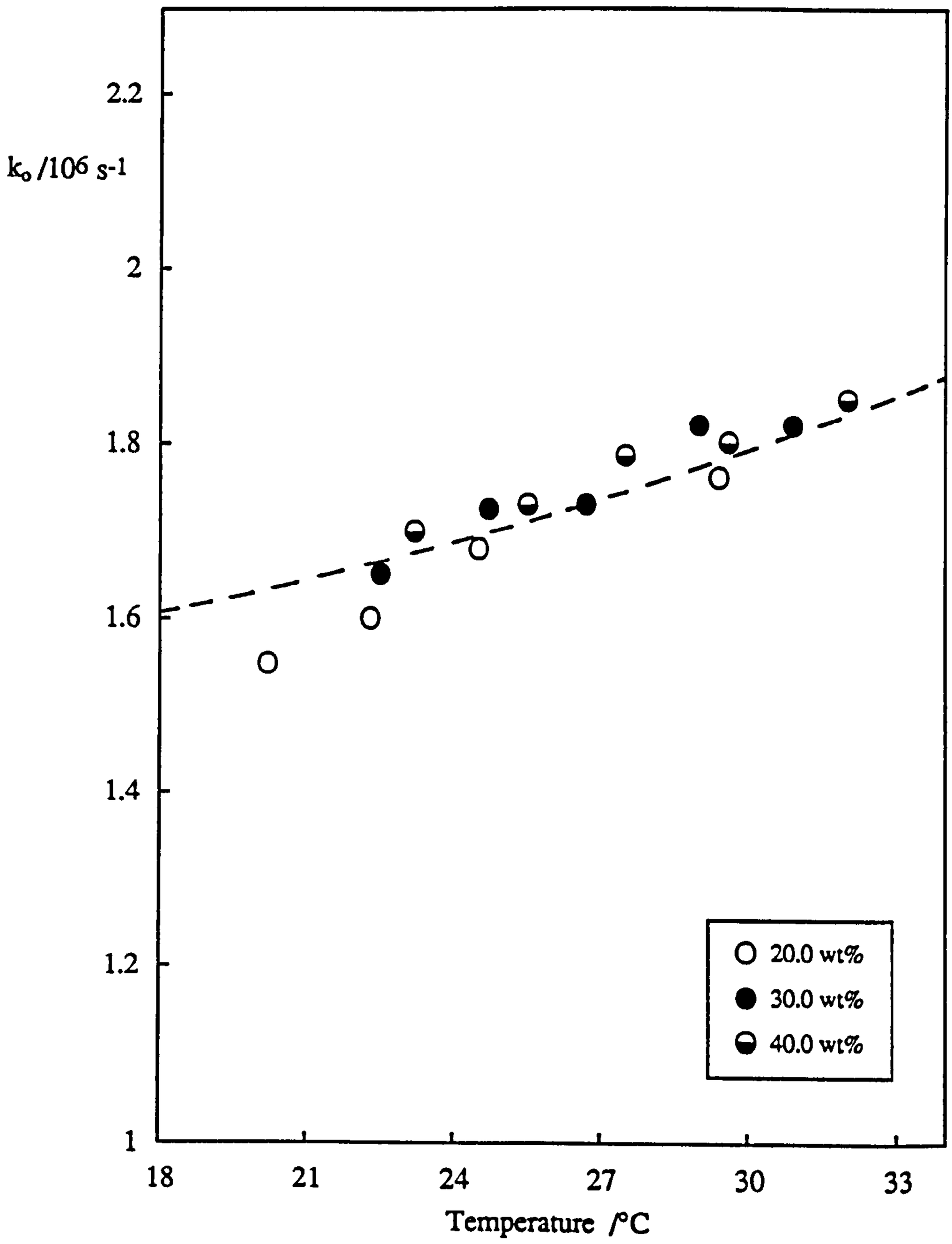

Figure 5.16.

First order exchange rate constant (k_t) versus droplet concentration for $R'_{water} = 15$ water-in-50% MCT microemulsions stabilised by $C_{12}E_4$. The temperatures correspond to positions within the one phase stability region.

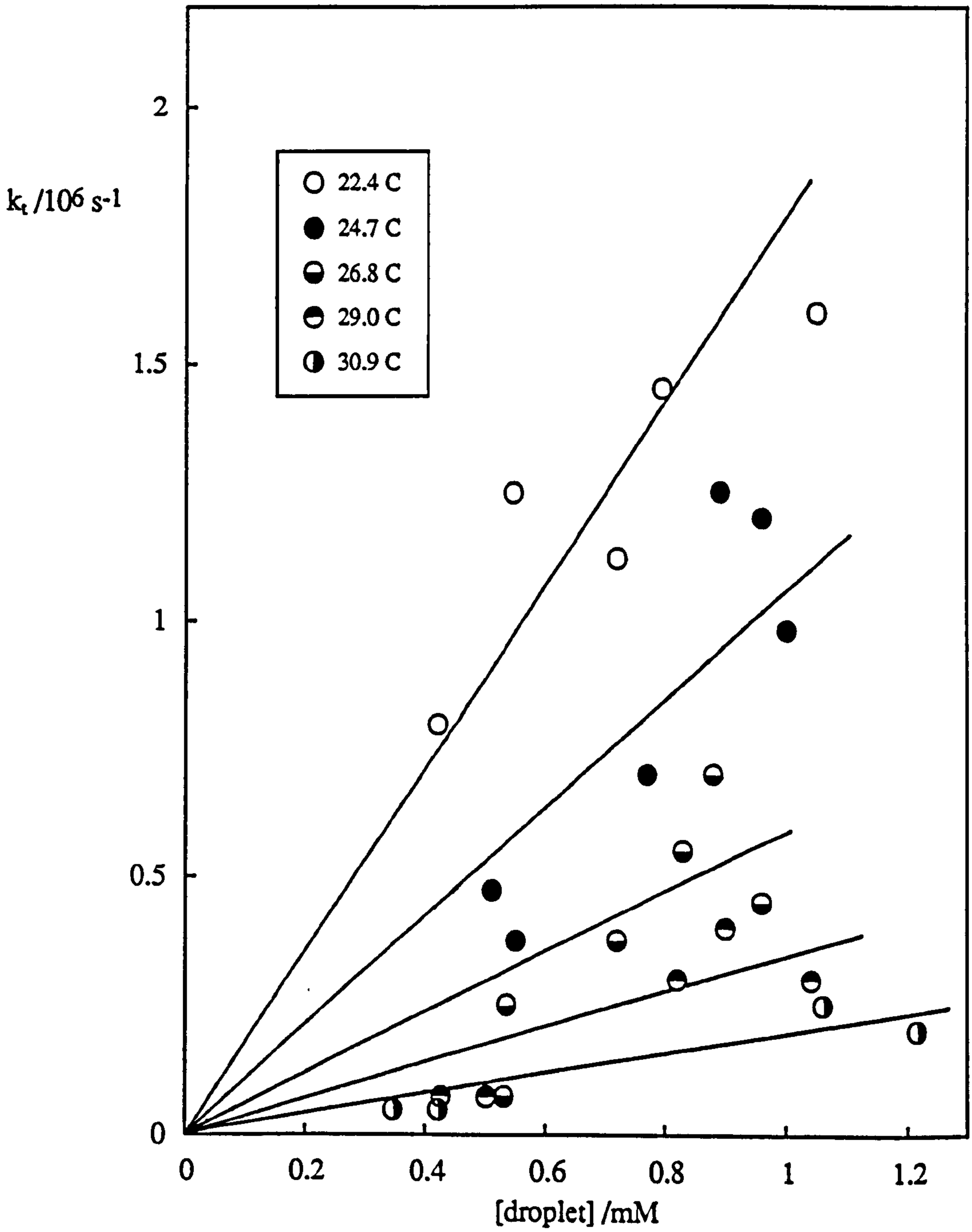

Figure 5.17.

Arrhenius plot of the second order exchange rate constant versus temperature for R'_{water} = 15 W/O microemulsion droplets stabilised by $C_{12}E_4$ in 50% MCT. The dashed line indicates the behaviour expected for a diffusion-controlled rate constant.

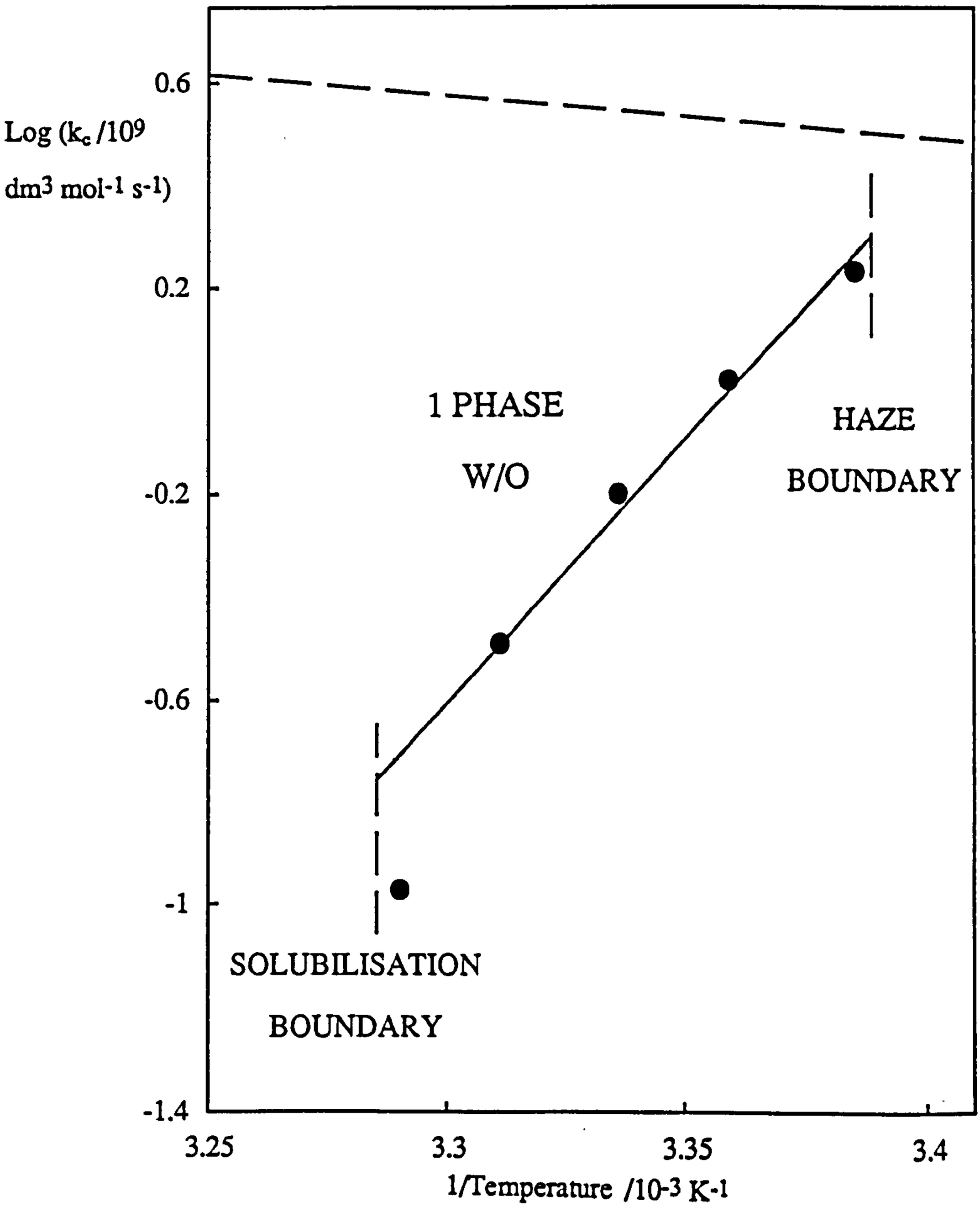

As for heptane as the oil phase, the exchange rate is slowest at the high temperature, solubilisation phase boundary. The dashed line indicates the variation of the diffusion controlled rate constant k_{dc}, predicted for spheres having no energy barrier to coalescence. This value is approached at temperatures close to the haze curve phase boundary.

Table 5.2 below, shows the calculated second order diffusion controlled rate constant and also its ratio with the exchange rate constant at the solubilisation phase boundary for both 50% MCT and heptane as the oil phase. Expressing the rate constants in this way accounts for the different bulk viscosities and allows direct comparison between the two systems. Also tabulated are the cμc values measured at the solubilisation phase boundaries and the approximate estimates for the monolayer rigidities.

Table 5.2

Oil Phase	$k_{dc}/10^9$ M^{-1} s^{-1}	log (k_{dc}/k_c)	$(K+\bar{K}/2)$ /kT	cμc /M
50% MCT	3.9	1.45 ± 0.3	0.9 ± 0.6	0.29 ± 0.02
Heptane	16.9	1.60 ± 0.3	1.0 ± 0.6	0.06 ± 0.01

The exchange rates with respect to the diffusion controlled limit, are approximately the same for the two systems. Clark *et al.* investigating water-in-heptane microemulsions (R'_{water} = 16) stabilised by $C_{12}E_5$, reported a value for log (k_{dc}/k_c) of 1.30 (55). The critical microemulsion concentration had previously been determined to be ~0.08 M and $(K+\bar{K}/2)$, from the tension-size relationship, was estimated to be 1.1 ± 0.5 kT (29). These are of comparable magnitude to those determined for $C_{12}E_4$ in heptane. The enhanced rate postulated for systems with high critical microemulsion concentrations is therefore not observed. It may be that larger cμc variations are required to achieve significant differences in k_{dc}/k_c. Furthermore, since the errors

associated with the parameters ($K+\bar{K}/2$) are large, differences between the two systems due to the $c\mu c$, may be partially offset by changes in the rigidity parameters. Ideally, direct measurements of K and $\bar{K}$ separately, are required before reliable correlations may be performed with the exchange rates.

5.6 Conclusions.

From this study of the equilibrium properties of microemulsions formed in triglyceride / alkane oil mixtures, a number of important observations have been made.

(1). Upon increasing the concentration of triglyceride in the oil phase the minimum concentration of surfactant required for the formation of aggregates dramatically increases. The calculated molar enthalpy of transfer of one mole of surfactant from oil to the preferred microemulsion monolayer curvature decreases from -42 ± 10 kJ mol^{-1} in heptane to -26 ± 5 kJ mol^{-1} in 50% MCT and -19 ± 8 kJ mol^{-1} in 75% MCT.

(2). The degree of maximum water solubilisation is reduced and the one phase microemulsion stability region is shifted to higher temperatures upon increasing the concentration of MCT above 25%. This is consistent with a reduced solvation of the surfactant tails by the bulkier triglyceride molecule. For triglyceride contents less than or equal to 25%, the one phase region is shifted to slightly lower temperatures suggesting penetration of the MCT into the alkyl tail region of the surfactant for this concentration range.

(3). The value of the rigidity parameter ($K+\bar{K}/2$) estimated from tension-size relationship for 50% MCT is of the order of kT. This is of similar magnitude to values reported previously for other systems using this treatment.

(4). The microemulsion exchange rate relative to the diffusion controlled limit is found to be little affected by the presence of 50% MCT in the oil phase. The enhanced rate expected for this system due to the high concentration of non-adsorbed surfactant in the continuous phase is not observed.

6. POSSIBLE CORRELATIONS BETWEEN MONOLAYER BENDING RIGIDITIES, MICROEMULSION EXCHANGE RATES AND MACROEMULSION STABILITY.

CHAPTER 6.

6.1 Introduction; the Work of Lee *et al.*

In the previous chapters, attempts have been made to correlate properties of microemulsion systems with factors which may have a direct bearing on the formation and stability of the corresponding macroemulsions. The rate of exchange of probe molecules between microemulsion aggregates has been measured by time-resolved fluorescence and the relevance of the cμc and the monolayer rigidity to the magnitude of the exchange rate constant discussed. For the majority of systems studied by TRF to date, only approximate estimates of the parameter $(K+\bar{K}/2)$ have been reported from a tension-size relationship. The relative contributions of both K and $\bar{K}$ within these parameters is unknown. Additionally, the experimental errors in the values of $(K+\bar{K}/2)$ are typically of the same order of magnitude as the values themselves.

Recently, Lee *et al.* (167) used an ellipsometry technique to determine values of the rigidity constant K for planar monolayers of three nonionic surfactants. The measurements were performed on oil-water interfaces produced by combining the excess oil and water phases of Winsor III systems. In order to maintain the temperature range of the Winsor III regions within suitable experimental operating conditions (i.e. 15 - 30°C), the alkyl chain length and degree of ethoxylation of the surfactant and the chain length of the oil had to be varied. The three systems investigated were $C_{12}E_5$/hexane, $C_{10}E_4$/octane and C_8E_3/decane. The experimental values of K were renormalised to the same length scale (7.5 Å) so that they could be directly compared. They observed that for C_8E_3 and $C_{10}E_4$, K increased with the length of the surfactant molecule as predicted previously by Safinya *et al.* (177). Problems with obtaining "clean" interfaces however, (interfaces devoid of unresolved emulsion particulates) restricted the measurements with the $C_{12}E_5$ system and only limited data was obtained. These indicated a larger value of K for this system than obtained for either of the other

two. Indeed, we may speculate here that the problem of obtaining a "clean" interface in this case may be a consequence of the higher monolayer rigidity. A quantitative value of K for $C_{12}E_5$ monolayers was not reported. Table 6.1 below tabulates the three systems investigated and their reported renormalised rigidity constants.

Table 6.1

System	K/kT
$C_{12}E_5$/hexane	-
$C_{10}E_4$/octane	0.76
C_8E_3/decane	0.35

If it is assumed that the bending energy dominates the microemulsion coalescence process, then it may be predicted that the microemulsion exchange rate at the solubilisation phase boundary should follow the order $C_8E_3 > C_{10}E_4 > C_{12}E_5$. Similarly, macroemulsion stability with respect to coalescence might also be predicted to follow this order when compared at the same system HLB.

In this chapter, the extent of the one phase W/O microemulsion regions are presented for the surfactant systems $C_{12}E_5$/hexane, $C_{10}E_4$/octane and C_8E_3/decane. Variation of the microemulsion droplet size with R'_{water} is reported and the area per surfactant molecule at the droplet surface calculated. Interfacial tensions are presented and exchange rates are determined for each system at the solubilisation phase boundary for microemulsion droplets of $R'_{water} = 8$. The results are interpreted in terms of differences in monolayer rigidities as determined by Lee *et al.* Finally, the possible correlation between microemulsion exchange rate and macroemulsion coalescence is investigated for the three surfactant systems.

6.2 W/O Microemulsion Phase Boundaries for Three Nonionic Surfactant + Alkane + Water Systems.

One phase W/O microemulsion stability regions for the three surfactant systems $C_{12}E_5$/hexane, $C_{10}E_4$/octane and C_8E_3/decane are shown in Figures 6.1, 6.2 and 6.3. It is clearly evident that the degree of maximum solubilisation increases in the order C_8E_3/decane < $C_{10}E_4$/octane < $C_{12}E_5$ /hexane. For each system the temperature corresponding to maximum solubilisation is approximately 30°C.

Critical microemulsion concentrations for each system as a function of temperature are shown in Figure 6.4. At a fixed temperature it is clear that the cμc increases in the order $C_{12}E_5$ < $C_{10}E_4$ < C_8E_3. The enthalpies of transfer of one mole of each surfactant from the monomeric state in the oil to the "preferred" monolayer curvature at the solubilisation phase boundary have been calculated from Figure 6.5. The results are tabulated below in Table 6.2.

Table 6.2

System	$\Delta H_{micelle}$/kJ mol^{-1}
$C_{12}E_5$/hexane	-35 ± 6
$C_{10}E_4$/octane	-30 ± 15
C_8E_3/decane	-30 ± 5

The results of Shinoda *et al.* show that the enthalpy change for a series of dodecyl tail group surfactants in decane, decreases (i.e. become more negative) by approximately 2 kJ mol^{-1} per additional ethoxy group (151). Changing the surfactant chain length at a constant number of ethoxy units was shown to have negligible effect. For the systems investigated here, the alkane and the length of the surfactant alkyl tail change in addition to the number of ethoxy groups. The observed change in the transfer

Figure 6.1.

One phase water-in-hexane stability region for microemulsions stabilised by $C_{12}E_5$. The open points denote the haze boundary and the filled points the solubilisation boundary.

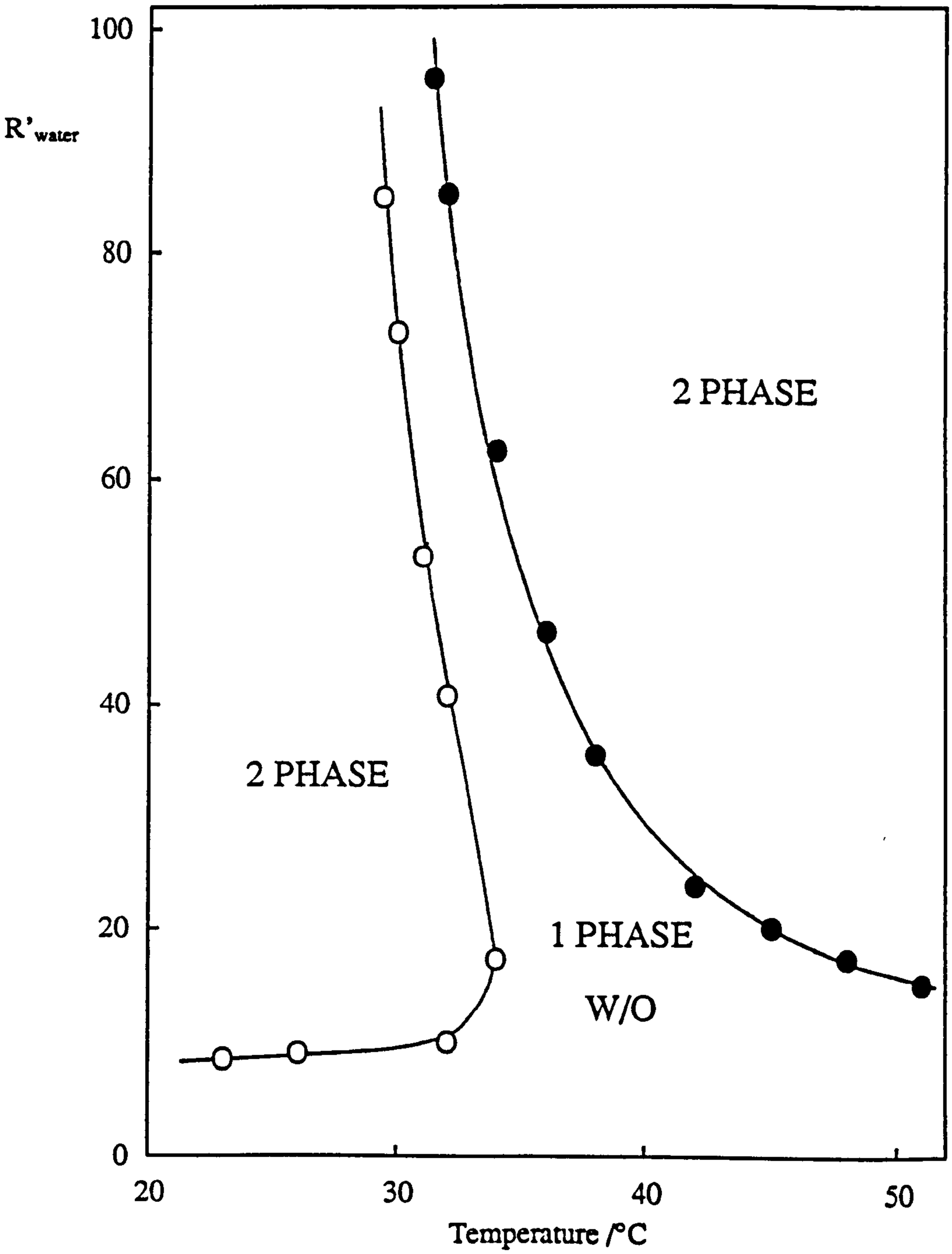

Figure 6.2.

One phase water-in-octane stability region for microemulsions stabilised by $C_{10}E_4$. The open points denote the haze boundary and the filled points the solubilisation boundary.

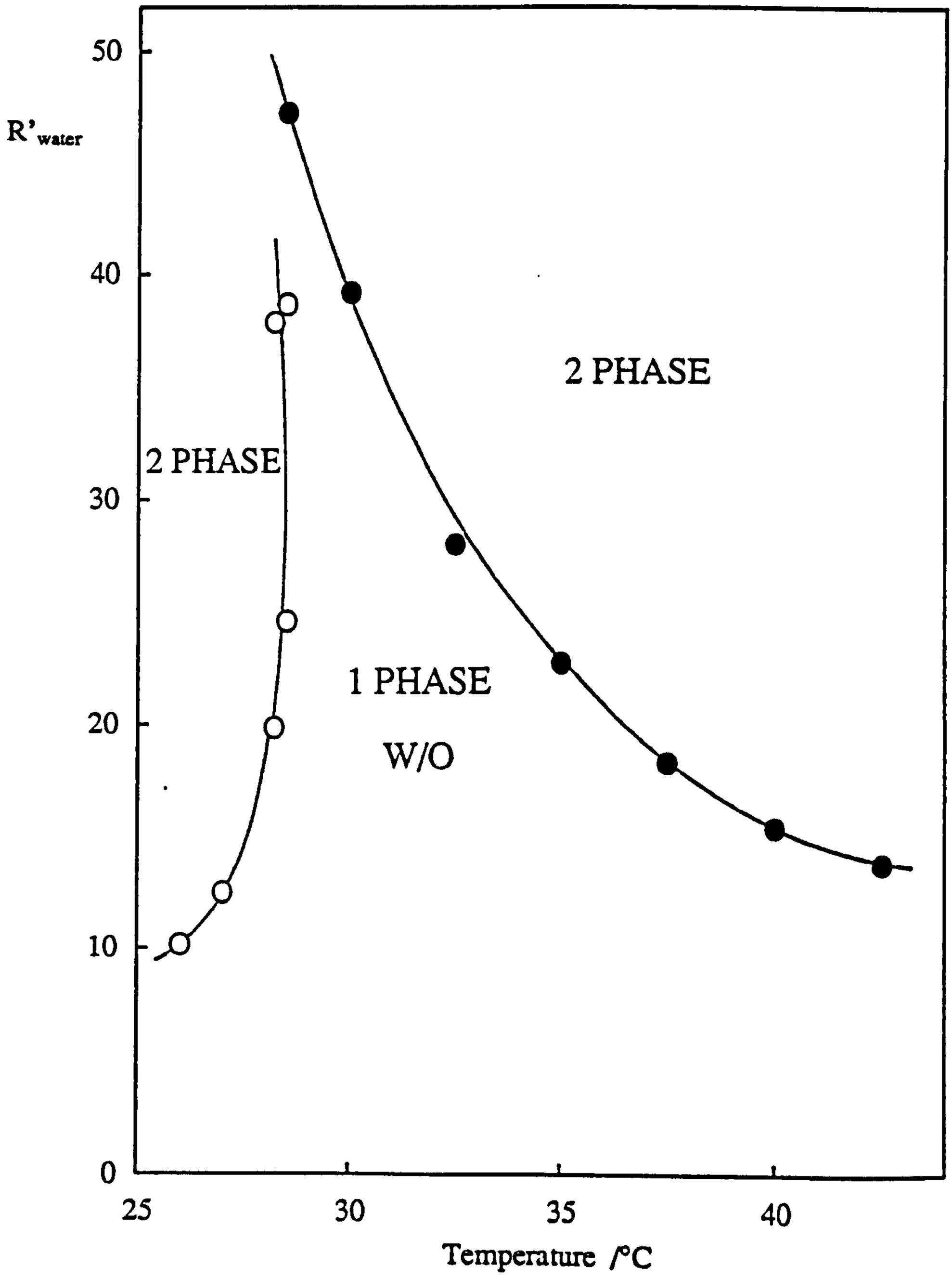

Figure 6.3.

One phase water-in-decane stability region for microemulsions stabilised by C_8E_3. The open points denote the haze boundary and the filled points the solubilisation boundary.

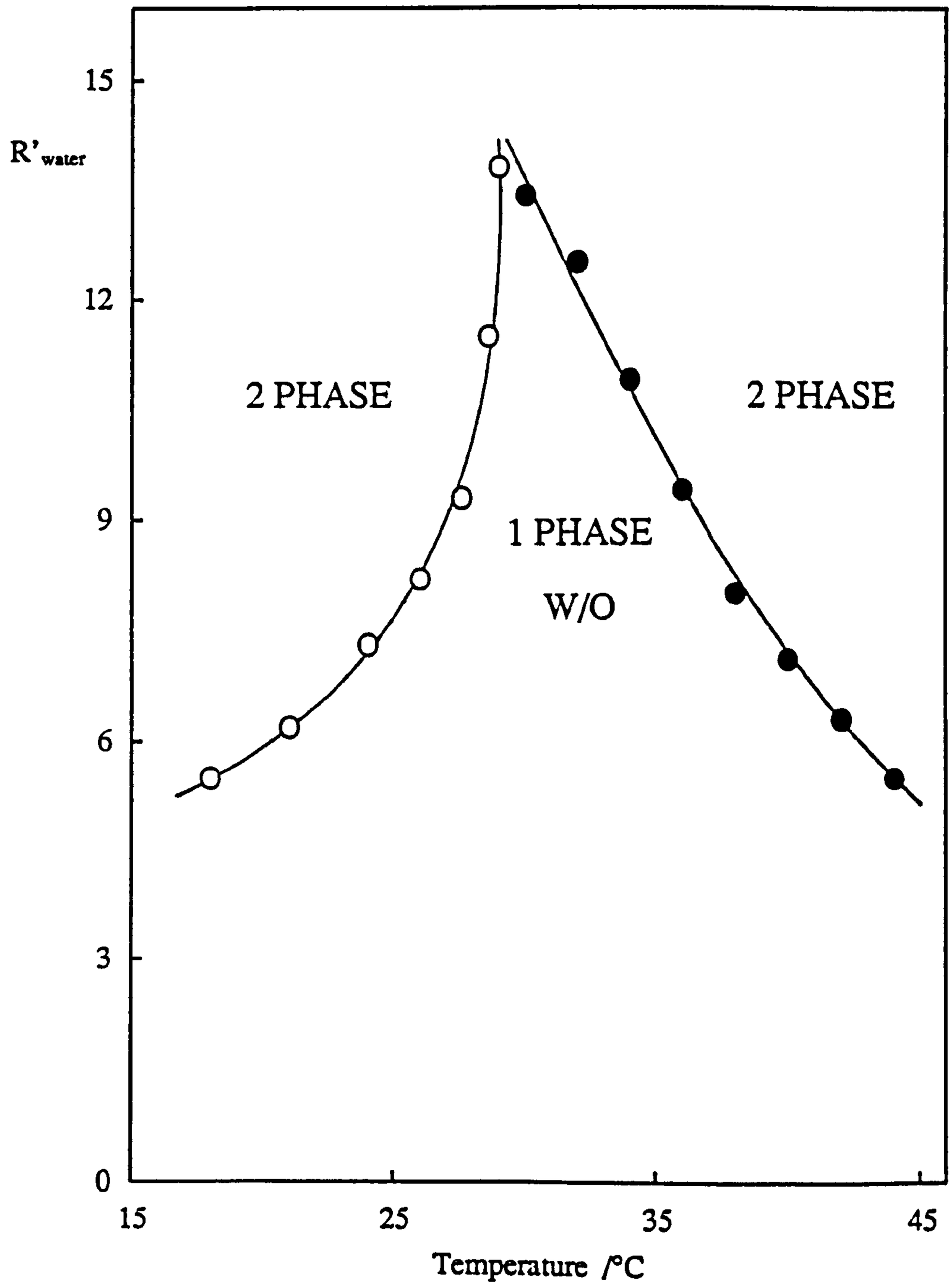

Figure 6.4.

Variation of the critical microemulsion concentration with temperature for the three surfactant systems shown in the legend.

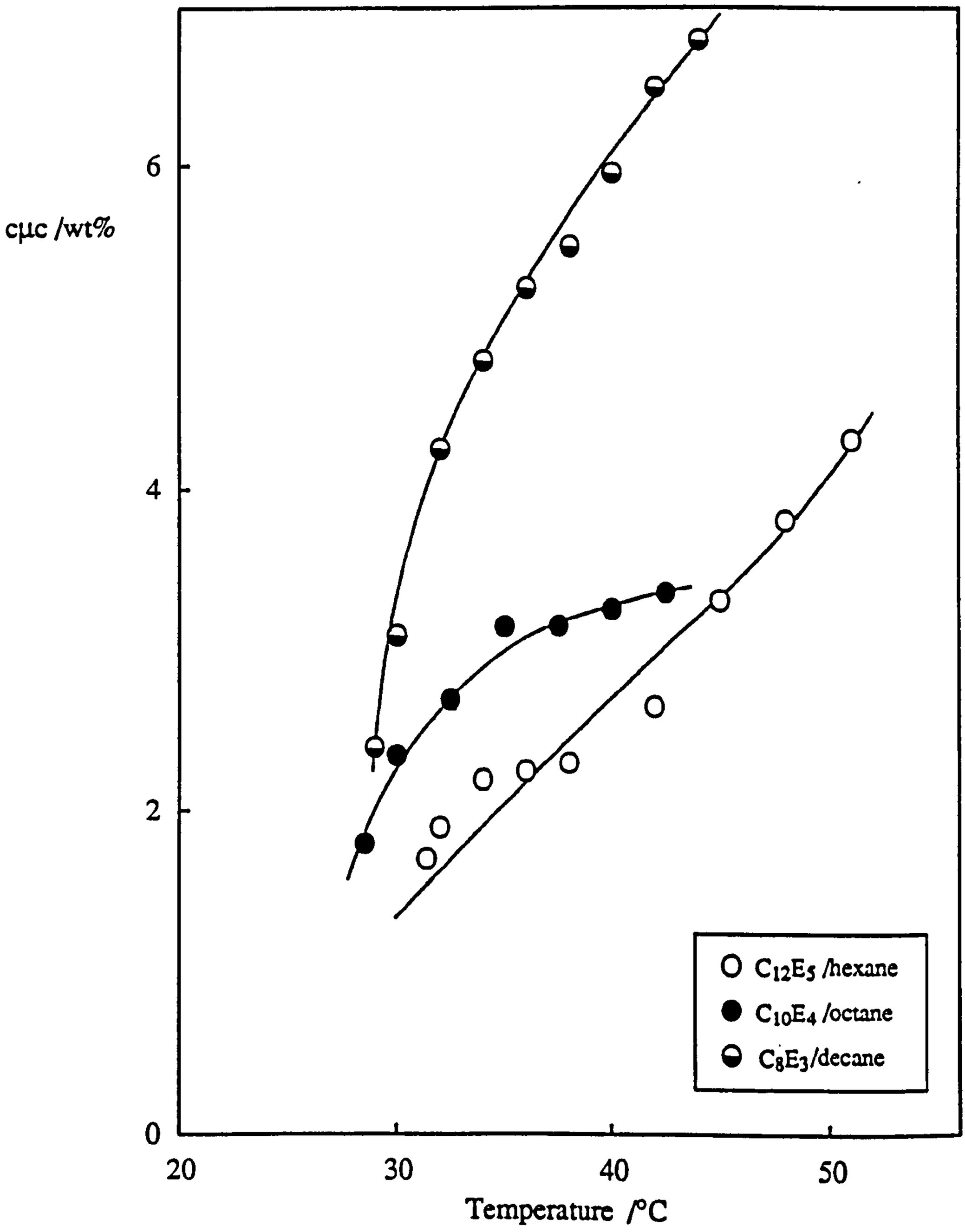

Figure 6.5.

Variation of log cμc with 1/temperature for the three surfactant systems shown in the legend.

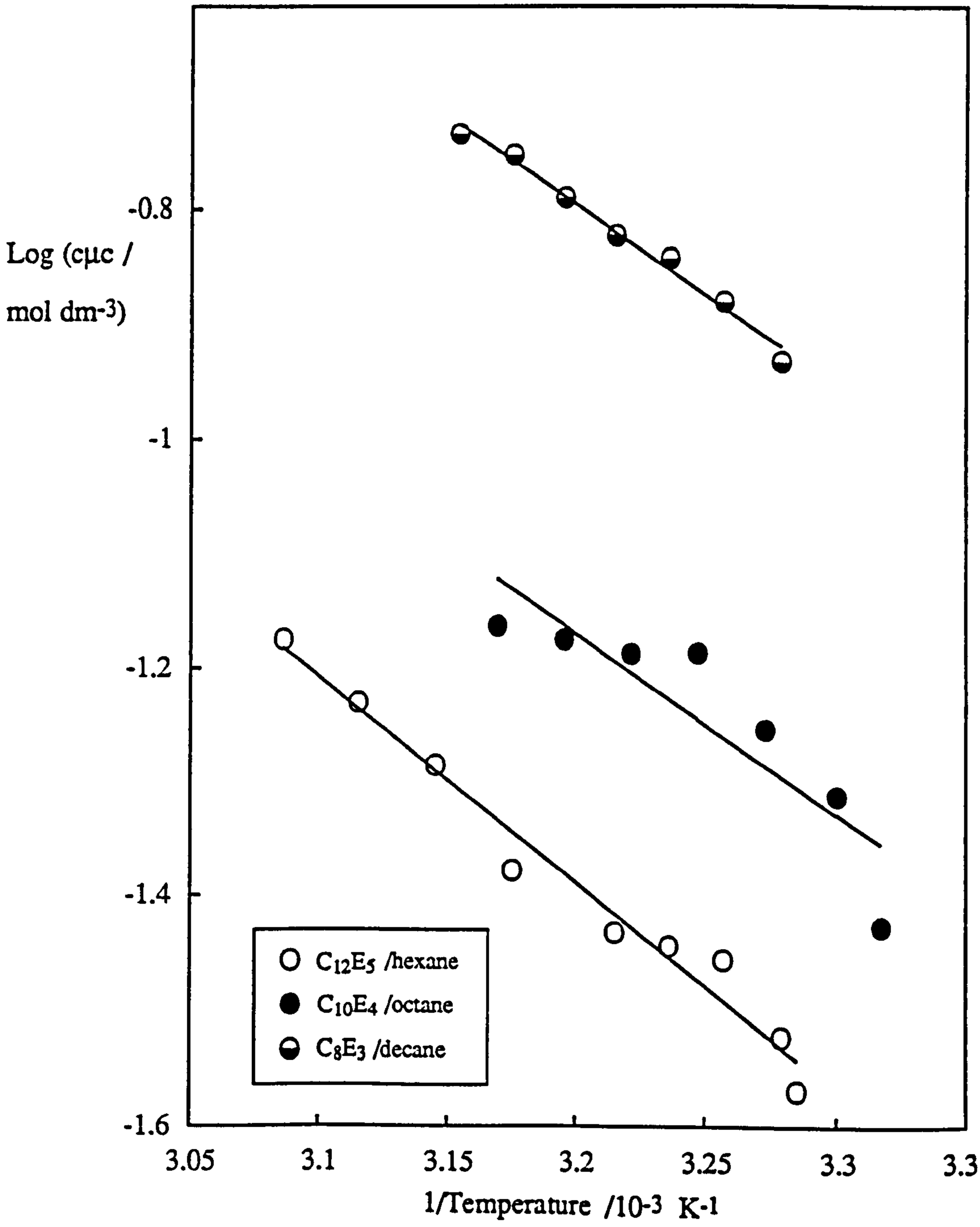

enthalpy, from -30 ± 5 kJ mol^{-1} for C_8E_3/decane to -35 ± 6 kJ mol^{-1} for $C_{12}E_5$/hexane, is consistent with that expected for two additional ethoxy units.

6.3 Measurement of Microemulsion Droplet Sizes by Photon Correlation Spectroscopy.

As before, microemulsion droplet sizes were measured at temperatures very close to the excess water solubilisation phase boundaries where inter-droplet interactions are minimum. Variation of the apparent diffusion coefficient with dispersed phase volume fraction is shown for each system in Figures 6.6a-c. The dependence of the diffusion coefficient on volume fraction is small and the aggregates mostly appear to behave "ideally". For microemulsions stabilised by C_8E_3, only aggregates of composition R'_{water} = 12 were large enough to be measured and the hydrodynamic radius was found to be 6.0 ± 1.5 nm.

The hydrodynamic radii (obtained from extrapolation of the apparent diffusion coefficients to infinite dilution) are shown as a function of R'_{water} in Figures 6.7 and 6.8 for $C_{12}E_5$ and $C_{10}E_4$ respectively. An approximate linear relationship between r_H and R'_{water} is seen to hold for both systems in accordance with the geometrical expression previously presented (equation 4.2). In Figure 6.8, the point at R'_{water} = 41 appears to deviate significantly from the linear dependence. This presumably arises from the larger error in the cμc values for this system (Figure 6.5) and the large dependence of R'_{water} on the temperature at 30°C (Figure 6.2). For $C_{12}E_5$ the data conforms to the following empirical relationship.

$$r_H/\text{nm} = 0.217\, R'_{water} + 2$$

Figure 6.6a.

Variation of the apparent diffusion coefficient with dispersed phase volume fraction, for water-in-hexane microemulsions stabilised by $C_{12}E_5$.

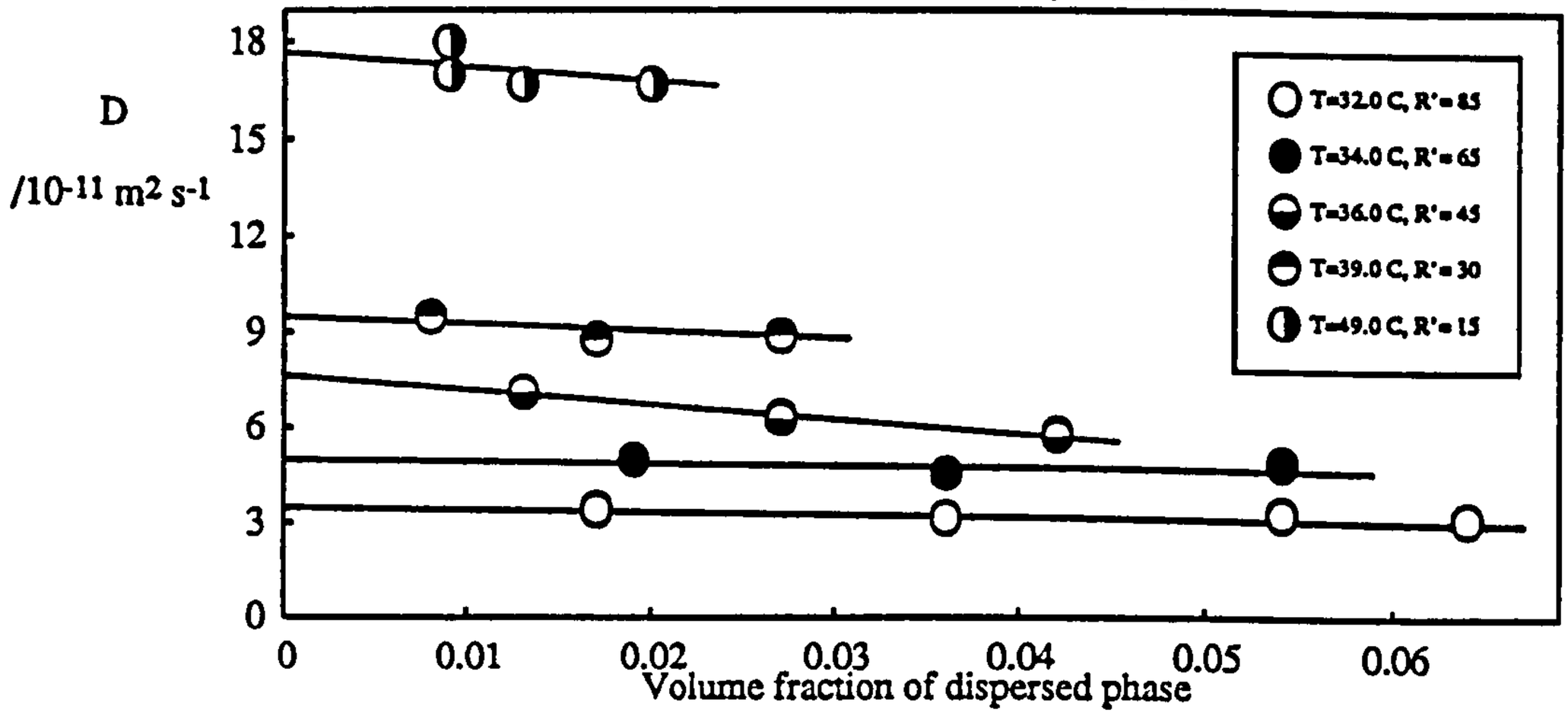

Figure 6.6b, water-in-octane microemulsions stabilised by $C_{10}E_4$.

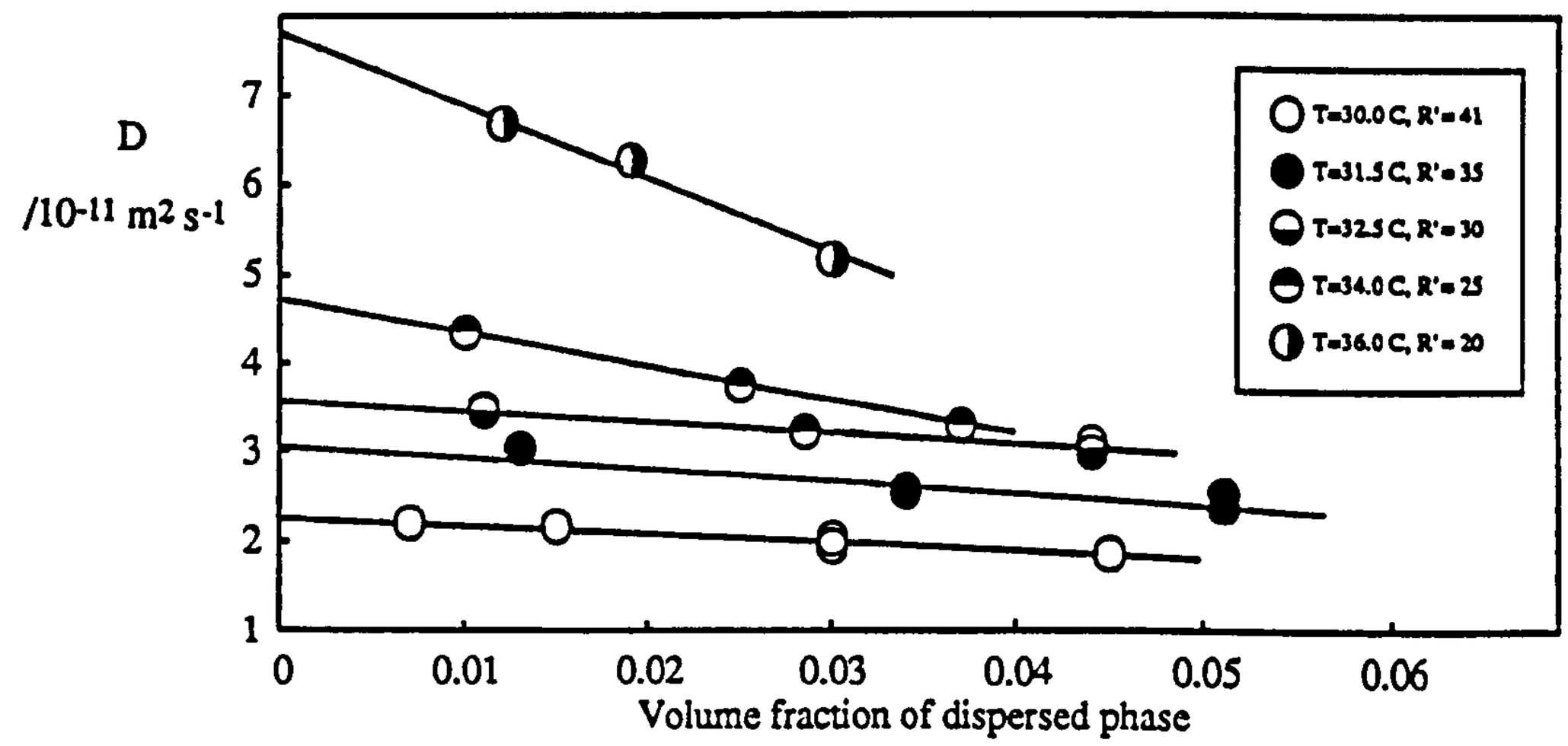

Figure 6.6c, water-in-decane microemulsions stabilised by C_8E_3 .

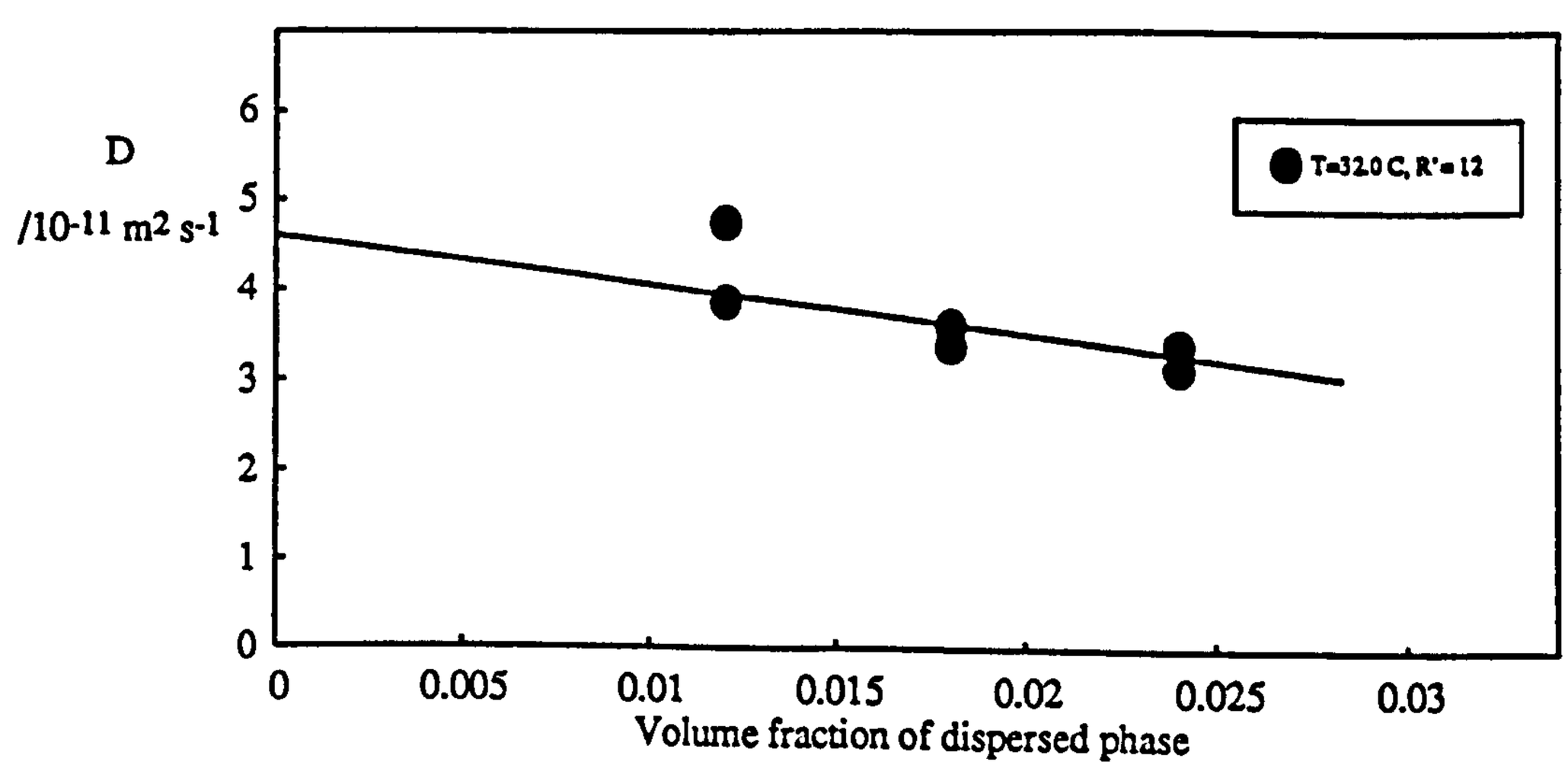

Figure 6.7.

Hydrodynamic radii measured close to the solubilisation boundary versus R'_{water} for water-in-hexane microemulsions stabilised by $C_{12}E_5$. Open point is derived from TRF data assuming two molecules of hexane per $C_{12}E_5$ solvation.

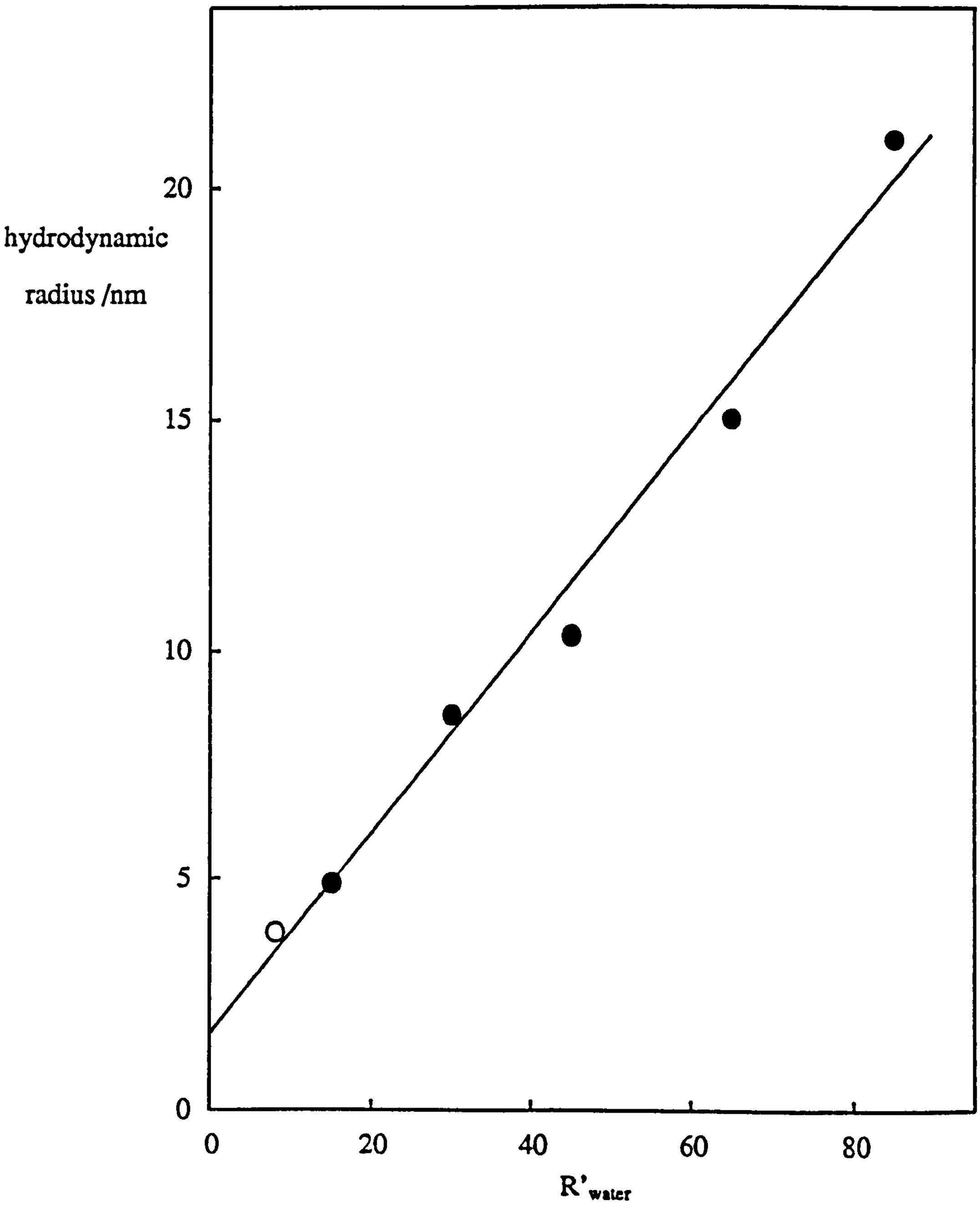

Figure 6.8.

Hydrodynamic radii measured close to the solubilisation boundary versus R'_{water} for water-in-octane microemulsions stabilised by $C_{10}E_4$. Open points are values derived from TRF data assuming two molecules of octane per $C_{10}E_4$ solvation.

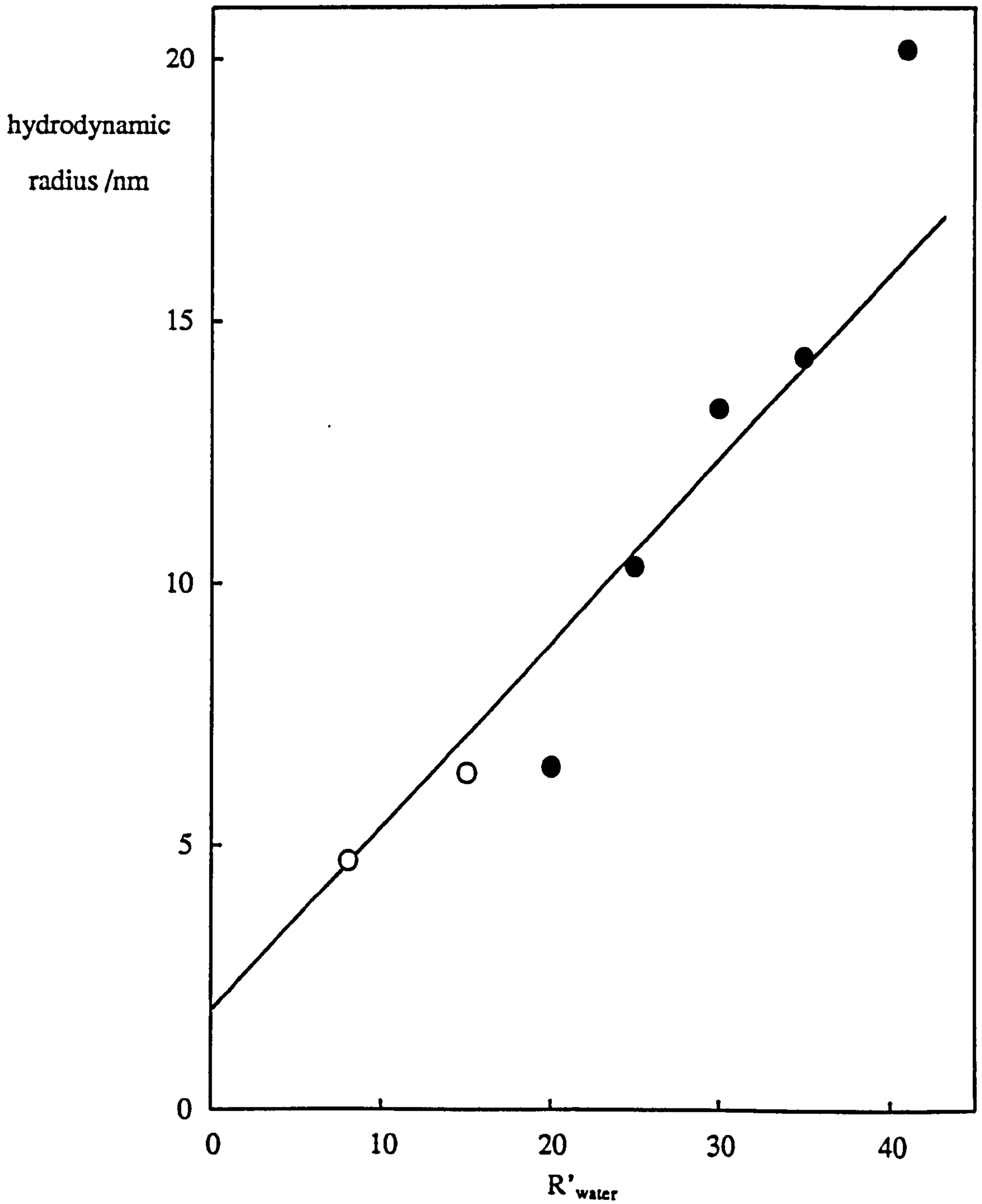

The area per surfactant molecule at the interface between the droplet core and the surfactant monolayer is calculated to be $0.41 \pm 0.06\ nm^2$. This is slightly larger than the value of $0.35 \pm 0.06\ nm^2$ reported for $C_{12}E_5$ in heptane (29). The interfacial thickness is estimated from the intercept to be 2 ± 2 nm. For aggregates stabilised by $C_{10}E_4$ in octane the following relationship approximately describes the data.

$$r_H / nm = 0.345\ R'_{water} + 2$$

This corresponds to an area per surfactant molecule of $0.26 \pm 0.07\ nm^2$ and an interfacial thickness of 2 ± 2 nm. This area is similar to values of $0.32 \pm 0.06\ nm^2$ and $0.26 \pm 0.06\ nm^2$ determined for $C_{12}E_4$ in heptane and tetradecane respectively. For the W/O systems investigated here, the area is primarily dependent on the number of ethoxy units in the head group and is less dependent on the chain length of the alkyl tail and on the nature of the oil phase.

6.4 Post-cμc Oil-Water Interfacial Tension as a Function of Temperature.

Figure 6.9 shows the variation of the interfacial tension between the upper and lower phases of Winsor I, II, and III systems for the three surfactant systems shown in the legend. The values of the minimum tension increase in the order $C_{12}E_5 < C_{10}E_4 < C_8E_3$. Kunieda and Shinoda have correlated the depth of the tension minima with the temperature range over which the three phase region exists (161). For the three systems of interest here, Table 6.3 demonstrates this correlation.

Figure 6.9.

Oil-water interfacial tension as a function of temperature for the three nonionic surfactant systems shown in the legend.

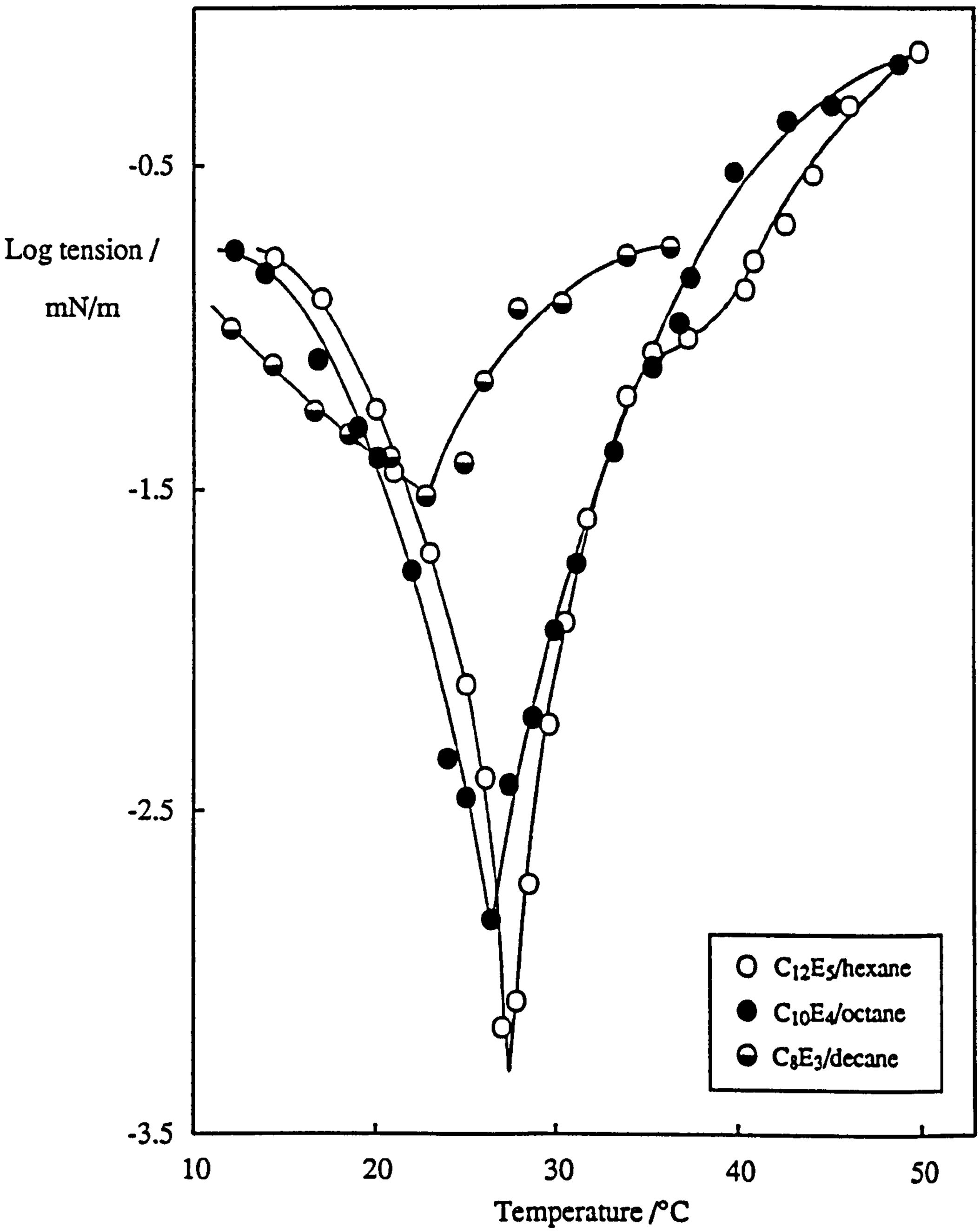

Table 6.3

System	ΔT_{III} (lit.)/°C	Log γ_{min}	T*/°C
$C_{12}E_5$/hexane	27 - 29 (34)	-3.30	28.0
$C_{10}E_4$/octane	23 - 28 (34)	-2.85	26.0
C_8E_3/decane	16 - 28 (34)	-1.55	23.0

It can be seen that the lowest oil-water interfacial tensions are attained when the temperature range of the three phase region is smallest. Also tabulated are the temperatures at which the tension minima are observed, T*. These values are seen to coincide approximately with the midpoints of the three phase temperature intervals as has been previously observed (40, 188).

The values of the oil-water interfacial tension as determined here by the spinning drop technique, are in good agreement with those determined with surface laser light scattering by Lee *et al.* (167). Similar agreements between these two techniques have previously been reported in the literature (189, 190).

The values of $(K+\bar{K}/2)$ may be estimated using the approximate relationship between the interfacial tension and the droplet size given in section 1.2.5. Despite having values of K for the three systems measured directly by ellipsometry, it is interesting to see how the parameter $(K+\bar{K}/2)$ relates to these values. The relationship between the interfacial tension and the droplet size is shown in Figure 6.10 for $C_{12}E_5$ and $C_{10}E_4$. Values for aggregates stabilised by C_8E_3 are not shown since the microemulsion sizes were too small to be determined. In the case of $C_{12}E_5$, the data is seen to approximately fit the radius^{-2} dependence expected from the theory. However, for aggregates stabilised by $C_{10}E_4$, the fit is poor and the data appears to conform to a radius$^{-3.5}$ dependence. The calculated values for $(K+\bar{K}/2)$ are both approximately kT (within 1 kT or so) and hence are of a similar magnitude to K.

Figure 6.10.

Variation of log tension with log radii for W/O microemulsions formed with $C_{10}E_4$ in octane and $C_{12}E_5$ in hexane. The lines are the best fits to the data assuming a gradient of -2.

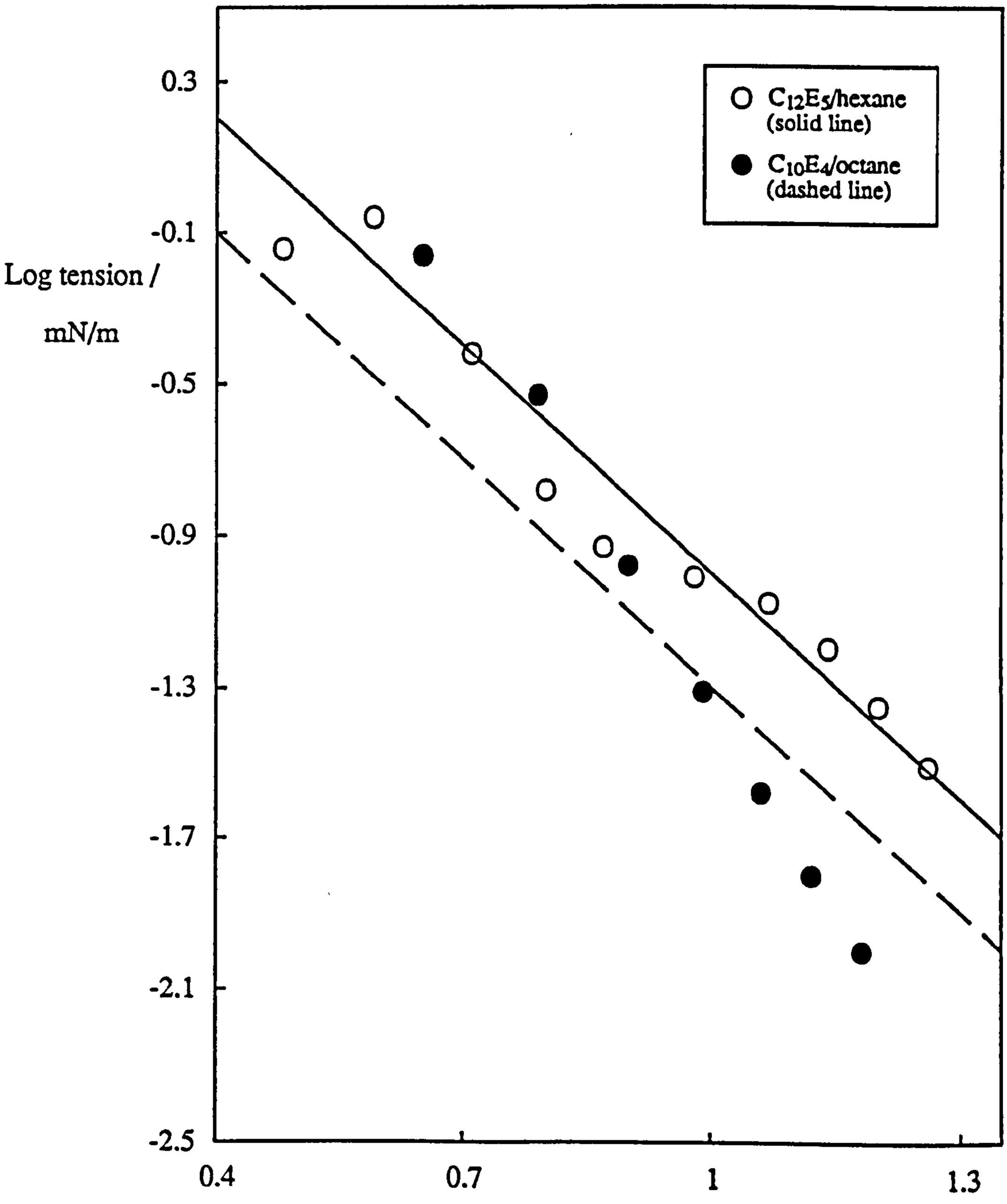

6.5 Time-Resolved Fluorescence Results For W/O Microemulsions Formed with $C_{12}E_5$/Hexane, $C_{10}E_4$/Octane and C_8E_3/Decane.

Microemulsion dynamics were investigated using a time-resolved fluorescence technique for $R'_{water} = 8$ droplets of each of the three systems. The one phase stability regions, critical microemulsion concentrations and interfacial tensions corresponding to $R'_{water} = 8$ for each system are tabulated below in Table 6.4.

Table 6.4

System	γ_c /mN m^{-1}	ΔT /°C	cμc /10^{-2} M
$C_{12}E_5$/hexane	2.00*	10 - 60*	8.4 ± 0.8*
$C_{10}E_4$/octane	0.66	22 - 48*	7.9 ± 1.0*
C_8E_3/decane	0.18	26 - 37	15.0 ± 1.0

* Estimated by extrapolation.

Samples were investigated at surfactant concentrations between 10 and 30 wt% and ruthenium tris-bipyridyl and methyl viologen were used as fluorescer and quencher probes respectively. In the case of all three surfactants, a fluorescent impurity was observed to slightly perturb the first few channels of the decay trace. However, as for $C_{12}E_4$, the intensity decay curves were corrected by subtracting the trace of a "blank" microemulsion sample before fitting. Generally, χ^2 values were better than about 1.5.

Plots showing the variation of the microemulsion droplet size with temperature across the one phase stability region ($R'_{water} = 8$) are displayed in Figures 6.11a-c. The radii are calculated using equation 4.18. The sizes are seen to be independent of temperature and show little dependence on the droplet concentration. The results are tabulated below.

Figure 6.11a.

Variation of microemulsion droplet radii (unsolvated) across the one phase stability region, for $R'_{water} = 8$ water-in-hexane droplets stabilised by $C_{12}E_5$.

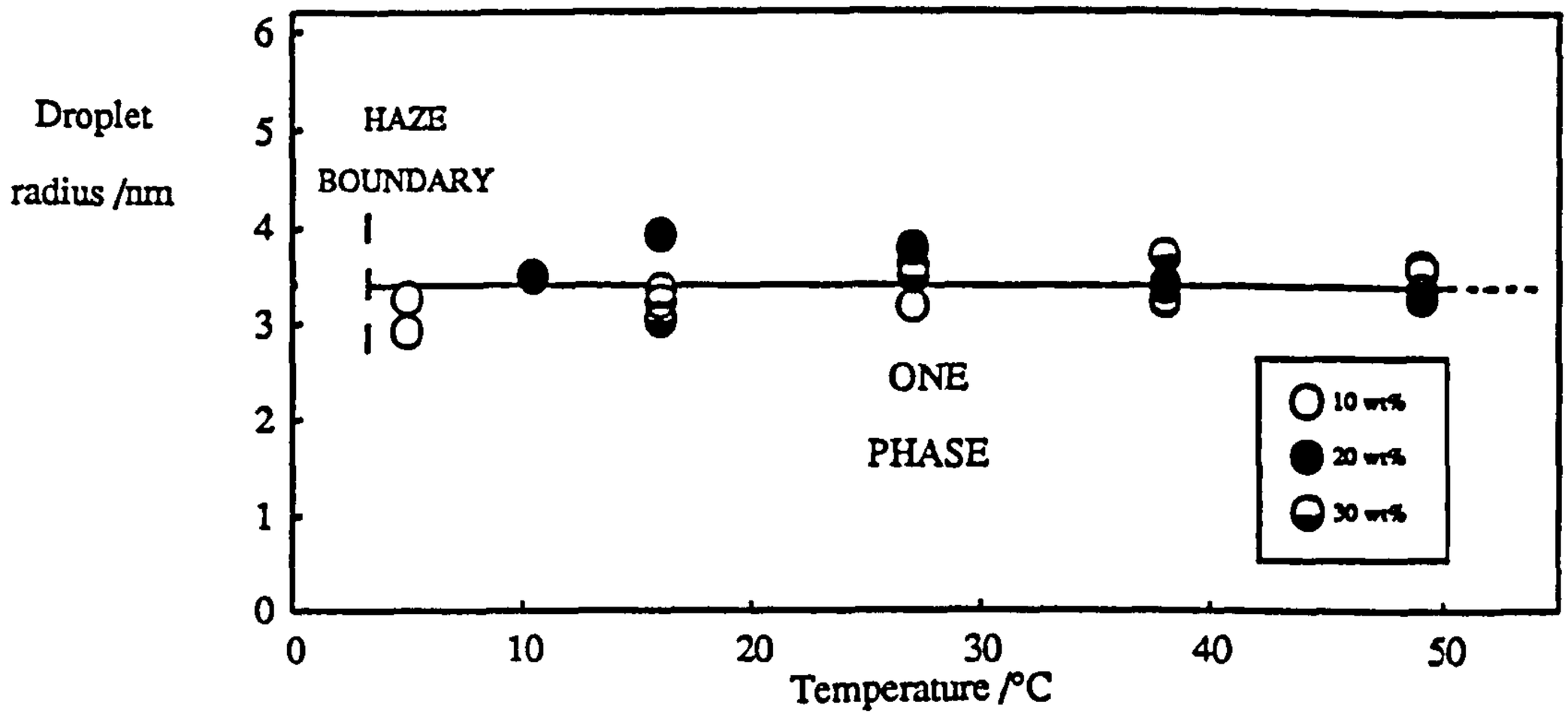

Figure 6.11b, $R'_{water} = 8$ water-in-octane microemulsions stabilised by $C_{10}E_4$.

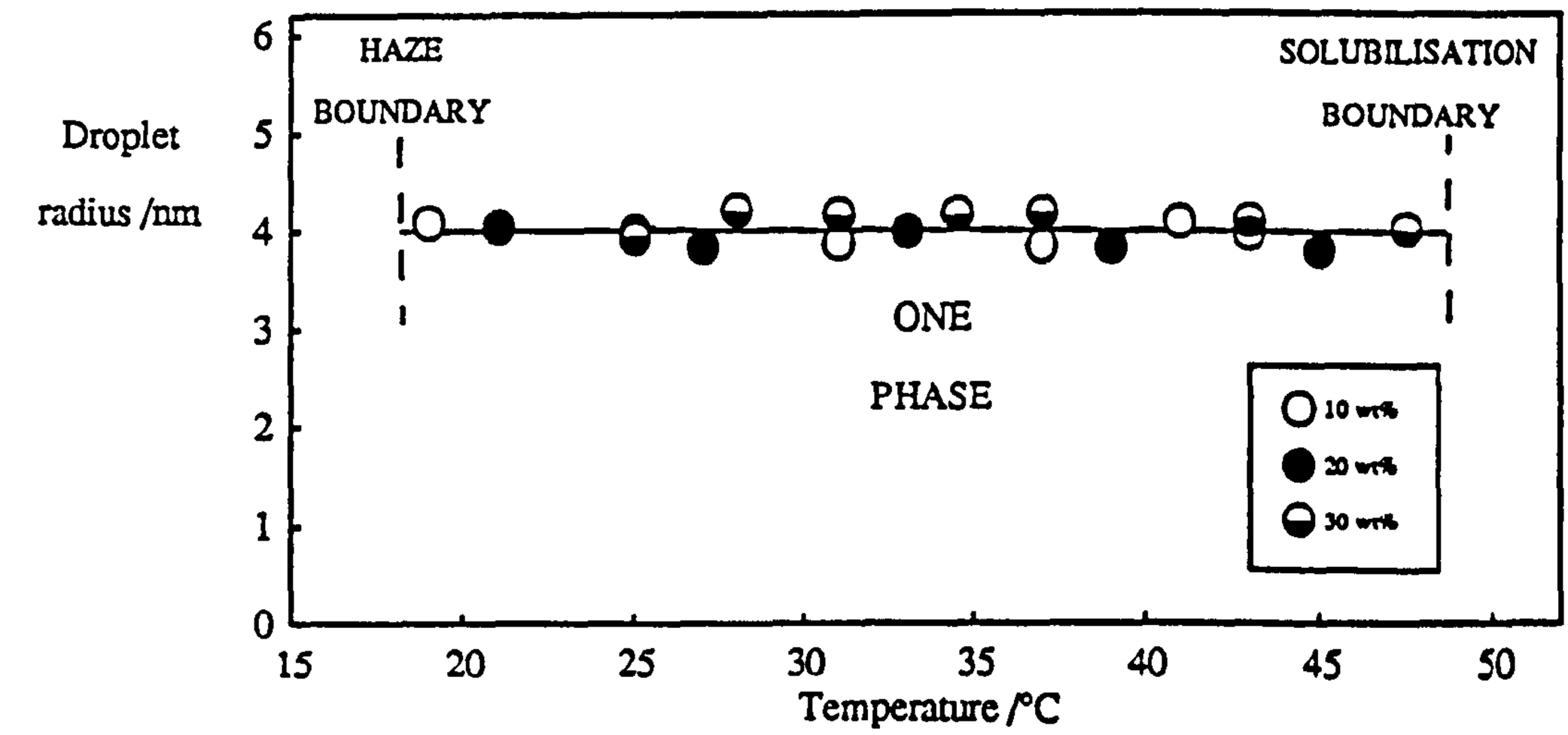

Figure 6.11c, $R'_{water} = 8$ water-in-decane microemulsions stabilised by C_8E_3.

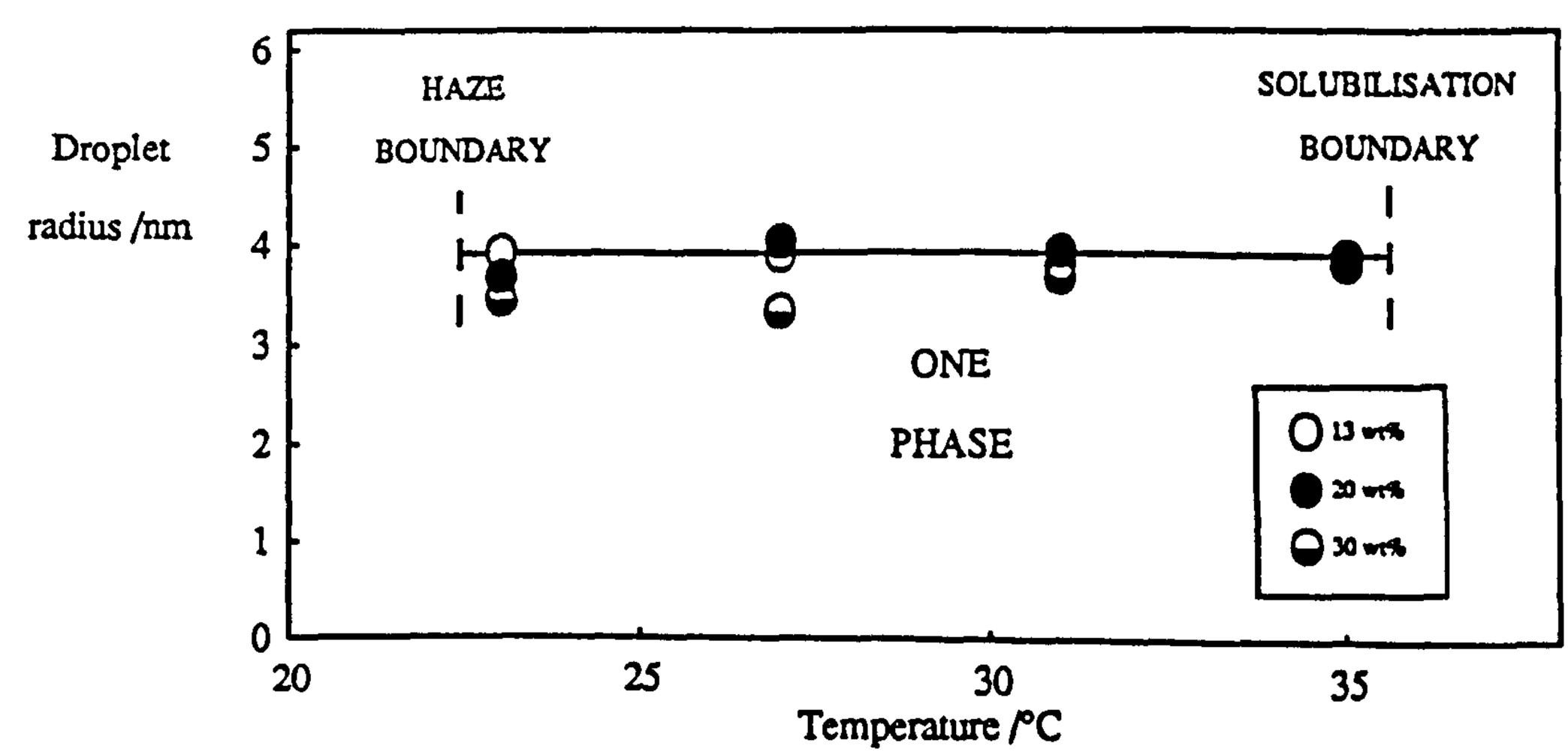

Table 6.5

System	r /nm	N_{agg}
$C_{12}E_5$/hexane	3.4 ± 0.3	180 ± 50
$C_{10}E_4$/octane	4.0 ± 0.2	330 ± 50
C_8E_3/decane	3.9 ± 0.3	370 ± 60

The smaller aggregation number in the case of $C_{12}E_5$ presumably reflects the larger area per surfactant head group expected for this molecule. Table 6.6 below compares values for the area occupied by the surfactant molecule at the interface between the droplet core and the surfactant monolayer calculated from the above aggregation numbers with those obtained through PCS measurements.

Table 6.6

System	A_h(TRF)/nm^2	A_h(PCS)/nm^2
$C_{12}E_5$/hexane	0.33 ± 0.04	0.41 ± 0.06
$C_{10}E_4$/octane	0.27 ± 0.02	0.26 ± 0.07
C_8E_3/decane	0.26 ± 0.02	-

Good agreement is seen for $C_{10}E_4$, however a difference is observed for $C_{12}E_5$. The value obtained by TRF is however, in agreement with a value of 0.35 ± 0.06 nm^2 reported by Aveyard *et al.* for $C_{12}E_5$ in heptane (29). It appears therefore that the value calculated from PCS may be slightly too large.

Figure 6.12 shows the variation of log (k_q N_{agg} R'_{water}) (predicted by equation 4.19 to be inversely proportional to the microviscosity) with temperature for the three surfactant systems. The R'_{water} = 8 droplets show a similar microviscosity to the R'_{water} = 15 systems shown in Figures 4.31 and 5.14. The values are all of the order of 10 cP.

Figure 6.12.

Log (k_q N_{agg} R'_{water}) versus 1/temperature for the W/O microemulsion systems shown in the legend. The dashed line indicates the values calculated for a microviscosity equal to that of bulk water.

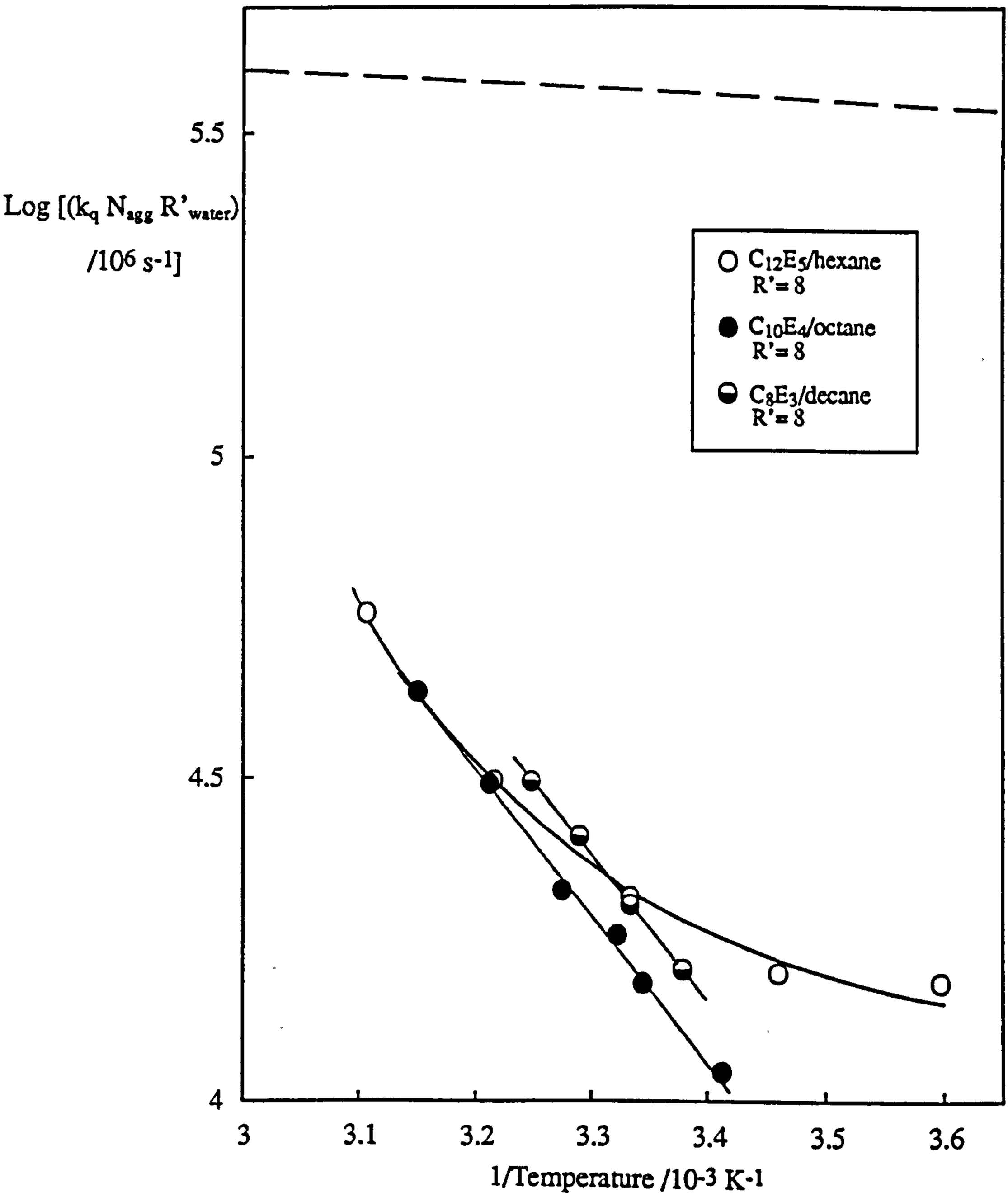

The first order fluorescence decay rate constant k_o is shown in Figure 6.13 as a function of temperature for the three surfactant systems discussed here and those discussed previously in Chapters four and five. There appears to be a slight dependence on R'_{water} with a higher rate constant being observed for larger values of R'_{water}. A similar result has been observed by Jada *et al.* for aggregates stabilised by cationic surfactants (54). This dependence on R'_{water} indicates that the micro-environment experienced by the probe (e.g. polarity, hydration etc.) changes with droplet size. At large droplet sizes, k_o tends towards the value observed in bulk water (176).

Calculated values of the first order exchange rate constant k_t, assuming a "fusion-fission" mechanism, are shown in Figures 6.14a-c as a function of droplet concentration. As in previous studies, an approximate linear dependence is observed. The second order exchange rate constants k_c, corresponding to the different temperatures within the one phase region are obtained from the slopes. These are displayed in Figures 6.15a-c. The dashed lines indicate the variation of the diffusion controlled rate constant calculated from equation 4.20. As in the previous studies, the slowest exchange rate for each system is observed at the high temperature solubilisation phase boundary. In the case of $C_{12}E_5$, the rate constant could not be determined directly at the solubilisation boundary since this occurred at a temperature outside the operating conditions of the instrument. This was however estimated by linear extrapolation.

Table 6.7 below tabulates the exchange rate constants at the solubilisation boundary for each system as a ratio with the diffusion controlled rate constant. This ratio allows direct comparison of systems exhibiting different continuous phase viscosities. The diffusion controlled rate constant alone is also tabulated along with the renormalised bending rigidity constants as reported by Lee *et al.* (167), cμc values and the all-trans length of each surfactant molecule (ML) as measured from molecular models.

Figure 6.13.

Variation of the unquenched fluorescence decay rate constant k_o, for RB in the W/O microemulsion systems shown in the legend. The dashed line indicates the behaviour in water (121).

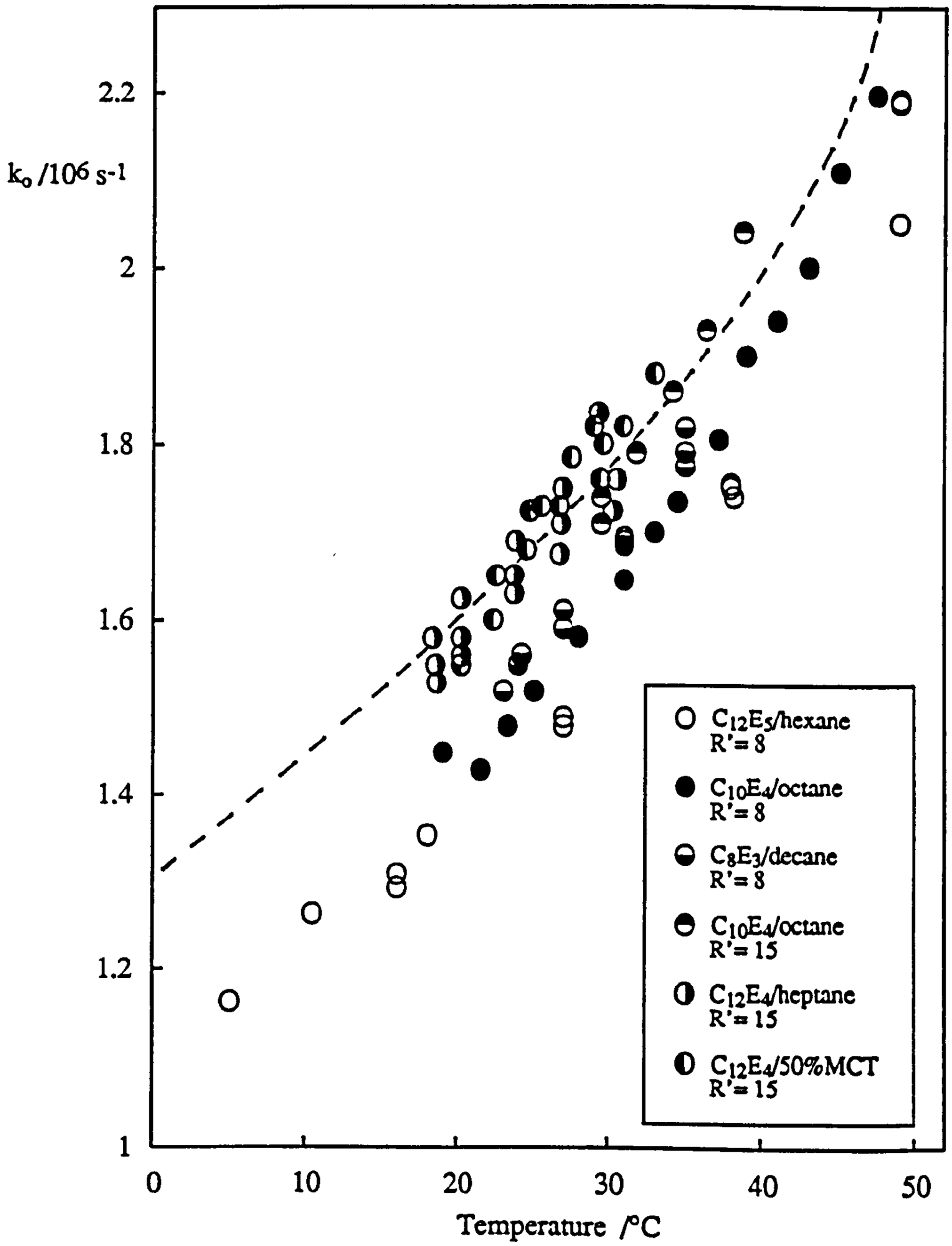

Figure 6.14a.

First order exchange rate constant k_t, versus droplet concentration, for $R'_{water} = 8$ water-in-hexane microemulsions stabilised by $C_{12}E_5$.

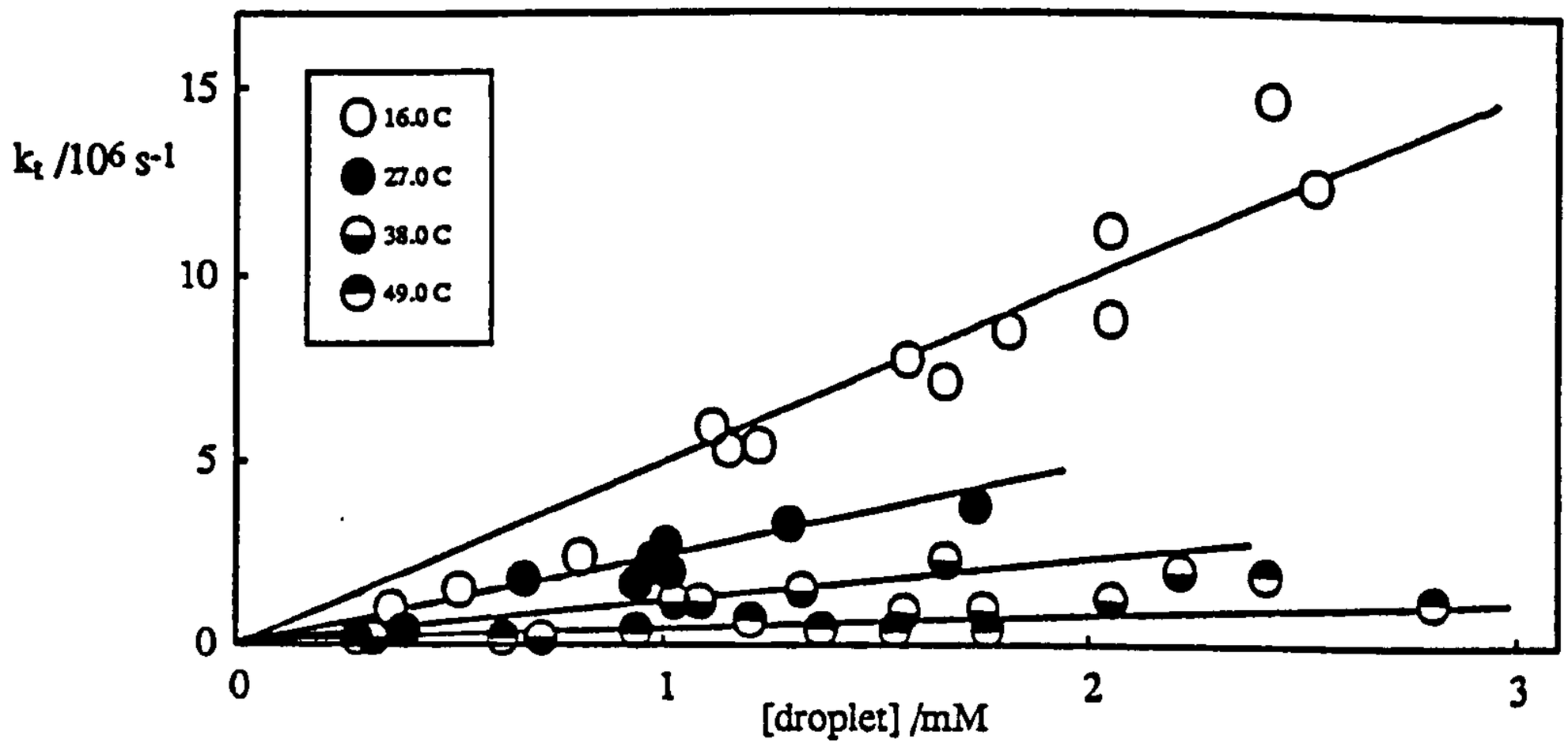

Figure 6.14b, $R'_{water} = 8$ water-in-octane microemulsions stabilised by $C_{10}E_4$.

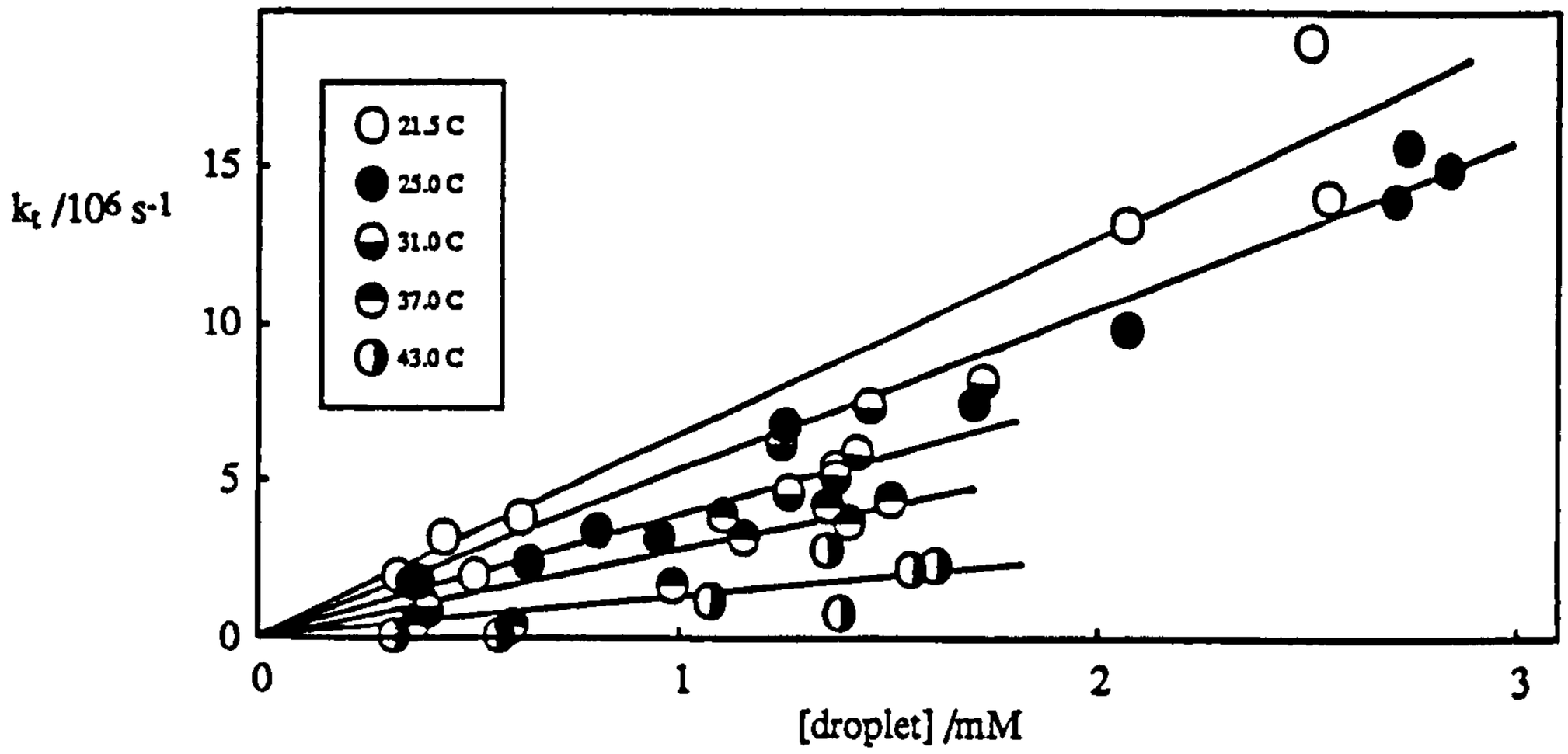

Figure 6.14c, $R'_{water} = 8$ water-in-decane microemulsions stabilised by C_8E_3.

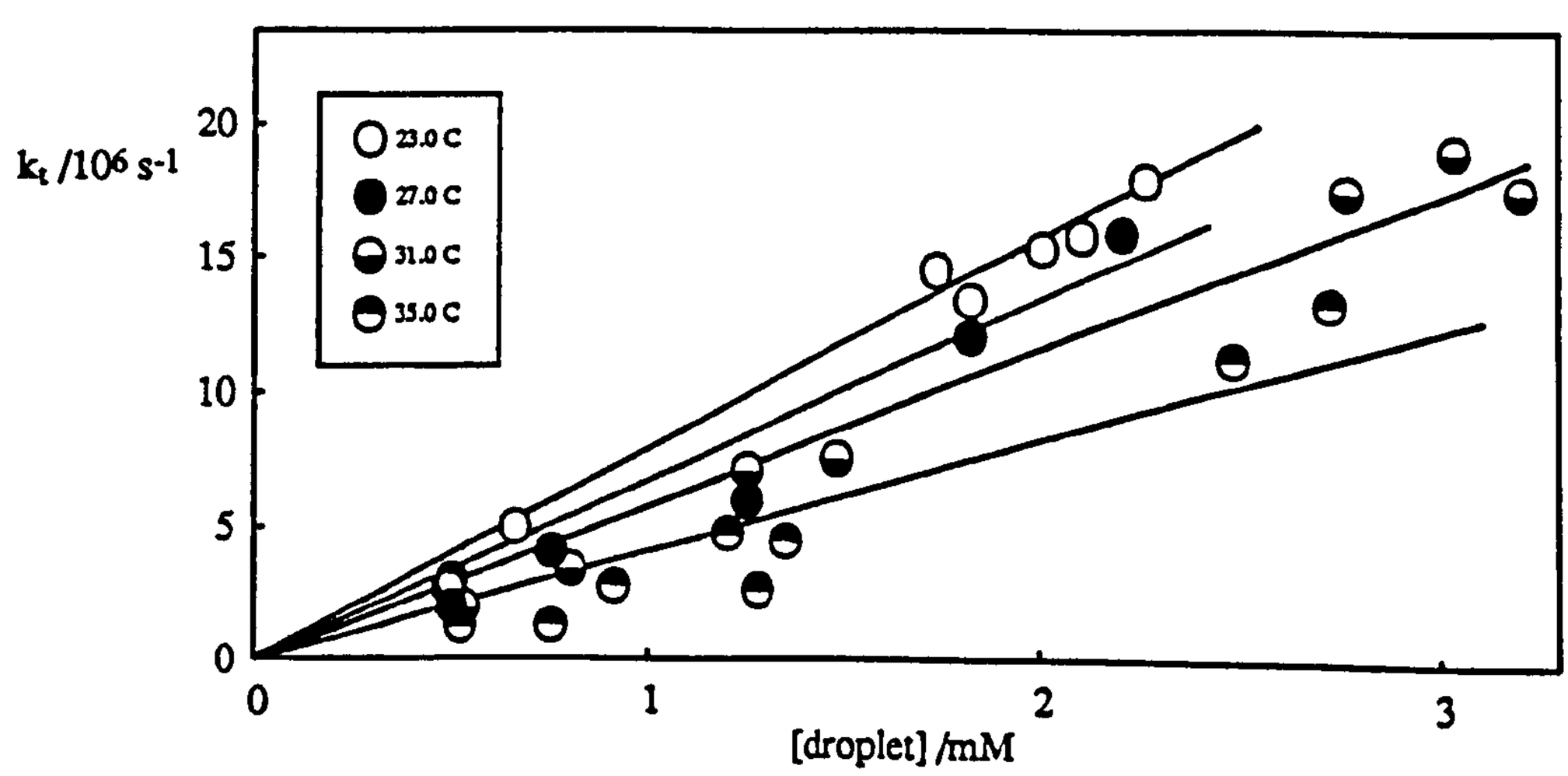

Figure 6.15a

Log k_c versus 1/temperature for $R'_{water} = 8$ water-in-hexane microemulsions stabilised by $C_{12}E_5$. The dashed line indicates diffusion-controlled behaviour.

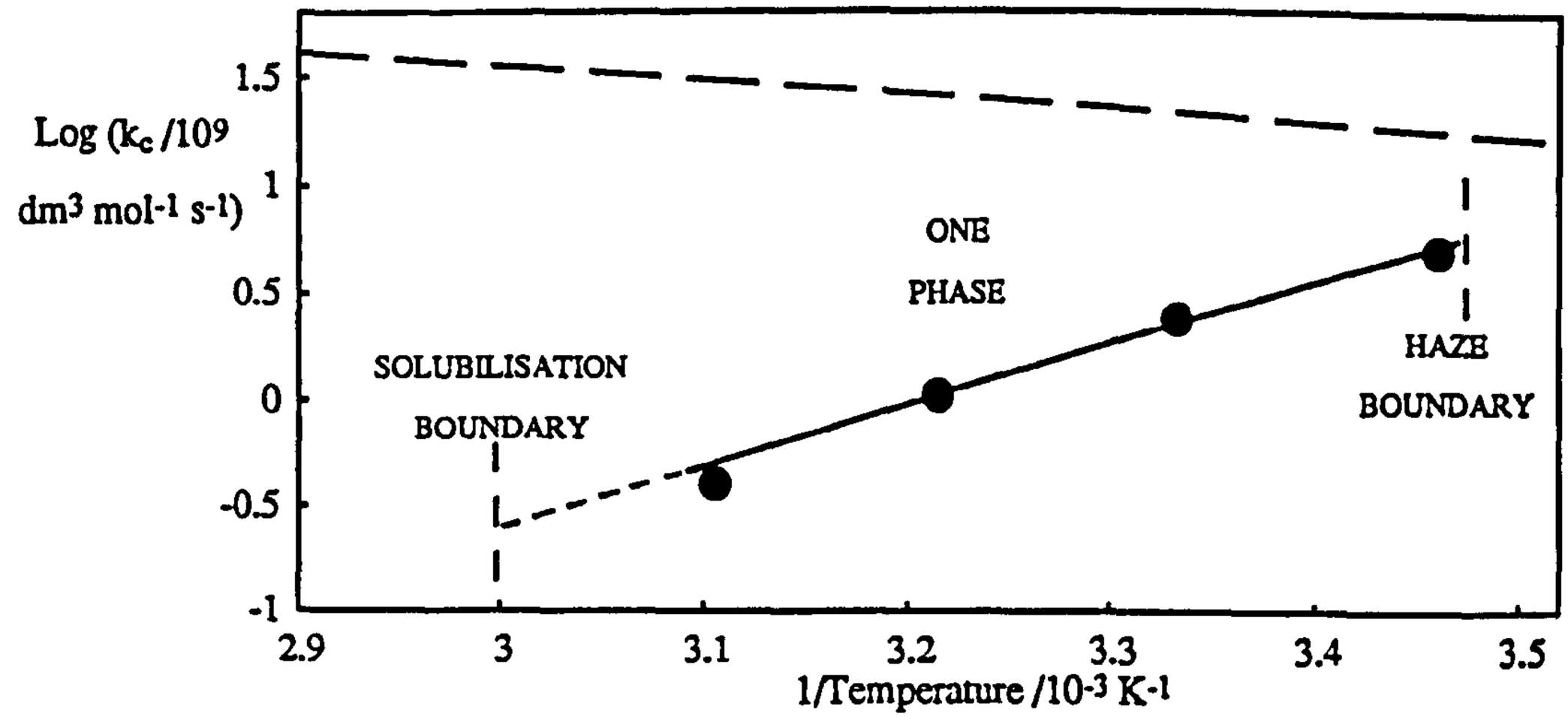

Figure 6.15b, $R'_{water} = 8$ water-in-octane microemulsions stabilised by $C_{10}E_4$.

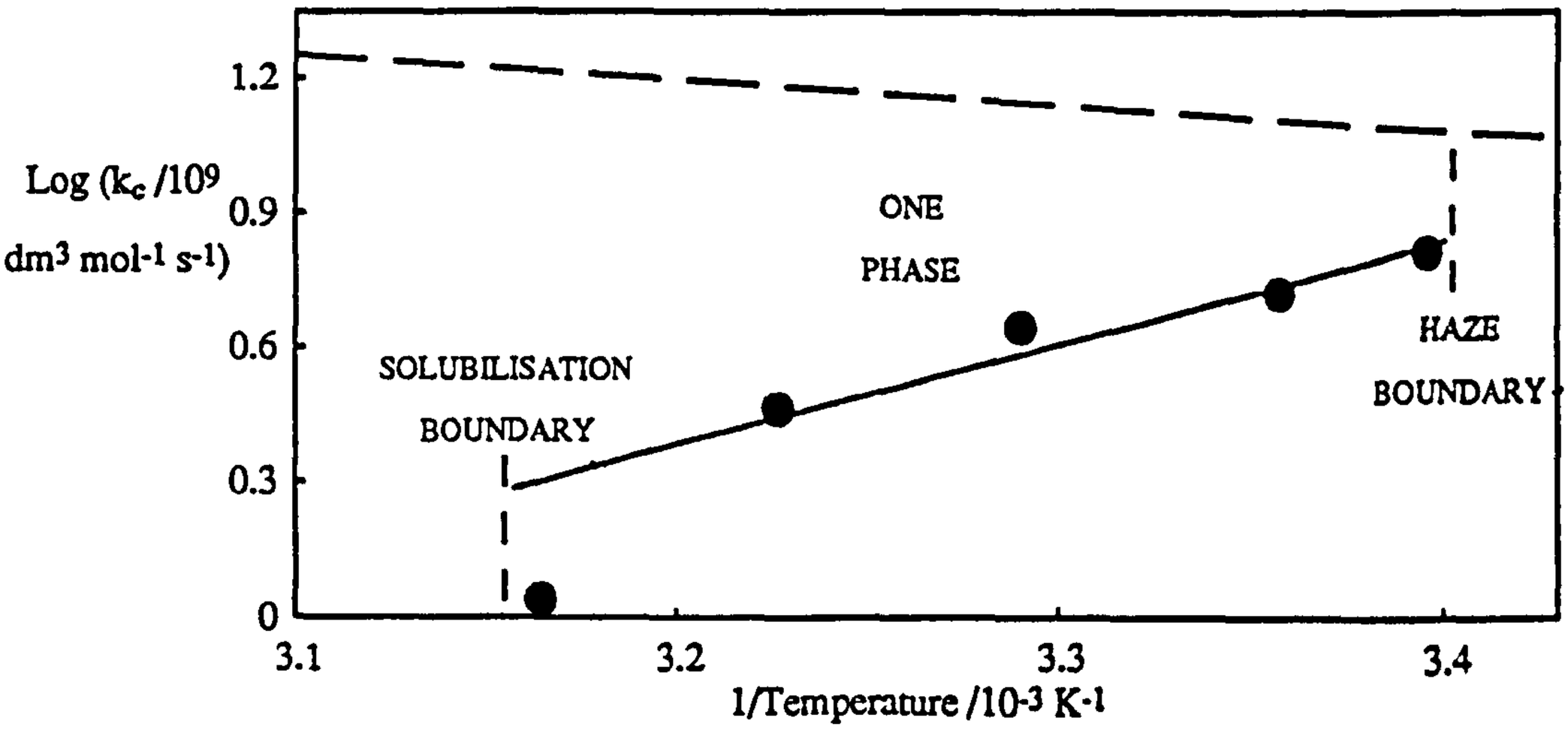

Figure 6.15c, $R'_{water} = 8$ water-in-decane microemulsions stabilised by C_8E_3.

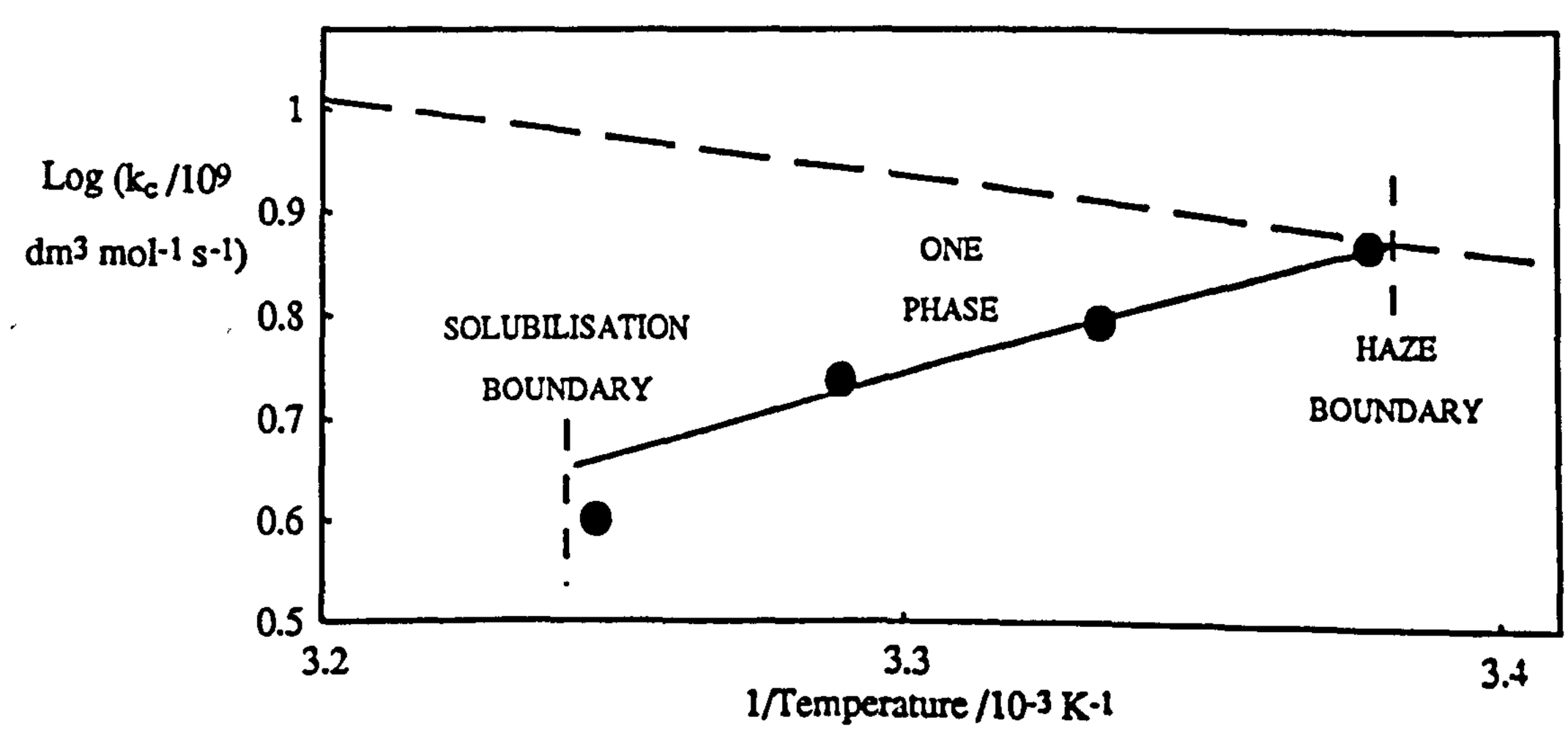

Table 6.7

System	k_{dc} /10^9 $M^{-1}s^{-1}$	Log (k_{dc}/k_c)	K /kT	cμc /10^{-2}M	ML /nm
$C_{12}E_5$/hexane	33.6	2.20 ± 0.2	-	8.4 ± 0.8	3.6
$C_{10}E_4$/octane	17.7	1.06 ± 0.2	0.76	7.9 ± 1.0	3.0
C_8E_3/decane	9.7	0.36 ± 0.1	0.35	15.0 ± 1.0	2.4

It is clear from this table that the exchange rate at the solubilisation phase boundary dramatically increases in the order $C_{12}E_5 < C_{10}E_4 < C_8E_3$. For $C_{10}E_4$ and C_8E_3 this order parallels the increase in rigidity for these two systems. The faster rate in the case of C_8E_3 may also be facilitated by a cμc that is approximately twice that of $C_{10}E_4$. As mentioned, Lee *et al.* could not determine a reliable value for the rigidity constant for the $C_{12}E_5$ system due to the presence of unresolved emulsion particulates perturbing the interface. Safinya *et al.* have recently predicted that the rigidity should scale with the cube of the surfactant length (177), i.e.

$$K/kT = B\ (\text{surfactant length}/nm)^3 \qquad (6.1)$$

where B is a proportionality constant. From the data for $C_{10}E_4$ and C_8E_3 an average value of 0.0267 kT nm^{-3} can be calculated for B. This corresponds to values for K of 0.72 kT and 0.37 kT, assuming all-trans surfactant lengths of 3.0 and 2.4 nm for $C_{10}E_4$ and C_8E_3 respectively. An estimate of the rigidity of the $C_{12}E_5$ monolayer can then be made with this equation taking the length of the surfactant molecule to be 3.6 nm. This corresponds to a value for K of 1.25 kT. Since the cμc values for both $C_{12}E_5$ and $C_{10}E_4$ are approximately 0.08 M it appears therefore, that increasing the monolayer rigidity dramatically reduces the microemulsion exchange rate for these systems.

The only other system for which monolayer rigidities and microemulsion exchange rates have been measured directly is the AOT/heptane system. Binks *et al.*

have recently determined the renormalised monolayer rigidity to be 1.65 kT which is the highest value reported to date for surfactant monolayers (191). The rate of exchange of probe molecules has been measured for this system and the ratio k_{dc}/k_c is found to be of the order of 100 times slower than that measured here for $C_{12}E_5$ (50). The results are therefore consistent with the expectation that systems with high monolayer rigidities exhibit slow microemulsion exchange rates. However, a direct comparison of the AOT system with the three nonionic surfactant systems reported here is difficult to perform for the following reasons.

(1). The exchange rate for the AOT system has only been measured at the solubilisation phase boundary using a stopped flow technique. As previously discussed in the Introduction, exchange rates measured by time-resolved fluorescence and stopped flow using different probe molecules are not directly comparable. The measured rates for AOT have been found to be faster when measured by TRF which might indicate that the probes used in the TRF experiment are exchanging through mechanisms other than "fusion-fission".

(2). The value of the cμc for AOT in heptane ($\sim 10^{-3}$ M) is much lower than those reported here for the three nonionic surfactant systems. This might also contribute to the slower rate observed overall.

(3). Upon coalescence of two microemulsion droplets, repulsive electrostatic interactions between surfactant head groups on the inner surface of the droplet may disfavour the formation of the "hour glass" shaped transition state. Consequently the exchange rate may be reduced with respect to nonionic surfactant systems.

6.6 Correlation Between Microemulsion Exchange Rate, Monolayer Rigidity and Macroemulsion Stability for Systems Containing $C_{12}E_5$/Hexane, $C_{10}E_4$/Octane and C_8E_3/Decane.

In the previous section it was shown that systems with large monolayer rigidities exhibit slow microemulsion droplet exchange rates at the solubilisation phase boundary. The rates were seen to follow the order $C_8E_3 > C_{10}E_4 > C_{12}E_5$. As mentioned in the Introduction, the type of macroemulsion formed when a microemulsion and excess dispersed phase is shaken is generally the same as the type of microemulsion initially present. It is of interest to explore whether a correlation exists between the microemulsion exchange rate and the stability of the corresponding macroemulsion. For the three surfactant systems, the rates of oil and water phase resolution are reported for W/O macroemulsions prepared from Winsor II systems at temperatures in which the R'_{water} value was 8 in each case. The three systems were therefore at "corresponding" system HLB values. The oil-water interfacial tensions of these systems are tabulated in Table 6.5. The emulsions were prepared for each system with a surfactant concentration of 6 wt% above the cμc in the oil. The significance of a constant concentration of post-cμc surfactant will be discussed in Chapter 7. The droplet sizes of emulsions prepared with $C_{12}E_5$ and $C_{10}E_4$ were estimated using optical microscopy to be of the order of 1 μm. Phase resolution of emulsions prepared with C_8E_3 was too rapid for an estimation of the size to be performed. As far as possible therefore, the three systems were investigated at approximately the same emulsion conditions.

In Figure 6.16 the resolution of the water-in-hexane emulsion stabilised by $C_{12}E_5$ is shown. The results from two identical experiments are presented and the agreement between them is reasonable. It can be seen from Figure 6.16a that initially (0 - 10 hours) the water droplets undergo sedimentation with concomitant oil resolution. This produces a concentrated emulsion which after ~10 hours starts to undergo coalescence and water

Figure 6.16a.

Oil resolution for the W/O emulsion prepared with 11.40 wt% $C_{12}E_5$ in hexane at 59.7°C, $R'_{water} = 8$. The results from two identical experiments are presented.

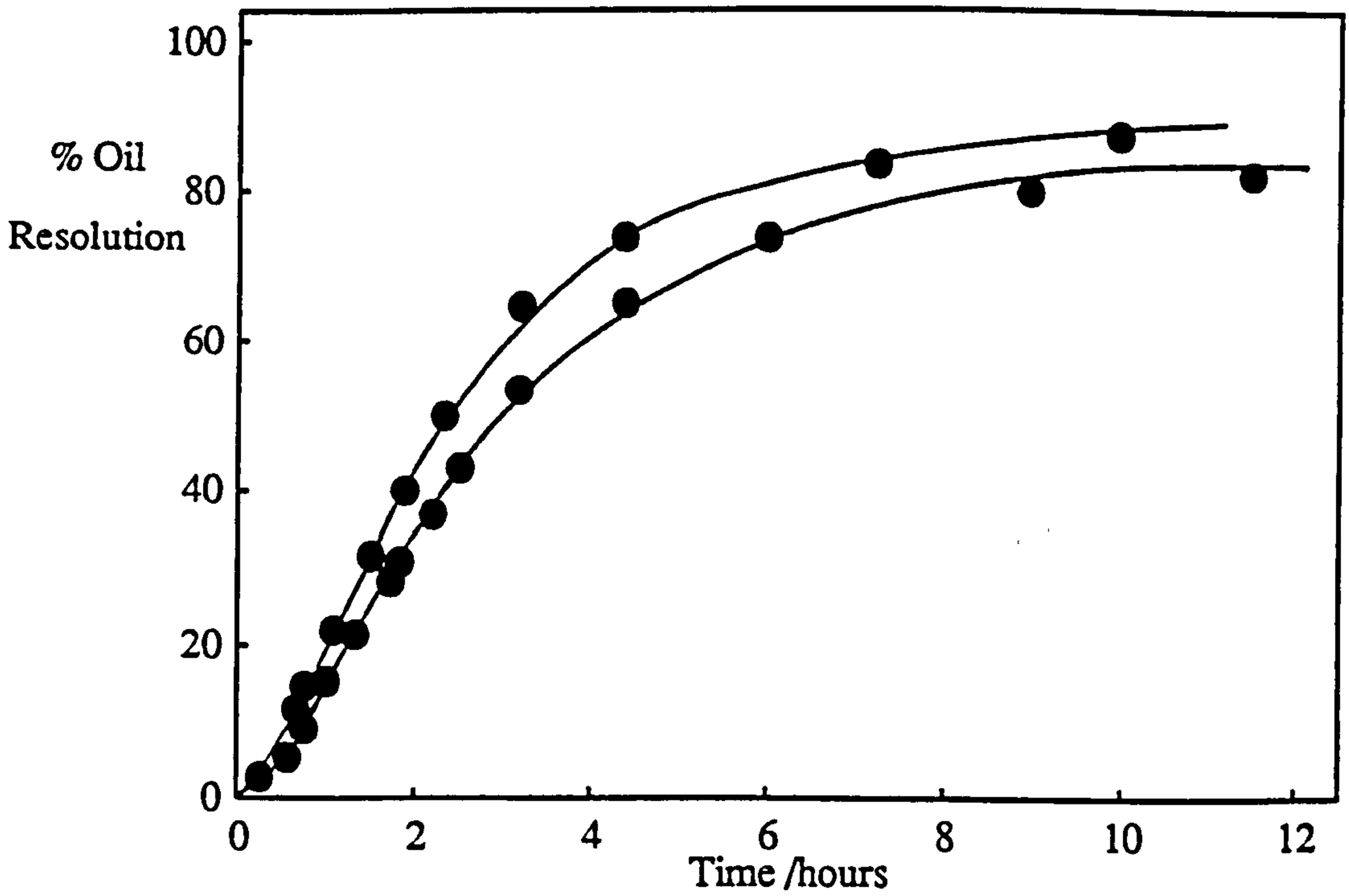

Figure 6.16b.

Water resolution for the W/O emulsions outlined above.

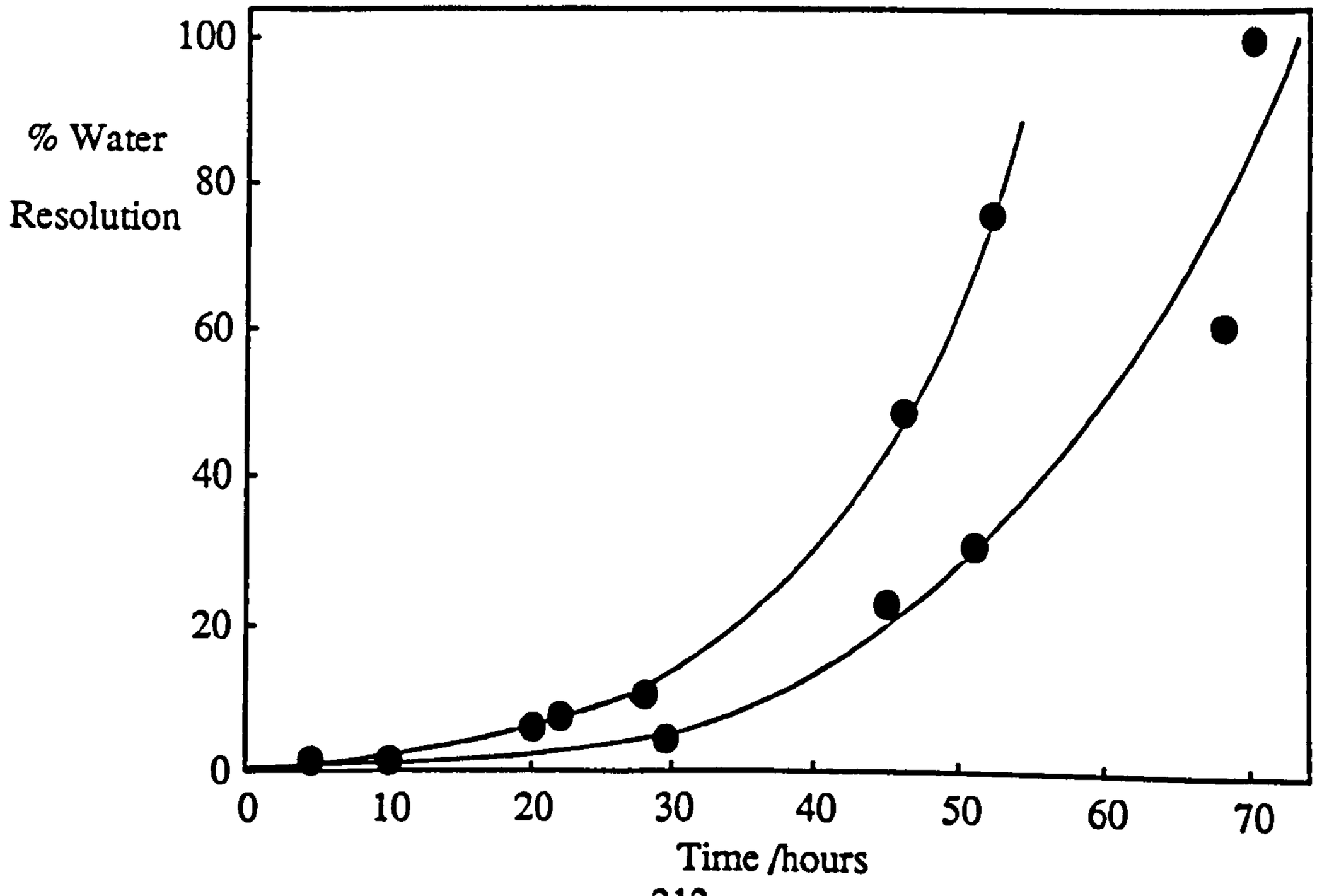

is resolved as shown in Figure 6.16b. Similarly, Figures 6.17a and 6.17b show the corresponding results for the W/O emulsion prepared with $C_{10}E_4$ in octane. In this case both sedimentation and coalescence occur simultaneously and complete resolution of both phases occurs within 10 hours. Resolution of the emulsion stabilised by C_8E_3 is shown in Figures 6.18a and 6.18b. Once again the oil and water phases resolve simultaneously. However in this case, complete resolution of both phases is observed within about 2 minutes. It is interesting to observe that for each system studied, there appears to be an induction period before the maximum oil or water resolution rate is obtained.

The water concentration in the upper oil phase was checked for each system by Karl Fischer titration at the end of the monitoring period. By assuming that all the surfactant resided in the oil phase (which is reasonable since W/O aggregates are formed and the cμc in water is very low) the R'_{water} value for each oil phase was calculated. These were all found to be within the range 7 - 10 in reasonable agreement with the value of 8 expected from the phase studies.

In Table 6.8 below, the water resolution rate of each emulsion has been compared by measuring the time taken for 20% of the aqueous phase to resolve ($t_{20\%}$). This is compared with the values for the microemulsion exchange rate at the solubilisation phase boundary and the reported monolayer rigidity constant.

Table 6.8

System	$t_{(20\%)}$ /hours	k_{dc}/k_c	K /kT
$C_{12}E_5$/hexane	40 ± 10	160	1.25*
$C_{10}E_4$/octane	1.8 ± 0.5	11.5	0.76
C_8E_3/decane	0.013 ± 0.01	2.3	0.35

* Estimated from K /kT = 0.0267 (surfactant length /nm)^3

Figure 6.17a.

Oil resolution for the W/O emulsion prepared with 9.90 wt% $C_{10}E_4$ in octane at 49.0°C, $R'_{water} = 8$.

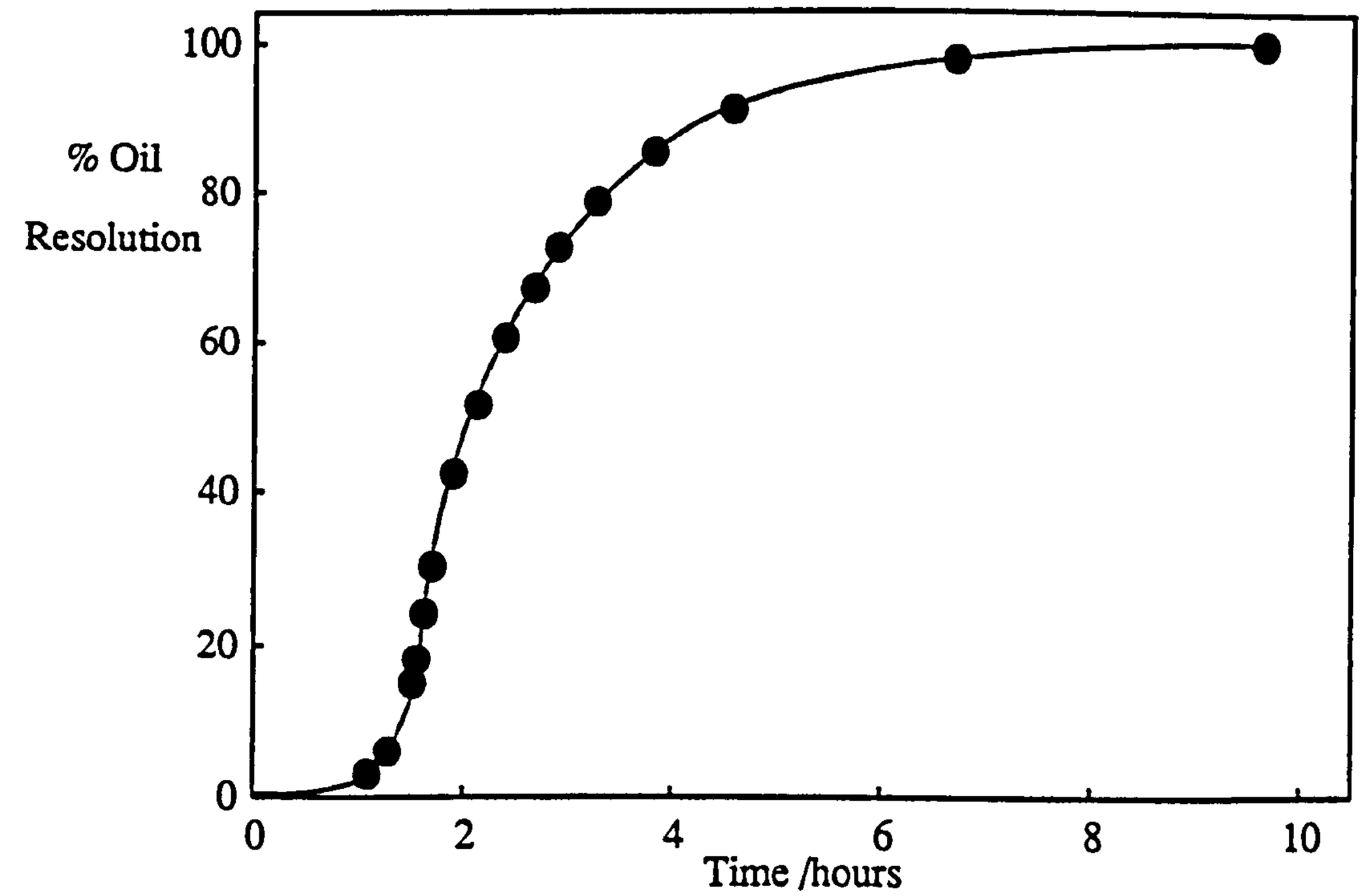

Figure 6.17b.

Water resolution for the W/O emulsion outlined above.

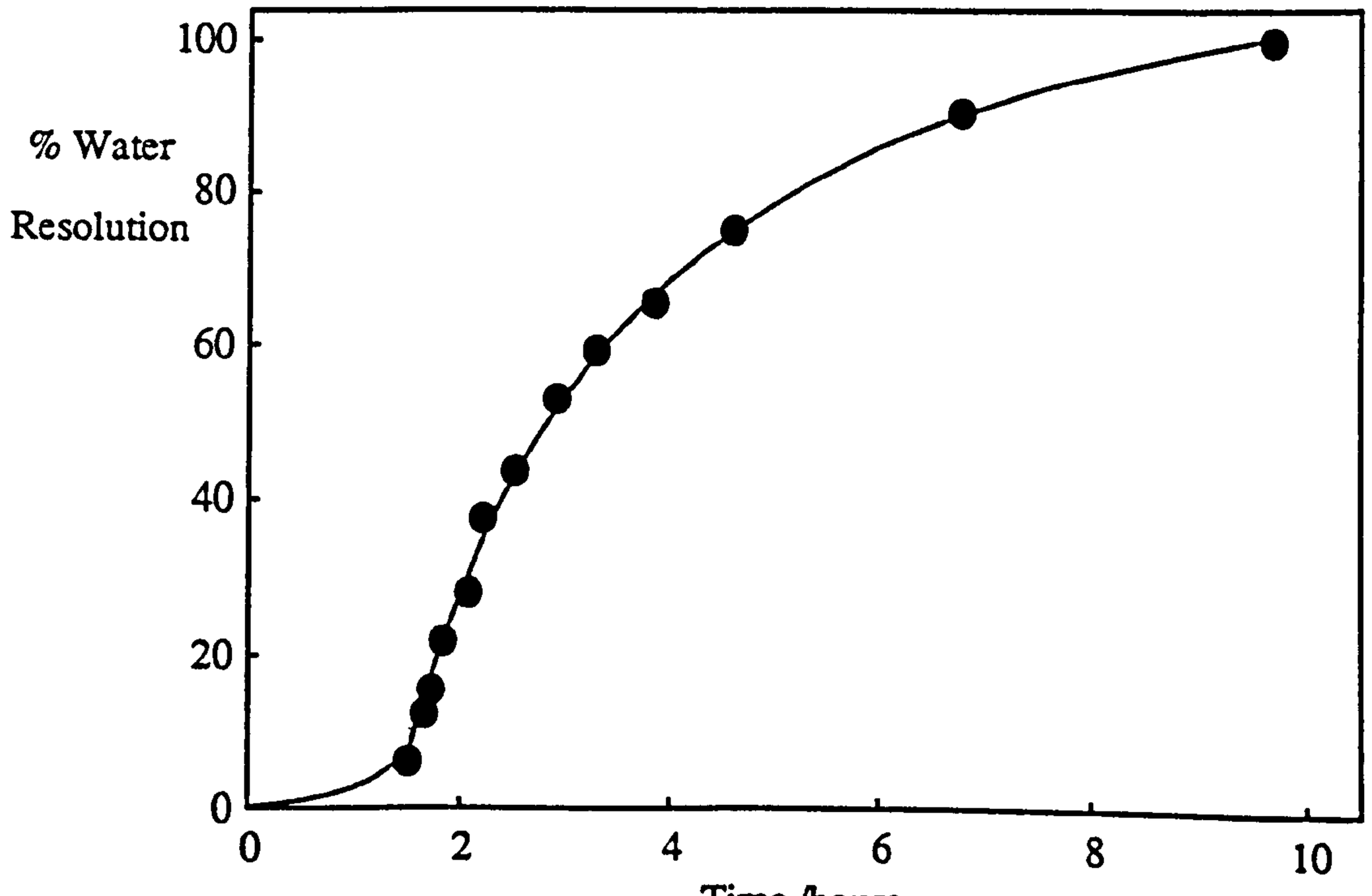

Figure 6.18a.

Oil resolution for the W/O emulsion prepared with 11.40 wt% C_8E_3 in decane at 37.0°C, $R'_{water} = 8$.

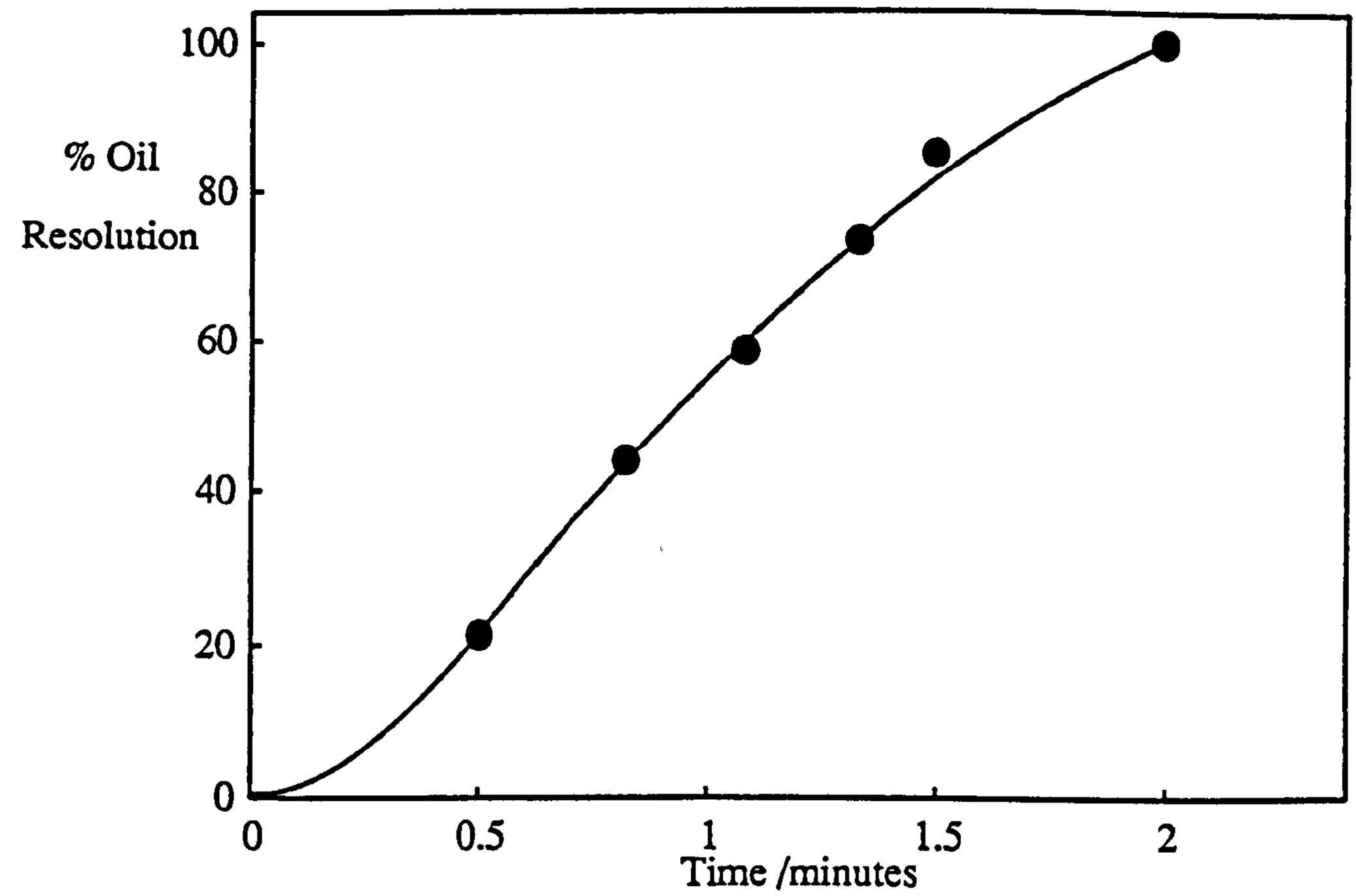

Figure 6.18b.

Water resolution for the W/O emulsion outlined above.

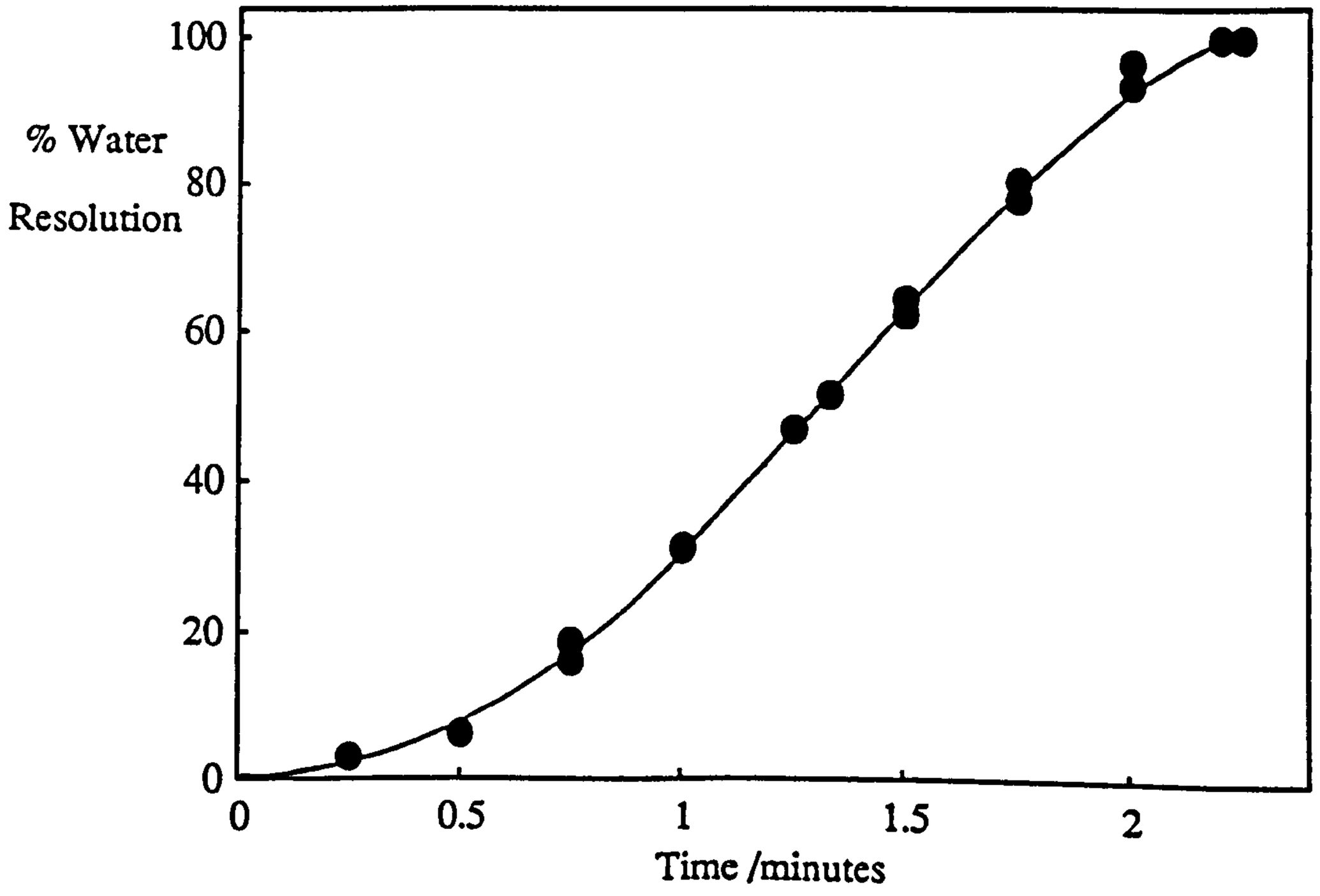

For these systems, a correlation exists between the macroemulsion water resolution rate, the monolayer bending rigidity and the microemulsion exchange rate. Water resolution is seen to be vastly accelerated for systems which exhibit low monolayer bending rigidities.

6.7 Conclusions.

From this study, the following conclusions may be made.

(1). For the three systems investigated, the microemulsion exchange rates at the solubilisation phase boundaries correlate with monolayer rigidity values reported by Lee *et al.* The following order of increasing exchange rate (and decreasing rigidity) is observed $C_{12}E_5 < C_{10}E_4 < C_8E_3$.

(2). For the corresponding macroemulsions compared at similar system HLB values, a similar order is observed. The fastest water phase resolution rates occur for the systems with the lowest monolayer rigidities.

7. INVESTIGATION INTO THE STABILITY OF W/O MACROEMULSIONS FORMED WITH OIL + WATER + $C_{12}E_4$.

CHAPTER 7.

7.1 Introduction.

Emulsions are of considerable industrial importance and consequently have been studied extensively over many years. As already discussed, they are thermodynamically unstable but may exhibit considerable kinetic stability. Breakdown can occur through several processes as previously outlined in section 1.3.2 e.g. coalescence, creaming/sedimentation, Ostwald ripening, flocculation. In general, the overall breakdown of an emulsion may involve a combination of several if not all of these mechanisms operating to a greater or lesser extent. Consequently, quantitative determination of emulsion stability is highly difficult to perform. For this reason, despite the large volume of literature dedicated to emulsion behaviour, many aspects of their stability still remain poorly understood (192, 193).

In the previous chapter, it was observed that the order of emulsion water resolution for three different surfactant systems, paralleled that observed for the microemulsion exchange rates at the solubilisation phase boundaries. This was seen to correlate with values for the monolayer bending rigidities, faster coalescence rates being observed for systems with low rigidity constants. To date however, only a limited number of studies have been reported focussing on the relationship between microemulsion behaviour and macroemulsion stability. Shinoda (136) and Salager *et al.* (146) have shown that the type of emulsion formed when a microemulsion plus excess dispersed phase is emulsified, is generally the same as the initial type of microemulsion present. The continuous phase of the emulsion therefore contains microemulsion aggregates. They also observed that emulsion stability was a minimum at conditions corresponding to the formation of a Winsor III microemulsion system.

In this study, oil and water phase resolution rates have been determined for W/O emulsions stabilised by $C_{12}E_4$ in heptane and heptane / MCT mixtures. These emulsions

were prepared by emulsifying Winsor II systems of water plus W/O microemulsion phases. Thus the continuous phase of the emulsion contained W/O microemulsion droplets. For emulsions containing an equal phase volume ratio of water : oil the effects of changing the concentration and size of the *microemulsion droplets* in the continuous phase has been determined. The results are seen to be reasonably consistent with predictions from a theoretical model. Correlations between the cμc and emulsion stability are also presented.

7.2 Stability of W/O Emulsions Prepared with Water + Heptane + $C_{12}E_4$

The major breakdown process for water-in-heptane emulsions prepared with $C_{12}E_4$ at concentrations in excess of the cμc, was that of droplet sedimentation. The rate of oil phase resolution observed was determined as previously described in Chapter two and interpreted as providing a measure of the sedimentation rate. For emulsions prepared with heptane as the oil phase, resolution of the dispersed aqueous phase was not observed (for surfactant concentrations > cμc) indicating that the rate of coalescence in these systems was minimal. A typical profile for oil resolution is shown in Figure 7.1. There is an induction period before the maximum resolution rate is achieved and at longer times the resolution asymtotically approaches ~100%. The system then consists of a separated W/O microemulsion phase and a highly concentrated emulsion. The composition of this emulsion is similar to that of the high internal phase emulsion gels described in a series of papers by Solans *et al.* (194 - 196). Indeed, these sedimented systems have been shown recently to form such gels when shaken with glass beads (197).

The effect of increasing the surfactant concentration on the stability of water-in-heptane emulsions at 26°C was investigated. The emulsions were prepared separately

Figure 7.1.

Typical oil resolution profile for W/O emulsions prepared with $C_{12}E_4$ + heptane + water. The oil contains 3.2 wt% $C_{12}E_4$, temperature = 26.0°C.

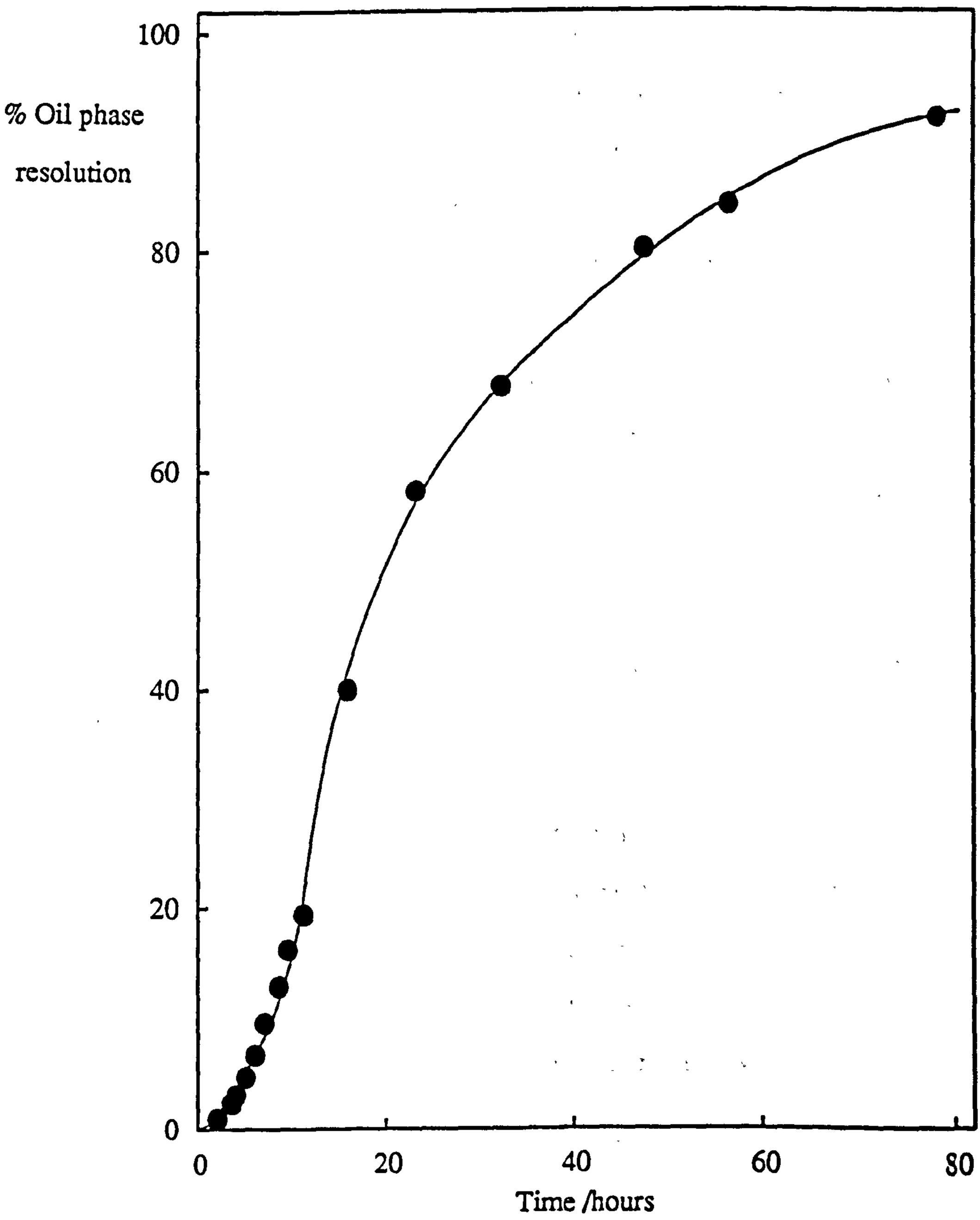

with different surfactant concentrations in the oil phase. This will be referred to as method I. The average emulsion drop size was estimated using optical microscopy to be of the order of 1 μm and independent of surfactant concentration above the cμc. Below the cμc the emulsion drops were polydisperse in the range of 10 - 30 μm. The resolution of oil phase with time for emulsions prepared with different surfactant concentrations is shown in Figure 7.2. For surfactant concentrations below the critical microemulsion concentration, resolution of both water and oil phases was observed. In these cases, the stabilising surfactant monolayer surrounding the droplets presumably is not saturated and therefore might be expected to offer low resistance to droplet coalescence. For all surfactant concentrations in excess of the cμc, resolution of water is not evident over the timescale of the observations (~7 days) and the emulsion breaks down through sedimentation of the dispersed droplets. A convenient parameter for comparing the effect of surfactant concentration on the rate of oil phase resolution is the time for 15% of the oil phase to resolve ($t_{15\%}$). This is plotted in Figure 7.3 as a function of surfactant concentration. It is clear that maximum emulsion stability occurs around a surfactant concentration of 3 wt% which coincides with the cμc for this system. Increasing the surfactant concentration beyond the cμc dramatically destabilises the emulsion.

A fraction of the additional surfactant in excess of the cμc, is present as monolayer coating the emulsion droplets. This concentration of surfactant, which is required to completely saturate the emulsion droplets, can be estimated if the droplet diameter is taken to be 1 μm and the area per surfactant molecule at the droplet surface is assumed to be 0.6 nm^2 (equal to the measured area at the planar oil-water interface) (38). For emulsions considered here where the dispersed phase volume fraction is 50%, this concentration is estimated to be 0.85 wt% in the oil. This value is highly dependent upon the value taken for the emulsion drop size e.g. for drops of diameter 4 μm a concentration of only 0.21 wt% is required. Thus, the majority of the additional surfactant in excess of the cμc is present in the form of W/O *microemulsions* in the

Figure 7.2.

Oil resolution curves for W/O emulsions prepared with $C_{12}E_4$ + heptane + water at 26.0°C (R'_{water} = 18) for different surfactant concentrations in the oil.

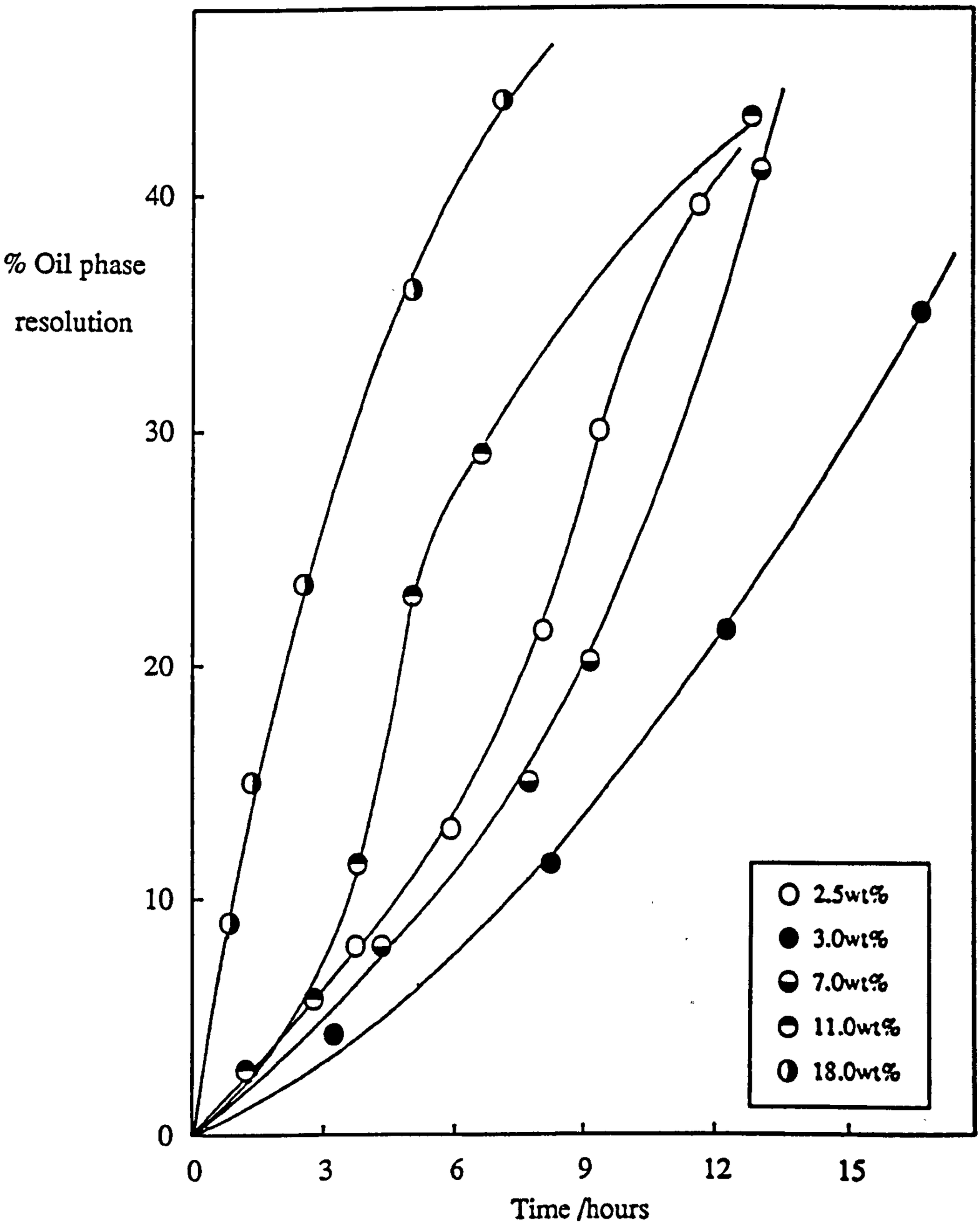

Figure 7.3.

Variation of $t_{(15\%)}$ with surfactant concentration in heptane. The emulsions were prepared by method I at 26.0°C, R'_{water} = 18, cμc = 3.0 wt%.

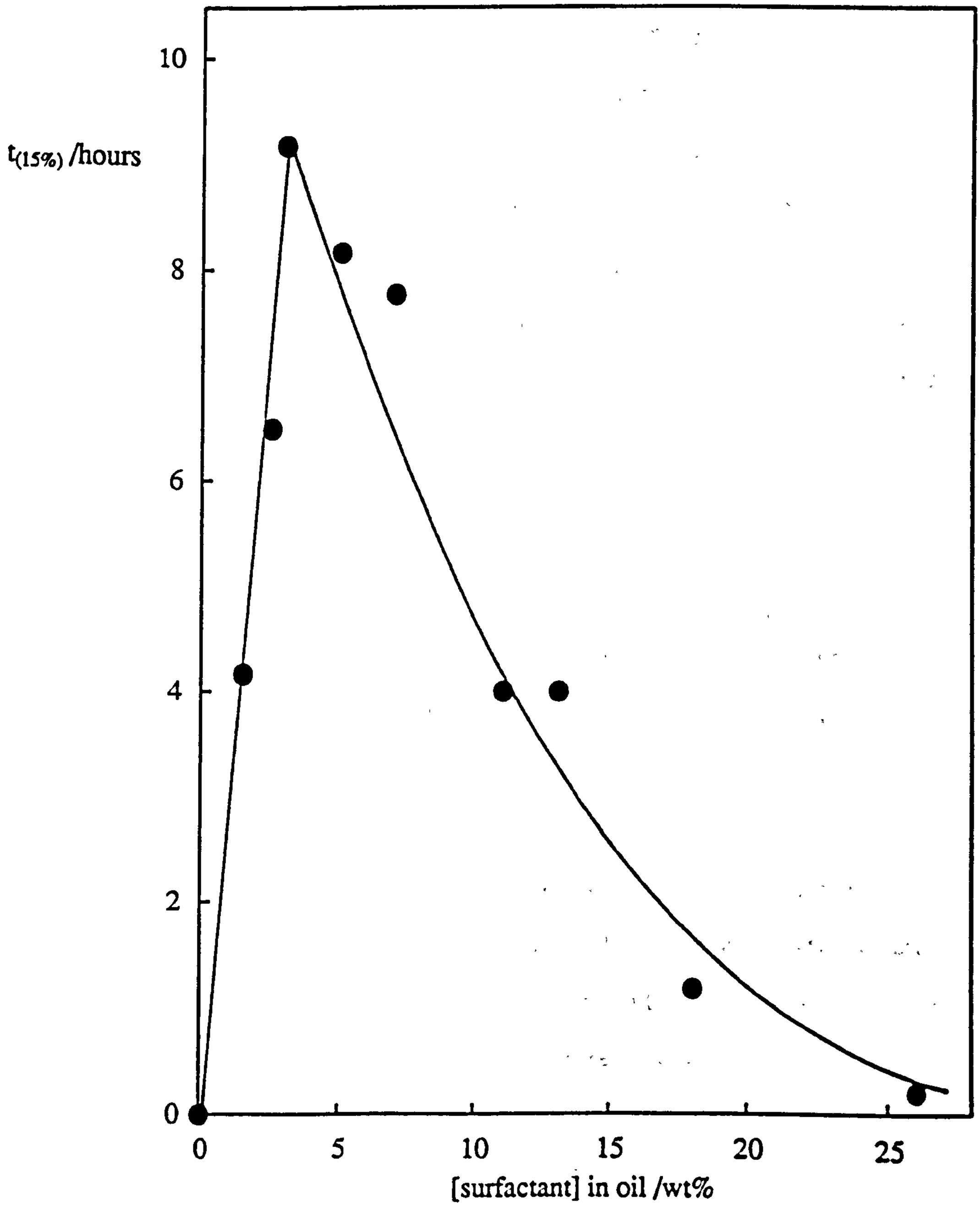

continuous phase of the emulsion. It appears therefore, that the accelerated oil phase separation observed for emulsions prepared with high surfactant concentrations, may be due to the presence of microemulsions in the continuous phase.

A similar effect has been found by Aronson *et al.* for the creaming of oil-in-water emulsions stabilised by a series of nonionic surfactants (86, 198). The effect was ascribed to a depletion flocculation interaction of the emulsion droplets induced by the presence of the O/W aggregates. He reported results for the effect of changing the emulsion droplet size and the type of nonionic surfactant. One purpose of the present study was to investigate the effects of changing the size of the *microemulsion aggregates* in the continuous phase of the emulsion. This has been achieved through changing the temperature at which the emulsion is prepared.

Three microemulsion droplet sizes were investigated corresponding to R'_{water} values of 43, 18 and 7. The relevant parameters corresponding to these droplet compositions are tabulated below in Table 7.1.

Table 7.1

R'_{water}	Temp /°C	cμc /wt%	r_H /nm	γ_c /mN m^{-1}
43	17.0	1.5 ± 0.4	13.7	0.045
18	26.0	3.0 ± 0.4	6.5	0.36
7	40.0	5.4 ± 0.8	3.1	1.14

Figure 7.4 shows the variation of $t_{(15\%)}$ with surfactant concentration in the oil for three different temperatures. For this comparison the emulsions were prepared separately at each surfactant concentration i.e. method I. Consequently Figure 7.4b is identical to Figure 7.3. For the three microemulsion droplet sizes, the values of $t_{(15\%)}$ are seen to pass through maxima corresponding approximately to the cμc in each system. Water resolution was only observed at surfactant concentrations less than the cμc.

Figure 7.4a.

Variation of $t_{(15\%)}$ with surfactant concentration in heptane. The emulsions were prepared by method I. Temperature = 17.0°C, $R'_{water} = 43$.

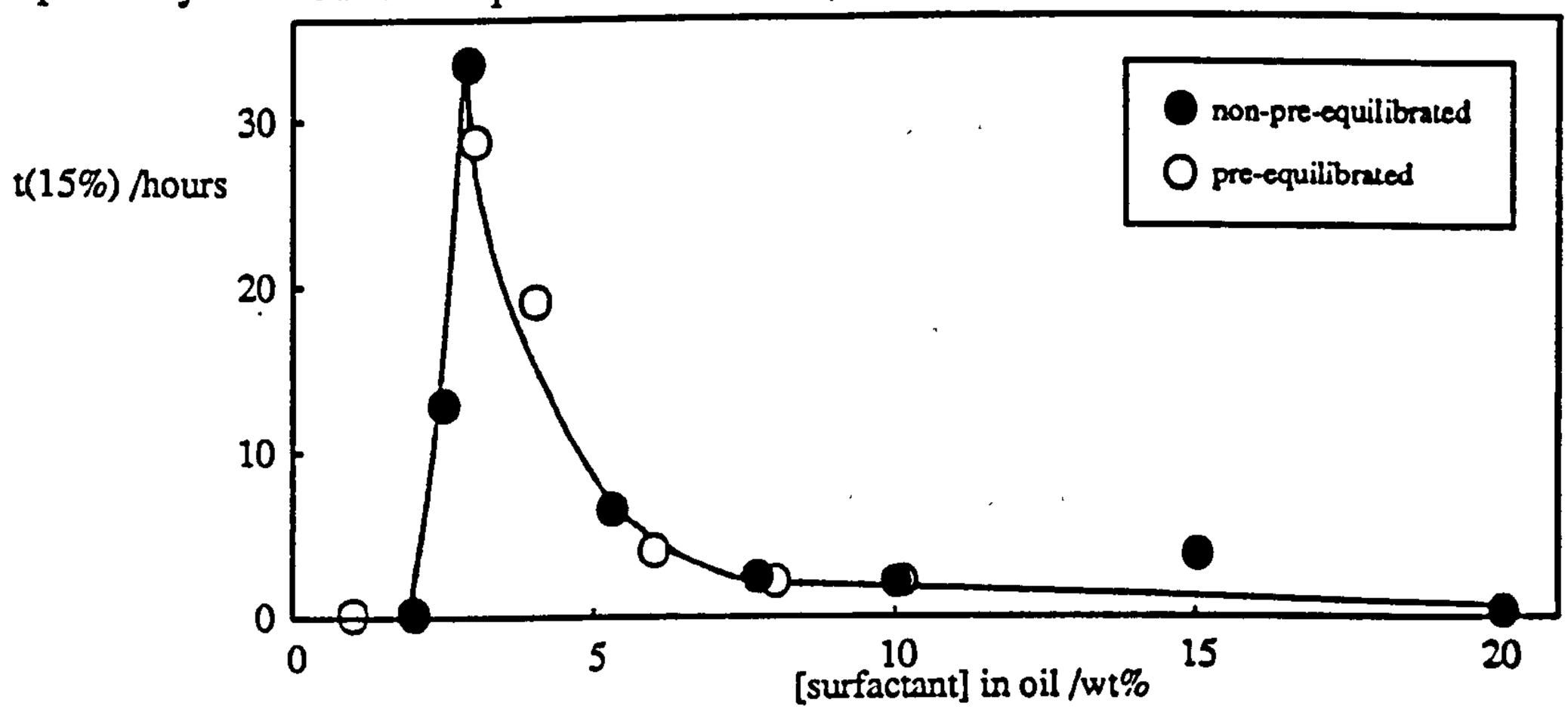

Figure 7.4b, temperature = 26.0°C, $R'_{water} = 18$.

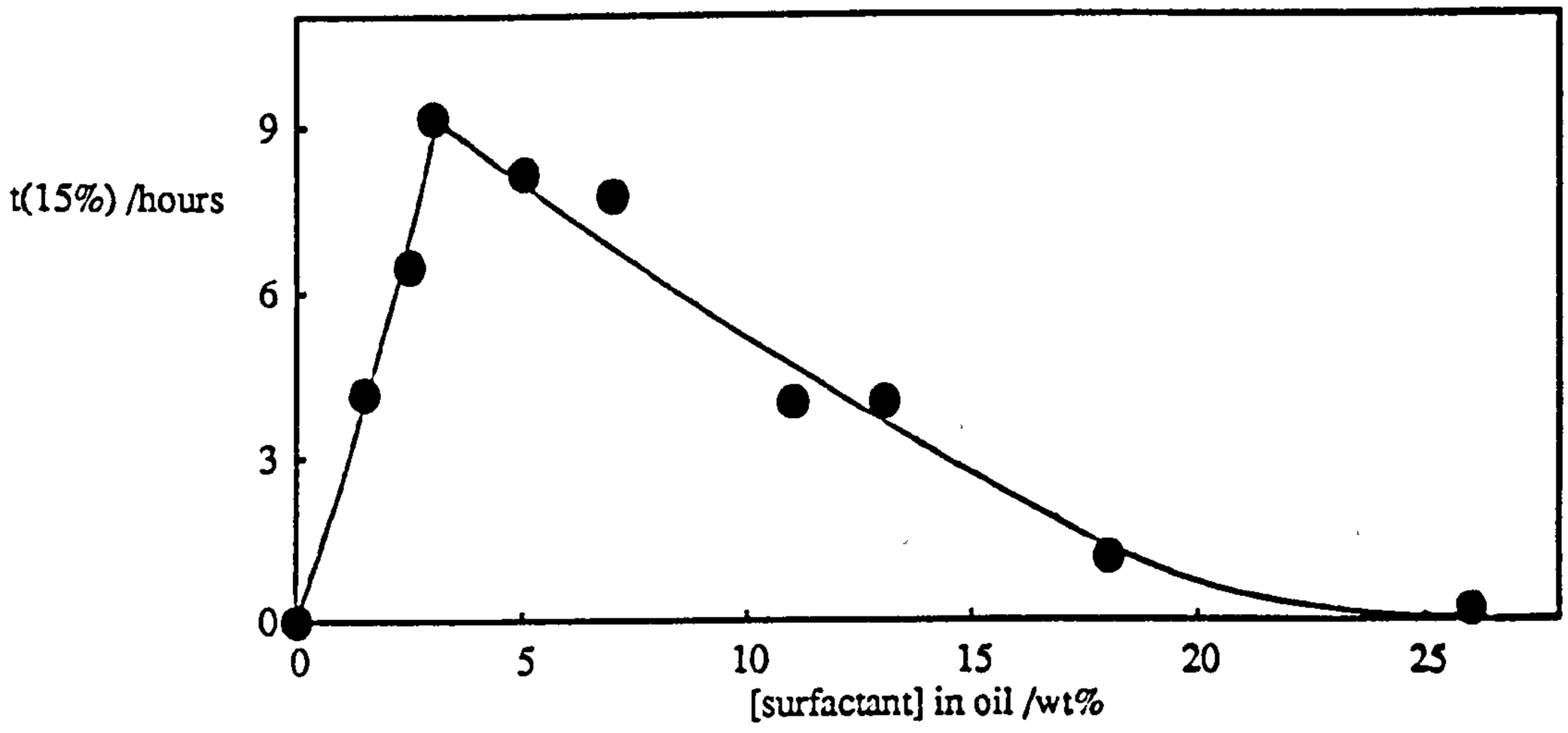

Figure 7.4c, temperature = 40.0°C, $R'_{water} = 7$.

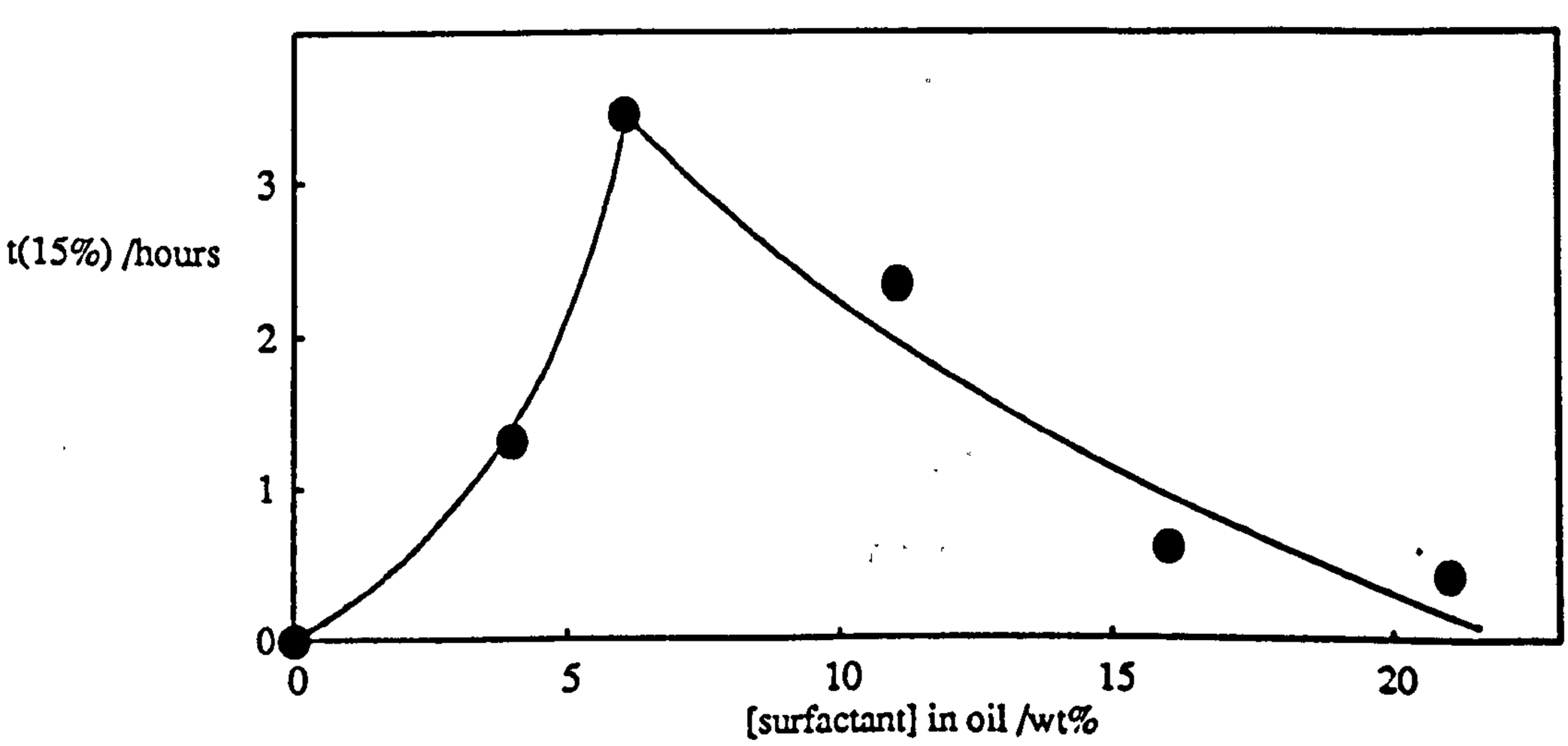

In Figure 7.4a, the results from emulsions prepared with oil and water phases that had been pre-equilibrated for 18 hours are also presented. The two sets of data are seen to be in excellent agreement. This indicates that an equilibrium surfactant distribution is reached within a few minutes for these systems. The observed dependence of the emulsion stability on the surfactant concentration is therefore not a consequence of a changing surfactant distribution with time. The effects of the different microemulsion droplet sizes on the rate of oil phase separation may be judged by comparing the concentration of surfactant which is required to reduce $t_{(15\%)}$ from the maximum to half that value. Figure 7.4 suggests that the $R'_{water} = 43$ microemulsion droplets produce the greatest accelerating effect and that droplets of $R'_{water} = 18$ and 7 produce similar rate enhancements. Additionally, the maximum value of $t_{(15\%)}$ decreases with decreasing microemulsion size and increasing cμc.

The results shown in Figure 7.4 were obtained using emulsions prepared separately at each surfactant concentration and temperature. Although the mean emulsion drop sizes were judged to be similar, the observed effects may be due to slightly differing emulsion size distributions. In order to overcome this ambiguity in interpretation, the resolution experiments were repeated using an alternative method of preparing the emulsions.

In the second method, method II, a large volume of stock emulsion containing surfactant at a concentration close to the cμc (~0.5 wt% > cμc) was prepared at each of the three temperatures investigated. The oil : water ratio of the emulsion was 2 : 3. The emulsion was divided into 10 cm^3 aliquots and 2 cm^3 samples of pre-equilibrated W/O microemulsions were added with hand shaking but no additional homogenisation. The final oil : water ratio was approximately 1 : 1 as in the previous emulsions prepared by method I. In this way, a series of emulsions of constant initial drop size distribution (equal to that in the stock emulsion) but containing different concentrations of microemulsion droplets were obtained for each temperature. The average emulsion drop

size was confirmed using optical microscopy. The sizes were determined after approximately 15 minutes of preparation and then subsequently after four days. The results for each temperature are shown in Figures 7.5, 7.6 and 7.7. For emulsions prepared with concentrations of surfactant less than the cμc, the initial emulsion drop diameter was of the order of 1 μm. For 17°C a slightly larger initial drop size was apparent. After four days the emulsion drops had grown extensively (~25 - 50 μm) and, as previously mentioned, some resolution of both water and oil was observed. For surfactant concentrations slightly greater than each cμc, the initial drop sizes were of the order of 1 μm and very little drop growth was observed at each temperature after four days. For emulsions containing high concentrations of surfactant (equivalent to high concentrations of microemulsion droplets), the initial average emulsion drop size was again approximately 1 μm. However, large flocculated structures were seen which co-existed with regions of oil phase devoid of drops. After four days the emulsions prepared at 17 and 26°C showed only slight signs of drop growth, whereas the emulsion prepared at 40°C contained drops in the range 5 - 10 μm.

Variation of $t_{(15\%)}$ with surfactant concentration is shown in Figure 7.8 for emulsions prepared by method II. The pattern of behaviour is similar to that obtained when the emulsions were prepared by method I. It appears therefore, that the acceleration in oil phase separation rate after the cμc is *not* associated with changing emulsion drop sizes.

Using method II, since different stock emulsions were used for the different temperatures the size distribution may vary between the three temperatures. It is of interest here to compare the oil resolution accelerating effect of different microemulsion sizes and to do this it is necessary to ensure a constant emulsion droplet size for the different temperatures. This was achieved by preparing a global stock emulsion at 26°C, splitting it into aliquots, which were then used for the series of resolution experiments at different temperatures following the addition of different microemulsion droplet

Figure 7.5.

Photographs of emulsions prepared by method II at 17.0°C, $R'_{water} = 43$. Bar = 25 μm.

(a). 1.2 wt%, t = 15 mins.

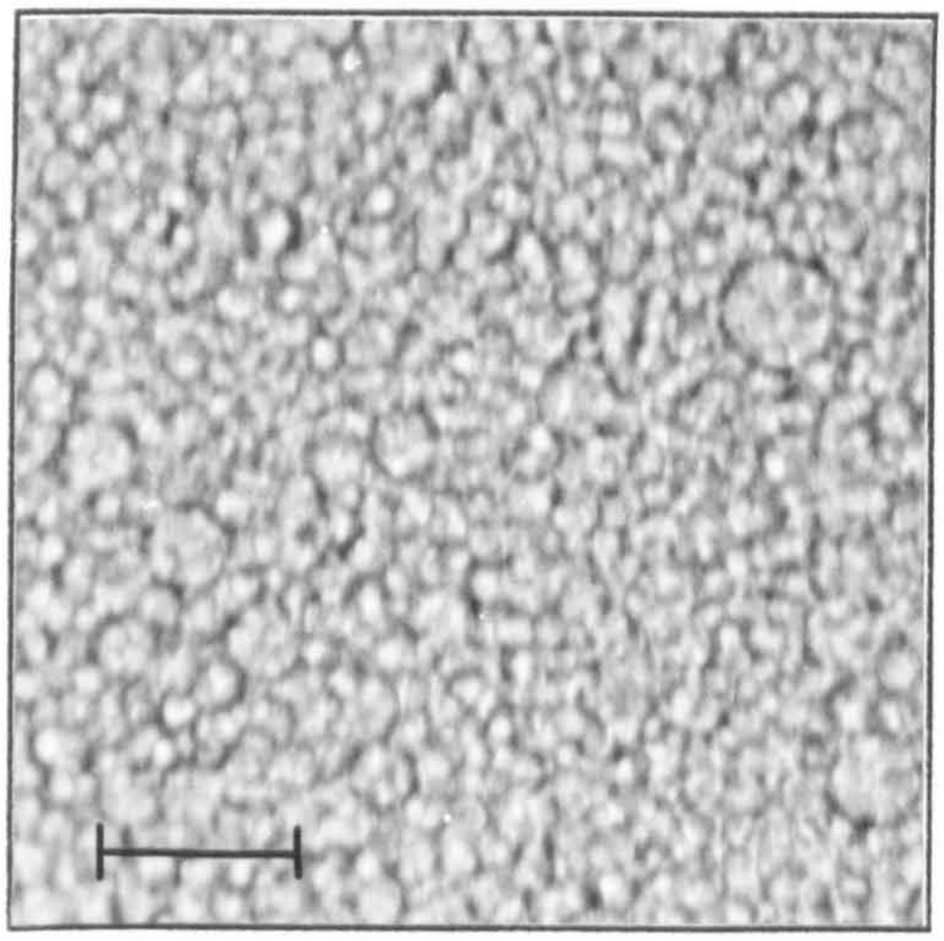

(b). 1.2 wt%, t = 4 days.

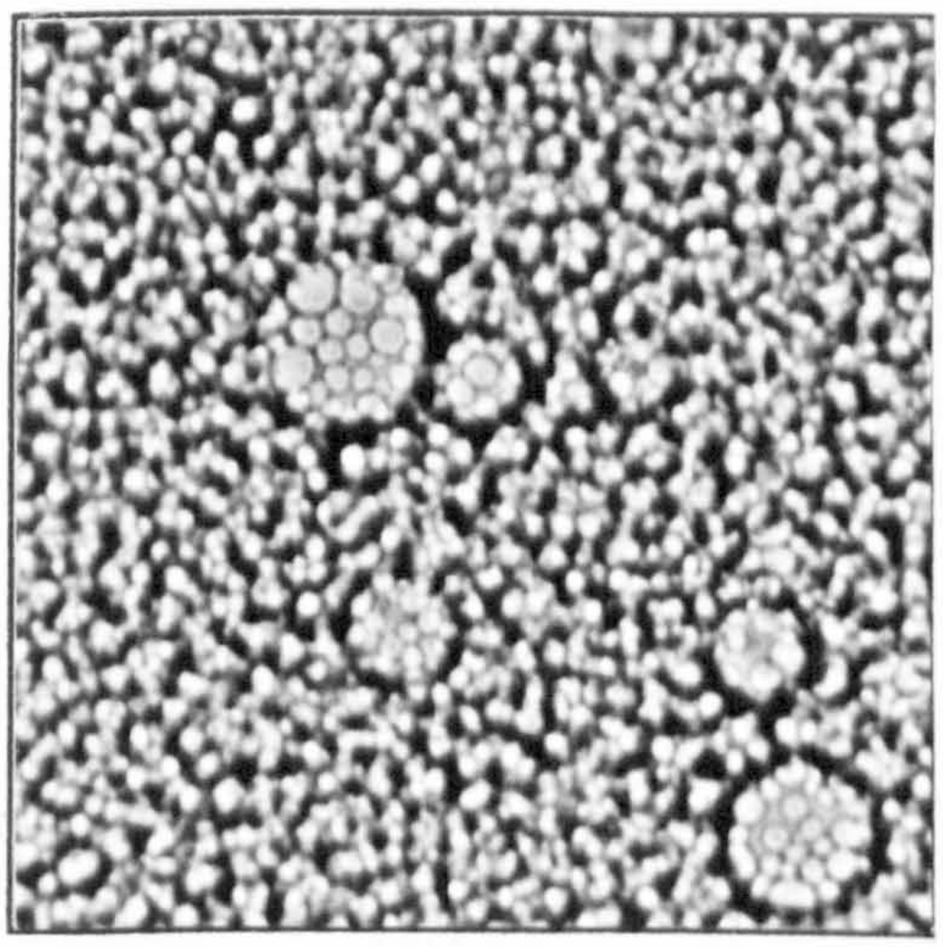

(c). 2.4 wt%, t = 15 mins.

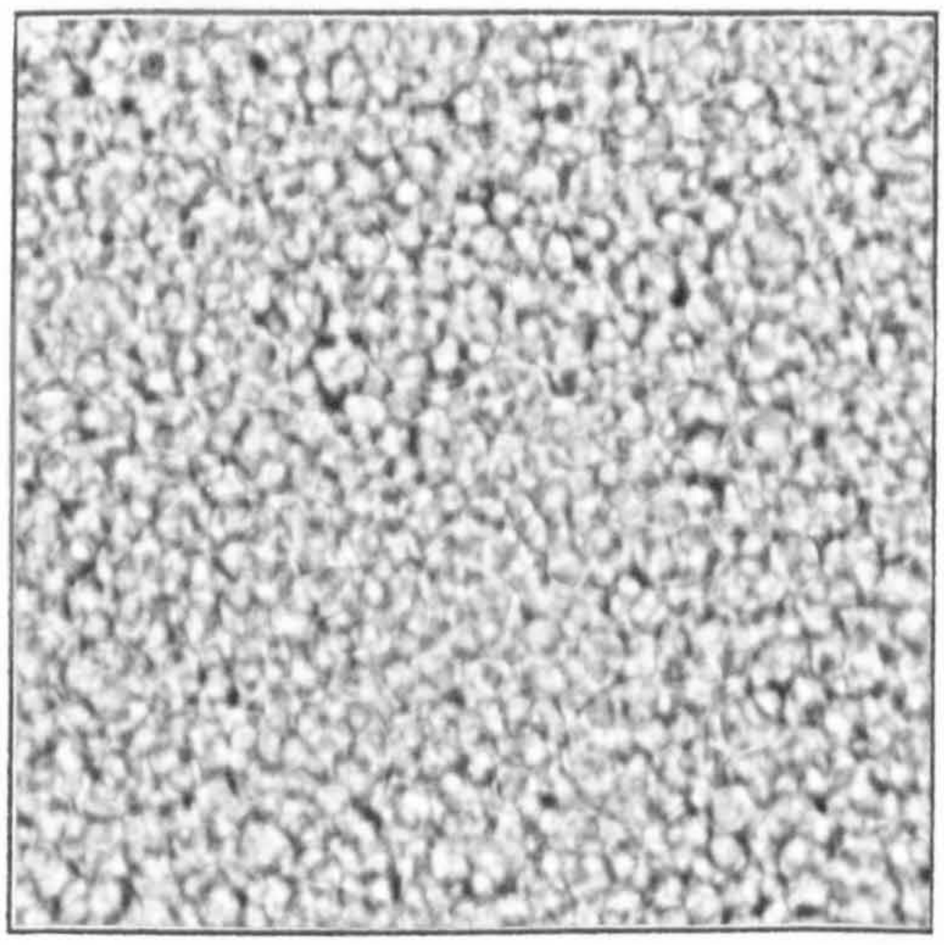

(d). 2.4 wt%, t = 4 days.

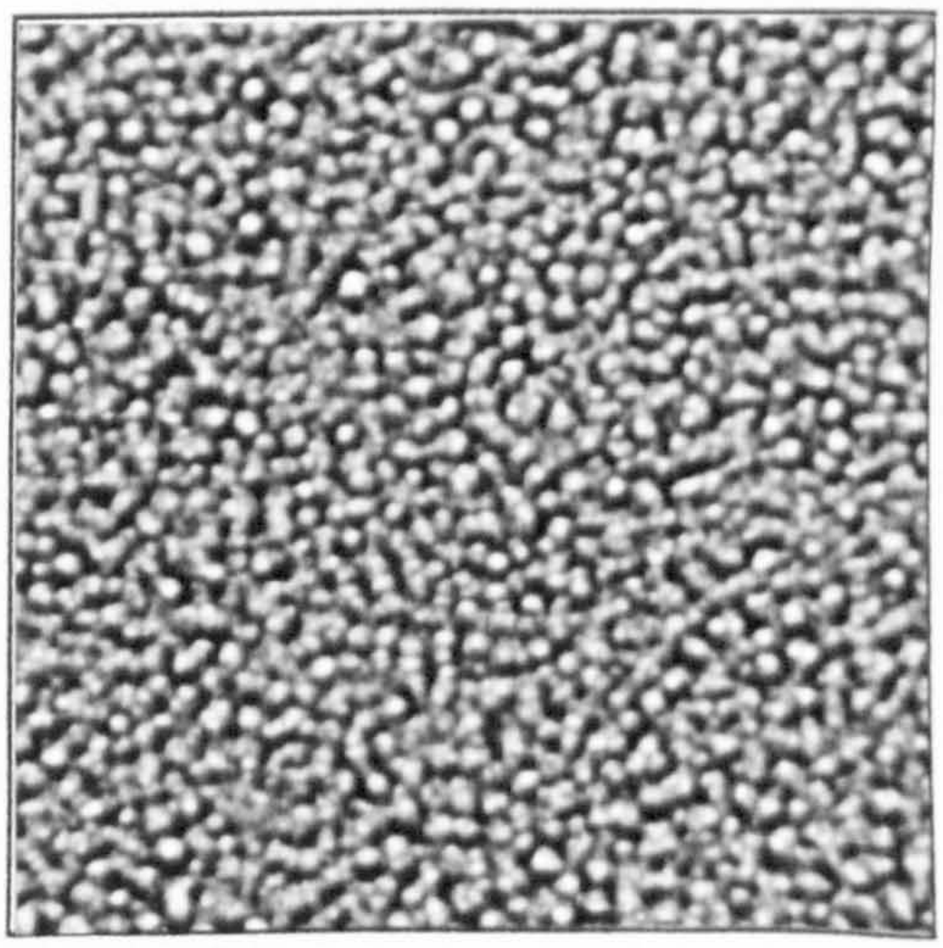

(e). 9.0 wt%, t = 15 mins.

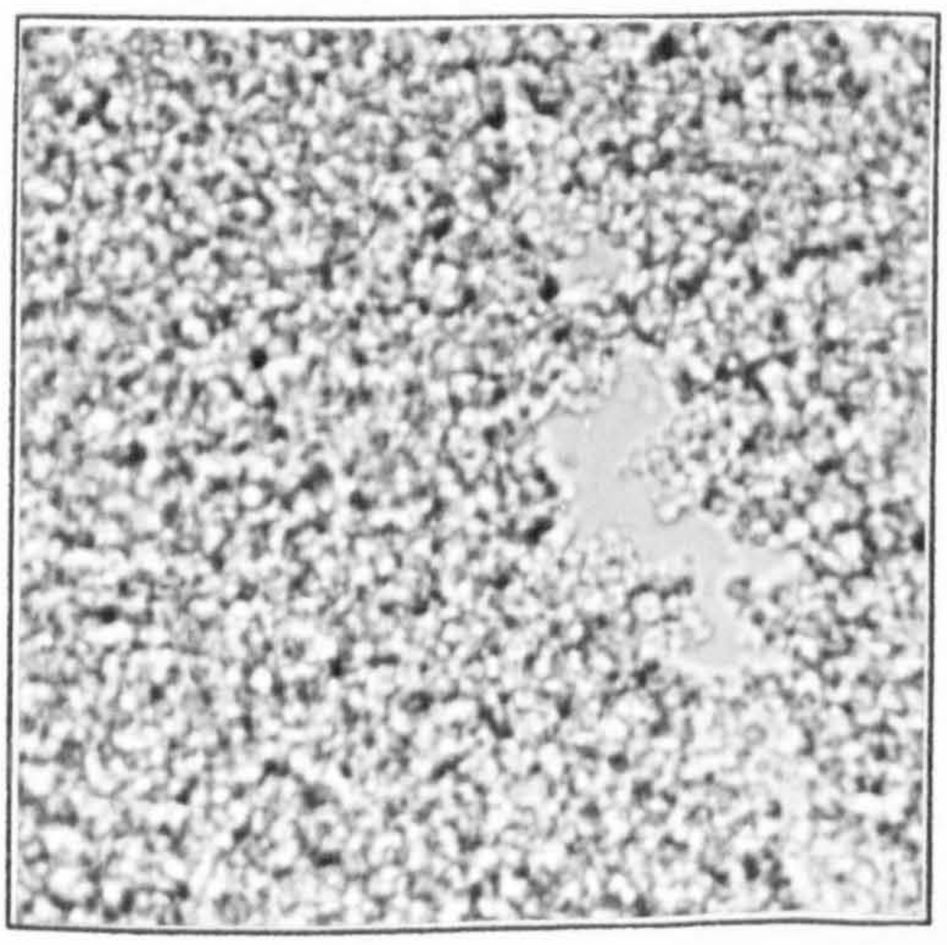

(f). 9.0 wt%, t = 4 days.

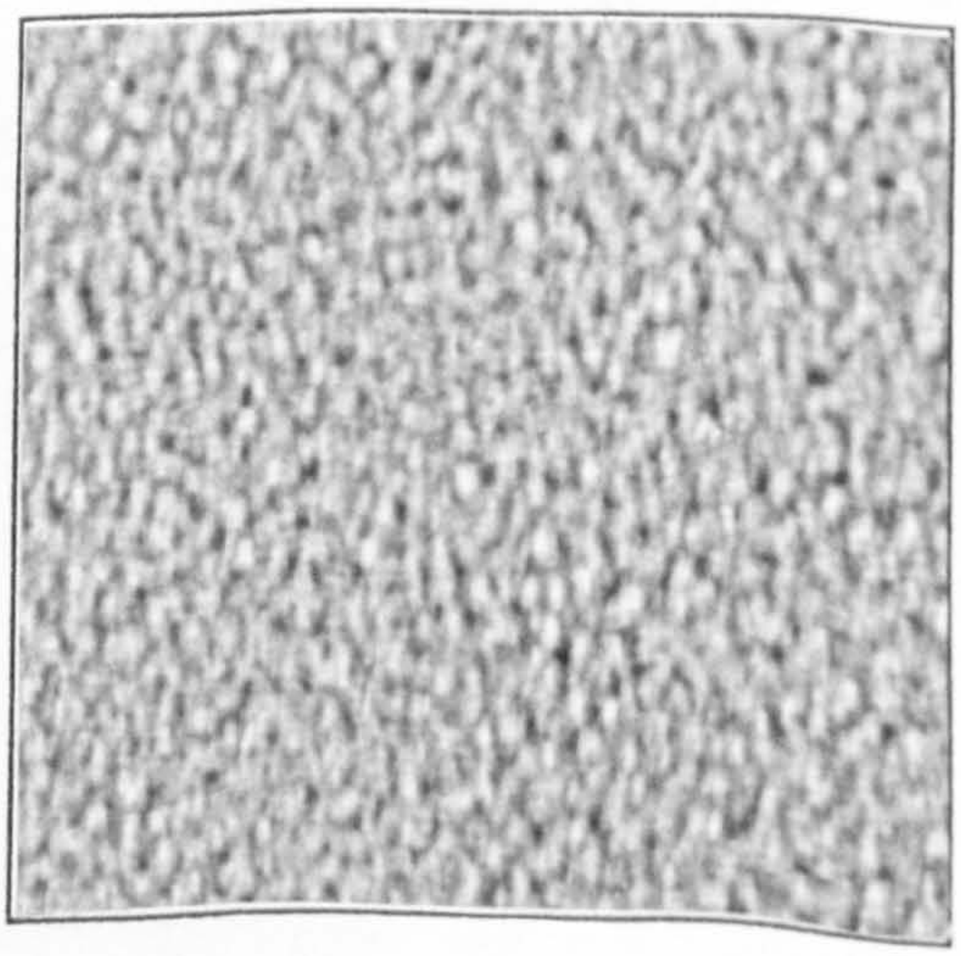

Figure 7.6.

Photographs of emulsions prepared by method II at 26.0°C, $R'_{water} = 18$. Bar = 25 μm.

(a). 2.5 wt%, t = 15 mins.

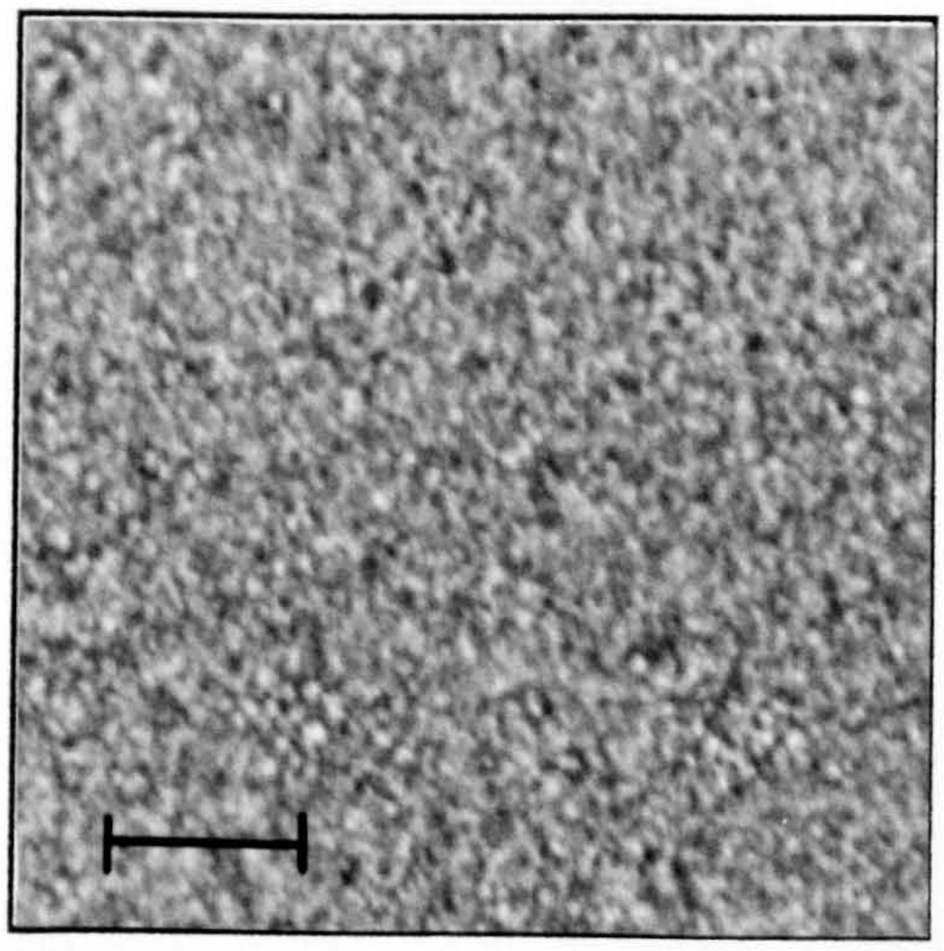

(b). 2.5 wt%, t = 4 days.

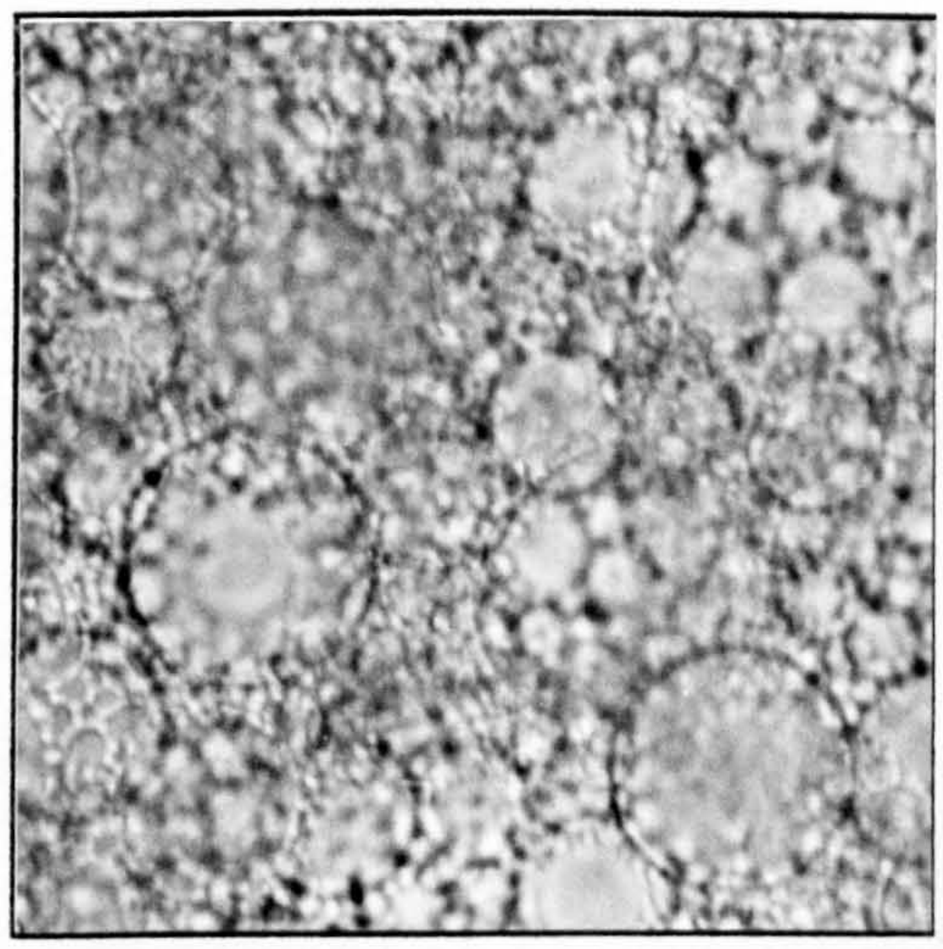

(c). 3.2 wt%, t = 15 mins.

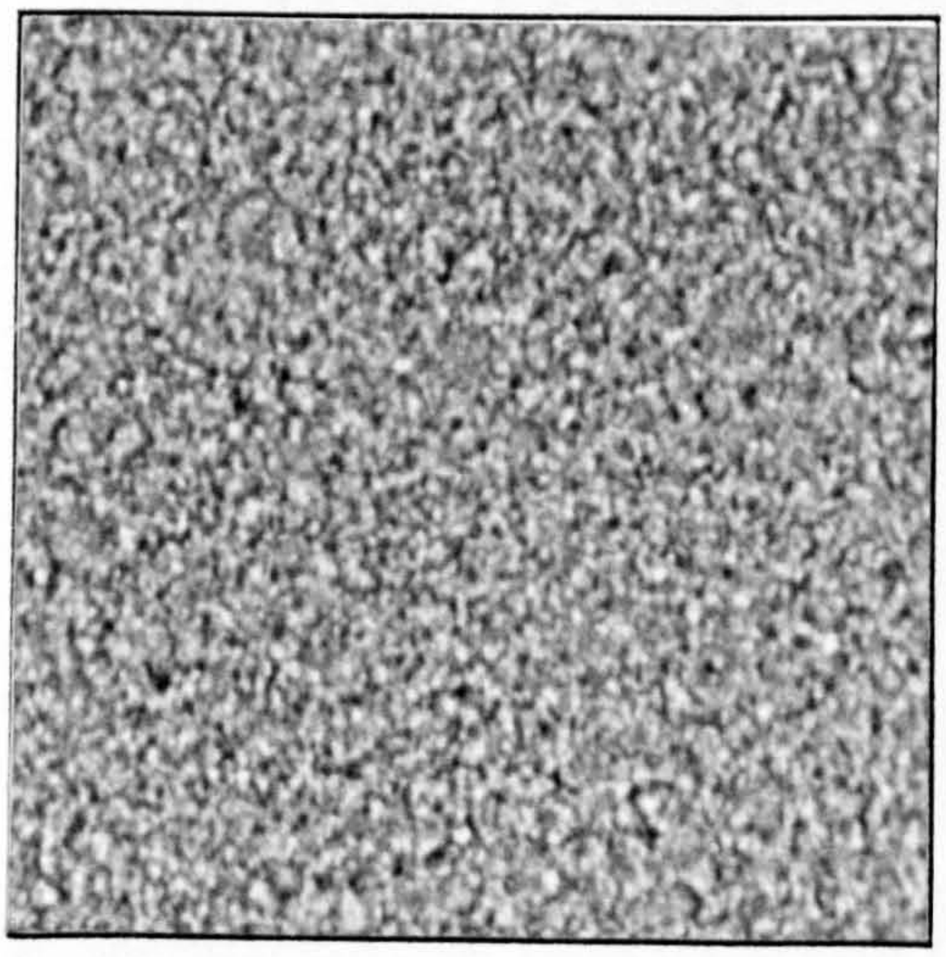

(d). 3.2 wt%, t = 4 days.

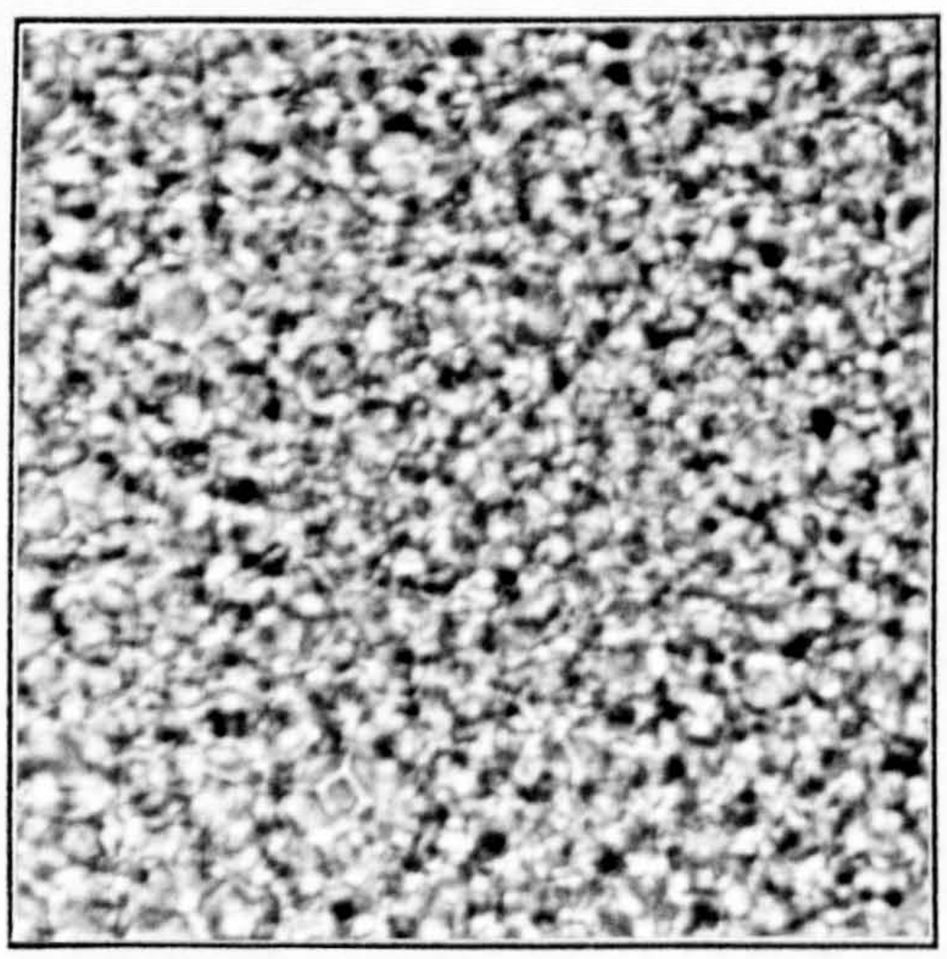

(e). 15.9 wt%, t = 15 mins.

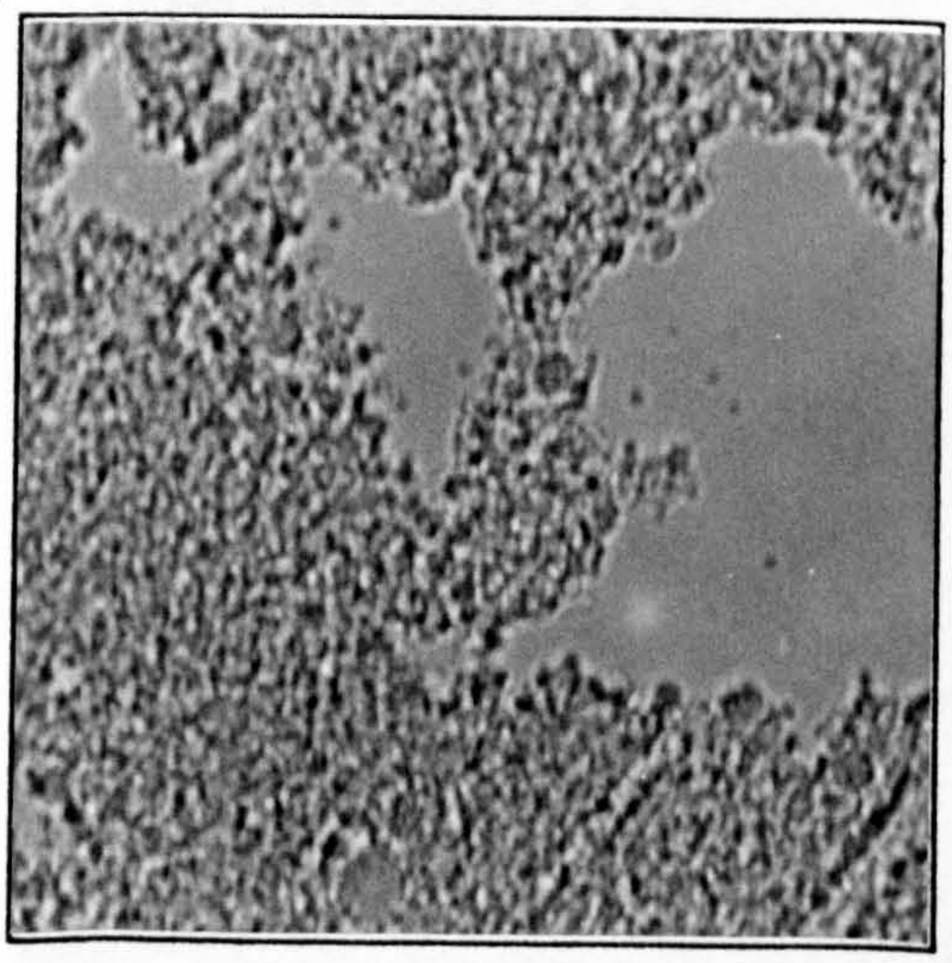

(f). 15.9 wt%, t = 4 days.

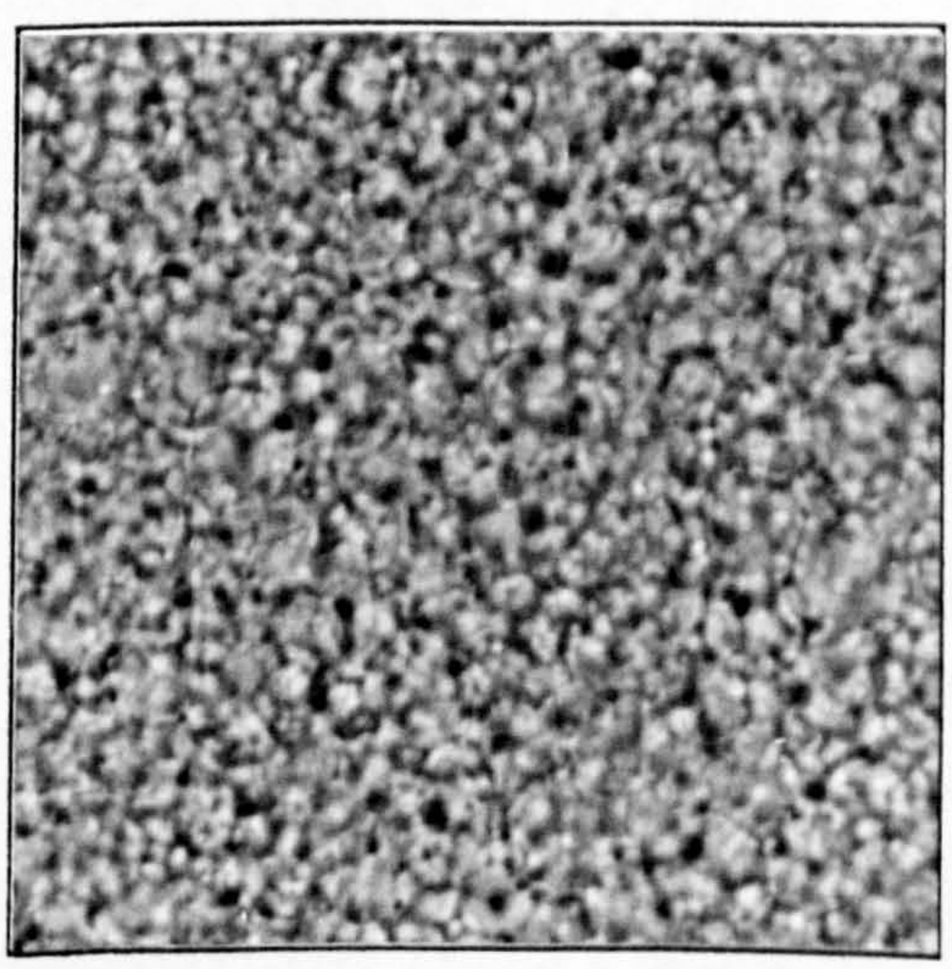

Figure 7.7.

Photographs of emulsions prepared by method II at 40.0°C, $R'_{water} = 7$. Bar = 25 μm.

(a). 4.0 wt%, t = 15 mins.

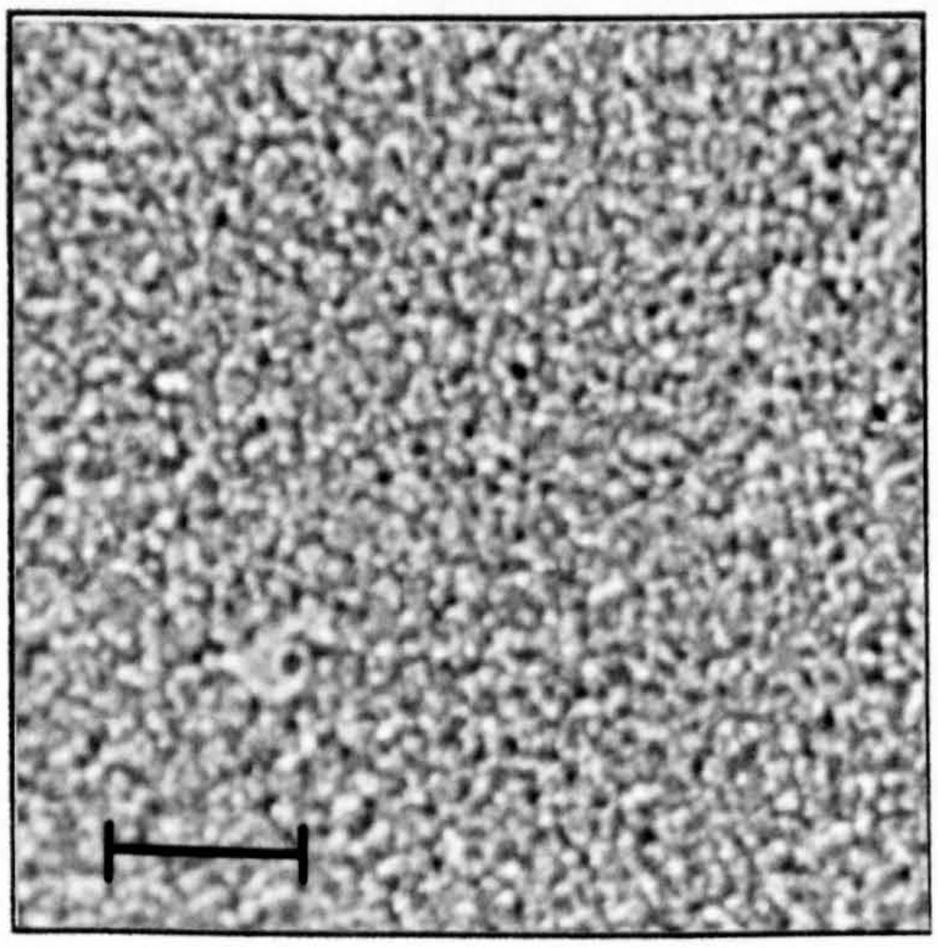

(b). 4.0 wt%, t = 4 days.

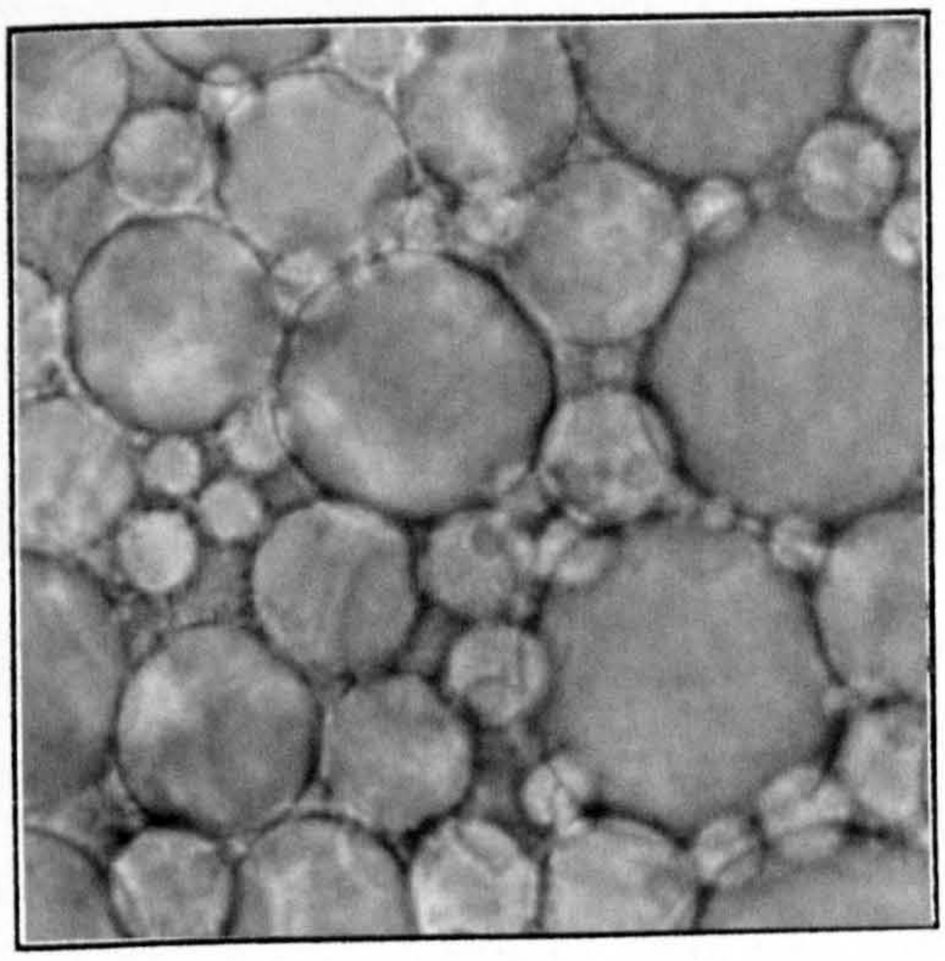

(c). 5.5 wt%, t = 15 mins.

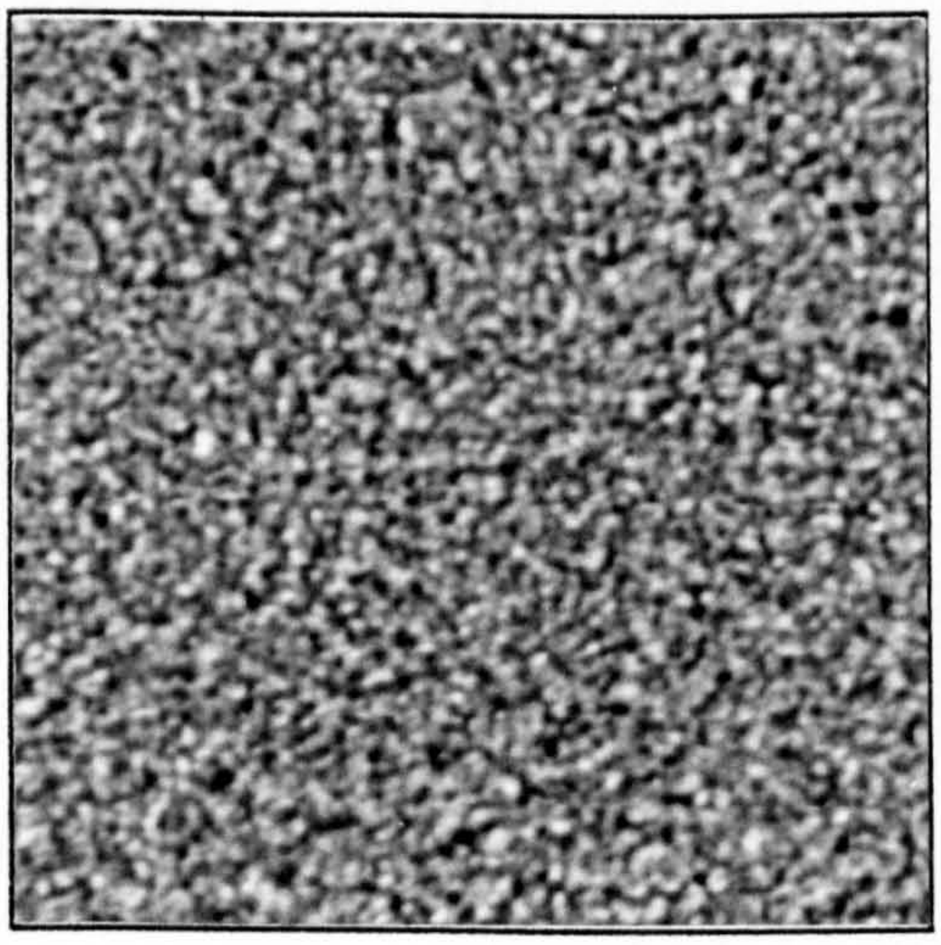

(d). 5.5 wt%, t = 4 days.

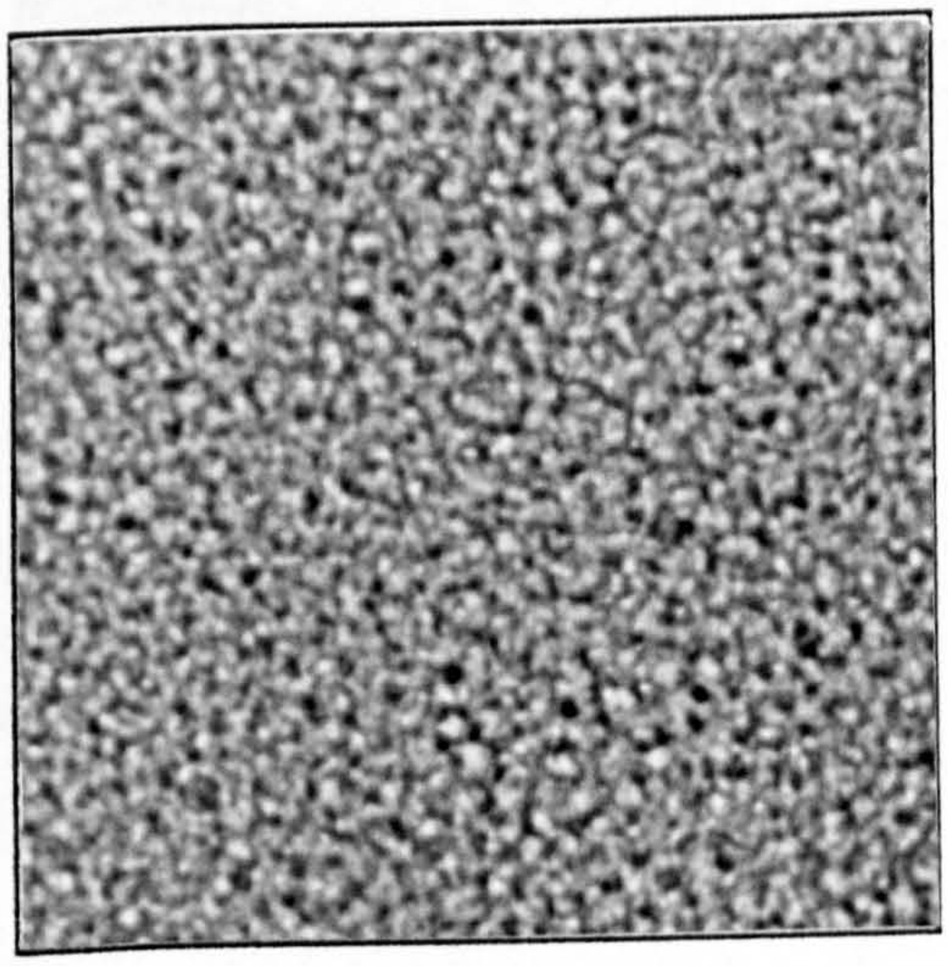

(e). 14.8 wt%, t = 15 mins.

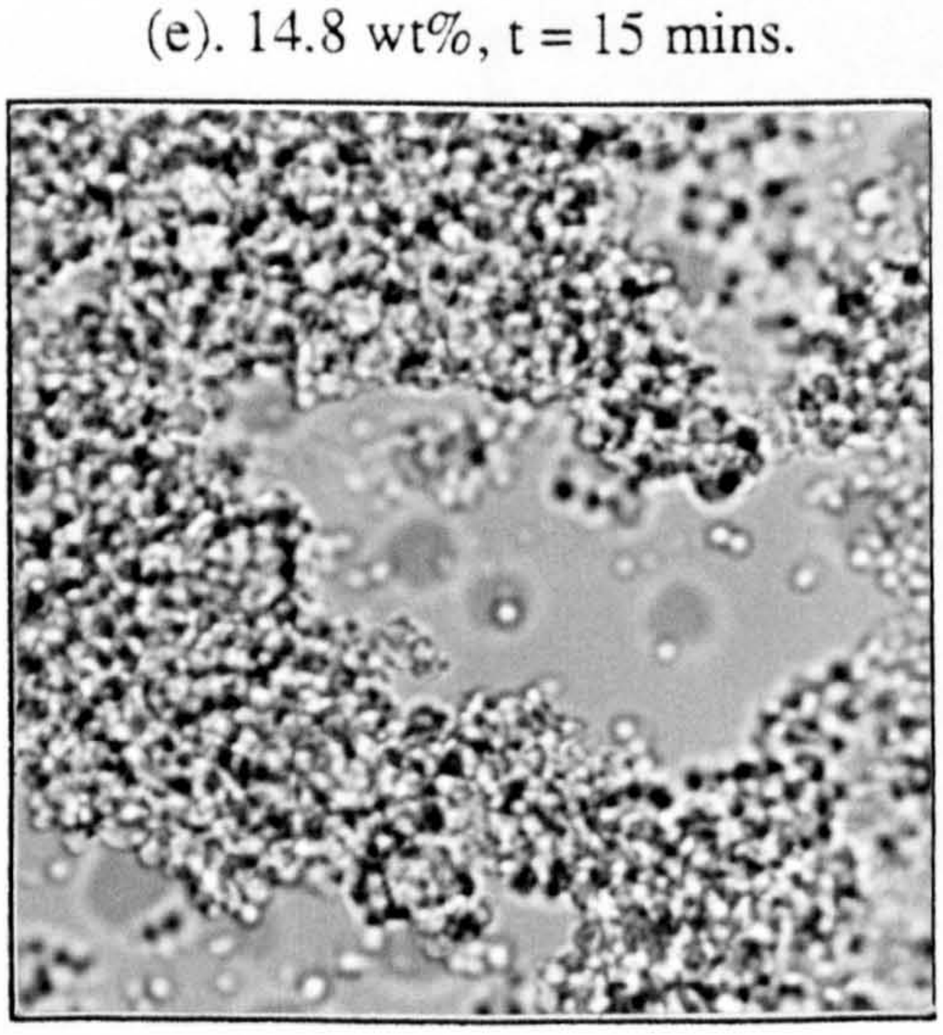

(f). 14.8 wt%, t = 4 days.

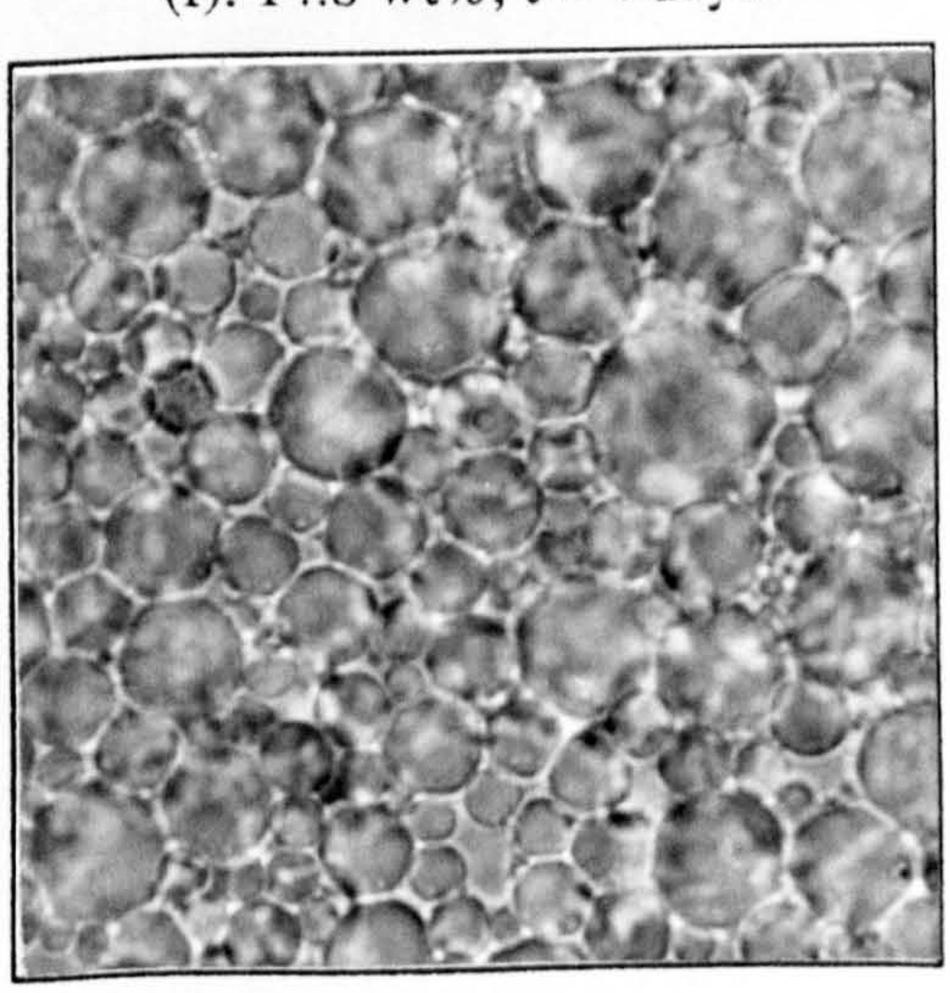

Figure 7.8a.

Variation of $t_{(15\%)}$ with surfactant concentration in heptane. The emulsions were prepared by method II. Temperature = 17.0°C, $R'_{water} = 43$.

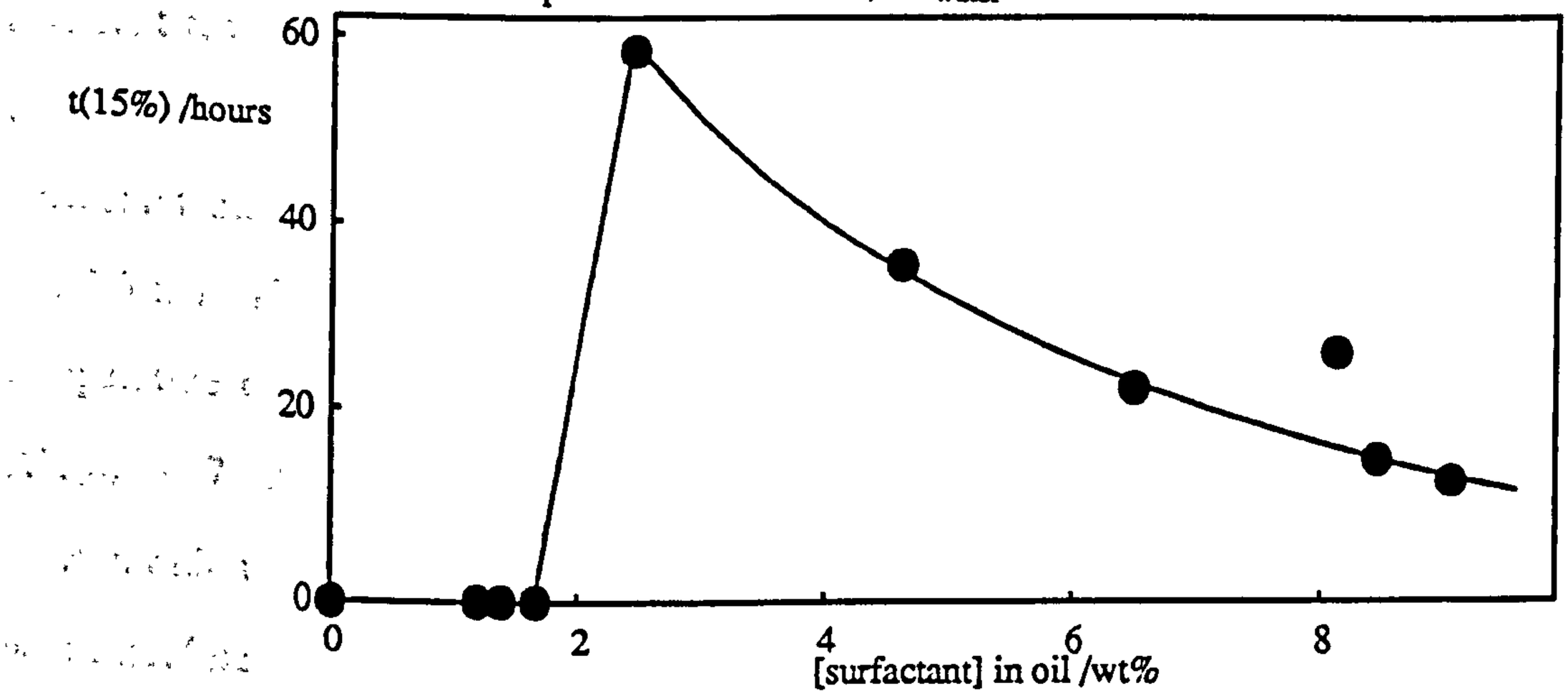

Figure 7.8b, temperature = 26.0°C, $R'_{water} = 18$.

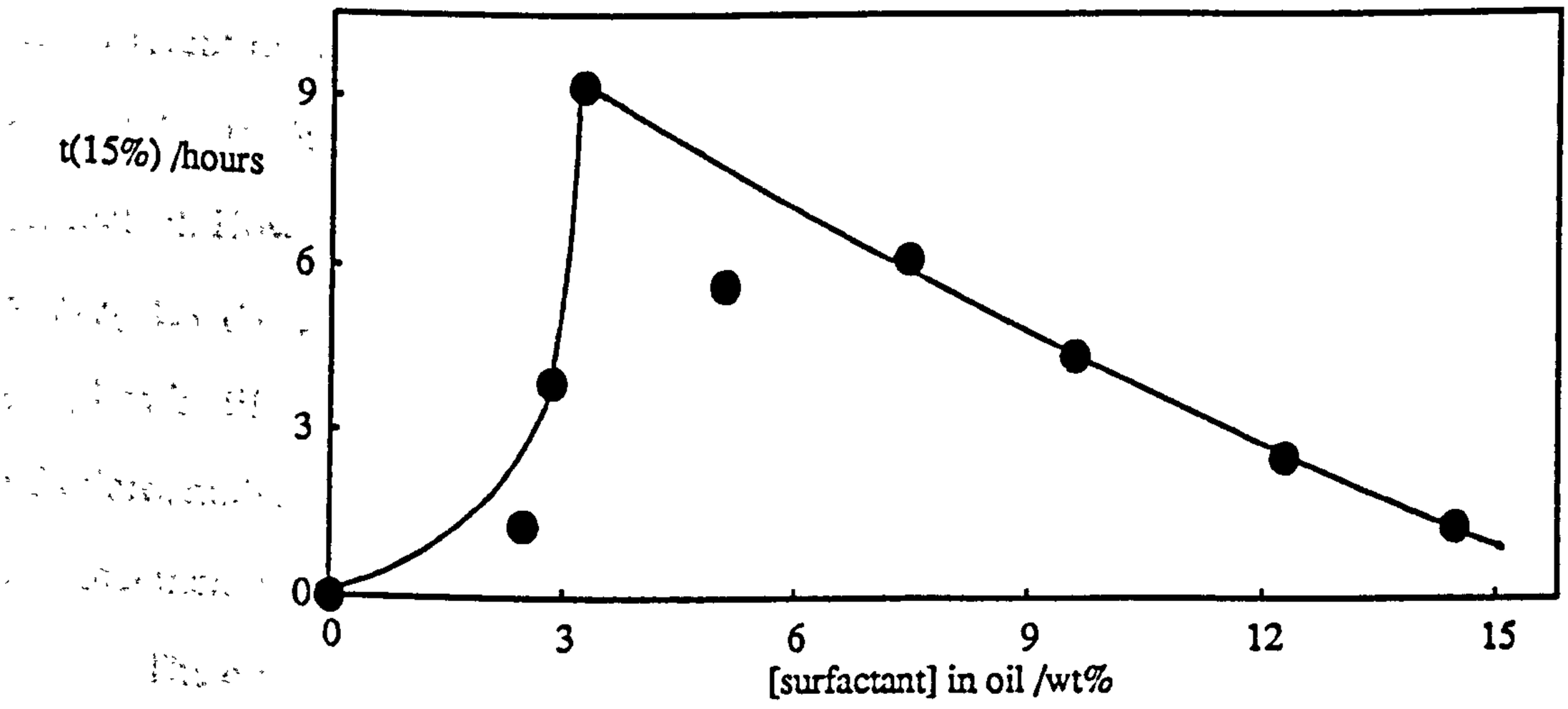

Figure 7.8c, temperature = 40.0°C, $R'_{water} = 7$.

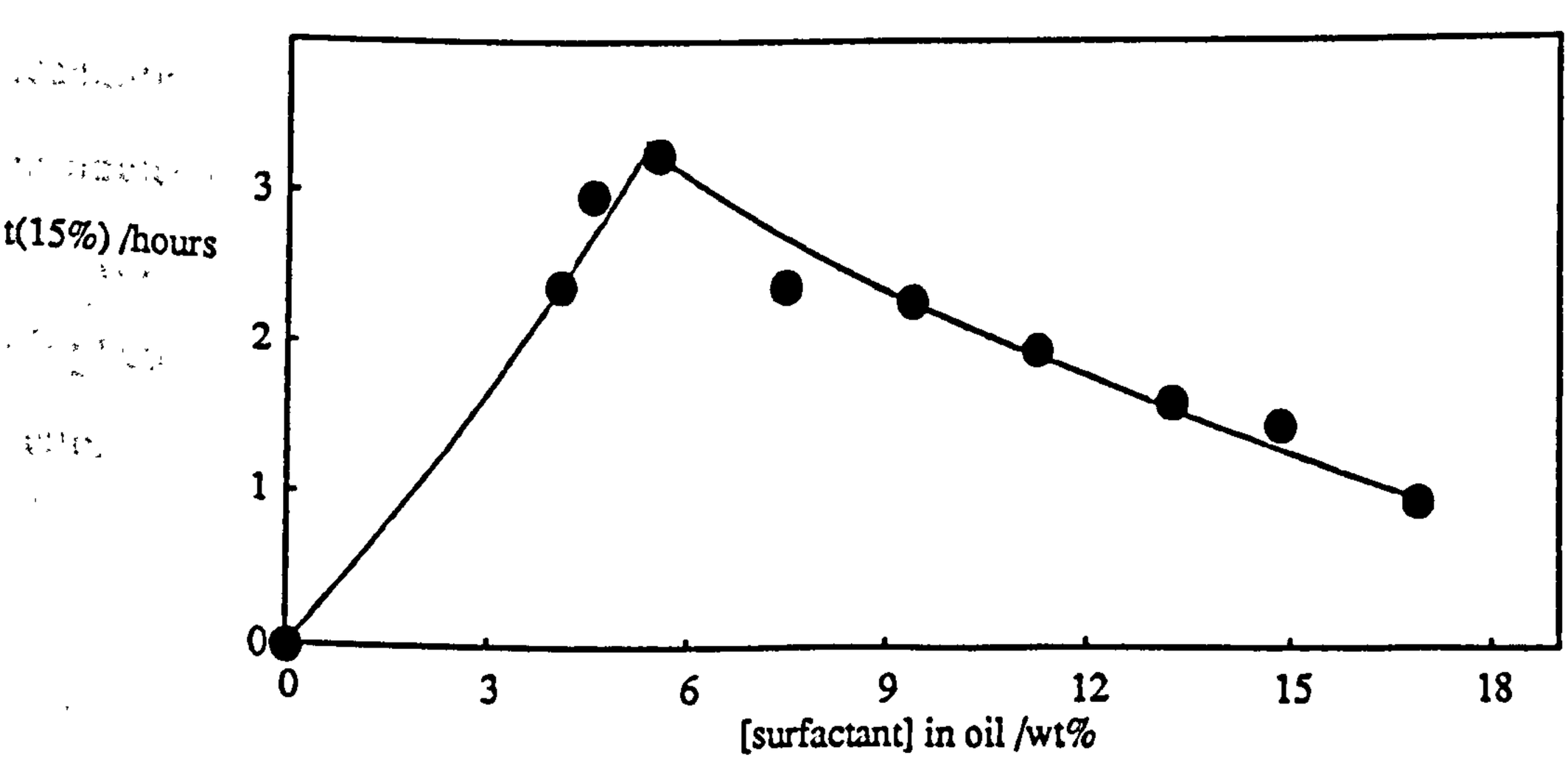

concentrations (method III). Thus, in method III the same emulsion was used for the different temperatures, whereas in method II different stock emulsions were used at each temperature. Since the cμc varies with temperature, some slight adjustment of the surfactant distribution within the emulsion must occur when the temperature of the emulsion is altered. The stock emulsion temperature was not raised to obtain the temperature corresponding to a microemulsion droplet composition corresponding to R'_{water} = 7 since this would cause the cμc to increase beyond the surfactant concentration in the original stock emulsion thereby making it unstable. This method was therefore restricted to microemulsion droplets of composition R'_{water} = 43 and 18 only. The results are shown in Figures 7.9a and 7.9b. As in methods I and II, the microemulsion droplets accelerate the oil phase resolution. The accelerating effect of the different microemulsion droplet sizes now appears similar i.e. for both droplet sizes, $t_{(15\%)}$ falls to 50% of its maximum determined value for the addition of ~5 wt% surfactant. However, since the aggregation numbers are different for R'_{water} = 43 and 18 aggregates (N_{agg} = 5700 and 1000 respectively), the concentration of microemulsion droplets is different in each case. If the results are compared at the same concentration of microemulsion in the continuous phase, then the larger aggregates produce a greater enhancement in the rate of oil resolution.

The emulsion behaviour can be summarised as follows.

(1). For emulsions prepared by all three methods, water resolution is only observed for surfactant concentrations less than the cμc. At higher surfactant concentrations, the emulsions resolve to give a W/O microemulsion phase and a highly concentrated emulsion.

(2). For each system investigated, maximum emulsion stability with respect to oil phase resolution is observed at a surfactant concentration approximately equal to the cμc.

Figure 7.9a.

Variation of $t_{(15\%)}$ with surfactant concentration in heptane. The emulsions were prepared by method III. Temperature = 17.0°C, R'_{water} = 43.

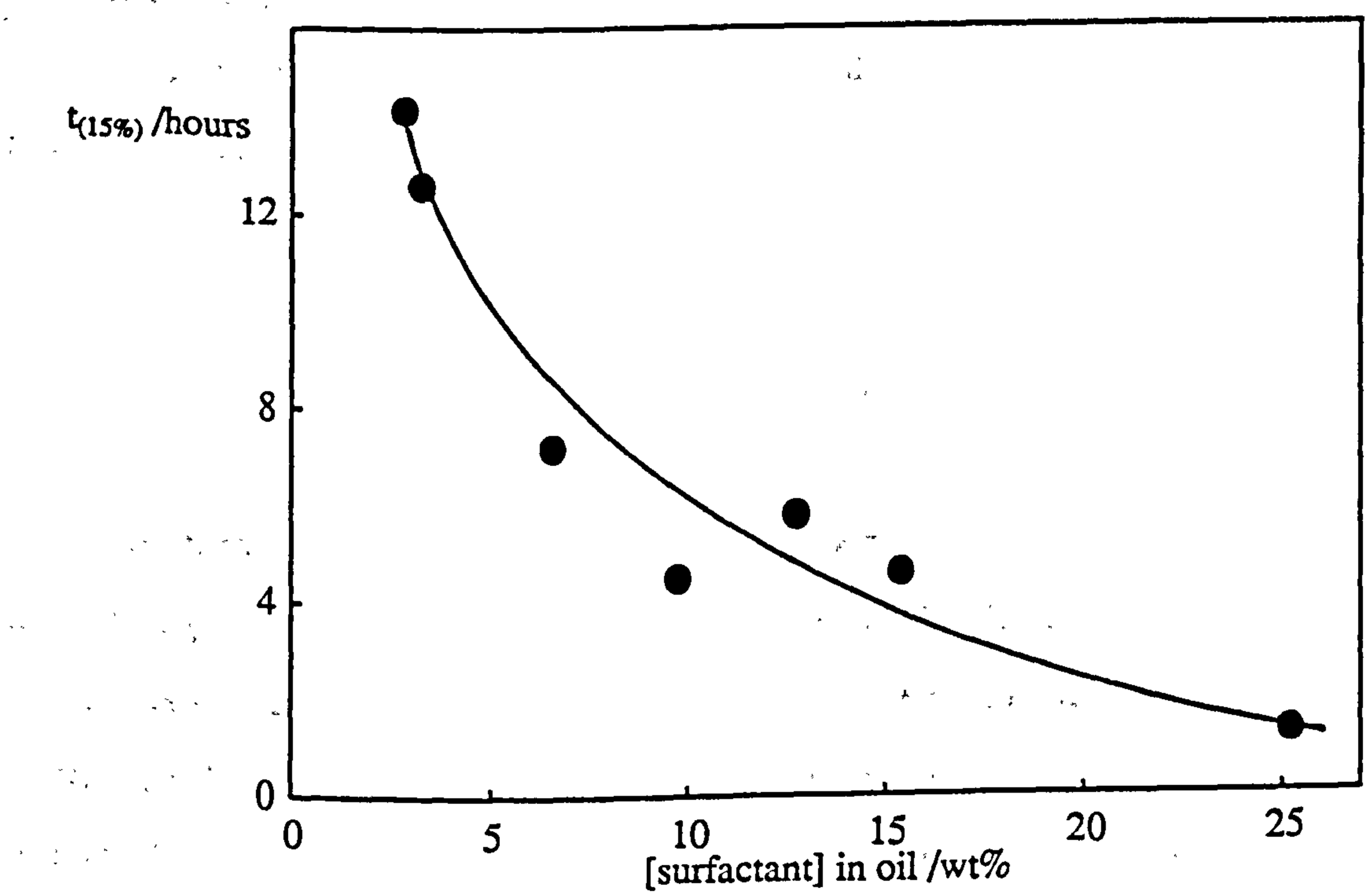

Figure 7.9b.

Temperature = 26.0°C, R'_{water} = 18.

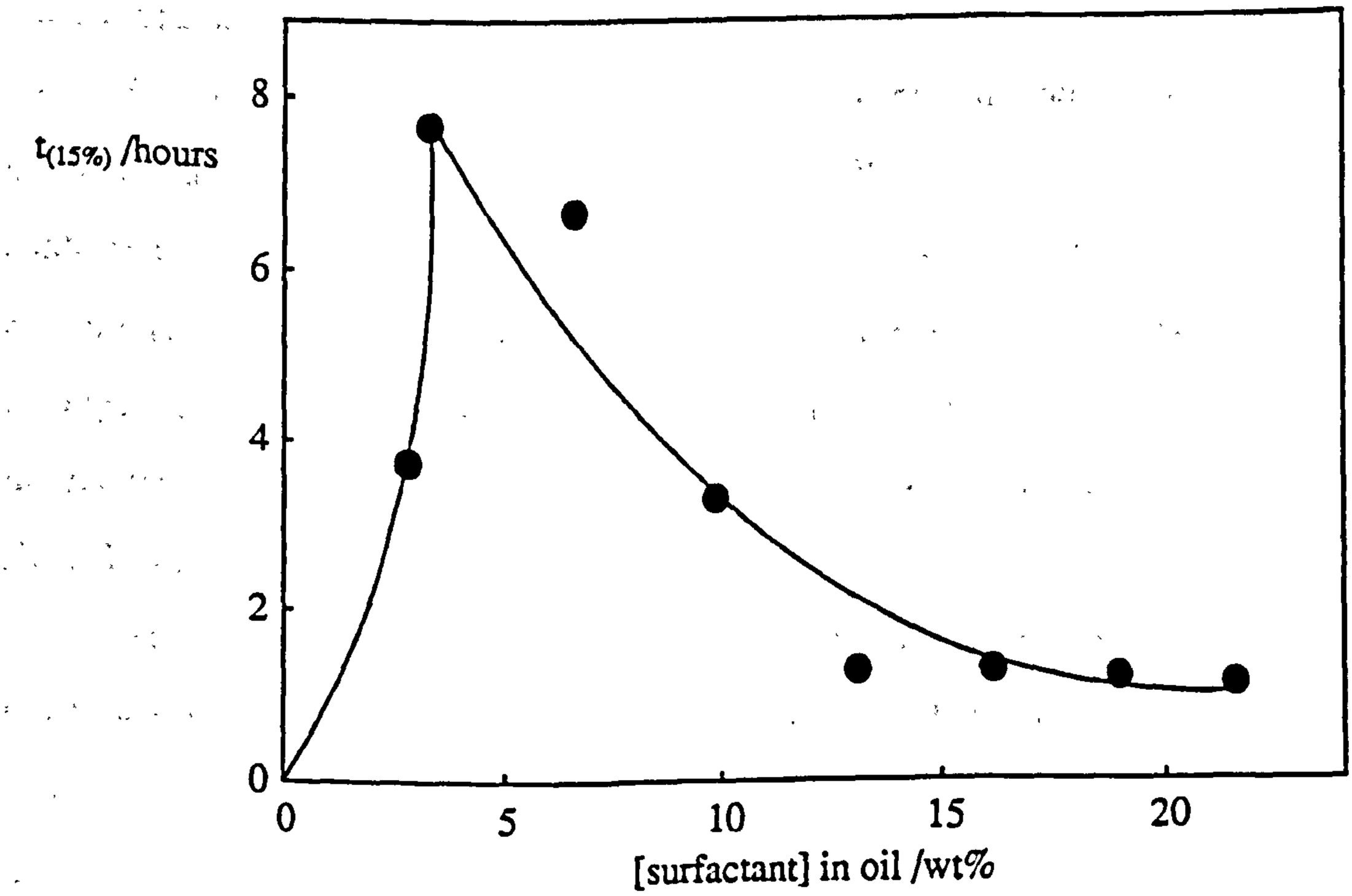

(3). For a fixed concentration of microemulsified surfactant, the accelerating effects of $R'_{water} = 43$ and 18 microemulsion droplets on the oil phase resolution rate are similar. However, when the two systems are compared at the same concentration of *microemulsion droplets*, an enhanced rate is observed for the emulsion containing larger microemulsion aggregates in the continuous phase.

7.3 The Depletion Flocculation Interaction.

As mentioned earlier, Aronson (86) has observed a similar enhancement in the rate of droplet creaming for O/W emulsions induced by the presence of surfactant aggregates in the continuous phase. He ascribed this effect to a depletion flocculation interaction. This type of interaction has previously been invoked to explain the effects of non-adsorbing polymers added to the continuous phases of various emulsion systems (97, 199, 200). Similarly, it has also been used to interpret the flocculation of polystyrene latex spheres by polymers (201, 202), and by nonionic surfactant aggregates (203). It therefore seems plausible that a similar effect is operating in the case of W/O emulsions studied here.

In the previous section the effect of increasing the concentration of microemulsion droplets in the continuous phase of W/O emulsions was investigated. Additionally, the size of the microemulsion aggregates was systematically varied and the results indicated that the oil phase separation rate was rather insensitive to the aggregate size (for a fixed concentration of aggregated surfactant). In this section, these observations are discussed to see if they are consistent with a mechanism of depletion flocculation.

The original depletion flocculation concept was developed by Asakura and Oosawa some 35 years ago (87, 88). In recent years however it has received an

increasing amount of attention (85, 202 - 204). The basic model, initially set up by Sperry to explain the flocculation of polystyrene latices by polymers (202) and later extended by Aronson to account for micellar effects (86), is as follows. The dispersed emulsion droplets are considered as large, non-deformable spheres in a continuous phase containing small, spherical, non-deformable, non-adsorbing surfactant aggregates (W/O microemulsion droplets in this case). The geometry associated with this model is shown below in Figure 7.10. (The relative sizes of the emulsion and microemulsion droplets are not to scale).*

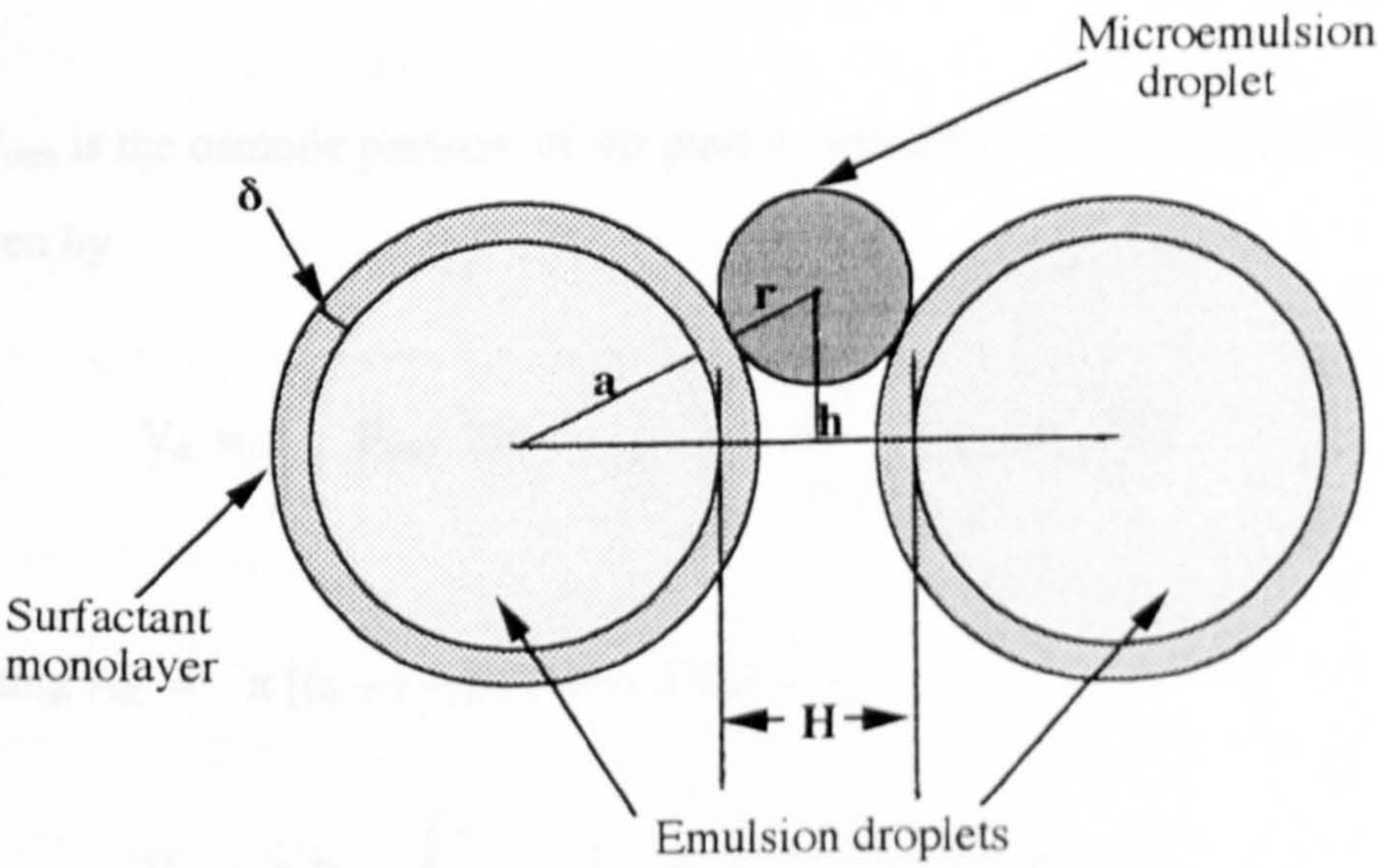

Figure 7.10

When the emulsion droplets approach sufficiently close such that the spacing between them H, is less than $2(r + \delta)$, the centres of gravity of the microemulsion aggregates are excluded from this region defined by the area A_R.

$$A_R = \pi h^2 \qquad (7.1)$$

*For the purposes of this discussion, it is not necessary to take account of the adsorbed film thickness (δ) and recasting the model without it would lead to some simplification of the equations. This was not done as these calculations were made using a computer program designed to allow the inclusion of other interaction terms for which inclusion of the adsorbed film was necessary.

$$\therefore \qquad A_R = \pi [(a + r + \delta)^2 - (a + H/2)^2] \qquad (7.2)$$

This causes an osmotic pressure between the droplet-free zone and the bulk continuous phase containing the microemulsion droplets. This osmotic pressure then serves to force the emulsion drops closer together. The magnitude of this attractive force is given by

$$F_{osm} = P_{osm} \; A_R \qquad (7.3)$$

where P_{osm} is the osmotic pressure of the particle solution. The attractive potential V_d, is then given by

$$V_d = \int_{\infty}^{H} F_{osm} \; dH \qquad = \int_{2(r+\delta)}^{H} P_{osm} \; A_R \; dH \qquad (7.4)$$

substituting $A_R = \pi [(a + r + \delta)^2 - (a + H/2)^2]$

$$V_d = \pi \, P_{osm} \int_{2(r+\delta)}^{H} [(a + r + \delta)^2 - (a + H/2)^2] \; dH \qquad (7.5)$$

The depletion interaction energy of the two emulsion drops is therefore given by

$$V_d = -(2 \pi P_{osm} a^3/3) \; \{[2(1 + r/a)^3 + (1 + H/2a)^3 - 3(1 + r/a)^2 (1 + H/2a)]$$
$$+ \; \delta/a \, [3(\delta/a) + 6(r/a) (\delta/a) + 6(r/a) + 6(r/a)^2 + 2(\delta/a)^2 - 3(H/2a) (\delta/a)$$
$$- 6(H/2a) - \; 6(H/2a) (r/a)]\} \qquad (7.6)$$

In the treatment of Aronson, the following expression was used for the osmotic pressure of the micellar solution

$$P_{osm} = (C\,R\,T/M)(1 + 2C/\rho) = (C\,R\,T/M)(1 + 2\phi) \qquad (7.7)$$

where C is the concentration of aggregated surfactant in g/cm3, M is the molecular weight of the surfactant aggregates, ρ is the surfactant aggregate density (taken to be equal to 1 for the W/O microemulsions considered here), ϕ is the volume fraction of microemulsions and R and T have their usual significance. This expression, which appears to have been chosen somewhat arbitrarily, is appropriate for fairly dilute solutions and corresponds to spherical particles with some degree of mutual attraction (the coefficient of ϕ for hard spheres with no mutual attraction is 4). The overall equation for the depletion flocculation interaction energy arising from non-adsorbing spherical micellar or microemulsion aggregates is then simply obtained by substituting this expression for P_{osm} into equation 7.6 above. A simple computer program was written to evaluate the interaction energies for choices of parameters appropriate to the experimental conditions.

The depletion interaction energies were calculated for a separation H equal to 2δ i.e. for two emulsion droplets in contact. Figure 7.11 shows the dependence of the contact interaction energy on the emulsion droplet size as a function of the concentration of aggregated surfactant. For the purposes of these calculations, δ was taken to be 2.5 nm, (consequently H = 5 nm) and the temperature was kept constant at 26°C which corresponds to $R'_{water} = 18$ and a microemulsion droplet radius of 6.5 nm. It is evident that substantial attractive forces are associated with the exclusion of microemulsion aggregates. The interaction energy increases with the concentration of microemulsion droplets in the continuous phase and is larger for the larger emulsion drops. Since it has been reported that interaction energies of only a few kT are sufficient to flocculate dispersions (205), the process appears adequate to account for the destabilisation observed in the experimental results of section 7.2.

Figure 7.11.

Theoretical contact depletion interaction energies as a function of surfactant concentration in the continuous phase for different emulsion droplet radii. Parameters used in the calculation are given in the text.

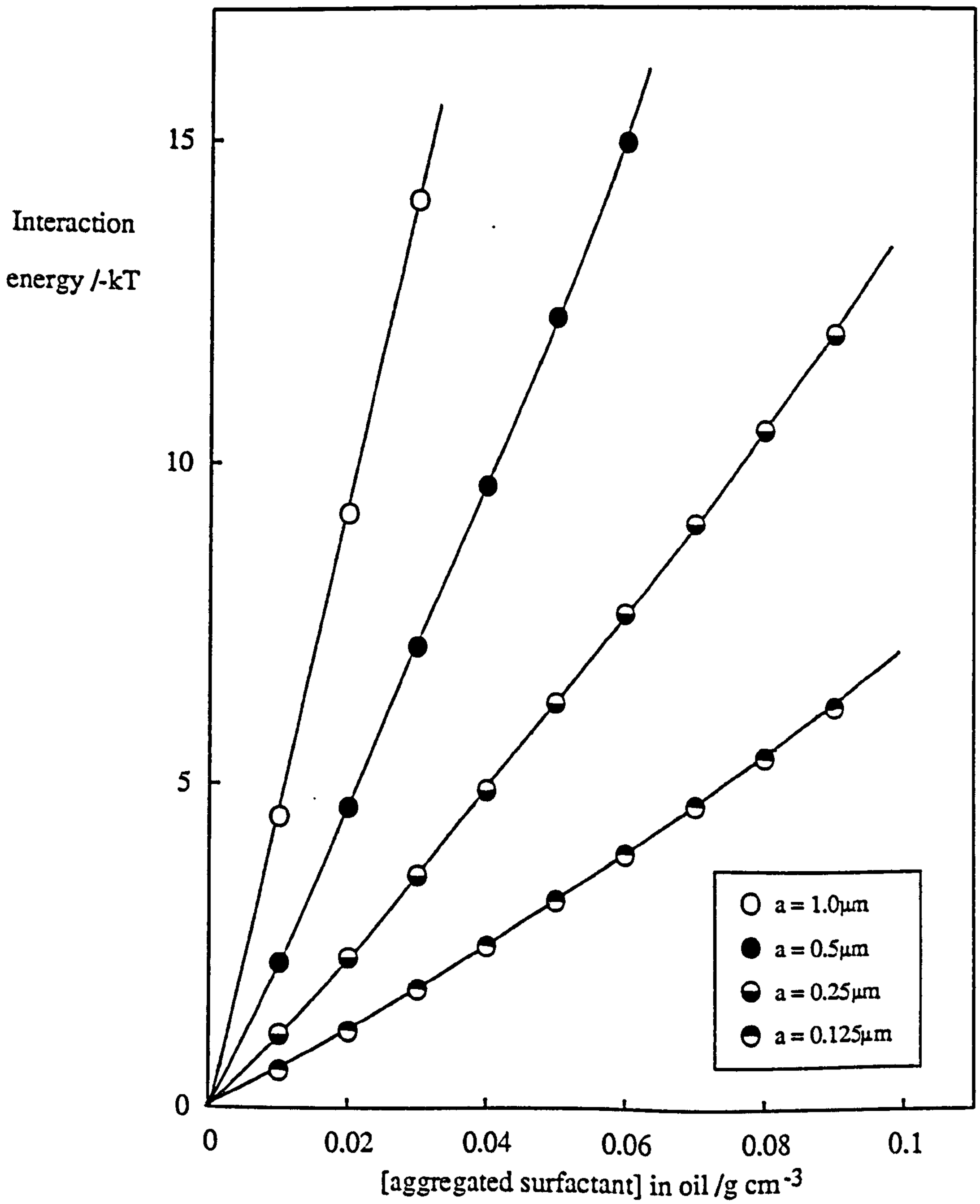

The effect of varying the microemulsion droplet size was also investigated experimentally for emulsions of approximate diameter 1 μm. This has been modelled for the three microemulsion droplet compositions, R'_{water} = 7, 18 and 43 which correspond to radii of 3.1, 6.5 and 12.7 nm respectively. The results are shown in Figure 7.12. For a fixed concentration of aggregated surfactant, the theory predicts that smaller microemulsion aggregates should lead to an increased attraction between emulsion droplets. This arises from there being a greater concentration of smaller droplets present at a fixed concentration and this outweighs the smaller effect of the individual droplets. The size dependence however, is contrary to the experimental observation that for a fixed concentration of aggregated surfactant the different microemulsion droplet sizes accelerate the oil phase resolution to approximately similar extents.

This apparent discrepancy has been investigated further by using an alternative expression for the osmotic pressure. If the microemulsion droplets are assumed to behave as hard spheres, as has been suggested for systems at the solubilisation phase boundary (206), the following equation (207, 208) is more appropriate than the virial expansion used by Aronson.

$$P_{osm} = (C\,R\,T/M)\,[(1 + \phi + \phi^2 - \phi^3)/(1 - \phi)^3] \qquad (7.8)$$

Calculated values of the contact interaction energy using this more realistic expression produces the curves shown in Figure 7.13. The effect of changing the microemulsion droplet size is now predicted to be relatively small. This is in agreement with the experimental findings.

Although it appears that these results for W/O emulsions and Aronson's data for O/W emulsions are reasonably consistent with the predictions of the depletion flocculation model, the possibility of other interactions cannot be rigourously

Figure 7.12.

Theoretical contact depletion interaction energies, assuming a virial expansion for the osmotic pressure, as a function of surfactant concentration for the three emulsion conditions investigated. Parameters used in the calculation are given in the text.

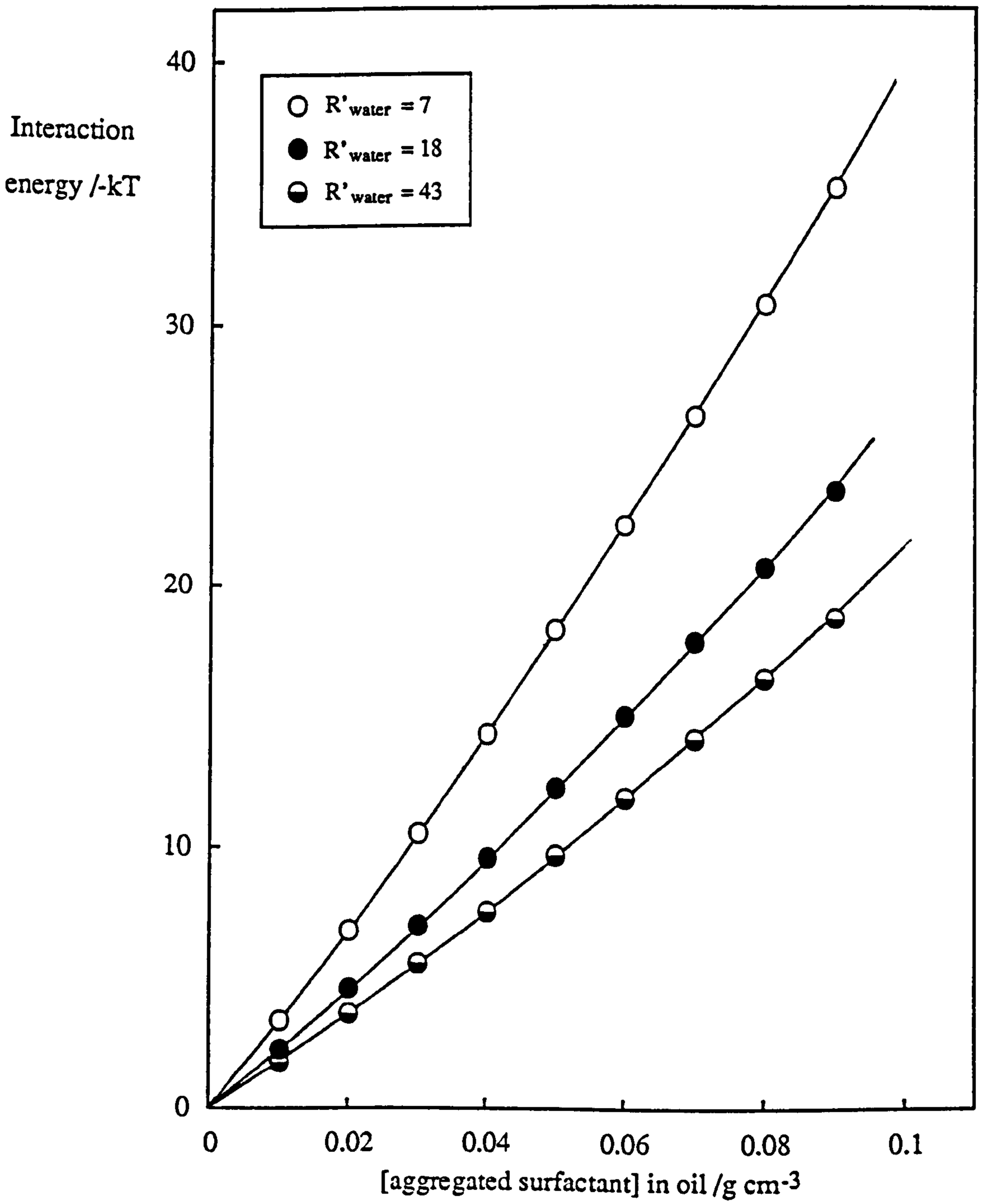

Figure 7.13.

Theoretical contact depletion interaction energies, assuming a hard sphere expression for the osmotic pressure, as a function of surfactant concentration for the three emulsion conditions investigated.

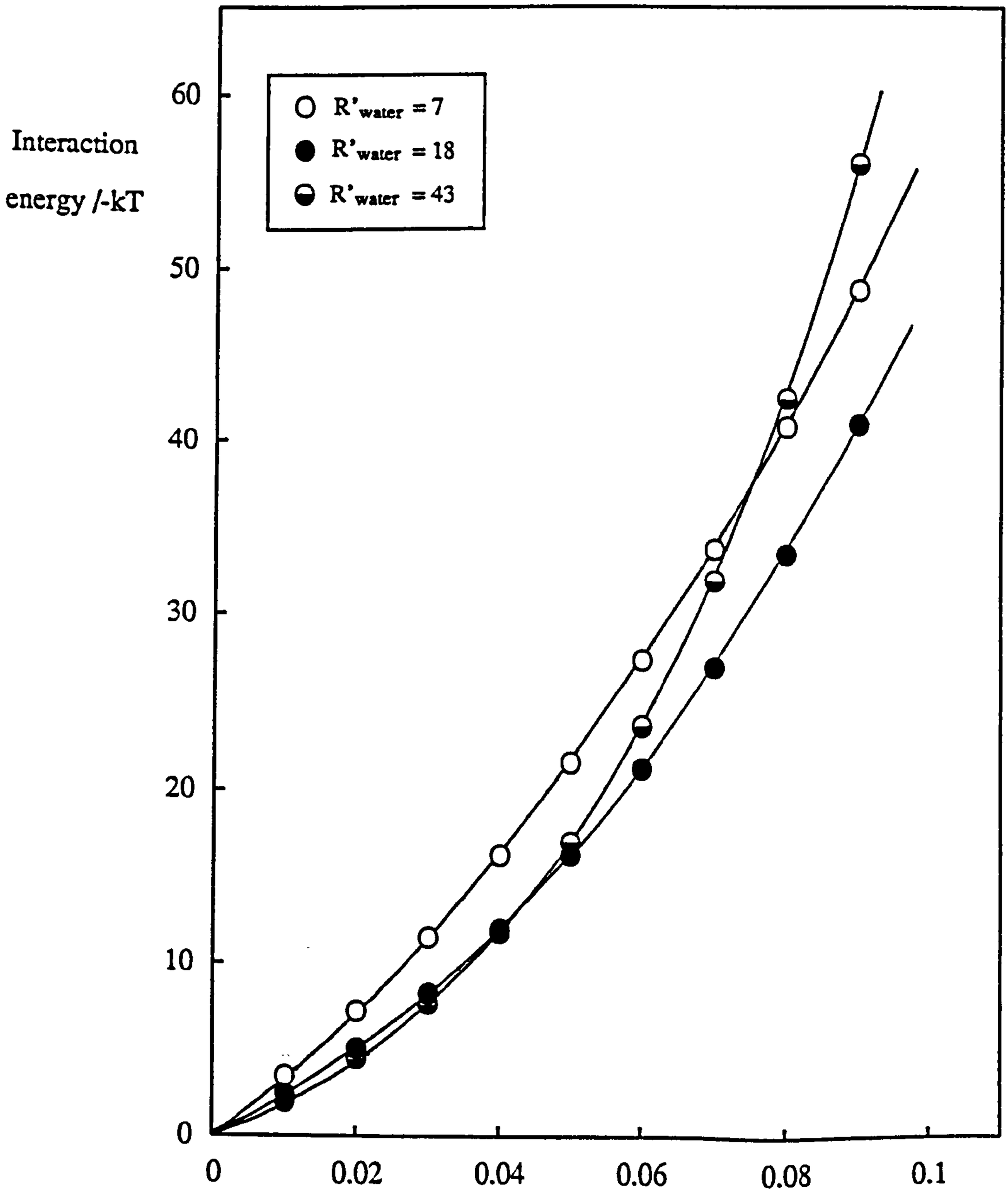

discounted at this stage. The surfactant monolayer coating the emulsions drops is essentially planar on a molecular scale whereas the monolayer coating the microemulsion droplets is highly curved. This difference in curvatures causes the interfacial tensions and monolayer compositions of these monolayers to be different (38). Hence it is possible that the interactions of emulsion-emulsion, microemulsion-microemulsion and emulsion-microemulsion surfaces are all different. On this basis an alternative explanation of the results described here may be that the microemulsion aggregates adsorb at the emulsion drop surfaces and may "bridge" two emulsion drops causing the observed flocculation effects. This "bridging" mechanism has previously been observed for systems containing polymers at low surface coverages (97). Higher surface coverages are observed to sterically stabilise the emulsion droplets. This may also be expected to occur at high concentrations of microemulsion droplets. To completely cover the surface of 1 μm diameter droplets requires between 2.5 and 5.0 wt% of aggregated surfactant for the microemulsion sizes investigated here. However, since no stabilisation has been observed at the highest concentrations of aggregated surfactant investigated (~20 wt%), it appears therefore that the bridging interaction seems less likely than the depletion mechanism.

7.4 Stability of W/O Emulsions Prepared with Triglyceride / Heptane + Water + $C_{12}E_4$.

In Chapter five it was shown that the main effect of incorporation of triglyceride into the oil phase was to increase the critical microemulsion concentration. For concentrations of MCT greater than about 25%, the one phase W/O microemulsion stability region was also shifted to slightly higher temperatures. Results from an investigation into the stability of W/O emulsions formed with 50% and 75% MCT in

heptane are presented in this section. An equilibrium R'_{water} value of 18 was chosen for each system to allow comparison with the corresponding 100% heptane system. Parameters relevant to this composition for both systems are compared to those for heptane alone as the oil phase in Table 7.2 below.

Table 7.2

System	Temp. /°C	cμc /wt%	r_H /nm	γ_c /mN m^{-1}
0% MCT	26.0	3.0 ± 0.4	6.5	0.36
50% MCT	27.3	10.3 ± 1.0	6.5	0.29
75% MCT	33.7	16 ± 1.5	6.5*	0.23

* The hydrodynamic radius of R'_{water} = 18 microemulsions in 75% MCT, was assumed to be the same as that for 50% MCT.

Figure 7.14a shows the variation of the time required for 15% oil resolution as a function of surfactant concentration for 50% MCT in the oil phase. The emulsion was prepared by method I. The behaviour is qualitatively similar to that observed for heptane alone as the oil phase. It is clear that the maximum stability is again observed close to the cμc which is now shifted to 10.3 wt%. It is interesting to observe that the oil resolution is much accelerated for this system, occurring in minutes rather than hours. A similar trend is observed when different microemulsion concentrations are added to portions of a stock emulsion, (i.e. method II), as shown in Figure 7.14b. The emulsion droplet size for this system was determined by optical microscopy to be approximately 1 μm. Resolution of water was observed for surfactant concentrations below the cμc. However, as in the case of heptane as the oil phase, no resolution was seen at higher concentrations over a monitoring period of five days.

Emulsions prepared with 75% MCT as the oil phase show a qualitatively different behaviour. Relatively rapid resolution of both oil and water phases is observed

Figure 7.14a.

Variation of $t_{(15\%)}$ with surfactant concentration in 50% MCT.

Temperature = 27.3°C, R'_{water} = 18. The emulsions were prepared by method I. .

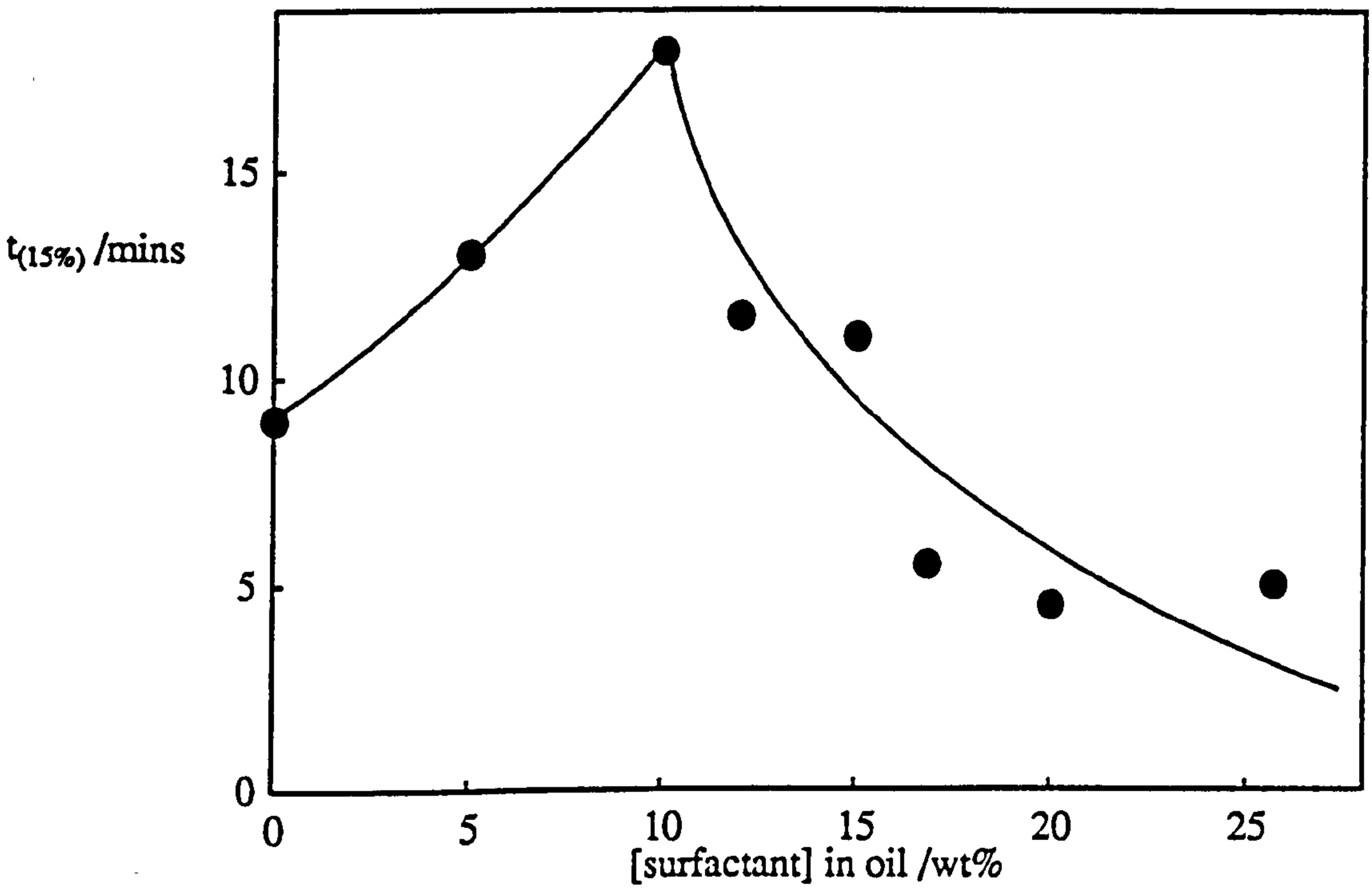

Figure 7.14b.

The emulsion was prepared by method II.

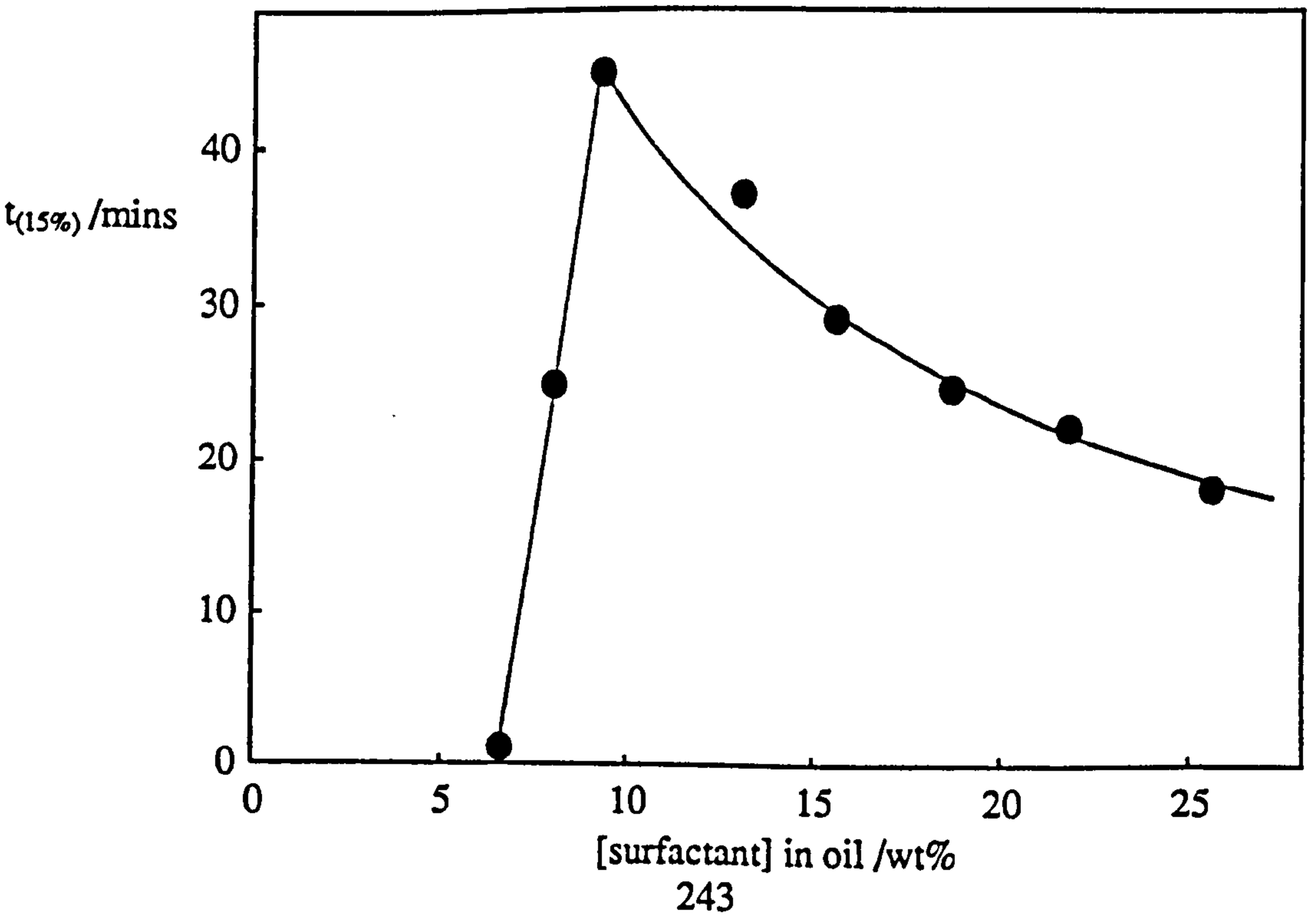

at all surfactant concentrations. Figure 7.15a shows the oil resolution versus time plots as a function of surfactant concentration for emulsions prepared by method I. For surfactant concentrations close to or slightly greater than the cμc, the oil phase is seen to resolve steadily until approximately 60% resolution is achieved. At this point resolution of the oil phase virtually ceases for a time dependent upon the concentration of surfactant present in excess of the cμc. Resolution of oil then starts again as separation of water commences as seen in Figure 7.15b.

This interesting effect appears to indicate that for surfactant concentrations at or slightly in excess of the cμc, coalescence can only proceed after approximately 60% of the oil phase has resolved. This corresponds to an emulsion drop volume fraction of approximately 0.70 in the sedimented emulsion which is similar to a value of 0.74 expected for cubic close-packing of non-deformable spheres. For this triglyceride concentration, the close proximity of emulsion drops leads to rupture of the stabilising monolayers and rapid resolution of water is observed. The concentration of aggregates in the continuous phase of the emulsion is seen to affect the time taken for the close-packed structure to be achieved. This subsequently determines the length of the induction period before water resolution is observed. This is displayed in Figures 7.16a and 7.16b where the time taken for 25% of the oil and water phases to resolve is shown as a function of surfactant concentration. The time $t_{(25\%)}$ is plotted here since the resolution rates are very fast and $t_{(15\%)}$ times were too short for reasonable accuracy. Maximum stability with respect to sedimentation and coalescence again occurs close to the cμc. The figure also highlights the fast oil resolution followed subsequently by coalescence of the dispersed aqueous phase. Drop size determinations could not be performed for these systems due to their highly unstable nature.

Figure 7.15a.

Oil resolution curves for W/O emulsions prepared with $C_{12}E_4$ + 75% MCT + water at 33.7°C, (R'_{water} = 18) for different surfactant concentrations in the oil.

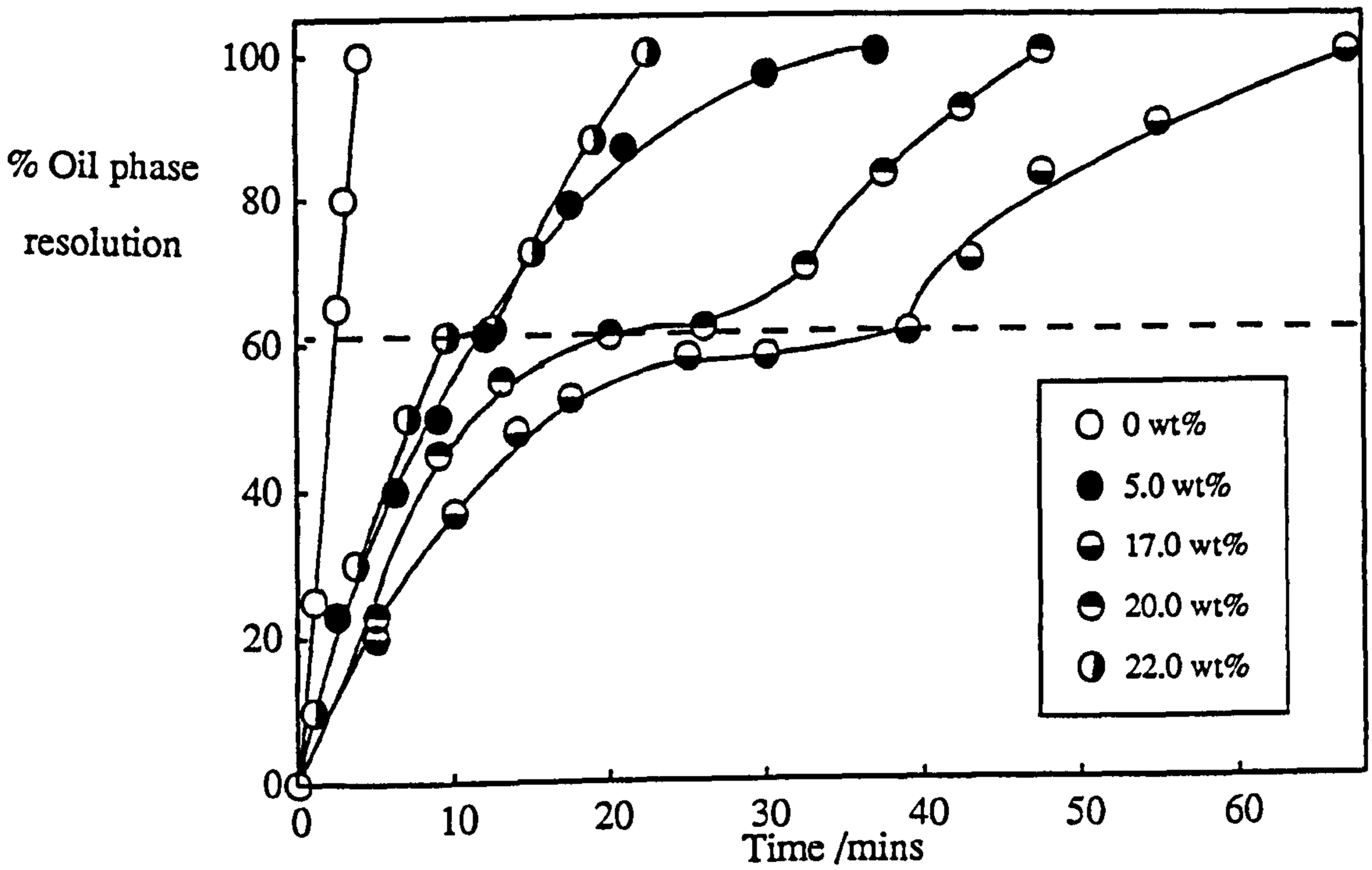

Figure 7.15b.

Water resolution curves corresponding to the emulsions outlined in the above legend.

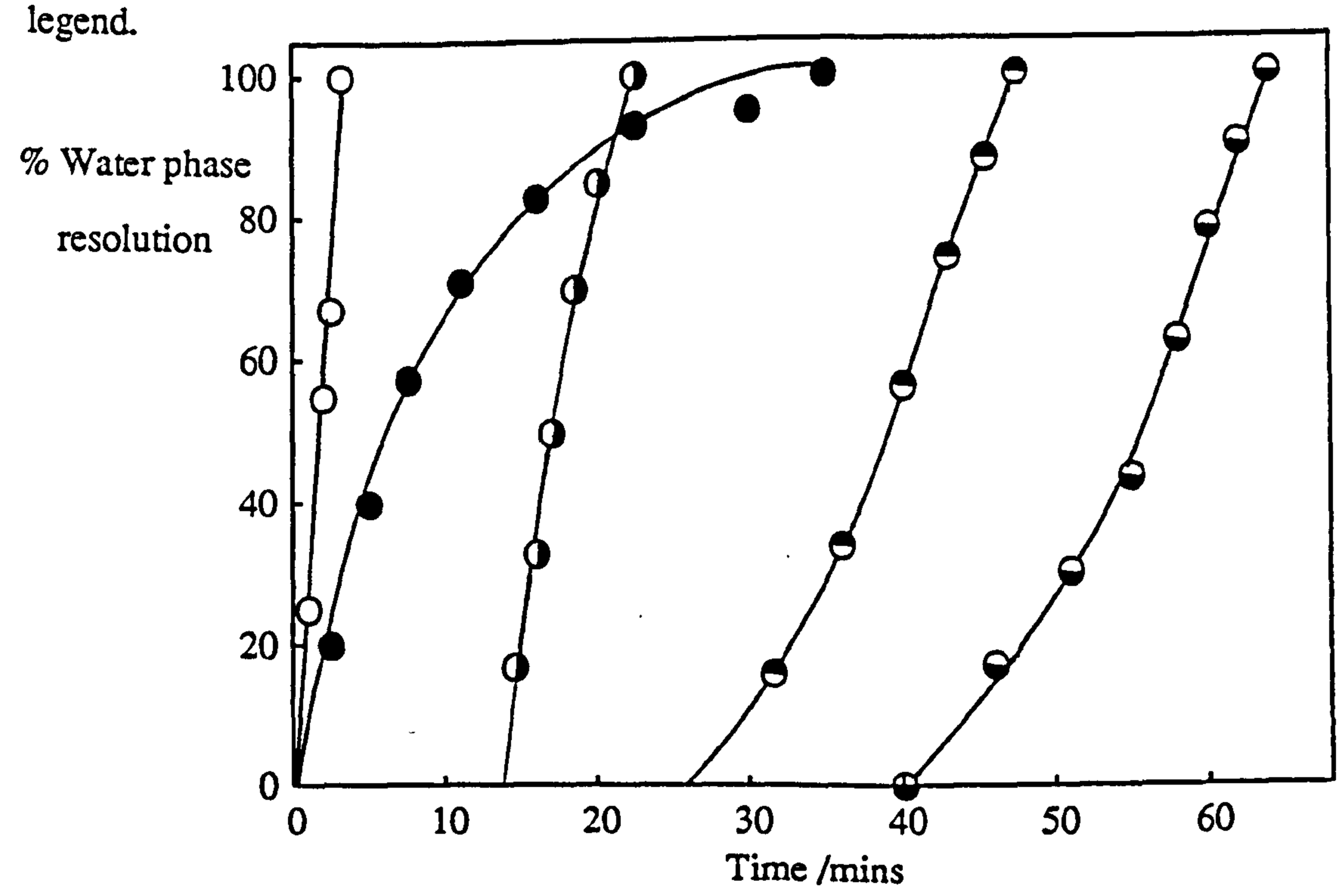

Figure 7.16a.

Variation of $t_{(25\%)}$ for oil resolution with surfactant concentration in 75% MCT. Temperature = 33.7°C, R'_{water} = 18. The emulsions were prepared by method I.

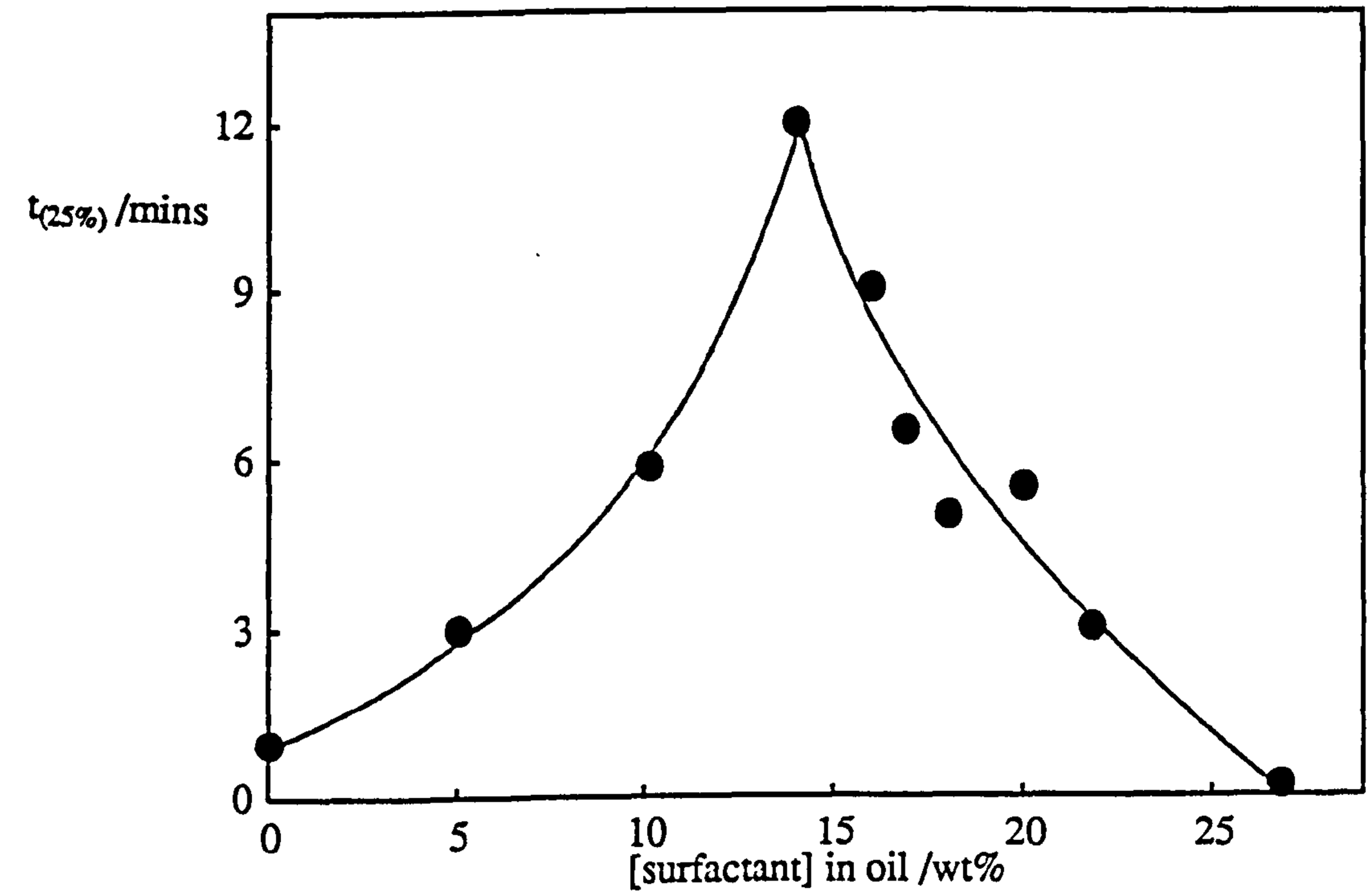

Figure 7.16b.

Variation of water resolution (droplet coalescence) with surfactant concentration for the emulsions outlined above.

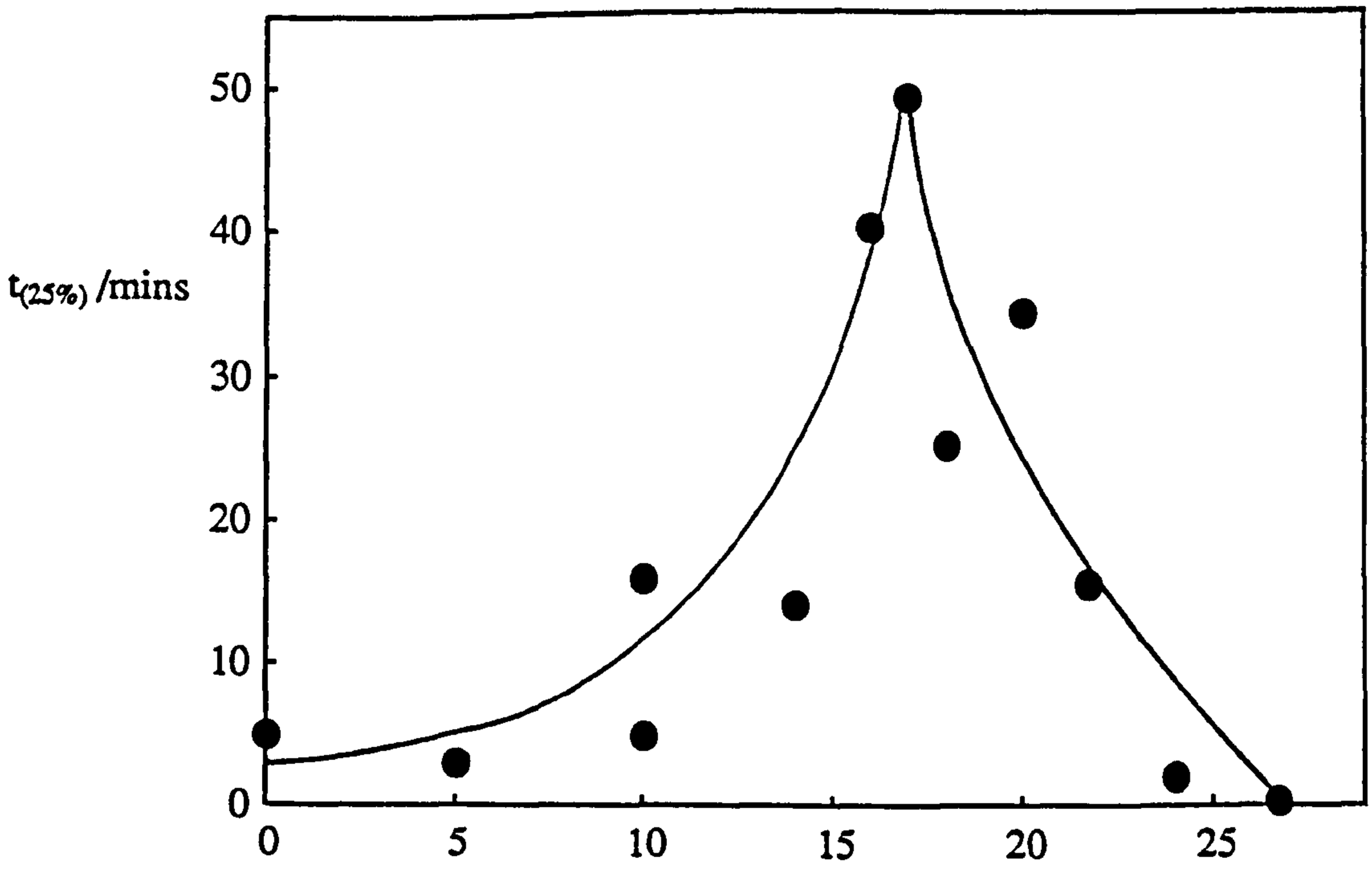

7.5 Conclusions.

From this study of W/O emulsions stabilised by $C_{12}E_4$ several important observations have been made relating microemulsion properties to emulsion stability.

(1). For all emulsions prepared with concentrations of surfactant less than the cμc, rapid resolution of both water and oil was observed. This is thought to be due to incomplete adsorption of surfactant at the oil-water interface.

(2). For emulsions prepared with surfactant at concentrations greater than the cμc, breakdown occurred primarily through a mechanism of droplet sedimentation. The concentration of surfactant required for maximum stability with respect to oil resolution, is plotted in Figure 7.17 against the critical microemulsion concentration for all systems investigated. The solid line shows a slope of unity. It is clear that maximum emulsion stability occurs at a surfactant concentration approximately equal to the cμc for the different surfactant systems investigated.

(3). The rate of oil phase resolution is accelerated by the presence of W/O microemulsion droplets in the continuous phase. For heptane as the oil phase the acceleration was observed to be rather insensitive to the size of the microemulsion aggregates for a fixed concentration of aggregated surfactant. These observations were shown to be reasonably consistent with a depletion flocculation mechanism if the microemulsion aggregates were assumed to behave like hard spheres.

(4). Increasing the cμc of the surfactant in the oil phase, either through the addition of MCT or by changing the temperature, was observed to produce a decrease in the stability of the emulsion. This is demonstrated in Figure 7.18 where the maximum value of the time for 15% oil resolution is plotted against the cμc for all the systems investigated. In the case of the highest cμc studied (75% MCT, cμc ≈ 16 wt%), the emulsion was highly unstable and resolution of both oil and water was observed. Since

Figure 7.17.

Correlation between the $C_{12}E_4$ concentration at which the slowest oil resolution is observed and the system cμc.

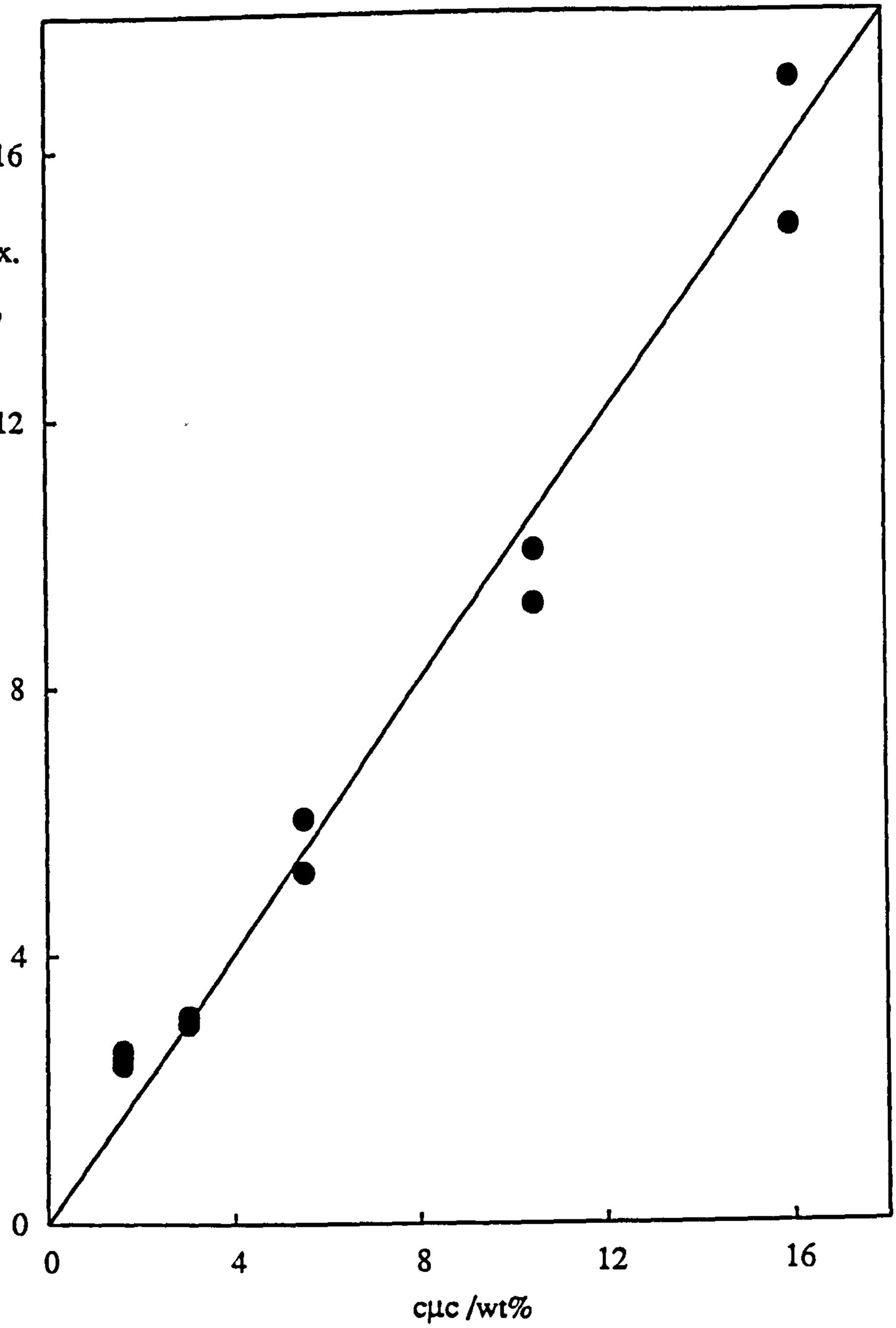

Figure 7.18.

Correlation between the maximum $t_{(15\%)}$ oil resolution (log scale) and the system cμc.

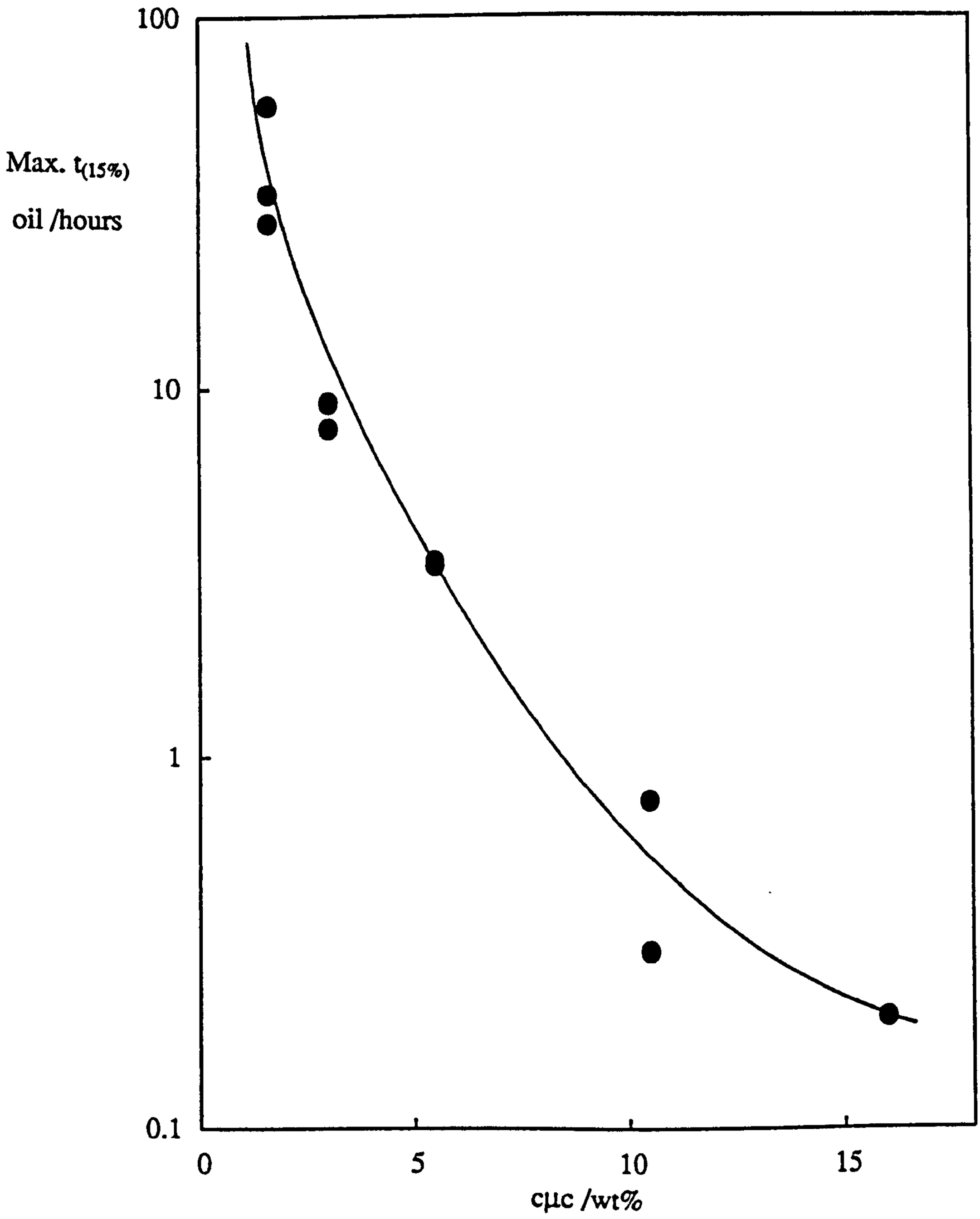

the maximum value of $t_{(15\%)}$ occurs close to the cμc where the microemulsion droplet concentration is effectively zero, the differences between the systems are presumably a consequence of some property of the monolayer stabilising the emulsion droplets. A possible explanation may be that, for low cμc systems, Marangoni tension gradients induced by emulsion droplet sedimentation act so as to resist the sedimentation process and hence slow down the oil phase resolution. Higher concentrations of surfactant in the oil phase i.e. higher cμc values, are expected to relieve the tension gradients and hence increase the rate of oil phase resolution.

7.6 Preliminary Observations of the Effects of BSA on the Stability of W/O Emulsions.

In commercial emulsion systems, stabilisation is rarely achieved by low molar mass surfactants alone. Frequently, macromolecules are also present which contribute to the overall stability of the product. In the case of food emulsions, these may be proteins or polysaccharides e.g. in margarine, the W/O emulsion is stabilised through a combination of monoglycerides and milk proteins (60).

Earlier in section 4.4.1, the effect of BSA on the position of the excess water solubilisation phase boundary was determined for water-in-heptane microemulsions stabilised by $C_{12}E_4$. In this final section, preliminary results for the effect of this protein on the stability of the corresponding macroemulsions are presented. As will be seen, the effects of added protein are complex and cannot be explained at present. At this preliminary stage, only the observations are reported.

Emulsions were prepared at 14.5°C which corresponded to a microemulsion droplet composition R'_{water}, of approximately 43 for the range of BSA concentrations investigated. Although the R'_{water} value is the same as that used for the no-protein systems, the temperature is shifted slightly due to the presence of the buffer. The cμc was previously determined to be virtually independent of protein concentration and was estimated to be 1.5 ± 0.5 wt%. The emulsions were prepared by method II, the initial stock emulsion being prepared with 2.4 wt% $C_{12}E_4$ in the oil and the aqueous phase containing the protein in 50 mM phosphate buffer at pH 7.0. The effect of the concentration of microemulsion aggregates was investigated for 0, 10 and 50 mg/ml BSA in the aqueous phase. The initial emulsion drop size was estimated by microscopy to be of the order of 1 μm in each case.

As was observed for the systems described in section 7.2 (i.e. containing no protein or phosphate buffer), water resolution was only observed for surfactant

concentrations below the cμc (1.5 wt%). For these surfactant concentrations, rapid oil resolution was also seen. For concentrations in excess of 1.5 wt% only resolution of the oil phase was observed with no water phase separation occurring over a monitoring period of fourteen days. As seen in Figure 7.19, the stability ($t_{(15\%)}$ of the oil phase) of the two protein containing systems passes through a maximum upon increasing the surfactant concentration. However, the surfactant concentrations corresponding to the maxima are significantly *higher* than the cμc for these BSA containing systems. Additionally, the oil phase resolution rates in each case are faster than those observed previously for water alone as the dispersed phase.

The cμc of the surfactant in the resolved oil phases was checked to see if it was in agreement with that found previously by turbidity titration. This was performed by; (i) extracting samples of the resolved oil phase and measuring the water content by Karl Fischer titrations, and (ii) determining the change in absorbance of samples of the oil phase upon warming to 30°C (i.e. detecting the change in turbidity upon crossing the solubilisation phase boundary). From these analyses the cμc for both protein concentrations was determined to be within the range 1.6 - 2.2 wt% in agreement with the values determined from the microemulsion phase studies. This check demonstrates that a significant fraction of the surfactant is not bound to the BSA dissolved in the aqueous phase. This finding is consistent with the protein-binding studies of Nishikido *et al.* who found that for a similar protein concentration, only four molecules of $C_{12}E_6$ were bound per BSA molecule (209).

The effects of BSA in shifting the concentration of surfactant required for maximum emulsion stabilisation and increasing the rate of oil phase resolution cannot be explained at present. Further detailed studies are required (e.g. into the composition of the monolayer and the effect of pre-equilibration) before these effects may be understood in terms of quantitative theories.

Figure 7.19.

Effect of BSA concentration on the variation of $t_{(15\%)}$ oil resolution with surfactant concentration in heptane. The W/O emulsions were prepared by method II, temperature = 14.5°C, R'_{water} = 43.

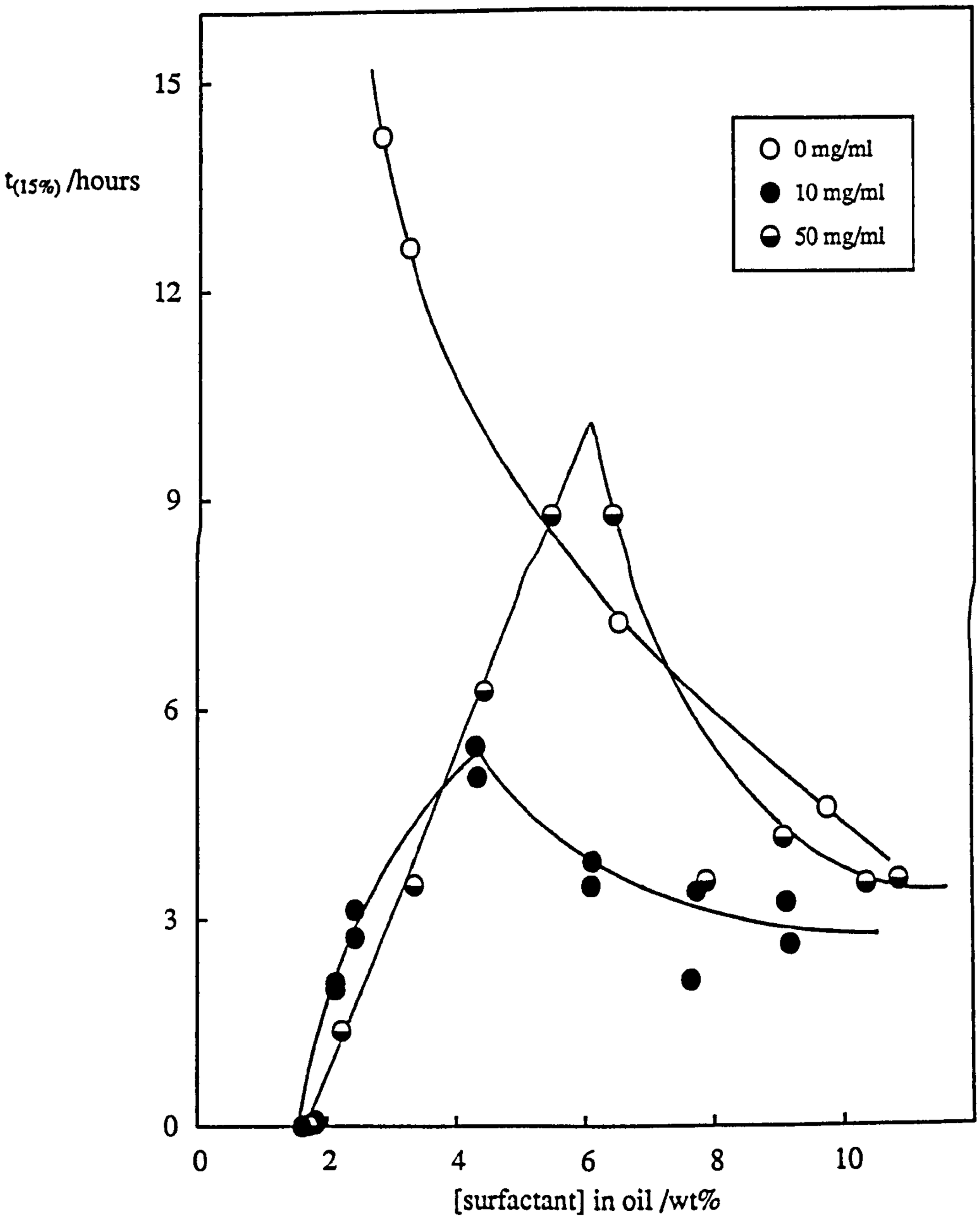

8. SUMMARY.

CHAPTER 8.

This thesis has been concerned with various microemulsion and macroemulsion properties of mixtures of oil + water + nonionic surfactant. Initially, studies were performed with commercial, food type surfactants. These are complex, poorly characterised mixtures which upon emulsification of two phase oil-water systems were observed to produce highly stable emulsions. Since initial microemulsion solubilisation studies did not indicate their behaviour to be peculiar or specific, it was decided to use the more amenable pure, nonionic surfactants of the type C_nE_m for all subsequent studies. The main conclusions relating to this work are summarised below.

(1) Microemulsions are observed to be formed in oil above a certain surfactant concentration, called the *critical microemulsion concentration*, cμc. The effect of several variables on the cμc have been determined. These are tabulated below in Table 8.1.

Table 8.1

Increase in	Change in cμc
Head group ethoxylation	Decrease
Alkane chain length	Decrease
Temperature	Increase
Salt concentration	Increase

An approximate correlation has been shown to exist between the cμc and the ratio of dispersed water to aggregated surfactant, R'_{water}.

(2) For all W/O microemulsion systems investigated, an approximate linear dependence is observed between the droplet size and the microemulsion composition

(R'_{water}). This suggests that the effective area per surfactant head group at the droplet surface remains constant. The variation of the droplet size (and hence droplet curvature) with temperature in a Winsor II system may be interpreted in terms of changes in the effective area per surfactant tail group. This may be induced through changes in the degree of oil penetration into the tail region. An alternative possibility is also considered in which changes in the droplet curvature are achieved through changes in the surfactant monolayer thickness. Both these limiting models are found to account for the observed solubilisation behaviour. In microemulsion systems, both may occur to varying extents to bring about changes in the preferred curvature of the surfactant monolayer.

(3) Using an approximate relationship between the interfacial tension and the microemulsion droplet size, values for the rigidity parameter ($K+\bar{K}/2$) have been estimated for several nonionic surfactant systems. In each case, the uncertainties in the values are of the same order of magnitude as the values themselves which are typically of the order of kT for all systems investigated. Furthermore, the rigidity modulii K and $\bar{K}$ cannot be estimated separately. It may be concluded for these reasons that this treatment is not a good method of estimating monolayer rigidity.

(4) Incorporation of triglyceride into the oil phase dramatically increases the cμc. When the oil phase comprises of 75% MCT, cμc values for $C_{12}E_4$ of the order of 20 wt% (~0.3 M) may be attained. The enthalpy change upon transfer of a mole of $C_{12}E_4$ from monomers in the oil phase to the aggregated state decreases from -42 ± 10 kJ mol^{-1} in heptane to -26 ± 5 kJ mol^{-1} in 50% MCT and -19 ± 8 kJ mol^{-1} in 75% MCT. This reflects the increasing affinity of the surfactant for the increasingly polar oil phase.

Upon increasing the concentration of MCT in the oil phase above 25%, the maximum degree of water solubilisation is decreased. The one phase stability region is

also shifted to higher temperatures presumably indicating a reduced penetration of the oil into the surfactant tail region. For lower MCT concentrations however, the one phase region is shifted to slightly lower temperatures. This may now indicate preferential solvation of the tail region by the triglyceride molecules.

(5) Using the technique of time-resolved fluorimetry, microemulsion droplet radii have been determined for several W/O microemulsion systems. The droplet sizes are found to be independent of droplet volume fraction and temperature at a constant R'_{water} value. Light scattering measurements show that the apparent diffusion coefficient of the droplets decreases as the temperature is decreased (on moving away from the solubilisation phase boundary towards the haze boundary). The combination of techniques shows that this is due to increasing attractive interactions between the droplets.

From the determination of the first order rate constant for quenching within a microemulsion droplet, an estimate of the dispersed phase microviscosity has been given. For all systems studied, these values appear to indicate that the viscosity is approximately ten times that of bulk water.

The second order microemulsion exchange rate constant is observed to be a minimum at the solubilisation phase boundary for all systems investigated. This corresponds to the situation at which inter-droplet attractions are a minimum and the microemulsion aggregates are closest to their natural curvature.

For W/O microemulsions stabilised by $C_{12}E_4$ in heptane and 50% MCT, the exchange rate constants at the solubilisation phase boundaries (after correcting for the effects of the different bulk phase viscosities) are observed to be similar. If the energy required to desorb surfactant from the droplet surface is a significant factor in the formation in the transition state, an enhanced rate might have been expected for the 50% MCT system since the cμc is approximately five times that in heptane. The fact

that this is not observed may indicate that other factors are more important in the formation of the transition state. One such factor may be the monolayer bending rigidity, K. Although the two systems exhibit similar values of $(K+\bar{K}/2)$ the large errors associated with these values and the relative magnitudes of the parameters K and $\bar{K}$ are unknown.

(6) Microemulsion exchange rates have been determined for three surfactant systems for which monolayer bending rigidities have been reported (167). The exchange rate constants have been determined at the solubilisation phase boundaries at a droplet composition of $R'_{water} = 8$. The rate constants are observed to follow the order $C_{12}E_5$/hexane < $C_{10}E_4$/octane < C_8E_3/decane. This order parallels that reported for the values of the monolayer bending rigidity constants (K) for these three surfactant systems i.e. the exchange rate increases as the monolayer rigidity decreases.

The surfactant monolayer rigidity may also be one of the factors expected to affect the rate of *macroemulsion* droplet coalescence. This has been investigated for W/O emulsions prepared with these three surfactant systems at temperatures corresponding to an R'_{water} value of 8 in the equilibrium microemulsion system. The water resolution rate is observed to decrease rapidly in the order in which the monolayer bending rigidity increases. A correlation appears therefore, to exist between the microemulsion exchange rate, the rate of macroemulsion water resolution and the monolayer bending rigidity.

(7) Investigations into the stability of W/O macroemulsions stabilised by $C_{12}E_4$ have been presented. For all emulsions prepared with surfactant concentrations less than the cμc, rapid resolution of both oil and water phases is observed. This is thought to be due to incomplete saturation adsorption at the oil-water interface. For emulsions prepared with $C_{12}E_4$ in heptane or 50% MCT as the oil phase at concentrations in excess of the

cμc, the major breakdown mechanism operative over the experimental time scale is that of droplet sedimentation. This leads to a concentrated W/O emulsion being formed at the base of the tube. Emulsions prepared with 75% MCT however, are observed to breakdown by resolution of both water and oil phases at all surfactant concentrations.

For all these systems, there is an optimum surfactant concentration at which maximum stability is achieved. This concentration is found in all cases to be approximately equal to the surfactant cμc in the oil phase. Additionally, systems with the lowest cμc values exhibited the highest maximum stabilities. The addition of microemulsion droplets to the oil phase is observed to accelerate the rate of oil phase resolution. For a fixed concentration of *aggregated* surfactant, the acceleration rate is observed to be rather insensitive to the size of the microemulsion droplets. These observations are reasonably consistent with a depletion flocculation mechanism if the microemulsion droplets are assumed to behave as hard spheres.

REFERENCES.

REFERENCES.

(1) N. Boden, *Chem. in Britain*, **26**, 345, (1990).

(2) P. Becher in *Microemulsions and Emulsions in Foods*, Eds. M. El-Nokaly, D. Cornell, A.C.S. Symposium Series 448, Washington D.C., (1991).

(3) S. S. Davis, J. Hadgraft and K. J. Palin, in *Encyclopedia of Emulsion Technology*, Vol. 2, pp. 159, Ed. P. Becher, Marcel Dekker Inc., New York, (1985).

(4) K. H. Raney, W. J. Benton and C. A. Miller, *J. Colloid Int. Sci.*, **117**, 282, (1987).

(5) D. Z. Becher in ref (3) above ch. 4, pp. 239.

(6) M. K. Sharma and D. O. Shah, in *Macro- and Microemulsions - Theory and Applications*, Ed. D. O. Shah, A.C.S. Symposium Series 272, Washington D.C., (1985).

(7) B. W. Davies in *Encyclopedia of Emulsion Technology*, Vol. 3, pp. 307, Ed. P. Becher, Marcel Dekker Inc., New York and Basel, (1988).

(8) J. W. McBain and C. S. Salmon, *J. Amer. Chem, Soc.*, **43**, 426, (1920).

(9) P. Mukerjee and K. J. Mysels, *Critical Micelle Concentrations of Aqueous Surfactant Systems*, National Bureau of Standards, Washington, (1971).

(10) C. Tanford, *The Hydrophobic Effect : Formation of Micelles and Biological Membranes*, 2nd Edition, Wiley, New York, (1980).

(11) J. M. Corkill, J. F. Goodman and J. R. Tate, *Trans. Faraday Soc.*, **60**, 996, (1964).

(12) L. Benjamin, *J. Phys. Chem.*, **68**, 3575, (1964).

(13) J. M. Corkill, J. F. Goodman and S. P. Harrold, *Trans. Faraday Soc.*, **60**, 202, (1964).

(14) *Surfactants and Interfacial Phenomena*, Ed. M. J. Rosen, John Wiley & Sons, New York, (1989).

(15) J. M. Corkill and J. F. Goodman, *Adv. Colloid Int. Sci.*, **2**, 297, (1969).

(16) R. H. Ottewill, *Ann. Rep. Chem. Soc.*, **A66**, 183, (1969).

(17) J. S. Clunie, J. F. Goodman and P. C. Symons, *Trans. Faraday Soc.*, **65**, 287, (1969).

(18) E. A. G. Aniansson, S. N. Wall, M. Almgren, H. Hoffmann, I. Kielmann, W. Ulbricht, R. Zana, J. Lang and C. Tondre, *J. Phys. Chem.*, **80**, 905, (1976).

(19) C. Tondre and R. Zana, *J. Colloid Int. Sci.*, **66**, 544, (1978).

(20) T. Yasunaga, K. Takeda and S. Harada, *J. Colloid Int. Sci.*, **42**, 457, (1973).

(21) J. Rassing, P. J. Sams and E. Wyn-Jones, *J. Chem. Soc.*, **69**, 180, (1973).

(22) P. Jones, E. Wyn-Jones and G. J. T. Tiddy, *J. Chem. Soc. Faraday Trans. 1*, **83**, 2735, (1987).

(23) F. Y.-F. Lo, B. M. Escott, E. J. Fendler, E. T. Adams, R. D. Larsen and P. W. Smith, *J. Phys. Chem.*, **79**, 2609, (1975).

(24) T. P. Hoar and J. H. Schulman, *Nature*, **152**, 102, (1943).

(25) V. K. Bansal and D. O. Shah, in *Microemulsions*, Ed. L. M. Prince, pp. 149, Academic Press, New York, London, (1977).

(26) B. H. Robinson, A. N. Khan-Lodhi and T. Towey, in *Structure and Reactivity in Reverse Micelles*, Ed. M. P. Pileni, pp. 198, Elsevier, Amsterdam, (1989).

(27) K. E. Goklen and T. A. Hatton, *Sep. Sci. Tech.*, **22**, 831, (1987).

(28) E. Ruckenstein and J. Chi, *J. Chem. Soc. Faraday Trans. II*, **71**, 1690, (1975).

(29) R. Aveyard, B. P. Binks and P. D. I. Fletcher, *Langmuir*, **5**, 1211, (1989).

(30) J. Kizling and P. Stenius, *J. Colloid Int. Sci.*, **118**, 482, (1987).

(31) K. Shinoda, H. Kunieda, T. Arai and H. Saijo, *J. Phys. Chem.*, **88**, 5126, (1984).

(32) K. Shinoda and H. Kunieda, *J. Disp. Sci. Tech.*, **3**, 233, (1982).

(33) M. Kahlweit, E. Lessner and R. Strey, *J. Phys. Chem.*, **87**, 5032, (1983).

(34) M. Kahlweit and R. Strey, *Angew. Chem. Int. Ed. Engl.*, **24**, 654, (1985).

(35) P. A. Winsor, *Trans. Faraday Soc.*, **44**, 376, (1948).

(36) R. Aveyard, *Chem. and Ind.*, July, 474, (1987).

(37) D. J. Mitchell and B. W. Ninham, *J. Chem. Soc. Faraday Trans. II*, 77, 601, (1981).

(38) R. Aveyard, B. P. Binks and P. D. I. Fletcher, in *The Structure, Dynamics and Equilibrium Properties of Colloidal Systems*, Eds. D. M. Bloor, E. Wyn-Jones, pp. 557, Kluwer Academic Pub., Amsterdam, (1990).

(39) R. Aveyard, B. P. Binks and J. Mead, *J. Chem. Soc. Faraday Trans. 1*, 81, 2169, (1985).

(40) R. Aveyard and T. A. Lawless, *J. Chem. Soc. Faraday Trans. 1*, 82, 2951, (1986).

(41) *Surfactant Systems - their chemistry, pharmacy and biology*, D. Attwood, A. T. Florence, Chapman and Hall, London and New York, (1983).

(42) R. Aveyard, B. P. Binks, S. Clark and P. D. I. Fletcher, *J. Chem. Soc. Faraday Trans.* 86, 3111, (1990).

(43) M. E. Cates, D. Andelman, S. A. Safran and D. Roux, *Langmuir*, 4, 802, (1988).

(44) W. Helfrich and W. Harbich, in *Physics of Amphiphilic Layers*, Eds. J. Meunier, D. Langevin, N. Boccara, Springer-Verlag, Berlin, Heidelberg, New York, (1987).

(45) P.-G. de Gennes and C. Taupin, *J. Phys. Chem.*, 86, 2294, (1982).

(46) B. P. Binks, J. Meunier, O. Abillon and D. Langevin, *Langmuir*, 5, 415, (1989).

(47) M. V. Z. Smoluchowski, Phys. Chem. 92, 129, (1917).

(48) P. D. I. Fletcher, *J. Chem. Soc. Faraday Trans. 1*, 83, 1493, (1987).

(49) A. Jada, J. Lang, S.-J. Candau and R. Zana, *Colloids and Surfaces*, 38, 251, (1989).

(50) P. D. I. Fletcher, A. M. Howe and B. H. Robinson, *J. Chem. Soc. Faraday Trans. 1*, 83, 985, (1987).

(51) P. D. I. Fletcher and J. F. Holzwarth, *J. Phys. Chem.*, 95, 2550, (1991).

(52) P. D. I. Fletcher and D. Parrott, in *Chemical and Biological Reactions in Compartmentalised Liquids*, Eds. W. Knoche, R. Schomacker, pp.53, Springer-Verlag, Berlin, (1989).

(53) A. Jada, J. Lang and R. Zana, *J. Phys. Chem.*, **93**, 10, (1989).

(54) A. Jada, J. Lang, R. Zana, R. Makloufi, E. Hirsch and S. J. Candau, *J. Phys. Chem.*, **94**, 387, (1990).

(55) S. Clark, P. D. I. Fletcher and X. Ye, *Langmuir*, **6**, 1301, (1990).

(56) H. F. Eicke, J. C. W. Shepherd and A. Steinmann, *J. Colloid Int. Sci.*, **56**, 168, (1976).

(57) S. S. Atik and J. K. Thomas, *J. Am. Chem. Soc.*, **103**, 3543, (1981).

(58) R. Zana and J. Lang, in *Physics of Amphiphilic Layers*, Eds. J. Meunier, D. Langevin, N. Boccara, Springer, Berlin, Heidelberg, New York, (1987).

(59) P. D. I. Fletcher and B. H. Robinson, *unpublished results*.

(60) D. F. Darling and R. J. Birkett in *Food Emulsions and Foams*, Ed. E. Dickinson, pp. 1, Royal Society of Chemistry, Special pub. No. 58, (1987).

(61) P. L. Luisi, P. Meier, V. E. Imre and A. Pande, in *Reverse Micelles*, Eds. P. L. Luisi, B. E. Straub, pp. 323, Plenum Press, New York and London, (1984).

(62) M. P. Pileni in *Structure and Reactivity in Reverse Micelles*, Ed. M. P. Pileni, pp. 44, Elsevier, Amsterdam, (1989).

(63) Yu. L. Khmelnitsky, A. V. Kabanov, N. L. Klyachko, A. V. Levashov and K. Martinek, in *Structure and Reactivity in Reverse Micelles*, Ed. M. P. Pileni, pp. 230, Elsevier, Amsterdam, (1989).

(64) S. Barbaric and P. L. Luisi, *J. Amer. Chem. Soc.*, **103**, 4239, (1981).

(65) C. Grand, R. E. Smith and P. L. Luisi, *J. Biol. Chem.*, **256**, 837, (1981).

(66) D. Han, P. Walde and P. L. Luisi, *Biocatalysis*, **4**, 153, (1990).

(67) P. L. Luisi, *Angew. Chem. Int. Ed. Engl.*, **24**, 439, (1985).

(68) P. D. I. Fletcher, G. D. Rees, B. H. Robinson and R. B. Freedman, *Biochimica et Biophysica Acta*, **832**, 204, (1985).

(69) P. D. I. Fletcher and B. H. Robinson, *J. Chem. Soc. Faraday Trans. 1*, **80**, 2417, (1984).

(70) C. Jolivalt, M. Minier and H. Renon, *J. Colloid Int. Sci.*, **135**, 85, (1990).

(71) K. E. Goklen and T. A. Hatton, *Bio. Tech. Prog.*, **1**, 1, (1985).

(72) J. Woll and T. A. Hatton, *Mol. Cell. Biol.*, **68**, 117, (1987).

(73) *Emulsions : Theory and Practice*, P. Becher, Krieger Pub., New York, (1977).

(74) N. Krog, *J. Amer. Oil Chem. Soc.*, **54**, 124, (1977).

(75) H. A. Bampfield and J. Cooper, in *Encyclopedia of Emulsion Technology*, Vol. 3, Ed. P. Becher, pp. 281, Marcel Dekker, New York and Basel, (1988).

(76) *The Theory of Emulsions and Their Technical Treatment*, 4th edn., W. Clayton, The Blackinston Co., New York, (1943).

(77) W. C. Griffin, *J. Soc. Cosmet. Chem.*, **1**, 311, (1949).

(78) W. C. Griffin, *J. Soc. Cosmet. Chem.*, **5**, 249, (1954).

(79) W. D. Bancroft, *J. Phys. Chem.*, **17**, 514, (1913).

(80) *Emulsions and Solubilisation*, K. Shinoda, S. Friberg, John Wiley and Sons, New York, (1986).

(81) J. T. Davies and E. K. Rideal, *Interfacial Phenomena*, 2nd edn., Academic Press, London, (1963).

(82) L. M. Baldauf, R. S. Schechter, W. H. Wade and A. Graciaa, *J. Colloid Int. Sci.*, **85**, 187, (1982).

(83) R. E. Anton and J. L. Salager, *J. Colloid Int. Sci.*, **111**, 54, (1986).

(84) E. Dickinson and S. R. Euston, in *Food Polymers, Gels and Colloids*, Ed. E. Dickinson, Royal Soc. Chem., Cambridge, (1991).

(85) R. I. Feigin and D. H. Napper, *J. Colloid Int. Sci.*, **75**, 525, (1980).

(86) M. P. Aronson, *Langmuir*, **5**, 494, (1989).

(87) S. Asakura and F. Oosawa, *J. Chem. Phys.*, **22**, 1255, (1954).

(88) S. Asakura and F. Oosawa, *J. Polym. Sci.*, **33**, 183, (1958).

(89) B. Vincent in *Surfactants*, Ed. Th. F. Tadros, pp. 175, Academic Press, London, (1984).

(90) J. B. Rijnbout, W. A. B. Donners and A. Vrij, *Nature*, **249**, 242, (1974).

(91) R. Buscall and R. H. Ottewill, in *Colloid Science*, Vol. 2, pp. 191, Ed. D. H. Everett, The Chemical Soc., Thanet Press, Margate, (1975).

(92) J. Boyd, C. Parkinson and P. Sherman, J. Colloid Int. Sci., 41, 359, (1972).

(93) J. Lyklema in *Colloidal Dispersions*, Ed. J. W. Goodwin, pp. 47, Royal Soc. Chem., London, (1982).

(94) B. V. Derjaguin and L. Landau, *Acta Physiochem. U.S.S.R.*, **14**, 633, (1941).

(95) *Theory of the stability of Lyophobic Colloids*, E. J. W. Verwey and J. Th. G. Overbeek, Elsevier, Amsterdam, (1948).

(96) D. H. Napper in *Colloidal Dispersions*, Ed. J. W. Goodwin, pp. 99, Royal Soc. Chem., London, (1982).

(97) *Polymeric Stabilisation of Colloidal Dispersions*, D. H. Napper, Academic Press, (1983).

(98) H. Saito and K. Shinoda, *J. Colloid Int. Sci.*, **35**, 359, (1971).

(99) B. Vonnegut, *Rev. Sci. Instr.*, **13**, 6, (1942).

(100) A. W. Adamson, *Physical Chemistry of Surfaces*, Wiley, New York, (1976), Ch. 1.

(101) H. M. Princen, I. Y. Z. Zia and S. G. Mason, *J. Colloid. Int. Sci.* **23**, 99, (1967).

(102) D. J. Donahue and F. E. Bartell, *J. Phys. Chem.* **56**, 480 (1952).

(103) B. P. Binks, *Ph.D. Thesis*, Chapter 2, Univ. of Hull, (1986).

(104) M. Kerker, *The Scattering of light*, Academic Press, New York, 1969.

(105) P. N. Pusey, in *Colloidal Dispersions*, Ed. J. W. Goodwin, pp.129, Royal Soc. Chem., London, (1982).

(106) A. M. Cazabat and D. Langevin, *J. Chem. Phys.* **74**, 3148, (1981).

(107) R. A. Day, B. H. Robinson, J. H. R. Clarke and J. V. Doherty, *J. Chem. Soc. Faraday Trans.* 1, **75**, 132, (1979).

(108) D. E. Koppel, *J. Chem. Phys.*, **57**, 4814, (1972).

(109) *Curve-Fitter*, J. Mead, University of Hull, (1987).

(110) M. Almgren and J.-E. Lofroth, *J. Colloid Int. Sci.*, **81**, 486, (1981).

(111) M. Almgren, J.-E. Lofroth and R. Rydholm, *Chem. Phys. Lett.*, **63**, 265, (1979).

(112) M. Almgren, J. Alsins, E. Mukhtar and J. van Stam, *J. Phys. Chem.*, **92**, 4479, (1988).

(113) N. J. Turro and P.-L. Kuo, *Langmuir*, **2**, 438, (1986).

(114) R. Makhloufi, E. Hirsch, S. J. Candau, W. Binana-Limbele and R. Zana, *J. Phys. Chem.*, **93**, 8095, (1989).

(115) R. Zana and B. Michels, *J. Phys. Chem.*, **93**, 2643, (1989).

(116) J. Lang in *The Structure, Dynamics and Equilibrium properties of Colloidal Systems*, Eds. D. M. Bloor and E. Wyn-Jones, pp. 1, Kluwer Academic Publishers, Amsterdam, (1990).

(117) R. Zana in *Surfactant Solutions - New Methods of Investigation*, Ed. R. Zana, Ch. 5, Surfactant Science Series, Vol. 22.

(118) W. R. Ware in *Time - Resolved Fluorescence Spectroscopy in Biochemistry and Biology*, Eds. R. B. Cundall and R. E. Dale, pp. 23, Plenum Press, (1983).

(119) D. J. S. Birch and R. E. Imhof in *Picosecond Chemistry and Biology*, Eds. T. A. M. Doust and M. A. West, Science Reviews, (1984).

(120) Edinburgh Instruments 199 user manual.

(121) J. Van Houten and R. J. Watts, *J. Am. Chem. Soc.*, **98**, 4853, (1976).

(122) J. N. Demas, D. Diemente and E. W. Harris, *J. Am. Chem. Soc.* , **95**, 6864, (1973).

(123) *Handbook of Chemistry and Physics*, C. R. C. Press, 62nd Edition, (1981-82).

(124) K. Fischer, *Angew. Chem.* **48**, *394*, *(1935)*.

(125) N. Garti, E. Wellner, A. Aserin and S. Sarig, *J. Amer. Oil Chem. Soc.* **60**, 1151, (1983).

(126) Manufacturers specifications.

(127) M. Andrangui, F. Puisieux, M. Seiller, E. Morszanyi and A.-M. Orecchioni, *Pharm. Acta Helv.*, **54**, 214, (1979).

(128) J. Timmermans, *Physiochemical Constants of Pure Organic Compounds*, (Elsevier, New York, (1950).

(129) K.-V. Schubert, R. Strey and M. Kahlweit, *J. Colloid Int. Sci.*, **141**, 21, (1991).

(130) P. G. Righetti and T. Caravaggio, *J. Chromatography*, **127**, 1, (1976).

(131) *Data for Biochemical Research*, 3rd edn, Eds. R. M. C. Dawson, D. C. Elliott, W. H. Elliott, K. M. Jones, Clarendon Press, Oxford, (1986).

(132) *Milk Proteins: Chemistry and Molecular Biology*, Vol. 2, Ed. H. A. McKenzie, Academic Press, New York, (1970).

(133) K. Shinoda, *Progr. Colloid Polymer Sci.* **68**, 1, (1983).

(134) D. O. Shah and M.-J. Hou, *Langmuir* **3**, 1086, (1987).

(135) D. O. Shah and R. Leung, *J. Colloid Int. Sci.* **120**, 320, (1987).

(136) K. Shinoda, *J. Colloid Int. Sci.* **24**, 4, (1967).

(137) R. Aveyard, B. P. Binks, P. D. I. Fletcher and J. R. Lu, *J. Colloid Int. Sci.* **139**, 128, (1990).

(138) K. Shinoda and H. Kunieda, *J. Colloid Int. Sci.* **42**, 381, (1973).

(139) K. Shinoda and H. Arai, *J. Colloid Int. Sci.* **25**, 396, (1967).

(140) M. Kahlweit, *J. Colloid Int. Sci.* **90**, 197, (1982).

(141) M. Kahlweit, E. Lessner and R. Strey, *J. Phys. Chem.* **88**, 1937, (1984).

(142) Information supplied by Unilever (Colworth).

(143) B. Vincent, R. Davies and D. E. Graham, *J. Colloid Int. Sci.* **116**, 88, (1986).

(144) K. A. Johnson and D. O. Shah in *Surfactants in Solution*, Eds. K. L. Mittal, P. Bothorel, Vol. 6, pp. 1441, Plenum Press, (1986).

(145) K. Shinoda and T. Ogawa, *J. Colloid Int. Sci.* **24**, 56, (1967).

(146) J. L. Salager, I. Loaiza-Maldonado, M. Minana-Perez and F. Silva, *J. Dispers. Sci. Technol.* **3**, 279, (1982).

(147) J. C. Ravey, M. Buzier and C. Picot, *J. Colloid Int. Sci.* **97**, 9, (1984).

(148) M. Kahlweit, *J. Colloid Int. Sci.*, **118**, 436, (1987).

(149) R. Aveyard, B. P. Binks and J. Mead, *J. Chem. Soc. Faraday Trans. 1*, **82**, 1755, (1986).

(150) S. Mukherjee, C. A. Miller and T. Fort, *J. Colloid Int. Sci.* **91**, 223, (1983).

(151) K. Shinoda, K. Fukuda and A. Carlsson, *Langmuir*, **6**, 334, (1990).

(152) E. Dickinson and C. Woskett, in *Food Colloids*, pp. 74, Royal Soc. Chem., Special Pub. 75, (1989).

(153) J. A. De Feijter, J. Benjamins and M. Tamboer, *Colloids and Surfaces*, **27**, 243, (1987).

(154) E. Dickinson, B. S. Murray and G. Stainsby, in *Advances in Food Emulsions and Foams*, Eds. E. Dickinson, G. Stainsby. Elsevier Applied Science. London (1988).

(155) D. M. Blow in *The Enzymes*, 3rd Edition, Vol. 3, Ed. P. D. Boyer, pp 185-212, Academic Press, New York, London, (1971).

(156) A. K. Wright and M. R. Thompson, *J. Biophys.* **15**, 137, (1975).

(157) E. Dickinson and G. Stainsby, *Colloids in Food*, Applied Science, London, (1982).

(158) L. K. Creamer and G. D. Berry, *J. Dairy Res.* **42**, 169, (1975).

(159) G. K. Batchelor, *J. Fluid Mech.* **74**, 1, (1976).

(160) R. Aveyard, B. P. Binks, T. A. Lawless and J. Mead, *J. Chem. Soc. Faraday Trans.* 1, **81**, 2155, (1985).

(161) H. Kunieda and K. Shinoda, *Bull. Chem. Soc. Jpn.* **55**, 1777, (1982).

(162) J. Meunier, *J. Physique Lett.* **46**, 1005, (1985).

(163) E. van der Linden, *Ph.D. Thesis*, Leiden, 1990.

(164) B. Farago, D. Richter, J. S. Huang, S. A. Safran and S. T. Milner, *Phys. Rev. Lett.* **65**, 3348, (1990).

(165) A. Brun and J.- M. di Meglio, *Mol. Cryst. Liq. Cryst.* **159**, 1, (1988).

(166) B. P. Binks, J. Meunier and H. Kellay, in press *Euro. Phys. Lett.*, (1991).

(167) L. T. Lee, D. Langevin, J. Meunier, K. Wong and B. Cabane, *Prog. Colloid Polym. Sci.* **81**, 209, (1990).

(168) J. Meunier, *J. Physique*, **48**, 1819, (1987).

(169) W. Helfrich, *J. Physique*, **46**, 1263, (1985).

(170) L. Peliti and S. Leibler, *Phys. Rev. Lett.* **54**, 1690, (1985).

(171) P. Infelta, M. Gratzel and J. K. Thomas, *J. Phys. Chem.* **78**, 190, (1974).

(172) M. Tachiya, *Chem. Phys. Lett.* **33**, 289, (1975).

(173) M. Almgren, J.-E. Lofroth and J. van Stam, *J. Phys. Chem.* **90**, 4431, (1986).

(174) O. Johanson, A. W. H. Mau and W. H. F. Sasse, *Chem. Phys. Lett.* **94**, 113, (1983).

(175) R. Johannsson, M. Almgren and J. Alsins, E.C.I.S. Sept 1990 meeting, Italy.

(176) J. V. Caspar and T. J. Meyer, *J. Amer. Chem. Soc.*, **105**, 5583, (1983).

(177) C. R. Safinya, E. B. Sirota, D. Roux and G. S. Smith, Phys. Rev. Lett. 62, 1134, (1989).

(178) M. Kotlarchyk, S. H. Chen, J. S. Huang and M. W. Kim, *Phys. Rev. A*, **29**, 2054, (1984).

(179) *Handbook of Lipid Research 4. - The Physical Chemistry of Lipids*, D. A. Small, Plenum Press, New York and London, Ch. 10.

(180) N. Funasaki, S. Hada and K. Suzuki, *Chem. Pharm. Bull.*, **24**, 731, (1976).

(181) H. Kunieda, H. Asaoka and K. Shinoda, *J. Phys. Chem.*, **92**, 185, (1988).

(182) H. Kunieda, *J. Colloid Int. Sci.*, **133**, 237, (1989).

(183) F. Mori, J. C. Lim, O. G. Raney, C. M. Elsik and C. A. Miller, *Colloids and Surfaces*, **40**, 323, (1989).

(184) P. J. Doyle, *M. Phil. Thesis*, Liverpool Poly.,(1990).

(185) M. Kako and S. Kondo, *J. Colloid Int. Sci.*, **69**, 163, (1979).

(186) C. C. Thiel, *J. Council Sci. Ind. Research*, **16**, 139, (1943).

(187) R. Aveyard, B. P. Binks, P. D. I. Fletcher and X. Ye, *in preparation*

(188) R. Aveyard, B. P. Binks, S. Clark and P. D. I. Fletcher, *Progr. Colloid Polym. Sci.*, **79**, 202, (1989).

(189) R. Aveyard, B. P. Binks, T. A. Lawless and J. Mead, *Can. J. Chem.*, **66**, 3031, (1988).

(190) D. Chatenay, D. Langevin, J. Meunier, D. Bourbon, P. Lalanne and A. M. Bellocq, *J. Disp. Sci. Tech.*, **3**, 245, (1982).

(191) B. P. Binks, J. Meunier and D. Langevin, *Progr. Colloid Polym. Sci.*, **79**, 208, (1989).

(192) S. Friberg, in *Food Emulsions*, Ed. S. Friberg, Food Science, Marcel Dekker, New York, **5**, 3982, (1976).

(193) Th. F. Tadros and B. Vincent, in *Encyclopedia of Emulsion Technology*, Ed. P. Becher, Vol. 1, pp. 129, Marcel Dekker, New York, (1983).

(194) H. Kunieda, C. Solans, N. Shida and J. L. Parra, *Colloids and Surfaces*, **24**, 225, (1987).

(195) C. Solans, N. Azemar and J. L. Parra, *Progr. Colloid Polym. Sci.*, **76**, 224, (1988).

(196) H. Kunieda, N. Yano and C. Solans, *Colloids and Surfaces*, **36**, 313, (1989).

(197) P. D. I. Fletcher and B. P. Binks, *unpublished results*

(198) D. Fairhurst, M. P. Aronson, M. L. Gum and E. D. Goddard, *Colloids and Surfaces*, **7**, 153, (1983).

(199) A. Lips, I. J. Campbell and E. G. Pelan, in *Food Polymers, Gels and Colloids*, Ed. E. Dickinson, pp. 1, Royal Soc. Chemistry, Cambridge, (1991).

(200) S. J. Gouldby, P. A. Gunning, D. J. Hibberd and M. M. Robins, in ref. (196) pp. 244.

(201) C. Cowell, R. Li-In-On and B. Vincent, *J. Chem. Soc. Faraday Trans. 1*, **74**, 337, (1978).

(202) P. R. Sperry, *J. Colloid Int. Sci.*, **87**, 375, (1981).

(203) C. Ma, *Colloids and Surfaces*, **28**, 1, (1987).

(204) S. Rawson, K. Ryan and B. Vincent, *Colloids and Surfaces*, **34**, 89, (1988).

(205) R. Hogg and K. Yang, *J. Colloid Int. Sci.*, **56**, 573, (1976).

(206) J. Th. G. Overbeek, G. J. Verhoeckx, P. L. de Bruyn and H. N. W. Lekkerkerker, *J. Colloid Int. Sci.*, **119**, 422, (1987).

(207) N. F. Carnahan and K. E. Starling, *J. Chem. Phys.*, **51**, 635, (1969).

(208) N. F. Carnahan and K. E. Starling, *J. Chem. Phys.*, **53**, 600, (1970).

(209) N. Nishikido, T. Takahara, H. Kobayashi and M. Tanaka, *Bull. Chem. Soc. Jpn.*, **55**, 3085, (1982).

(199) A. Lips, I. J. Campbell and E. G. Pelan, in *Food Polymers, Gels and Colloids*, Ed. E. Dickinson, pp. 1, Royal Soc. Chemistry, Cambridge, (1991).

(200) S. J. Gouldby, P. A. Gunning, D. J. Hibberd and M. M. Robins, in ref. (196) pp. 244.

(201) C. Cowell, R. Li-In-On and B. Vincent, *J. Chem. Soc. Faraday Trans. 1*, **74**, 337, (1978).

(202) P. R. Sperry, *J. Colloid Int. Sci.*, **87**, 375, (1981).

(203) C. Ma, *Colloids and Surfaces*, **28**, 1, (1987).

(204) S. Rawson, K. Ryan and B. Vincent, *Colloids and Surfaces*, **34**, 89, (1988).

(205) R. Hogg and K. Yang, *J. Colloid Int. Sci.*, **56**, 573, (1976).

(206) J. Th. G. Overbeek, G. J. Verhoeckx, P. L. de Bruyn and H. N. W. Lekkerkerker, *J. Colloid Int. Sci.*, **119**, 422, (1987).

(207) N. F. Carnahan and K. E. Starling, *J. Chem. Phys.*, **51**, 635, (1969).

(208) N. F. Carnahan and K. E. Starling, *J. Chem. Phys.*, **53**, 600, (1970).

(209) N. Nishikido, T. Takahara, H. Kobayashi and M. Tanaka, *Bull. Chem. Soc. Jpn.*, **55**, 3085, (1982).